UNIVERZITA KARLOVA

Přírodovědecká fakulta

Katedra biochemie

Doktorský studijní program: Biochemie

Mgr. Pavla Vaňková

Studium struktury a dynamiky proteinů a proteinových komplexů

The study of structure and dynamics of protein molecules and protein complexes

DISERTAČNÍ PRÁCE

Školitel: RNDr. Petr Man, Ph.D.

Praha 2020

Prohlášení

Prohlašuji, že jsem závěrečnou práci zpracovala samostatně a že jsem uvedla všechny použité informační zdoje a literaturu. Tato práce ani její podstatná část nebyla předložena k získání jiného nebo stejného akademického titulu.

V Praze ……

……

Mgr. Pavla Vaňková

Prohlášení o autorství

Prohlašuji, že Mgr. Pavla Vaňková přispěla v deklarovaném rozsahu ke všem experimentům a vědeckým publikacím zahrnutým v této disertační práci.

V Praze ……

……

RNDr. Petr Man, Ph.D.

Poděkování

Na tomto místě bych ráda vyjádřila svou nesmírnou vděčnost všem, kteří mě doprovázeli po celou dobu doktorského studia.

Obrovské díky patří mému školiteli a rádci, Petru Manovi, za rozsáhlé seznámení s technikou vodík/deuteriové výměny, za jeho motivující přístup při řešení experimentů, za poskytnutí možnosti podílet se na řešení řady zajímavých projektů, za jeho cenné rady a zejména za jeho bezbřehou trpělivost.

Velké poděkování patří také Petru Novákovi a všem ostatním členům Laboratoře strukturní biologie a buněčné signalizace, kteří se v průběhu času stali spíše rodinou, za vytvoření příjemného pracovního prostředí. Předně pak Petru Pompachovi a Zdeňku Kukačkovi za jejich nedocenitelné praktické rady a Františku Filandrovi za jeho ochotu kdykoli pomoci.

Filipu Trčkovi, Michalu Ďurechovi a Veronice Vandové z brněnského Regionálního centra aplikované molekulární onkologie, s nimiž nás dohromady svedla spolupráce při řešení projektu spojeného s výzkumem molekulárních chaperonů, patří další veliké poděkování za jejich inspirativní přístup k práci a schopnost vytvořit týmového ducha i přes tuto vzdálenost. Angelu L. Peyovi z Granadské Univerzity dále děkuji za možnost spolupráce při řešení dynamiky NQO1 a poskytnutí dalšího úhlu pohledu na techniku vodík/deuteriové výměny.

Veliké díky pak patří mým rodičům a partnerovi za jejich neutuchající podporu a trpělivost.

Abstrakt

Proteiny v buňce dosahují své nativní konformace za asistence molekulárních chaperonů. Tyto vysokomolekulární dynamické komplexy kromě toho vykonávají další funkce přispívající ke stabilitě buněčného proteomu. Řadí se mezi ně mimo jiné i transport proteinů do cílového kompartmentu nebo obrana proti oxidativnímu stresu. Dynamické strukturní změny chaperonů Hsp70 a NQO1 a ko-chaperonu Tomm34, jež se podílejí na výše zmíněných procesech, a jejich interakce s ligandy jsou zde charakterizovány kombinací strukturní hmotnostní spektrometrie, biofyzikálních a molekulárně biologických technik.

V této práci byla popsána ATP-dependentní dimerizace lidské inducibilní formy Hsp70 (HSPA1A) a charakterizováno evolučně konzervované dimerizační rozhraní. Dále byly identifikovány vysoce konzervované aminokyselinové zbytky, které vytvářejí síť kontaktů stabilizující obě krajní konformace HSPA1A (nízko- i vysokoafinitní) v průběhu ATPasového cyklu. Jedním z ko-chaperonů ovlivňujících ATPasový cyklus Hsp70 je TPR ko-chaperon Tomm34 spolupodílející se na transportu jádrem kódovaných mitochondriálních prekurzorů do mitochondrií. Zde je popsán význam jeho fosforylace cAMP-dependentní proteinkinasou A a následná interakce s proteinem 14-3-3γ při regulaci tohoto procesu. V případě chaperonu NQO1, který má kromě stabilizačního vlivu na několik vazebných partnerů i enzymatickou aktivitu, se podařilo strukturně charakterizovat velmi dynamickou apoformu NQO1 v kontextu formy s navázaným kofaktorem, jenž tuto flexibilní strukturu rozsáhle stabilizuje, a inibitorem, který způsobuje další stabilizaci makromolekuly. Protože se jedná o proteiny, které jsou ve velké míře zahrnuty v procesech karcinogeneze a předčasného stárnutí buněk, znalost struktury, alosterické komunikace mezi podjednotkami a jejich interakce s ligandy má velký potenciál uplatnění v terapii těchto patologických procesů.

Klíčová slova: strukturní hmotnostní spektrometrie, vodík/deuteriová výměna, proteostasa, molekulární chaperony, ko-chaperony, HSPA1A, Tomm34, NQO1, dimerizace, ATPasová aktivita, alosterie proteinů, interakční rozhraní, fosforylace, 14-3-3γ, transport mitochondriálních proteinů

Abstract

Inside the cellular milieu, proteins are reaching their native conformation with the assistance of molecular chaperones. These high mass dynamic complexes perform other functions that are contributing to the stability of the cellular proteome. Transport of proteins into the target compartment or defence against oxidative stress rank among these as well. Dynamic structural changes of chaperones Hsp70 and NQO1 and co-chaperone Tomm34 that are participating in above mentioned processes and their interactions with ligands are characterized here by the combination of structural mass spectrometry, biophysical and molecular biology techniques.

In this thesis the ATP-dependent dimerization of human inducible isoform Hsp70 (HSPA1A) and the characterization of its evolutionarily conserved dimerization interface were described. Further, highly conserved amino acid residues crucial for allosteric movements were identified. These residues create a network of contacts stabilizing both extreme conformations of HSPA1A (low and high-affinity) during the ATPase cycle. One of the co-chaperones that can affect Hsp70 ATPase cycle is TPR co-chaperone Tomm34. This co-chaperone is participating on the transport of the nuclear encoded mitochondrial precursors into the mitochondria. Here we described regulation of this process, through Tomm34 phosphorylation by cAMP-dependent protein kinase A and its subsequent interaction with 14-3-3 protein. Further, we investigated the chaperone NQO1, which in addition to the stabilization effect on several binding partners also has enzymatic activity. Structural characterization of highly dynamic NQO1 apo-form was carried out in the context of holo-form and inhibitor bound holo-form. Based on the findings, we concluded, that the dynamic environment of NQO1 is extensively stabilized by cofactor binding and that the inhibitor binding causes further stabilization of the NQO1 dimer. Since all these proteins are engaged in the processes of carcinogenesis and cell aging, the detailed knowledge of their structural properties, allosteric communication and their interactions with ligands has a great application potential in the therapy of the pathological processes.

Keywords: structural mass spectrometry, hydrogen/deuterium exchange, proteostasis, molecular chaperones, co-chaperones, HSPA1A, Tomm34, NQO1, dimerization, ATPase activity, protein allostery, interaction interface, phosphorylation, 14-3-3γ, mitochondrial protein transport

Obsah

Seznam zkratek

ADP	adenosindifosfát
Aha1	ko-chaperon aktivující ATPasovou aktivitu Hsp90 (*Activator of Hsp90 ATPase protein 1*)
AhR	transkripční faktor (*Aryl hydrocarbon receptor*)
ATP	adenosintrifosfát
BiP	eukaryotický homolog Hsp70 z ER (*Binding immunoglobulin protein*)
BS2G	bis-(sulfosukcinimidyl) glutarát
CAEMI	chaperonem asistovaná endosomální mikroautofagie
CAMA	chaperonem asistovaná makroautofagie
CCS	kolizní průřez (*Collisional cross-section*)
CID	kolizně indukovaná disociace (*Collision-induced dissociation*)
CIU	kolizně indukovaná postupná destabilizace terciární struktury (*Collision induced unfolding*)
CMA	chaperonem zprostředkovaná autofagie (*Chaperone-mediated autophagy*)
CTD	C-terminální doména Hsp90 nebo NQO1
CUPS	chaperonem asistovaná degradace zprostředkovaná UPS (*Chaperone-assisted ubiquitin-proteasome system*)
DBS	vazebné místo pro dikumarol (*Dicoumarol binding site*)
DCPIP	2,6-dichlorfenolindofenol
DSA	di-(N-sukcinimidyl) adipát
ECD	disociace záchytem elektronu (*Electron capture dissociation*)
ER	endoplasmatické retikulum
ESI	ionizace elektrosprejem (*Electrospray ionization*)

ETD	disociace přenosem elektronu (*Electron transfer dissociation*)
FAD	flavinadenindinukleotid
FBS	vazebné místo pro FAD (*FAD binding site*)
FT-ICR	hmotnostní analyzátor s iontově cyklotronovou resonancí a Fourierovou transformací (*Fourier Transform Ion Cyclotron Resonance*)
Grp94	eukaryotický homolog Hsp90 z ER (*94-kDa Glucose-regulated protein*)
HDX	vodík/deuteriová výměna (*Hydrogen/deuterium exchange*)
HDX-MS	vodík/deuteriová výměna kombinovaná s hmotnostní spektrometrií
HIF-1α	hypoxií indukovaný faktor 1 (*Hypoxia-induced factor 1*)
Hip	ko-chaperon interagující s Hsp70 (*Hsp70-interacting protein*)
Hop	TPR ko-chaperon interagující s Hsp70/Hsp90 (*Hsp70/90 organizing protein*)
HPLC	vysokoúčinná kapalinová chromatografie (*High-performance liquid chromatography*)
Hsc70	cytoplasmatický homolog Hsp70 (*Heat shock cognate 70*)
Hsp	proteiny teplotního šoku (*Heat shock protein*)
HtpG	prokaryotický homolog Hsp90 (*High temperature protein G*)
CHIP	TPR ko-chaperon interagující s C-koncem Hsp70 (*Carboxyl terminus of Hsp70-interacting protein*)
IM	iontová mobilita
IM-MS	iontová mobilita kombinovaná s hmotnostní spektrometrií
ITC	isotermální titrační kalorimetrie (*Isothermal titration calorimetry*)
JDP	ko-chaperony z rodiny J-proteinů obsahujících J-doménu (*J-domain proteins*)
LAMP2A	s lysozomem asociovaný membránový protein typu 2A (*Lysosome-associated membrane protein type 2A*)

LC	kapalinová chromatografie (*Liquid chromatography*)
MALDI	ionizace laserem za přítomnosti matrice (*Matrix-Assisted Laser Desorption/Ionization*)
MD	středová doména Hsp90 (*Middle domain*)
MMI	rozhraní dimeru (*Monomer:monomer interface*)
MS	Hmotnostní spektrometrie (*Mass spectrometry*)
NAD(P)H	Nikotinamidadenindinukleotid(fosfát)
NBD	Nukleotid-vázající doména Hsp70 (*Nucleotide binding domain*)
NEF	protein usnadňující výměnu hydrolyzovaného nukleotidu (*Nucleotide exchange factor*)
nESI	ionizace nanoelektrosprejem
NMR	nukleární magnetická resonance
NQO1	NAD(P)H:chinonoxidoreduktasa 1 (*NAD(P)H:quinone oxidoreductase 1*)
Nrf2	transkripční faktor (*Nuclear factor erythroid 2-related factor 2*)
NTD	N-terminální doména Hsp90 nebo NQO1
PES	2-fenylethynsulfonamid
PET-16	trifenyl(fenylethynyl)fosfonium bromid
PKA	cAMP-dependentní proteinkinasa A
PTM	posttranslační modifikace
SAXS	maloúhlový rozptyl rentgenového záření (*Small-angle X-ray scattering*)
SBD	substrát-vázající doména Hsp70 (*Substrate binding domain*)
SEC	gelová permeační chromatografie (*Size exclusion chromatography*)
SPR	povrchová plasmonová resonance (*Surface plasmon resonance*)
SRP	ribonukleoproteinový komplex rozpoznávající signální sekvenci (*Signal recognition particle*)

Sti1	homolog ko-chaperonu Hop z *S. cerevisiae* (*Stress-inducible protein 1*)
TCEP	tris(2-karboxyethyl)fosfin
TOM	translokační komplex vnější mitochondriální membrány (*Translocase of outer mitochondrial membrane*)
Tomm34	34-kDa translokasa vnější mitochondriální membrány (*34-kDa Translocase of outer mitochondrial membrane*)
TPR	34-aminokyselinové opakující se strukturní/sekvenční motivy (*Tetratricopeptide repeats*)
TRAP1	mitochondriální eukaryotický homolog Hsp90 (*Tumor necrosis factor receptor-associated protein 1*)
Ubl	N-terminální doména BAG1 podobná ubikvitinu (*Ubiquitin-like domain*)
UHPLC	ultra-vysokoúčinná kapalinová chromatografie (*Ultra-high performance liquid chromatography*)
UPS	ubikvitin-proteasomový degradační systém
UVPD	fotodisociace ultrafialovým zářením (*Ultraviolet photodissociation*)
XL-MS	chemické zesítění proteinů v kombinaci s hmotnostní spektrometrií (*Chemical cross-linking mass spectrometry*)

1 LITERÁRNÍ ÚVOD

1.1 Molekulární chaperony a jejich význam

Buňka, elementární jednotka všech organismů, je ekosystémem, jehož funkčnost je zajišťována koordinovanou součinností proteinových makromolekul. Jejich přítomnost je odrazem genetického kódu složeného z nukleových kyselin nesoucích primární informaci pro život jako takový. Integrita buněčného proteomu, proteostasa, je základním předpokladem zajišťujícím bezchybnou souslednost všech dějů vykonávaných těmito stěžejními jednotkami, které mohou nabývat nezměrného množství prostorových uspořádání podmiňujících jejich biologické funkce. Jak je však s ohledem na obrovský počet stupňů volnosti, jichž mohou proteinové řetězce složené z jednotlivých aminokyselin dosáhnout, zabezpečeno, že protein nabude ve velmi krátkém čase v řádu μs až s jediné nativní konformace, tedy konformace s nejnižší dosažitelnou volnou energií[1]? Touto skutečností založenou na Anfinsenovu dogmatu se zabývá myšlenkový experiment známý jako Levinthalův paradox. Anfinsenovo dogma, jinak označované jako termodynamická hypotéza, postuluje, že pro malé globulární proteiny je jejich trojrozměrná struktura definována pořadím aminokyselin v řetězci a dokáží tak reverzibilně dosáhnout své biologicky aktivní konformace, která odpovídá termodynamicky stabilnímu stavu s nejnižší potenciální energií konfigurace[2]. Levinthal navrhl alternativní pohled, kdy nativní protein dosahuje konkrétního metastabilního stavu, při němž potenciální energie dosahuje lokálního minima, nikoli absolutního. Tento model předpokládá, že nativní protein není v rovnovážném stavu s denaturovanou formou, kdy náhodně nalézá svou biologicky aktivní trojrozměrnou strukturu, což by trvalo nekonečně dlouho, ale že při hledání své nativní struktury postupně prochází sérií konkrétních stavů vedoucích k dané optimální konformaci[3].

Mezi fyzikálně-chemické vlivy, které udržují proteinový řetězec v jeho nativní konformaci se řadí hydrofobní interakce, tvorba vodíkových vazeb charakteristických pro α-helikální nebo β-listové uspořádání, van der Waalsovy interakce, elektrostatické interakce kladně nebo záporně nabitých postranních řetězců aminokyselin, geometrické preference určitých hodnot dihedrálních úhlů ϕ (vazba N–C_α) a ψ (C_α–C_β) mezi atomy proteinové páteře a v neposlední řadě taktéž tzv. efekt vyloučeného objemu vyvolaný zhuštěným makromolekulárním prostředím *in vivo*[4,5].

Rozsáhlé bádání v oblasti molekulárních chaperonů v průběhu 80. let začalo postupně zpochybňovat a následně i vyvracet všeobecně rozšířený koncept předpokládající, že skládání proteinů *in vivo* je nekatalyzovaný proces[6]. Srovnání chaperony asistovaného vs. neasistovaného sbalování proteinového řetězce je graficky znázorněno v *Obr. 1*[7]. Tato rozmanitá skupina evolučně konzervovaných proteinů, jejichž přítomnost je pro životaschopnost buněk esenciální, byla poprvé identifikována v buňkách slinných žláz larev *Drosophily melanogaster*. V reakci na vystavení buněk vyšší teplotě byla pozorována zvýšená exprese těchto všudypřítomných proteinů a odtud také vychází jejich označení *proteiny teplotního šoku*, Hsp (z angl. Heat shock protein)[8,9]. Později bylo potvrzeno, že buňky vykazují zvýšenou expresi Hsp jako kompenzační mechanismus i na další environmentální zátěž.

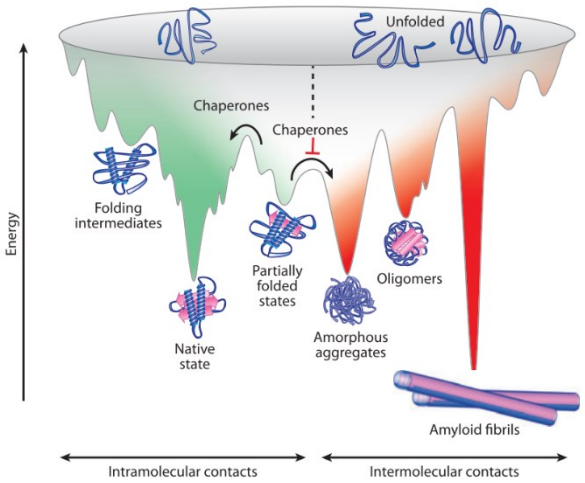

Obrázek 1. *Schematické znázornění procesu sbalování proteinů. Proteiny se snaží dosáhnout nativního stavu s nejnižší potenciální energií. Bez asistence chaperonů (červená část) dochází k nespecifické oligomerizaci nebo agregaci proteinů. S podporou chaperonových komplexů (zelená část), které zabraňují nespecifické agregaci při sbalování a napomáhají proteinu překonat energetické bariéry, protein zpravidla dosáhne své nativní konformace. (převzato z Kim, 2013)*[7]

Chaperony zabraňují agregaci kotraslačně, když je proteinový řetězec postupně uvolňován z ribozomu[10,11], čímž usnadňují, aby byl správně uspořádán do své nativní konformace, nebo ho udržují ve stavu kompetentním pro transport do konkrétního buněčného kompartmentu[12,13]. Vedle toho se podílejí na jeho dalším osudu, např. sekreci ven z buňky[7] nebo napomáhají rozvolňovat agregáty[14] a proteinové komplexy[15]. Dalším významným příspěvkem chaperonů k udržování proteostasy je jejich úloha při rozpoznávání nesprávně sbalených proteinů, které mohou být za jejich asistence disagregovány, strukturně rozvolněny a opětovně sbaleny opakovanou vazbou na tyto molekulární kontrolory kvality buněčného proteomu. Nedosáhnou-li ani tak své správné konformace, jsou podrobeny degradaci buď prostřednicvím ubikvitin-proteasomového systému (UPS) nebo autofagie. Všechny výše zmíněné funkce molekulárních chaperonů

jsou shrnuty v *Obr. 2*. Protože jsou substrátové preference dvou nejabundantnějších rodin chaperonů Hsp70 a Hsp90 velmi nespecifické, jejich specifita pro konkrétní substrát a jeho další osud je modulována interakcí s tzv. ko-chaperony.

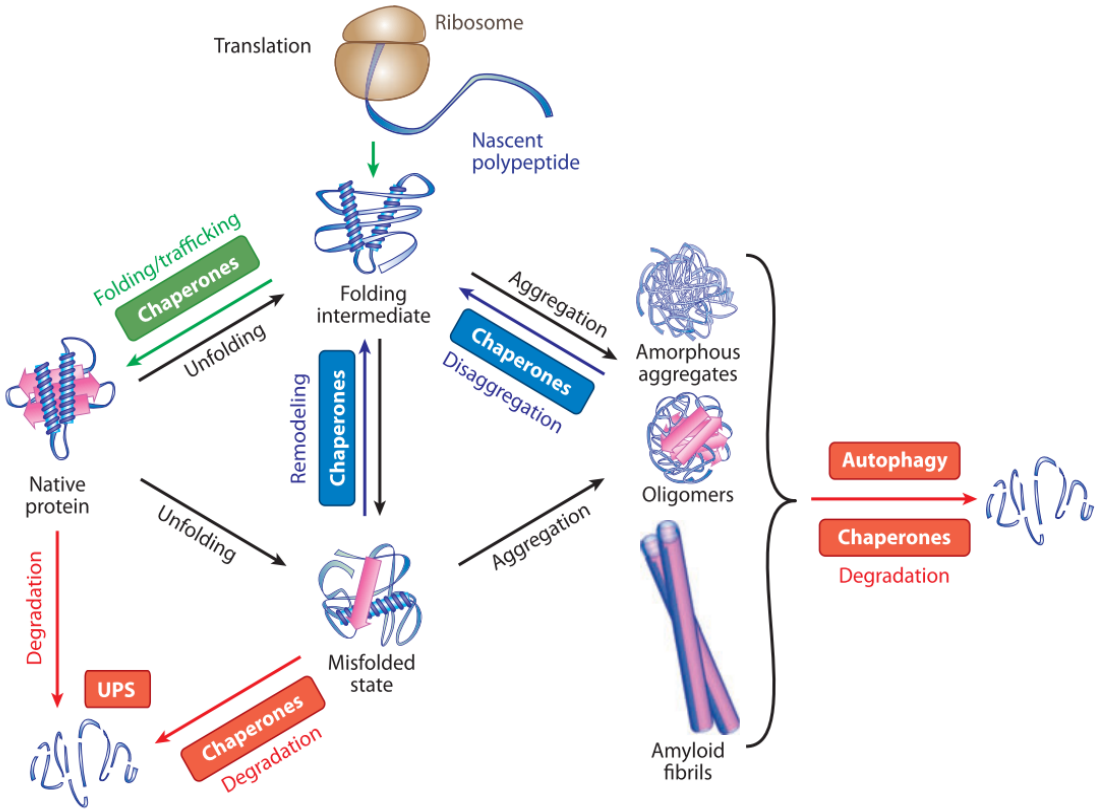

Obrázek 2. *Proteostatická síť integrující různorodé funkce chaperonů. Chaperony napomáhají protein už při jeho syntéze na ribozomu udržovat v neagregované formě, která je kompetentní pro jeho transport do místa určení a dosažení nativního stavu. Nabyl-li protein nesprávné konformace, napomáhají ho převést zpět do stavu, z něhož může opět nabýt správného sbalení. Dále se podílí na disagregaci proteinových agregátů. Pokud nejsou proteiny schopny dosáhnout nativní konformace, chaperony se podílejí na jejich degradaci prostřednictvím UPS nebo autofagie. (převzato z Kim, 2013)*[7]

V souvislosti s různými stresovými stavy dochází na buněčné úrovni k deregulaci funkce molekulárních chaperonů. To se může negativně projevit například nedostatečným odbouráváním proteinových agregátů, s čímž je spojována Alzheimerova choroba (β-amyloidové plaky α-synucleinu), Parkinsonova choroba (amyloidogenní protein Tau) nebo Huntingtonova nemoc (agregáty huntingtinu)[16]. S negativní prognózou je pak spojována zvýšená přítomnost Hsp70 a Hsp90 chaperonů v případě karcinogeneze[17]. Negativním prognostickým markerem je v rakovinných buňkách, které jsou ve stavu hypoxie, rovněž zvýšená exprese transkripčního faktoru HIF-1α (z angl. Hypoxia-induced factor 1), který je hlavním regulátorem homeostasy kyslíku[18]. Nedávno byla studována jeho interakce s NAD(P)H:chinonoxidoreduktasou 1 (NQO1; z angl. NAD(P)H:quinone oxidoreductase 1; EC 1.6.5.2), jejíž exprese

je rovněž za hypoxických podmínek zvýšena a která na HIF-1α působí jako stabilizující chaperon. Touto interakcí je totiž snížena jeho ubikvitinace uvnitř cytoslu, odkud pak může být importován přímo do jádra, kde zahajuje svou transkripční aktivitu[19,20]. Mimo chaperonového působení na několik dalších substrátů funguje NQO1 primárně jako enzym, kdy mechanismem dvouelektronové redukce chinonů brání tvorbě reaktivních a potenciálně cytotoxických semichinonů nebo redukcí superoxidových radikálů chrání buňku před působením reaktivních forem kyslíku[21].

1.2 Hsp70

Rodina dynamických, všudypřítomných a vysoce homologních 70-kDa Hsp70 proteinů čítá u člověka celkem 13 členů (*Tab. 1*[22]), zatímco pro *Escherischii coli* byly dosud identifikovány pouze tři zástupci a pro *Saccharomyces cerevisiae* 11 homolgů[23]. Z pohledu evoluce, kdy lze pozorovat vysoký stupeň sekvenční, strukturní i funkční konzervace napříč všemi organismy od archeí přes rostliny až ke člověku, jde o nejvíce konzervovanou rodinu proteinů vůbec, a například prokaryotický ortholog DnaK sdílí s eukaryotickými Hsp70 proteiny přibližně 50% sekvenční shodu[22,24].

Tabulka 1: *Vybraní zástupci lidské proteinové rodiny Hsp70. (převzato z Daugaard, 2007; upraveno)*[22]

Protein	Alternative names	Homology to Hsp70-1a (%)	Locus	Accession	Localization	Affymetrix annotation	Cellular localization	Stress-induced
Hsp70-1a	Hsp70, Hsp72, Hsp70-1	100	*HSPA1A*	NM_005345	6p21.3	200799_at	Cytosol, Nucleus, Lysosomes	Yes
Hsp70-1b	Hsp70, Hsp72, Hsp70-1	99	*HSPA1B*	NM_005346	6p21.3	202581_at	Cytosol, Nucleus, Lysosomes	Yes
Hsp70-1t	Hsp70-hom	91	*HSPA1L*	NM_005527	6p21.3	210189_at	Cytosol, Nucleus	No
Hsp70-2	Hsp70-3, HspA2	84	*HSPA2*	NM_021979	14q24.1	211538_s_at	Cytosol, Nucleus	No
Hsp70-5	Bib, Grp78	64	*HSPA5*	NM_005347	9q33-q34.1	211936_at	ER	No
Hsp70-6	Hsp70B′	85	*HSPA6*	NM_002155	1cen-qter	213418_at	Cytosol, Nucleus	Yes
Hsc70	Hsp70-8, Hsp73	86	*HSPA8*	NM_006597[a]	11q23.3-q25	210338_s_at	Cytosol, Nucleus	No
Hsp70-9	Grp75, mtHsp75, Mortalin	52	*HSPA9*	NM_004134	5q31.1	200690_at	Mitochondria	No

[a]A 54 kDa Hsc70 splice variant (NM_153201) has been reported, but its functional significance remains unclear

U všech eukaryot jsou proteiny Hsp70 kódovány více než jedním genem[22]. U člověka mají pro udržování proteostasy za fyziologických podmínek nezastupitelnou úlohu zejména ve většině tkání konstitutivně exprimované cytosolické Hsc70 (HSPA8), jejž můžeme nalézt i v jádře, mitochondriální Grp75/mtHsp75 (HSPA9) a BiP/Grp78 (z angl. Binding immunoglobulin protein) (HSPA5), který je lokalizován do endoplasmatického retikula (ER). Cytosolický Hsc70 zabraňuje agregaci proteinů a uplatňuje se primárně při skládání lineárního nascentního proteinového řetězce do definovaného trojrozměrného uspořádání, při translokaci proteinových řetězců přes membrány, pomáhá rozrušit kompaktní strukturu klathrinového pláště na povrchu endocytických váčků[25] nebo se podílí na chaperonem zprostředkované autofagii[26]. BiP usnadňuje transport nově syntetizovaných proteinů v lumen ER a jejich následné sbalení do správné konformace a Grp75 má analogickou funkci v mitochondriálním

lumen. Za stresových podmínek jsou pak pro lidskou buňku esenciální inducibilně exprimovaní zástupci Hsp70 rodiny, jmenovitě Hsp70 (HSPA1A), Hsp70-2 (HSPA1B) a Hsp70B (HSPA6)[22,27]. Inducibilní Hsp70, Hsp70-2 a Hsp70B se vyskytují v cytoplasmě a jádře a kromě Hsp70B je lze nalézt i v lysozomech[22]. Cytoprotektivní působení těchto forem spočívá zejména v jejich antiapoptotické aktivitě, kdy je na různých úrovních předcházeno programované buněčné smrti[28,29,30]. Rozsáhlá exprese Hsp70 v buňkách maligních nádorů různého původu koreluje s jejich zvýšenou proliferací, klinickým stadiem a špatnou prognózou[17,31]. V *Tab. 2*[22] je uveden přehled myších fenotypů po vyřazení funkce genů pro konkrétní homology Hsp70.

Tabulka 2: *Přehled projevů vyřazení genů pro jednotlivé homology Hsp70 v myším fenotypu. (převzato z Daugaard, 2007; upraveno)*[22]

Protein	Gene locus	Chromosomal localization	Analogous Human gene	Phenotype
Hsp70.1	*Hspa1a*	17 B1	*HSPA1A*	Viable and fertile. Susceptible to UV, osmotic stress, ischemia, TNF, pancratitis and heat
Hsp70.3	*Hspa1b*	17 B1	*HSPA1B*	Viable and fertile. Susceptible to Heat
Hsp70.1 + Hsp70.3	*Hspa1a + Hspa1b*	17 B1	*HSPA1A + HSPA1B*	Viable and fertile. Susceptible to radiation and sepsis. Increased genomic instability
Hsp70.2	*Hspa2*	17 B1	*HSPA2*	Viable and female fertility. Meiotic defects in male germ cells
Hsc70	*Hspa8*	9 A5.1	*HSPA8*	Not applicable. Knockout cells are non-viable
Bip, GRP78	*Hspa5*	2 B	*HSPA5*	Lethal at embryonic day 3.5

1.2.1 Struktura Hsp70

Nativní struktura Hsp70 je tvořena dvěma funkčními doménami, které jsou vzájemně propojené krátkým vysoce flexibilním úsekem hydrofobní sekvence, tzv. linkerem (*Obr. 3* na s. 18). První doména ve směru od N-konce (45-kDa) je zodpovědná za vazbu a hydrolýzu adenosintrifosfátu (ATP), od čehož je odvozen její název NBD (z angl. Nucleotide binding domain). Druhá doména (25-kDa), vázající substrát (SBD; z angl. Substrate binding domain), představuje C-terminální část Hsp70. Vazba substrátu je přechodná, bez jakékoli sekvenční specifity a zacílená na krátké úseky proteinů sestávající z hydrofobních aminokyselin lemovaných pozitivně nabitými aminokyselinovými zbytky[32]. Absence sekvenční specifity vůči těmto všudypřítomným krátkým hydrofobním oblastem, které se s výjimkou vnitřně neuspořádaných proteinů opakují v primární sekvenci přibližně každých 30–40 aminokyselin a jsou vystaveny na povrchu nesbalených nebo špatně poskládaných proteinů[15], eliminuje limitaci velikosti navázaného substrátu.

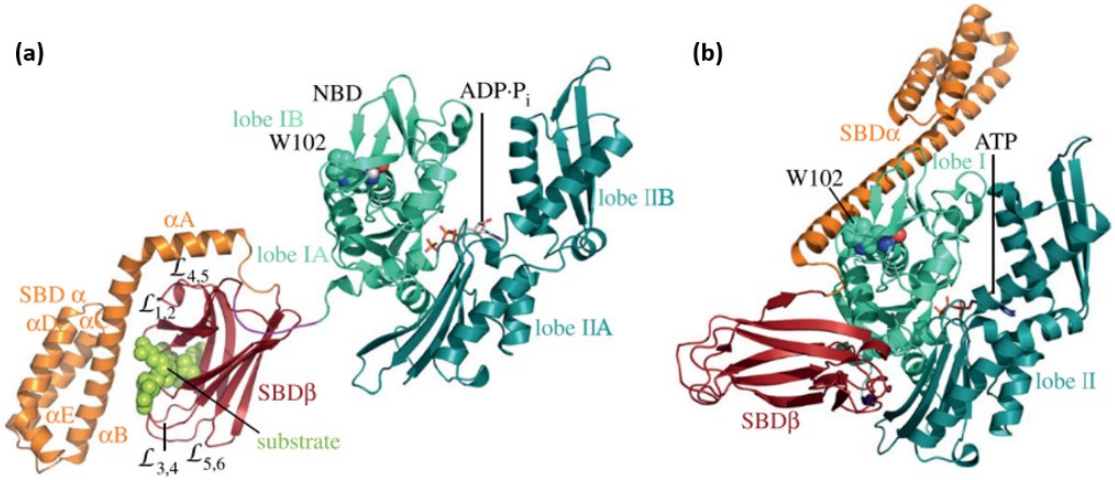

Obrázek 3. *Struktura bakteriálního homologu Hsp70, DnaK. (a) Vysokoafinitní uzavřená konformace, kdy je mezi rameny NBD IA/B (světle zelená) a IIA/B (tyrkysová) koordinován hydrolyzovaný ATP, ve formě ADP. Substrát (jasně zelená) navázaný v hydrofobní kapse SBDβ je stabilizován smyčkami $L_{1,2}$ a $L_{3,4}$ a subdoménou SBDα (oranžová). NBD a SBD propojené hydrofobním flexibilním linkerem jsou na sobě zcela nezávislé a tato ADP-vázající struktura je totožná s tzv. Apo stavem, strukturou bez navázaného nukleotidu. (PDB kód: 2KHO). (b) Nízkoafinitní ATP-vázající konformace s otevřenou substrát vázající doménou SBDβ. V NBD je koordinován ATP a vlivem rotace ramen NBD se mezi nimi v oblasti IA a IIA vytvořila štěrbina, do níž byl zasunut hydrofobní linker. Dále došlo k disociaci SBDβ a SBDα, které jsou teď dokovány na NBD poskytujíc nová interakční rozhraní NBD-SBDβ a NBD-SBDα. (PDB kód: 4B9Q). (převzato z Mayer, 2018; upraveno)*[34]

NBD, která je strukturně homologní s aktinem[33], je tvořena dvěma rameny, I a II, kdy je každé ještě rozděleno na dvě subdomény A a B (IA, IB, IIA, IIB). Uvnitř této struktury připomínající zalomené písmeno „V“ je hluboká štěrbina, na jejíž dno se váže molekula ATP, která je koordinována všemi čtyřmi subdoménami IA, IB, IIA, IIB. SBD je organizována do dvou subdomén, SBDβ a SBDα. Podjednotka beta, která sekvenčně navazuje na flexibilní linker, je tvořena dvěma čtyřvláknovými vzájemně pootočenými β-listy (β1-β2-β4-β5 a β3-β6-β7-β8), kde jsou jednotlivá vlákna propojena ven vybíhajícími smyčkami. Mezi β-vlákny β1-β2 a β3-β4 se nachází centrální úzká hydrofobní kapsa uzpůsobená vazbě jediného dlouhého hydrofobního aminokyselinového postranního řetězce leucinu substrátového peptidu, nad nímž se klenou k sobě orientované smyčky $L_{1,2}$ a $L_{3,4}$, které jsou navzájem stabilizovány vodíkovými vazbami a hydrofobními interakcemi[23,34]. Tato klenba stericky stabilizující substrát přispívá dále v pozicích −1 a +1 od centrálního leucinu k vazbě sousedících leucinů. Vazebná místa vně tuto centrální triádu jsou mnohem otevřenější a elektrostatický potenciál povrchu SBDβ je v těchto místech silně negativní[35]. Substrát vázající kapsa SBDβ je dále shora překryta helixy αA a αB ze subdomény SBDα, které zde tvoří v případě interakce se substrátem pomyslné víko. Zatímco při vazbě peptidu víko přímo dosedá na SBDβ, v případě rozlehlejšího substrátu bylo pozorováno, že zůstává v polootevřené konformaci[36]. Na helix αB plynule navazuje

helix αC, který dále tvoří svazek s helixy αD a αE. SBD je zakončena C-terminálním nestrukturovaným regionem nesoucím konzervovaný nabitý sekvenční motiv EEVD (Glu-Glu-Val-Asp) umožnující interakci s tzv. TPR (34-aminokyselinové opakující se strukturní/sekvenční motivy; z angl. Tetratricopeptide repeats) ko-chaperony[37].

1.2.2 ATPasový cyklus a alosterická povaha Hsp70

Hsp70 je velmi dynamická a flexibilní struktura a její celková konformace závisí na vazbě a hydrolýze ATP, kdy je pomocí alosterického mechanismu regulována vazba proteinového substrátu (*Obr. 4*). Hydrolýza navázaného ATP zvyšuje afinitu Hsp70 vůči substrátu v hydrofobní kapse SBDβ a naopak vazba substrátu urychluje hydrolýzu ATP. Pokud je v aktivním centru NBD molekula adenosindifosfátu (ADP) nebo je ve stavu bez nukleotidu, SBD váže substrát s vysokou afinitou (K_D = 0,1–1 μM) a zároveň s velmi nízkou rychlostí asociace a disociace. Vazba ATP naopak oslabuje afinitu SBD vůči substrátu (K_D se zvyšuje přibližně 10×) a rychlost asociace a disociace vzrůstá o dva až tři řády[23,38]. Na základě nedávných poznatků lze konstatovat, že je vazba a uvolnění substrátu nikoli náhodným, ale vysoce koordinovaným procesem.

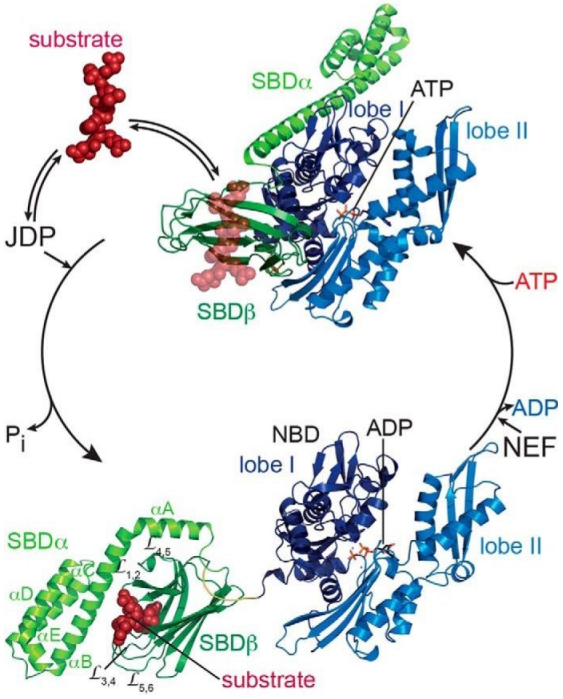

Obrázek 4. *ATPasový cyklus Hsp70. Do otevřené SBDβ Hsp70 v nízkoafinitním stavu s navázaným ATP je za asistence JDP ko-chaperonu vložen substrát. Ten je po hydrolýze ATP stericky uzavřen SBDα, neboť Hsp70 přechází do své vysokoafinitní konformace. Délka setrvání substrátu v SBDβ je regulována interakcí s ko-chaperony NEF, které zprostředkují výměnu ADP za nový ATP a Hsp70 přechází zpět do nízkoafinitní konformace s otevřenou SBDβ. (převzato z Mayer, 2019)*[55]

Vazba ATP do aktivního centra NBD vede ke vzájemnému pootočení ramen I a II, čímž dojde ve spodní části NBD (IA a IIA) ke vzniku štěrbiny, kam je posléze vložen hydrofobní linker. Dále je NBD skrze rameno I stabilizována rozsáhlou interakcí s SBDβ a SBDα, čímž je dosaženo konformace NBD nekompetentní pro hydrolýzu ATP, a hydrofobní kapsa pro vazbu substrátu v SBDβ je nyní široce rozevřená[39,40] (tzv. otevřená nízkoafinitní konformace Hsp70) (*Obr. 5a-II, 5b* na s. 20). Kromě tohoto široce otevřeného vazebného místa však

byla pro stav vázající ATP popsána i konformace, kdy smyčky $L_{3,4}$ a $L_{5,6}$, které se nacházejí v SBDβ na straně vzdálenější od NBD, jsou spolu s vlákny β3 a β4, které tvoří dno hydrofobní kapsy na stejné straně, rovněž rozevřené, ale v mnohem menším rozsahu[41] (tzv. částečně otevřená konformace SBDβ)) (*Obr. 5a-III, 5b*). Mimo tyto dvě konformace SBDβ, otevřenou a částečně otevřenou popsané pro DnaK-ATP, byla nedávno v případě lidského Hsp70 zástupce z ER, proteinu BiP, pozorována ještě třetí ATP-vazebná konformace, kdy je hydrofobní kapsa vázající substrát zcela uzavřená[42,43](*Obr. 5a-IV, 5b*). Na základě studií prováděných v roztoku bylo následně zjištěno, že tato plně uzavřená konformace, která není kompatibilní s vazbou substrátu, je v roztoku převládající formou[43].

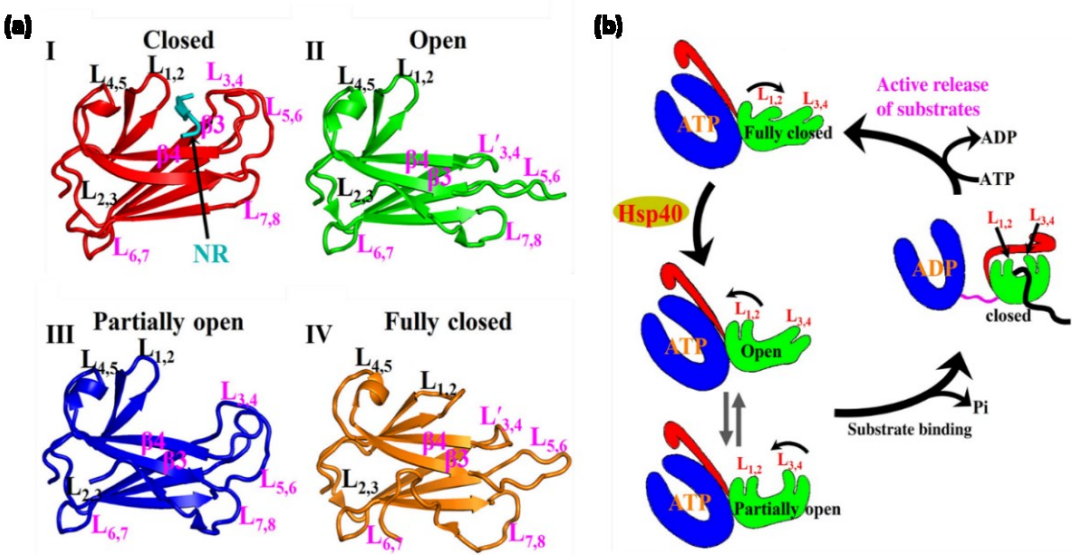

Obrázek 5. *Alosterický cyklus Hsp70. (a) Různé konformační stavy domény SBDβ – (I) uzavřená konformace izolované SBDβ DnaK s navázaným substrátem (PDB kód: 1DKX); (II) otevřená SBDβ DnaK-ATP (PDB kód: 4JNE); (III) částečně otevřená SBDβ DnaK-ATP (PDB kód: 4B9Q); (IV) plně uzavřená SBDβ z BiP-ATP (PDB kód: 8ASY). (b) Zjednodušené schéma znázorňující ATPasový cyklus a pravděpodobné strukturní přeměny SBDβ v jeho jednotlivých fázích. Ko-chaperonem Hsp40 je do otevřené SBDβ (zelená) Hsp70, která je v dynamické rovnováze se svou částečně otevřenou konformací, přenesen substrát (černá). Jejich součinností je usnadněna hydrolýza ATP, která spouští rozsáhlé strukturní změny a substrát je "uvězněn" v SBDβ s uzavřenou vysokoafinitní konformací. Následně v NBD (modrá) dochází za asistence NEF faktorů k výměně hydrolyzovaného ATP za nové, SBDα (červená) disociuje od SBDβ, která nabývá plně uzavřené konformace a substrát je aktivně uvolněn. Nakonec za asistence Hsp40, který s sebou nese nový substrát, získává SBDβ znovu otevřenou konformaci a celý cyklus se může opakovat. (převzato z Liu, 2020; upraveno)*[54]

Bazální hydrolytická aktivita, která je pro fungování Hsp70 esenciální a umožňuje přechod chaperonu do vysokoafinitní konformace vázající substrát, je velmi nízká. Rychlost hydrolýzy zvyšují ko-chaperony z rodiny J-proteinů (JDP; z angl. J-Domain proteins) a to až 15 000×[44,45,46]. Na základě krystalové struktury zachycující ATP-vázající strukturu DnaK z *E. coli,* který je z biofyzikálního hlediska nejlépe prostudovaným zástupcem proteinové rodiny Hsp70, v komplexu s J-doménou ko-chaperonu DnaJ

(Hsp40 u člověka) (*Obr. 6*), byl popsán evolučně konzervovaný mechanismus, jímž DnaJ, který na DnaK přenáší substrát[47], skrze rozsáhlé kontakty s SBDβ, linkerem i NBD propouští signál z kapsy vázající substrát až do NBD[48]. Zároveň jsou vazbou substrátu vyvolané konformační změny přenášeny do J-domény, kde motiv HPD (His-Pro-Asp) udržuje linker Hsp70 zanořený ve spodní části NBD, tedy v konformaci která zajišťuje, aby ramena a katalytické zbytky NBD byly v pozici optimální pro hydrolýzu ATP[48,49].

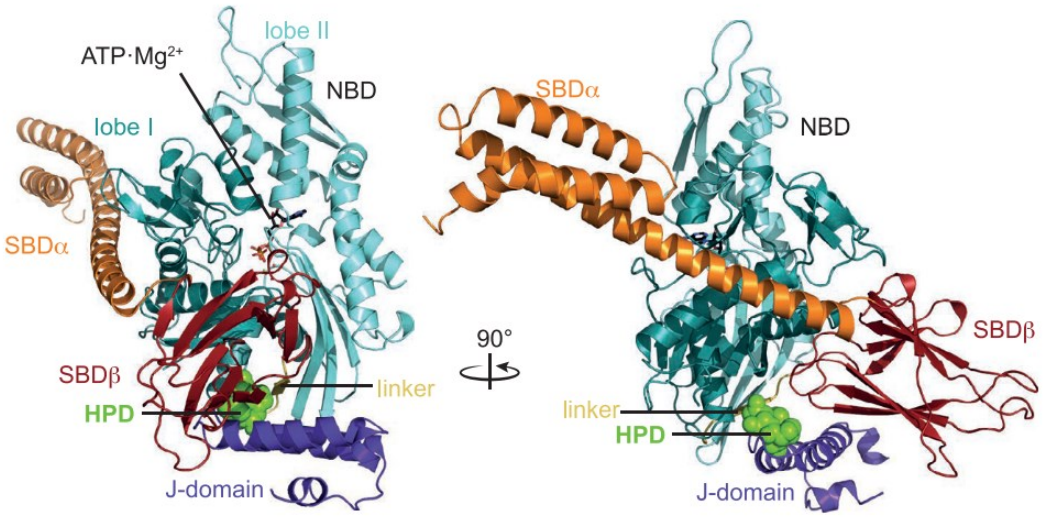

Obrázek 6. *Krystalová struktura DnaK-ATP z E. coli v komplexu s J-doménou DnaJ. Mezi rameny I (tyrkysová) a II (světle modrá) NBD je koordinováno ATP s Mg^{2+}. Flexibilní linker (žlutá) je vložen zespodu NBD do štěrbiny mezi jejími rameny a utváří se interakční rozhraní NBD-SBDβ (červená) a NBD-SBDα (oranžová). Struktura antiparalelního helixu reprezentující J-doménu ko-chaperonu DnaJ (fialová) kontaktuje domény SBDβ a NBD a skrze svůj HPD motiv (zelená) udržuje linker zanořený ve spodní části NBD. (PDB kód: 5NRO) (převzato z Kityk, 2018)[48]*

Aby však došlo k účinné vazbě ko-chaperonu Hsp40 k Hsp70 a následnému přenosu substrátu, musí se Hsp70-ATP nacházet ve formě antiparalelního dimeru, jehož existence byla popsána na základě krystalové struktury DnaK[50,51]. Dimerizační rozhraní zde bylo definováno aminokyselinami R56, T301, N537 a D540 (*Obr 7* na s. 22)[50]. Později byla tato funkčně relevantní na ATP závislá dimerizace potvrzena i pro eukaryotický homolog Hsp70[52]. Nedávno bylo zjištěno, že JDP ko-chaperony jsou nezbytné pro převedení zcela uzavřené konformace SBDβ v ATP vázajícím stavu Hsp70 na konformaci otevřenou, schopnou vazby substrátu, který je na ni posléze z ko-chaperonu přenesen[43]. Jakmile je substrát navázán, spolu s JDP rozsáhle stimulují ATPasovou aktivitu, Hsp70 tak přechází do vysokoafinitního ADP-vázajícího stavu, s uzavřenou SBDβ vázající substrát (*Obr. 5a-I, 5b* na s. 20) a JDP ko-chaperon disociuje

pryč. Pomocí měření nukleární magnetické resonance (NMR) byla odvozena struktura zachycující přechodné uspořádání mezi stavy vázajícími ATP a ADP[53].

Ve vysokoafinitním konformačním uspořádání Hsp70 vázajícím ADP jsou NBD a SBD na sobě zcela nezávislé, navzájem propojené pouze flexibilním linkerem, který je nyní exponován solventu, a namísto interakčního rozhraní NBD-SBDβ/SBDα se utváří nové SBDβ-SBDα se substrátem navázaným do hydrofobní kapsy (*Obr. 3a* na s. 18, kap. 1.2.1). Struktura jednotlivých domén v Hsp70 nyní odpovídá strukturám, které byly popsány v jejich izolovaném stavu a tato ADP-vazebná konformace se strukturně shoduje se stavem, kdy je protein ve stavu bez nukleotidu[54].

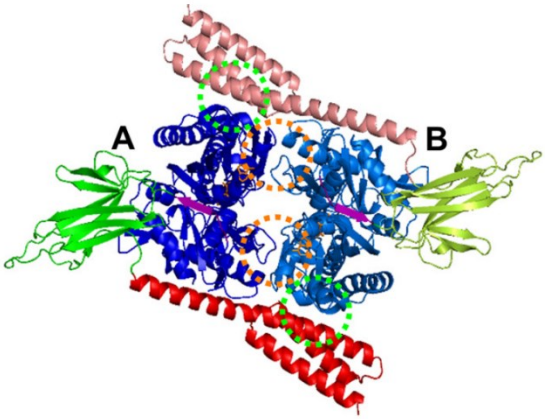

Obrázek 7. *Krystalová struktura antiparalelního dimeru DnaK. V rámci protomerů DnaK, A a B, jsou NBD vyznačeny odstíny modré, flexibilní linker fialovou, SBDβ odstíny zelené a SBDα odstíny červené barvy. Dimerizační rozhraní mezi NBD-NBD' protomeru A a B je vyznačeno oranžovými kruhy, rozhraní mezi NBD-SBDα' zelenými kruhy. (převzato z Sarbeng, 2015)[50]*

Výměna ADP za nový ATP je urychlena za asistence NEF (z angl. Nucleotide exchange factor) faktorů, které interagují zejména se subdoménou IIB NBD, čímž napomáhají otevření nukleotid-vazebné štěrbiny. K tomu může docházet dvěma různými mechanismy – buď NEF pomáhají naklánět subdoménu IIB směrem ven o 13–27° (GrpE, BAG a Hsp110 rodiny NEF), nebo usnadňují její rotaci kolem podélné osy (HspBP1 rodina NEF)[55]. Hsp70 po navázání nové molekuly ATP do aktivního centra v NBD opět nabývá v otevřené konformaci vázající ATP plně uzavřené konformace SBDβ, substrát je aktivně uvolněn a celý cyklus se může opakovat.

Jako antagonista NEF, který naopak stabilizuje ADP-vázající uzavřenou konformaci Hsp70 a prodlužuje tak jeho interakci se substrátem, slouží kofaktor Hip (z angl. Hsp70-interacting protein)[56]. Kromě interakce s ko-chaperony je aktivita Hsp70 dále regulována přítomností posttranslačních modifikací (PTM), zejména fosforylací[57].

1.3 Hsp90

Rodina v buňce všudypřítomných ATP-dependentních molekulárních chaperonů Hsp90 je stejně jako v případě Hsp70 evolučně vysoce konzervovaná, s 50% sekvenční podobností mezi bakteriálním zástupcem Hsp90 z *E. coli,* HtpG (z angl. High temperature protein G), a lidským cytoplasmatickým Hsp90[58]. Tyto 90-kDa molekulární chaperony se kromě archeí[59] nacházejí ve všech biologických říších, od bakterií, které mají nejčastěji jednoho zástupce, až po člověka, jehož genom kóduje celkem pět členů Hsp90 rodiny[27] – jmenovitě cytosolické Hsp90α (HSPC1), Hsp90α-A2 (HSPC2) a Hsp90β (HSPC3), dále Grp94 (z angl. 94-kDa Glucose-regulated protein) (HSPC4) sídlící v ER a mitochondriální TRAP1 (z angl. Tumor necrosis factor receptor-associated protein 1) (HSPC5). Zatímco cytosolická isoforma Hsp90β je exprimována konstitutivně, exprese Hsp90α je inducibilní, zvýšená za stresových podmínek[60].

Ačkoliv delece bakteriálního zástupce HtpG z *E. coli* není pro buňky letální a projevuje se pouze zvýšenou citlivostí na vyšší teploty s následným zhoršením růstu[61], pro jiné bakteriální kmeny je nepostradatelný[62,63], stejně jako v případě eukaryotických orthologů. Hsp90 jsou esenciální pro aktivaci, maturaci nebo degradaci svých strukturně a sekvenčně různorodých substrátů, jimiž jsou zejména kinasy[64], transkripční faktory[64,65], receptory steroidních hormonů[66,67], E3-ubikvitinligasy[64] nebo strukturní cytoskeletální proteiny jako aktin[68] a tubulin[69,70]. Touto cestou jsou chaperony rodiny Hsp90 napojeny na většinu buněčných biochemických procesů a zodpovídají tak za jejich správný průběh[71].

Se vzrůstající komplexitou eukaryotického proteomu vzrůstá i potřeba přesné regulace specifity Hsp90 směrem ke konkrétním substrátům. Rostoucí variabilita funkce Hsp90 je zabezpečena jednak navýšením repertoáru ko-chaperonů od žádného u bakteriálního HtpG nebo mitochondriálního TRAP1 a ER Grp94 až k přibližně 20 různým ko-chaperonům interagujícím s cytosolickými formami Hsp90[72]. Další úrovní regulace je přítomnost PTM, zejména fosforylace, acetylace, methylace, S-nitrosylace, ubikvitinace a SUMOylace, jak na molekulách samostných chaperonů Hsp90, tak i na jejich ko-chaperonech a substrátech[72]. Je známo, že Hsp90 kromě svých ko-chaperonů a substrátů interaguje také přímo i nepřímo s chaperonem Hsp70 a jeho ko-chaperony[73].

1.3.1 Struktura a konformační dynamika Hsp90

Hsp90 chaperony jsou v buňkách přítomny jako homodimery, kde protomery, jež jsou paralelně orientované, sestávají ze tří lineárně uspořádaných domén. N-terminální doména (NTD) váže a hydrolyzuje ATP, tzv. středová doména (MD; z angl. Middle domain) má regulační funkci ve smyslu hydrolýzy ATP a spolu s C-terminální doménou (CTD), která zodpovídá za konstitutivní dimerizaci, se účastní většiny interakcí s ko-chaperony a substráty. Nicméně residua v NTD se rovněž podílí na některých specifických interakcích se substráty Hsp90[58,74]. Mechanismu, jak Hsp90 rozpoznává a váže své substráty, však zatím není příliš detailně porozuměno. Oproti bakteriálnímu Hsp90 a mitochondriálnímu TRAP1, má eukaryotický cytosolický Hsp90 a ER Grp94 NTD propojenou s MD dlouhým nabitým flexibilním linkerem, který kontroluje rotaci NTD[75,76]. Lidský cytosolický Hsp90 má navíc oproti ER Grp94 nebo mitochondriálnímu TRAP1 homologu a bakteriálnímu HtpG ještě CTD zakončenou nestrukturovaným koncem nesoucím sekvenční motiv EEVD (Glu-Glu-Val-Asp) důležitý pro interakci s TPR ko-chaperony[37], stejně jako v případě Hsp70.

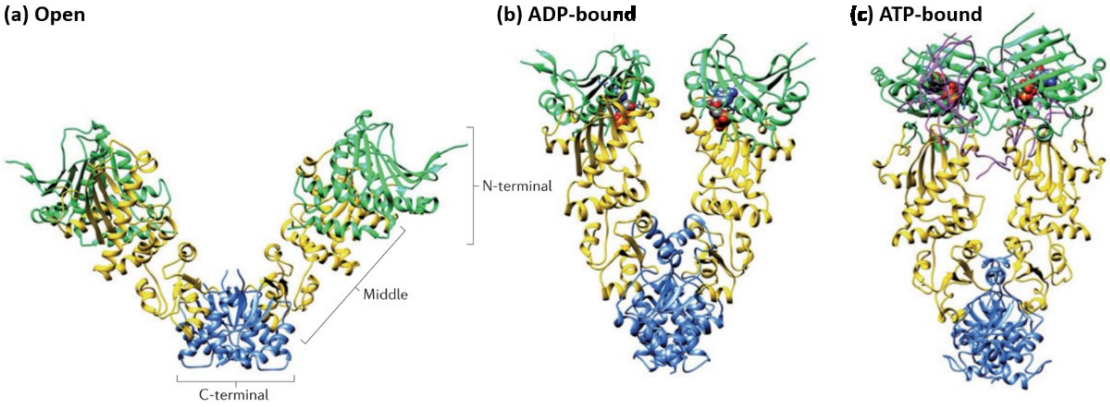

Obrázek 8. *Konformační stavy dimeru Hsp90. (a) Krystalová struktura otevřeného dimeru Hsp90 bez navázaného ATP. C-terminální domény (modrá), které spolu konstitutivně dimerizují jsou následovány MD (žlutá) a NTD (PDB kód: 2IOQ). (b) Krystalová struktura částečně otevřené konformace Hsp90 s navázaným ADP (PDB kód: 2O1V). (c) Krystalová struktura uzavřené konformace Hsp90 s navázaným ATP a substrátem (fialová) do obou NTD, které spolu přechodně dimerizují (PDB kód: 2CG9). (převzato z Saibil, 2013; upraveno)*[78]

Interakce Hsp90 se substráty je podmíněna ATPasovým cyklem, v jehož průběhu podstupuje dimer Hsp90 rozsáhlou sérii konformačních přeměn[77] (*Obr. 8*[78]), čímž poskytuje zcela unikátní rozhraní pro regulacii svými různorodými ko-chaperony, s nimiž po celou dobu chaperonového cyklu postupně přichází do kontaktu. Pokud není v dimeru Hsp90 v každé z NTD vázána molekula ATP, dimer zaujímá tzv. otevřenou konformaci připomínající písmeno „V“, kdy jsou do jeho vnitřního prostoru exponovány

hydrofobní zbytky[79] podílející se na vazbě substrátů (*Obr. 8a* na s. 24). Při vazbě ATP do vazebného místa uvnitř NTD dojde ke změnám v orientaci NTD a MD v rámci protomerů a následně spolu obě protilehlé NTD dimerizují (*Obr. 8c* na s. 24). Zároveň se NTD a MD v rámci protomeru přibližují a rozsáhle interagují, čímž je dosaženo katalyticky aktivní tzv. uzavřené konformace[76,79,80,81,82]. Na základě několika známých struktur se předpokládalo, že hydrolýza obou molekul ATP probíhá naráz a chaperonový cyklus je symetrický[79,81,82] (*Obr. 8b* na s. 24). Nedávná analýza mitochondriálního homologu Hsp90, TRAP1, který na rozdíl od cytosolického Hsp90 nespolupracuje s ko-chaperony, však odhalila, že v ATP-vázajícím stavu vykazuje nesymetrické uspořádání na interakčních rozhraních NTD-MD a MD-CTD jednotlivých protomerů[83], čímž je pravděpodobně simultánní hydrolýze ATP předcházeno[84,85]. Po hydrolýze ATP následuje uvolnění ADP a Hsp90 opět nabývá otevřené konformace.

1.4 Ko-chaperony regulující ATPasový cyklus Hsp70 a Hsp90

Jak již bylo nastíněno výše, k dosažení rozličných specifických funkcí a interakcí s konkrétními substráty napomáhá chaperonům Hsp70 a Hsp90 celá řada ko-chaperonů, které s nimi v průběhu celého ATPasového cyklu přechodně interagují a rozhodují o dalším osudu navázaného substrátu.

Zatímco pro chaperonovou funkci Hsp70 jsou stěžejní dvě hlavní skupiny ko-chaperonů, JDP a NEF, chaperonový cyklus eukaryotického cytosolického Hsp90 je mnohem komplexnější a je regulován součinností s širokým repertoárem ko-chaperonů, z nichž se velká většina váže k C-terminálnímu motivu EEVD skrze svou TPR doménu. Místa pro interakci s ko-chaperony se však nacházejí na všech třech funkčních doménách Hsp90[86]. Bakteriální HtpG, mitochondriální TRAP1 nebo ER Grp94 naopak pro svou regulaci ko-chaperony vůbec nevyužívají. Interakce s ko-chaperony jsou velmi rozmanité a některé striktně vážou pouze určitý konformační stav Hsp90, což umožňuje přesné načasování jednotlivých kroků chaperonového cyklu podle požadavků konkrétního substrátu[87]. Kompletní seznam všech známých ko-chaperonů a substrátů Hsp90 je průběžně sledován a aktualizován Picardovou laboratoří (www.picard.ch/downloads/Hsp90interactors.pdf; poslední přístup 23.9.2020).

Dobře zmapovanou skupinou ko-chaperonů Hsp90 jsou ko-chaperony podílející se na aktivaci steroidních receptorů nebo aktivaci kinas[72]. Chaperonový cyklus, který se podílí na aktivaci steroidních receptorů je zahájen vazbou ko-chaperonu Hop

(z angl. Hsp70/90 organizing protein; Sti1 (z angl. Stress-inducible protein 1) v kvasinkách) na dimer Hsp90, čímž inhibuje jeho N-terminální dimerizaci[88] a usnadňuje tak navázání substrátu do vnitřního prostoru Hsp90 dimeru[89]. Následně je za asistence plejády dalších ko-chaperonů, jmenovitě Fkbp51, Fkbp52, Cyp40, p23 a Pp5[90], které napomohou steroidnímu receptoru získat správnou konformaci, umožněna jeho interakce s odpovídajícím hormonem, vzniklý substrátový komplex je z chaperonu uvolněn a stává se transkripčně aktivní. V případě chaperonového cyklu proteinkinas se ko-chaperon Cdc37 váže nejdříve k proteinkinase a následně usnadňuje její asociaci s dimerem Hsp90[64,91]. Přesný mechanismus toho, jak dochází k aktivaci kinasy není znám, ale velmi pravděpodobnou se zdá hypotéza, že Hsp90 spolu s Cdc37 napomáhají kinasu stabilizovat proti degradaci během procesu výměny hydrolyzovaného ATP z kinasy za nové[72]. Jedním z nejlépe zmapovaných ko-chaperonů Hsp90 je Aha1 (z angl. Activator of Hsp90 ATPase protein 1), který funguje jako vysoce účinný aktivátor ATPasové aktivity Hsp90 tím, že mechanicky usnadňuje jeho N-terminální dimerizaci[92].

Zvýšení bazální ATPasové aktivity Hsp90 bylo pozorováno i v souvislosti s efektem tzv. makromolekulárního crowdingu, kdy je *in vitro* simulováno makromolekulami nabohacené vnitrobuněčné prostředí, které uvnitř buňky odpovídá přibližné koncentraci makromolekul 300–400 $mg.ml^{-1}$. Tato aktivace probíhá odlišným mechanismem než aktivace prostřednictvím ko-chaperonů a jsou navzájem nezávislé[93]. Na základě tohoto pozorování jsme pomocí vodík/deuteriové výměny v kombinaci s hmotnostní spektrometrií v přítomnosti polyethylenglykolu o koncentraci 100 $mg.ml^{-1}$ testovali hypotézu, zda jedna z nejlépe strukturně charakterizovaných interakcí Hsp90 s ko-chaperonem Aha1 nebude v tomto arteficiálním *in vivo* prostředí probíhat odlišným mechanismem. Výstup byl však srovnatelný s již dříve získanými výsledky[94,95,96], proto jsme tuto kapitolu uzavřeli.

1.4.1 TPR ko-chaperony regulující komunikaci mezi Hsp70/Hsp90

Velmi důležitou skupinu proteinů ve smyslu regulace chaperonové sítě představují TPR ko-chaperony, které u savců tvoří přibližně celou jednu třetinu chaperonového systému[97] a stejně jako ostatní ko-chaperony napomáhají diverzifikovat jeho funkce. Podílejí se zejména na procesu sbalování proteinů, kontrole kvality sbalení a případné degradaci, nebo translokaci proteinů přes membrány[98,99]. TPR domény charakteristické pro tyto proteiny sestávají z 34-aminokyselinových nepříliš konzervovaných amfipatických motivů struktury antiparalelního α-helixu (*Obr. 9a*), které se 3–16× opakují a tvoří superšroubovici[99,100] (*Obr. 9b*). TPR ko-chaperony interagující s cytosolickými eukaryotickými Hsp70 a Hsp90 mají své TPR domény tvořeny zpravidla třemi antiparalelními α-helixy, mezi nimiž vzniká amfipatický žlábek uzpůsobený pro vazbu proteinového ligandu, jímž je v tomto případě konzervovaný C-terminální sekvenční motiv EEVD.

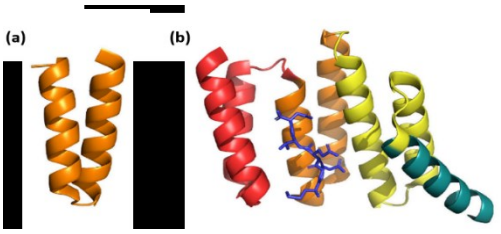

Obrázek 9. *Znázornění struktury TPR motivu. (a) 34-aminokyselinový antiparalelní helix. (b) Krystalová struktura TPR domény ko-chaperonu HOP tvořená třemi TPR motivy (červená, oranžová, žlutá), které koordinují substrát (modrý). (PDB kód: 1ELR) (převzato z Graham, 2019)*[98]

Vazebná selektivita ko-chaperonů, ve smyslu zda upřednostní vazbu k EEVD motivu Hsp70 nebo Hsp90, je vedle sítě elektrostatických interakcí mezi elektronegativním EEVD motivem a elektropozitivním povrchem TPR domény definována dodatečnými hydrofobními kontakty s aminokyselinovými zbytky lokalizovanými bezprostředně N-terminálně od EEVD motivu (Hsp70-***I***EEVD, Hsp90-***M***EEVD)[37,101]. Většina vazebné afinity TPR ko-chaperonů vůči Hsp70 a Hsp90 chaperonům však sídlí právě v síti elektrostatických kontaktů mezi pěti konzervovanými pozitivně nabitými aminokyselinami TPR domény, které koordinují dvě záporně nabité karboxylové skupiny C-terminálního aspartátu[37,100] (*Obr. 10* na s. 28). Tyto konzervované TPR domény slouží ke specifickým interakcím s konkrétním chaperonem, ale o tom, jakému osudu bude vystaven substrát zpracovávaný chaperonovým systémem, rozhodují zejména další funkční domény přítomné ve struktuře TPR ko-chaperonů a v neposlední řadě také PTM, ať už samotných TPR ko-chaperonů[102], chaperonů[37,103] nebo substrátů.

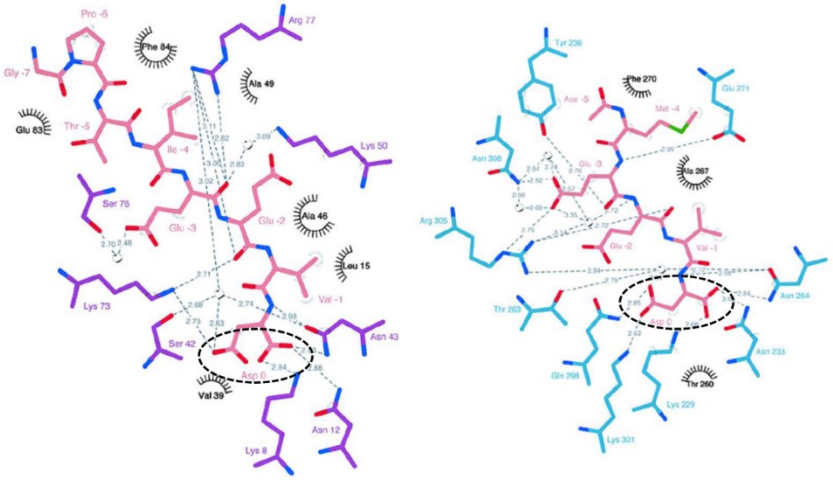

***Obrázek 10**. Schematické znázornění sítě elektrostatických a hydrofobních kontaktů mezi aminokyselinovými zbytky TPR1 a TPR2A domény ko-chaperonu Hop a substrátem. Černě jsou zvýrazněny záporně nabité karboxylové skupiny C-terminálních Asp z EEVD motivů Hsp70 a Hsp90, které jsou koordinovány pěti konzervovanými pozitivně nabitými aminokyselinami TPR domény. (převzato z Scheufler, 2000)*[100]

1.4.1.1 Ko-chaperon Hop

K nejlépe prostudovaným TPR ko-chaperonům se řadí Hop, který díky své flexibilitě zprostředkovává fyzické propojení mezi C-terminálními motivy EEVD Hsp70 a Hsp90 a usnadňuje tak přenos částečně sbaleného substrátu z Hsp70 na Hsp90, kde je dokončena jeho aktivace, pro niž je nezbytná přítomnost na aspartát a prolin bohatých domén DP1 (ve struktuře Hop za doménou TPR1) a DP2 (ve struktuře Hop za doménou TPR2B)[104] (*Obr. 11* na s. 29). N-terminální doména TPR1 ko-chaperonu Hop, která interaguje s Hsp70, je propojena dlouhým flexibilním linkerem s C-terminálním modulem sestávajícím z domén TPR2A a TPR2B[89]. Zatímco doména TPR2A interaguje s C-koncem monomeru Hsp90, úloha TPR2B nebyla dosud plně specifikována. Byla však pozorována její interakce jak s MD Hsp90, tak s Hsp70[89,104] a pro Hsp70 byly navíc pozorovány i dodatečné přímé kontakty s Hsp90[105]. K čistě přímému kontaktu mezi Hsp70 a Hsp90 chaperony bez účasti ko-chaperonů pak dochází v případě prokaryot, které ko-chaperony postrádají, a rovněž i v kvasinkách[73]. Aby mohl být substrát na Hsp90 přenesen, je nutné, aby se chaperon nacházel ve své otevřené konformaci. To je zajištěno interakcí Hop s 24 N-terminálními aminokyselinami NTD Hsp90, kdy ko-chaperon působí jako nekompetitivní inhibitor ATPasové aktivity a zabraňuje tak jeho N-terminální dimerizaci[106]. Zvýšená exprese ko-chaperonu Hop bývá pozorována v rakovinných buňkách, kde byla zároveň potvrzena i zvýšená přítomnost fosforylovaných chaperonů

Hsp70 a Hsp90 a prokázáno, že jejich C-terminální fosforylace zvyšuje afinitu k Hop ko-chaperonu, čímž je výrazně podpořena buněčná proliferace[103].

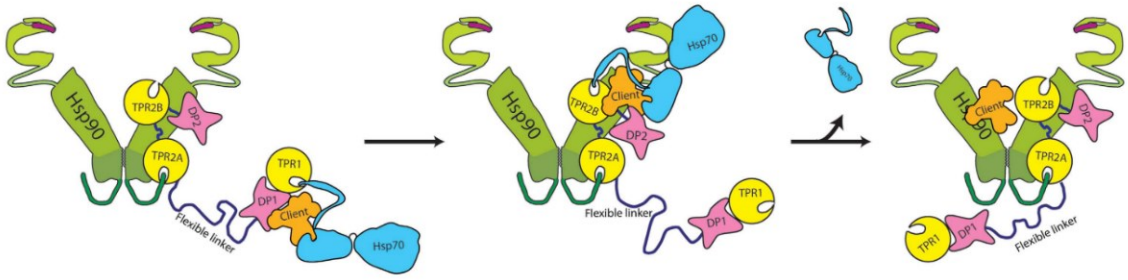

Obrázek 11. *Přenos substrátu z Hsp70 na Hsp90 asistovaný ko-chapronem Hop/Sti1. Hop/Sti1 sestávající z domén TPR1-DP1-flexibilního linkeru-TPR2A-TPR2B-DP2 tvoří mezičlánek mezi Hsp90, k jehož C-konci se váže skrze svou TPR2A doménu, a Hsp70, jejž váže skrze svou TPR1 doménu. Jejich fyzickým přiblížením Hop usnadňuje přenos substrátu z Hsp70 k jeho dalšímu zpracování za asistence Hsp90. (převzato z Schmid, 2012)*[104]

1.4.1.2 Ko-chaperon CHIP

V souvislosti se zvýšenou úrovní fosforylace uvnitř rakovinných buněk bylo dále pozorováno, že naopak v případě ko-chaperonu CHIP (z angl. Carboxyl terminus of Hsp70-interacting protein) dochází vlivem této PTM k výraznému poklesu afinity mezi ním a chaperony Hsp70 a Hsp90[37,103] a zároveň v tomto prostředí dochází k výraznému snížení úrovně jeho exprese[107]. Kromě jediné N-terminální TPR domény je CHIP vybaven tzv. U-box doménou s motivem zinkového prstu, která mu propůjčuje schopnost fungovat jako E3-ubikvitinligasa kooperující s enzymy E2-ubikvitinační kaskády[108] a řídící ubikvitinaci nesprávně sbalených substrátů Hsp70. Touto cestou CHIP zprostředkovává napojení chaperonového systému na UPS[109,110]. C-terminální U-box doména, která je zapojena

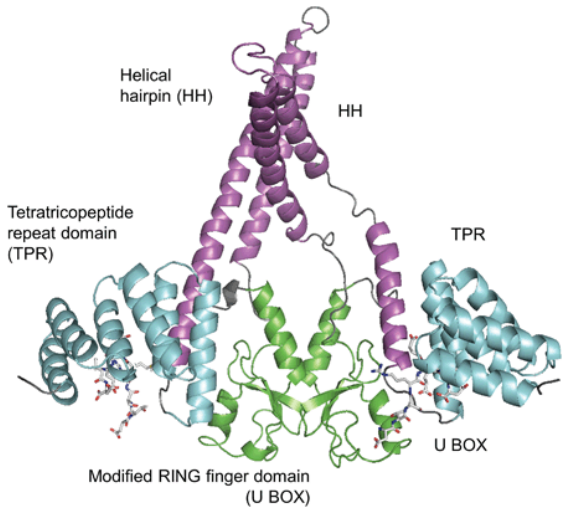

Obrázek 12. *Krystalová struktura asymetrického dimeru CHIP. N-terminální TPR doména (modrá) obsahující trojí repetici TPR motivu koordinuje C-terminální motiv peptidu Hsp90. Na ni plynule navazuje dynamický extendovaný α-helix (fialová) tvořící strukturu vlásenky a podílející se na dimerizaci. Na C-konci je struktura zakončena U-box doménou (zelená), která ko-chaperonu zajišťuje E3-ubikvitinligasovou aktivitu a je zodpovědná za dimerizaci. (PDB kód: 2C2L). (převzato z Edkins, 2015)*[110]

při paralelní dimerizaci s dalším protomerem, je s TPR doménou propojená skrze dlouhý extendovaný α-helikální region tvořící strukturu vlásenky. Ta rovněž přispívá k dimerizaci a pomocí krystalizace byla zachycena ve dvou různých konformacích[111,112], což odkazuje na flexibilitu a dynamické chování ko-chaperonu CHIP v roztoku[113,114]. Organizace jednotlivých domén ko-chaperonu CHIP je znázorněna pomocí krystalové struktury v *Obr. 12* na s. 29.

1.4.1.3 Ko-chaperon Tomm34

Dalším ko-chaperonem interagujícím jak s Hsp70, tak Hsp90 chaperonem je Tomm34 (z angl. 34-kDa Translocase of outer mitochondrial membrane)[115,116], který se účastní regulace transportu mitochondriálních preproteinů v cytosolu a jejich následného importu do mitochondrií pravděpodobně tak, že je napomáhá cyklickou interakcí mezi Hsp70 a Hsp90 udržovat ve stavu kompetentním pro translokaci[115,117] (*Obr. 13*).

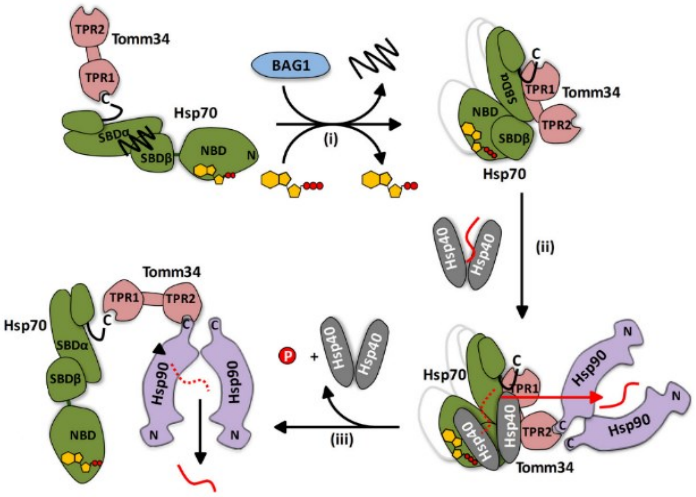

Obrázek 13. *Navrhovaný model mechanismu, jímž ko-chaperon Tomm34 zprostředkovává přenos substrátu z Hsp70 na Hsp90 v procesu cytoplasmatického transportu mitochondriálních proteinů. (i) Tomm34 skrze svou TPR1 doménu kontaktuje C-terminální motiv IEEVD Hsp70-ADP s navázaným substrátem. NEF BAG1 usnadní výměnu ADP za nové ATP a substrát je aktivně uvolněn. Hsp70 následně přechází do otevřené nízkoafinitní konformace a tvoří ATP-dependentní dimer s nímž Tomm34 rozsáhleji interaguje, jednak skrze TPR1 a dále přes blíže nespecifikované kontakty v oblasti flexibilního linkeru. (ii) Vazba Tomm34 k dimeru Hsp70-ATP interferuje s přenosem nového prekurzoru z dimeru ko-chaperonu Hsp40 do SBDβ Hsp70-ATP. Prekurzor je místo toho přenesen na Hsp90, jehož fyzické přiblížení k Hsp70 je zprostředkováno skrze kontakt C-terminálního motivu MEEVD s TPR2 doménou Tomm34. Zároveň vlivem hydrolýzy ATP usnadněnou Hsp40 přechází Hsp70 na ADP-vázající uzavřenou konformaci a Hsp40 disociuje pryč. (iii) Protože Hsp90 rozpoznává pouze substráty jejichž stav je blízký nativní konformaci, z Hsp40 přenesený preprotein jím není efektivně zpracován, je uvolněn a částečně sbalený prekurzor podstupuje další cyklus. Předpokládá se, že tímto přenosem mezi Hsp70-Hsp90 jsou preproteiny udržovány v částečně sbaleném stavu kompetentním pro transport, neboť je tak aktivně předcházeno jejich agregaci dokud nedosáhnou cílového kompartmentu. (převzato z Ďurech, 2016; upraveno)*[117]

Tomm34 sestává z N-terminální domény TPR1 a C-terminální TPR2, které jsou propojené dlouhým nestrukturovaným flexibilním linkerem. Zatímco doména TPR2 váže motiv MEEVD Hsp90 a vyžaduje, aby se chaperon nacházel v otevřené konformaci bez navázaného ATP, vazba k Hsp70 je komplexnější a vyžaduje jak elektrostatické interakce mezi C-terminálním motivem IEEVD Hsp70 a doménou TPR1, tak dodatečné hydrofobní kontakty mezi flexibilním linkerem ko-chaperonu a blíže nespecifikovanou částí Hsp70 v jeho ATP-vázajícím stavu[116,117].

1.5 NQO1

Dalším velmi důležitým článkem v procesu udržování proteostasy je všudypřítomný převážně cytoplasmatický homodimerní flavoproteinový enzym NQO1 katalyzující dvouelektronovou redukci chinonů, nitroaromátů, železitých solí a superoxidových radikálů, čímž hraje ústřední roli v procesech detoxifikace xenobiotik a udržování redoxní rovnováhy v buňce[21,118]. Katalytický mechanismus NQO1 zahrnuje dvoukrokovou reakci, která probíhá tzv. "ping-pong" mechanismem. Během první, velmi rychlé a na nikotinamidadenindinukleotid(fosfát)u (NAD(P)H) závislé redukující poloreakce se na holoenzym váže NAD(P)H, který redukuje flavinadenindinukleotid (FAD) v jednom ze dvou aktivních míst na $FADH_2$ a uvolňuje se $NAD(P)^+$. Redukovaný $FADH_2$ pak ve druhé pomalejší oxidativní poloreakci redukuje substrát navázaný v aktivním místě a holoenzym se regeneruje[21,119] (*Obr. 14*).

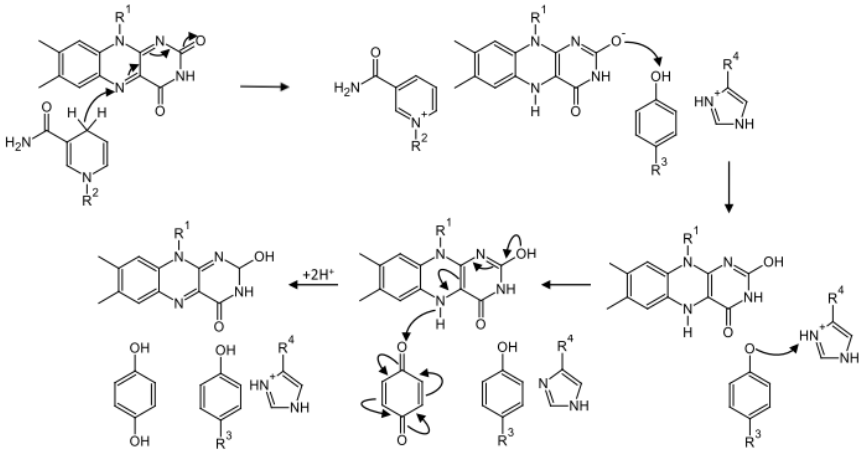

Obrázek 14. *Katalytický mechanismus NQO1. V první fázi je isoalloxazinový skelet FAD redukován kofaktorem NAD(P)H a získá záporný náboj, který je následně neutralizován přenosem H^+ z Tyr155. Ten je kompenzovaný His161. Redukce substrátu reprezentovaného chinonem je uskutečněna opačným tokem elektronů v isoalloxazinovém skeletu $FADH_2$ s využitím dvou H^+ z roztoku za vzniku ubichinonu. Ve schématu je předpokládáno, že NAD(P)H bezprostředně po redukci FAD disociuje pryč, zároveň jsou vykresleny pouze katalyticky aktivní části molekul a jejich zbytek je znázorněn jako R^{1-4}. (převzato z Beaver, 2019; upraveno)[21]*

Exprese NQO1 bývá zvýšena v odpovědi na různé druhy buněčného stresu skrze několik mechanismů zahrnujících transkripční faktory Nrf2 (z angl. Nuclear factor erythroid 2-related factor 2) nebo AhR (z angl. Aryl hydrocarbon receptor)[120,121,122]. Zvýšená hladina NQO1 je rovněž spojována s negativní prognózou v mnoha typech nádorů, pro něž je charakteristické hypoxické prostředí s vysokou mírou oxidativního stresu.

Bylo pozorováno, že NQO1 má i neenzymatickou funkci, kdy působí jako chaperon stabilizující celou řadu transkripčních faktorů jako je p53, p73α[123], HIF-1α[20] nebo protein Tat zahrnutý v infekci virem HIV[124] a tento stabilizační efekt může být zvrácen kumarinovými deriváty, z nichž nejlépe charakterizovaný biskumarin dikumarol je nejdéle známým kompetitivním inhibitorem NQO1 vázajícím se do jeho aktivního centra, kde blokuje přístup NAD(P)H[125,126,127].

1.5.1 Struktura a katalytický cyklus NQO1

Funkční jednotku NQO1 tvoří homodimer jehož dvě aktivní místa se nacházejí na rozhraní podjednotek a jsou tvořena aminokyselinovými zbytky z obou proteinových řetězců[128]. Každá 31-kDa podjednotka sestává z N-terminální domény (NTD) zahrnující aminokyselinové zbytky 1–224 a pevně vázající jednu molekulu FAD a z C-terminální domény (CTD) tvořené aminokyselinami 225–274 přispívajícími ke stabilizaci dimeru a vazbě koenzymu NAD(P)H a substrátů[128] (*Obr. 15*)

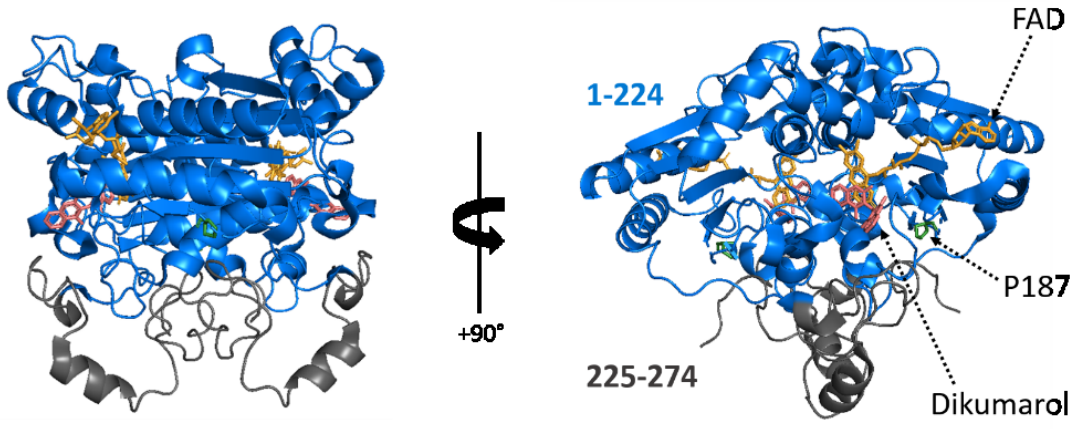

Obrázek 15. *Krystalová struktura dimeru NQO1 s navázaným kofaktorem FAD a kompetitivním inhibitorem dikumarolem. N-terminální doména (modrá) sestávající z aminokyselin 1-224 obsahuje vazebná místa pro FAD (žlutá) a dikumarol (červená). Extendovaná C-terminální doména (šedá) je tvořená zbytky 225-274. Zeleně je vyznačena pozice P187, jehož mutace P187S, která je nejabundantnějším polymorfismem, způsobuje výraznou destabilizaci struktury NQO1. (PDB kód: 2F1O) (vytvořeno v PyMOLu)*

Z funkčního i strukturního hlediska lze definovat různé ligační stavy NQO1. Apoforma NQO1 bez navázaných kofaktorů ($NQO1_{APO}$) existuje ve formě expandovaného konformačně flexibilního dimeru[21,129], kvůli čemuž není pro tento stav k dispozici žádná vysoce rozlišená struktura. Zejména vysoce flexibilní CTD funguje jako iniciační místo pro rychlou degradaci $NQO1_{APO}$ prostřednictvím UPS[130,131]. Vazba FAD pak spouští rozsáhlou konformační změnu, kdy se NQO1 s navázaným kofaktorem ($NQO1_{HOLO}$) stává kompaktnějším s vysoce uspořádanými prvky sekundární struktury a celkově dochází k poklesu flexibility dimeru, což bylo potvrzeno rentgenostrukturní analýzou, NMR a využitím limitované proteolýzy[132,133], a činí ho intracelulárně stabilním[123,134]. Krystalová struktura byla obdržena i pro $NQO1_{HOLO}$ formu s navázaným dikumarolem ($NQO1_{DIC}$)[127]. Pro tento stav je popsán další nárůst v uspořádanosti sekundární struktury, zvýšení jeho termální stability a resistence NTD a CTD vůči proteolýze[129]. Ze strukturního hlediska však není jasné, jakým mechanismem vazba dikumarolu snižuje vazebnou afinitu k interakčním partnerům $NQO1_{HOLO}$, kteří tak nejsou stabilizováni před degradací UPS.

Pro NQO1 byly doposud blíže charakterizovány pouze tři přirozeně se vyskytující mutace, které jsou spojené se zvýšeným rizikem výskytu rakoviny – P187S (NQO1*2), R139W (NQO1*3) a K240Q. Alelická frekvence polymorfismu p.P187S je zhruba 25 %, p.R139W 3 % populace[135]. Přestože je aminokyselinový zbytek P187 zanořen hluboko uvnitř struktury v blízkosti dimerizačního rozhraní (*Obr. 15* na s. 32), projevuje se tato mutace změnou dynamiky NTD v oblasti kolem vazebného místa pro FAD a zároveň výraznou destabilizací CTD[125,136], což poukazuje na přítomnost alosterické regulace uvnitř NQO1. Takto destabilizovaná forma je velmi rychle proteasomálně degradována.

Funkce a stabilita NQO1 může být rovněž modulována různými PTM. Fosforylace aminokyselinového zbytku T128 kinasou Akt ústí v polyubikvitinaci následovanou proteasomální degradací[137]. NQO1 nesoucí fosfomimetickou mutaci na S82 vykazuje sníženou afinitu vůči FAD s následnou destabilizací proteinu[130].

1.6 Hsp70, Hsp90, NQO1 a jimi zprostředkované základní proteostatické mechanismy

Kromě spolupráce s ko-chaperony, které napomáhají řídit chaperonový cyklus ve prospěch správného sbalení a aktivace substrátů, chaperony spolupracují s ko-chaperony kontrolujícími proteostasu. Je-li protein nesprávně sbalen a náchylný k agregaci nebo je vyžadována přesná časová regulace jeho aktivity (často jde o transkripční faktory nebo proteiny signalizačních kaskád[138]), napomohou komplexy chaperonů a ko-chaperonů buňce k jeho degradaci. Ta může být uskutečněna dvěma hlavními cestami, buď spoluprací s UPS nebo s využitím autofagie. Dalším důležitým dějem z pohledu buněčné proteostasy je dosažení správného buněčného kompartmentu daným proteinem, což je zajišťováno kooperací chaperonů s dalšími specializovanými ko-chaperony, které rozeznávají signalizační sekvenci a napomáhají protein udržet ve stavu kompetentním pro transport do konkrétní organely. Neméně důležitým aspektem z pohledu proteostasy je i homeostasa kyslíku, kdy jakákoli nerovnováha může nepříznivě ovlivnit stav buněčného proteomu.

1.6.1 Chaperonem asistovaná degradace prostřednictvím UPS

Chaperonem asistovaná degradace zprostředkovaná UPS (CUPS; z angl. Chaperone-assisted ubiquitin-proteasome system)[110,139], při níž je na chaperon navázaný substrát označen jednou nebo více molekulami ubikvitinu, se týká zejména chaperonů Hsp70 a Hsp90, které skrze svůj C-terminální motiv EEVD interagují s TPR doménou E3-ubikvitinligasy CHIP[110]. Ta inhibuje ATPasový cyklus Hsp70 a blokuje jeho schopnost sbalovat proteinový řetězec[140]. Navíc je prostřednictvím kooperace její U-box domény s E2-konjugačními enzymy z proteinové rodiny UBC4/5[141,142]

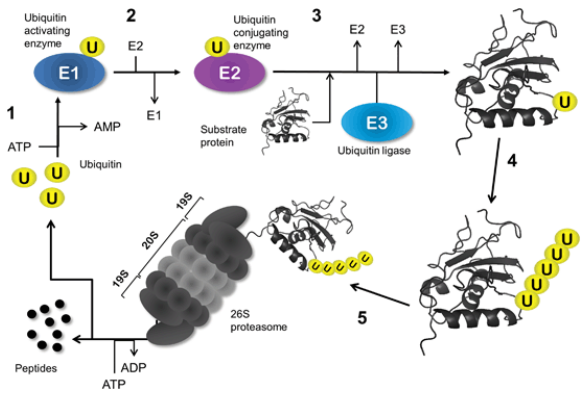

Obrázek 16. *Degradace proteinového substrátu skrze UPS. (1) Proces je zahájen aktivací ubikvitinu konjugací skrze thioesterovou vazbu s ubikvitin-aktivačním enzymem E1. (2) Aktivovaný ubikvitin je přenesen na ubikvitin-konjugační enzym E2, (3) který následně tvoří komplex s ubikvitinligasou E3 a substrátem. E3-ligasa přenese ubikvitin z E2 a připojí ho přes Lys k substrátu určenému k degradaci. (4) Kroky (1–3) se několikrát opakují za vzniku polyubikvitinového řetězce propojeného skrze Lys48, (5) ty slouží jako signál pro přenos substrátu do 26S proteasomu. (převzato z Edkins, 2015; upraveno)[110]*

na substrát kovalentně navázán ubikvitinový řetězec propojený skrze Lys48, což je signál charakteristický pro degradaci zprostředkovanou UPS[143] (*Obr. 16* na s. 34). Uvolnění takto označeného substrátu je pak iniciováno interakcí NBD Hsp70 s ko-chaperonem BAG1, který má kromě C-terminální NBD vázající BAG domény s NEF aktivitou zodpovědnou za výměnu ADP za nové ATP, i tzv. ubikvitinu podobnou N-terminální doménu (Ubl; z angl. Ubiquitin-like domain), jež interaguje s 26S proteasomem[144]. Pro BAG1 byla popsána existence ternárního komplexu Hsp70/BAG1/CHIP (*Obr. 17*), kdy je polyubikvitinovaný substrát po uvolnění z Hsp70 navázán na BAG1[145], který je ligasou CHIP rovněž polyubikvitinován[146]. V tomto případě jde však o propojení skrze Lys11, které slouží jako signál pro interakci BAG1 s proteasomem, pro nějž je tak prostorově usnadněna jeho interakce se substrátem určeným k degradaci.

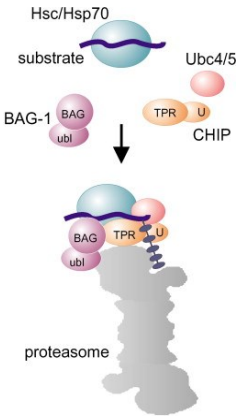

Obrázek 17. *Tvorba ternárního komplexu mezi Hsp70 a ko-chaperony BAG1 a CHIP a jeho interakce s 26S proteasomem. (převzato z Demand, 2001)[145]*

K ubikvitin-dependentní/independentní degradaci proteinů dochází i vlivem nízké hladiny exprese nebo nestability chaperonu NQO1, který působí stabilizačně na řadu svých interakčních partnerů, jimiž jsou např. klíčové regulační proteiny p53 a p73α[123], transkripční faktor HIF-1α[20] nebo protoonkoprotein c-Fos[147].

1.6.2 Autofagie

Ve stárnoucích buňkách, kde se zvyšuje poměr BAG3/BAG1[148], snižuje se hladina CHIP[149,150] a celkově klesá proteasomální aktivita[151], mohou být agregované, špatně sbalené či modifikované proteiny eliminovány prostřednictvím lysozomální (vakuolární u kvasinek a rostlin) autofagie. Tu lze klasifikovat podle mechanismu do tří skupin – chaperonem zprostředkovaná autofagie (CMA; z angl. Chaperone-mediated autophagy), chaperonem asistovaná endosomální mikroautofagie (CAEMI) a chaperonem asistovaná makroautofagie (CAMA) (*Obr. 18* na s. 36).

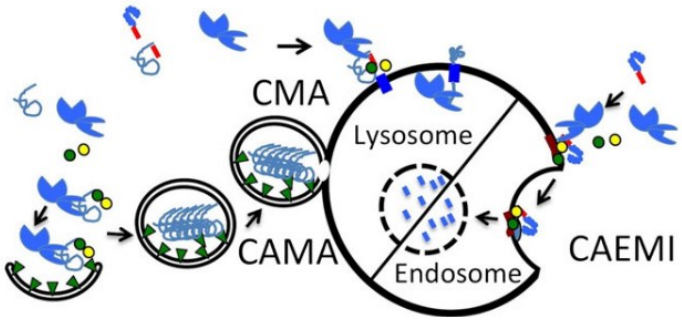

Obrázek 18. *Znázornění tří známých mechanismů autofagie – CMA, CAEMI a CAMA. Mechanismy autofagie zprostředkované Hsp70 probíhají za asistence chaperonů a ko-chaperonů (zelené a žluté kruhy), jejich konkrétní příspěvek k těmto procesům je však doposud ve velké míře neznámý. Červeně je vyznačen C-terminální sekvenční motiv KFERQ, zelený trojúhelník symbolizuje LC3. (převzato z Fernández-Fernández, 2017; upraveno)*[26]

CMA zahrnuje rozpoznání substrátů nesoucích C-terminální motiv KFERQ (Lys-Phe-Glu-Arg-Gln) chaperonem Hsc70[152]. Substrát je transportován k lysozomu, kde je navázán k monomernímu receptoru LAMP2A (z angl. Lysosome-associated membrane protein type 2A)[153]. Tato vazba následně indukuje tvorbu translokačního komplexu sestávajícího z několika kopií LAMP2A a jiných, dosud neidentifikovaných proteinů[154]. Skrze tento komplex je substrát za pomoci lysozomální formy Hsp70 a Hsp90 translokován do lumen lysozomu[155]. S CMA jsou spojovány i ko-chaperony Hsp40, Hop, Hip a BAG1, přesná povaha těchto interakcí však dosud nebyla plně objasněna[26].

V případě CAEMI dochází ke vchlípení lysozomální membrány nebo pozdního endosomu s cytoplasmatickým obsahem určeným k hydrolýze do lysozomálního lumen[156]. Stejně jako u CMA zde Hsc70 isoforma rovněž specificky rozpoznává KFERQ motiv.

Pro CAMA je cytoplasmatický substrát nejdříve identifikován rozpustnými receptory a adaptorovými proteiny v cytoplasmě a následně uzavřen uvnitř autofagosomu, dvojitou membránou ohraničené vesikuly, která pak přímo fúzuje s lysozomem[157]. Mechanismus rozpoznávání substrátu může být jak nespecifický, tak specifický[158]. Hsp70 interaguje s NEF BAG3, skrze nějž tvoří ternární komplex s tzv. malým heat-shock proteinem HspB8[159], a zároveň svým C-terminálním EEVD motivem interaguje s E3-ubikvitinligasou CHIP[158]. Tento komplex s polyubikvitinovaným substrátem je rozpoznán ubikvitin-vázajícím proteinem p62/SQSTM1, který se zároveň váže k LC3, a jeho lipidovaná forma LC3-II posléze asociuje s inicializační membránou autofagosomu, čímž je zahájeno uzavření membrány a vzniklý autofagosom může fúzovat s lysozomem[26].

1.6.3 Chaperony asistovaný transport proteinů

Proteiny určené pro sekreci ven z buňky a inkorporaci do endomembránových kompartmentů nebo plasmatické membrány prochází přes ER, ve kterém nabývají požadované konformace. Tam jsou translokovány pomocí trimerního komplexu Sec61 poté, co sem byly v drtivé většině vnořeny ko-translačně po usednutí ribozomu na receptor vázající tzv. SRP (z angl. Signal recognition particle) ribonukleoproteinový komplex navázaný na ribozom. Tato interakce je zprostředkována rozpoznáním N-terminální sekvence nově syntetizovaného proteinu signalizující jeho předurčení pro transport do ER[160]. Díky této ko-translační translokaci je eliminována nutnost doprovázet nově vznikající proteinový řetězec chaperonovými komplexy, které by zabraňovaly jeho agregaci. K translokaci skrze Sec61 translokon může docházet i posttranslačně, kdy je protein v cytoplasmě udržován ve stavu kompetentním pro transport za chaperonové asistence[161] (*Obr. 19*)

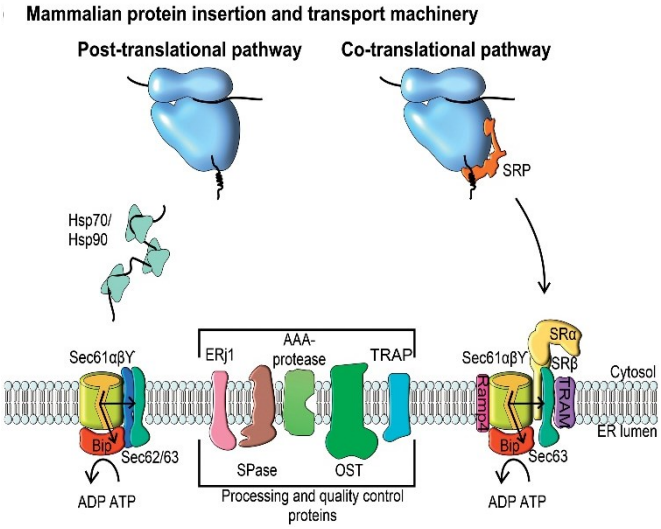

Obrázek 19. *Translokace proteinů do ER skrze Sec61 transokon. Dvě alternativní cesty transportu proteinů do ER – vpravo ko-translační a vlevo posttranslační, kdy je nutno eliminovat nespecifické hydrofobní interakce nově syntetizovaného proteinu za asistence ko-chaperonů Hsp70/Hsp90. (převzato z Denks, 2014)[161]*

Děje se tak i u jádrem kódovaných proteinů, které obsahují signalizační sekvenci pro transport do mitochondrie, kam jsou posttranslačně translokovány poté, co proběhla jejich syntéza na ribozomu uvnitř cytoplasmy. Od samého začátku je translace selektivně asistována chaperonovými komplexy. Nejabundantnější jsou zde chaperony Hsp70, Hsp90 a ko-chaperon Hsp40[162], přičemž je předpokládána asociace i s dalšími ko-chaperony jako např. Tomm34[115], které napomáhají udržovat proteinový řetězec neagregovaný a ve stavu kompetentním pro transport skrze translokační komplex vnější mitochondriální membrány TOM (z angl. Translocase of outer mitochondrial membrane). Ten sestává ze dvou až tří translokačních pórů, které jsou tvořeny proteinem Tom40 s charakteristickou strukturou β-barelu, receptorem Tom22 a malými stabilizačními a kontrolními podjednotkami Tom5–7. S TOM translokonem asociují dva další receptory

Tom20 a Tom70, které se preferenčně vážou k substrátům s různou signální sekvencí, ale jejich funkce je vzájemně redundantní[163]. Jak Tom20, tak Tom70 nesou TPR motivy, jejichž prostřednictvím mohou interagovat s C-terminálním motivem EEVD Hsp70 a Hsp90 chaperonů, od nichž převezmou substrát, který je pak přes Tom22 zacílen přímo do Tom40 a odtud dál putuje do konkrétního mitochondriálního kompartmentu[164].

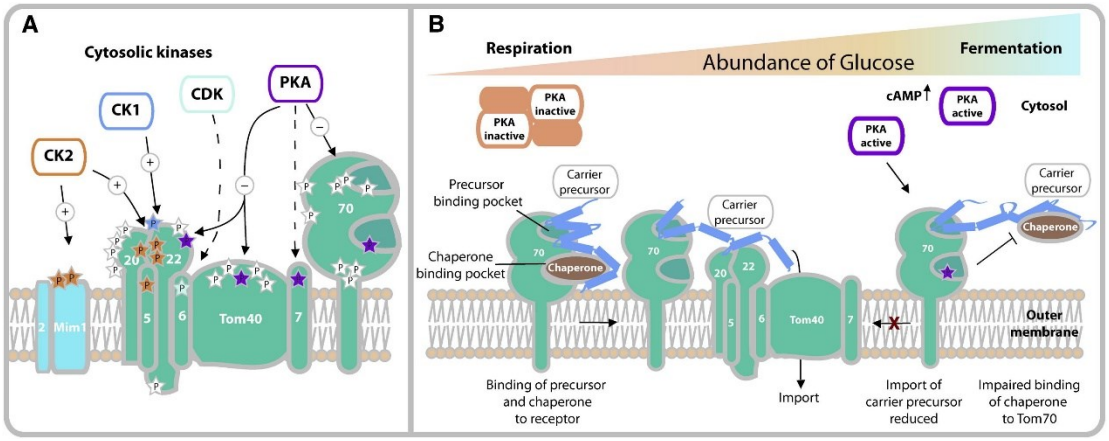

Obrázek 20. *Regulace mitochondriálního translokačního komplexu TOM cytoplasmatickými kinasami. (A) Všechny podjednotky translokačního komplexu vnější mitochondriální membrány TOM jsou fosforylovány cytoplasmatickými kinasami (CK1/2 – kaseinkinasa 1/2; CDK – cyklin-dependentní kinasa; PKA – cAMP dependentní proteinkinasa A) (fosforylované aminokyseliny jsou schematicky znázorněny hvězdičkami), které buď stimulují nebo inhibují biogenezi kritických částí translokační mašinerie. (B) Za fermentačních metabolických podmínek, kdy je snížená potřeba mitochondriálních proteinů, vzrůstá hladina cAMP, která aktivuje PKA. Ta selektivně fosforyluje Ser receptoru Tom70 v blízkosti vazebného místa pro chaperony Hsp70 a Hsp90, které sem jinak přinášejí hydrofobní prekurzory. Dále může fosforylovat Tom40 podjednotku, čímž je inhibována mitochondriální translokace, nebo Tom22 prekurzor v cytoplasmě, čímž je rovněž porušen import mitochondriálních preproteinů. (převzato z Harbauer, 2014)*[165]

Celý proces importu proteinových prekurzorů do mitochondrií je posttranslačně regulován na několika úrovních. Významná je fosforylace samotných prekurzorů, Hsp70 a zejména jednotlivých podjednotek TOM komplexu cytoplasmatickými kinasami v závislosti na metabolických potřebách buňky[165,166]. Zatímco Tom22 je fosforylován kaseinkinasou 2, která mitochondriální import stimuluje, receptor Tom70 je za anaerobních podmínek fosforylován c-AMP dependentní proteinkinasou A (PKA) (*Obr. 20a*). Touto fosforylací je narušena jeho interakce s cytoplasmatickým Hsp70, dochází k inhibici mitochondriálního importu[167] a proteinový prekurzor je k dispozici pro potřeby buňky (*Obr. 20b*).

Sekvenční motivy potenciálně fosforylovatelné PKA se nacházejí i v sekvenci cytoplasmatického ko-chaperonu Tomm34 – jedním z nich je Ser93 nacházející se v doméně TPR1, druhým je Ser160 v oblasti flexibilního linkeru[168]. Jak TPR1, tak flexibilní linker jsou zapojeny v ATP-dependentní interakci s Hsp70[117] a fosforylace

by tak v tomto procesu mohla hrát regulační roli. Flexibilní linker zároveň nese sekvenční motiv RXX(pS/pT)XP rozpoznávaný dimerickými všudypřítomnými regulačními proteiny 14-3-3[169], RWNS(160)LP, což je v souladu s typickou povahou 14-3-3 proteinů vázajících se k úsekům charakterizovaným strukturou postrádající prvky vnitřní uspořádanosti[170]. 14-3-3 se rovněž blíže nespecifikovaným mechanismem spolupodílí na procesu transportu mitochondiálních prekurzorů[171,172].

1.6.4 NQO1 a udržování buněčné redoxní rovnováhy

Redoxní stav buňky je dalším regulovatelným parametrem, který zodpovídá za správné fungování proteomu. Jedním z mechanismů, kterými jsou eliminovány reaktivní formy kyslíku, je dvouelektronová redukce solubilním cytoplasmatickým enzymem NQO1. Tento flavoprotein katalyzuje redukci chinonů a jejich derivátů[173], čímž zabraňuje vzniku reaktivních semichinonů, které mohou atakovat proteiny, lipidy nebo DNA[174]. Dále katalyzuje redukci nitroaromátů, železitých solí a superoxidových radikálů[21] (*Obr. 21*). Ztráta redukční aktivity NQO1 je nejčastěji spojována s rizikem karcinogeneze[21] a procesem stárnutí buněk[151].

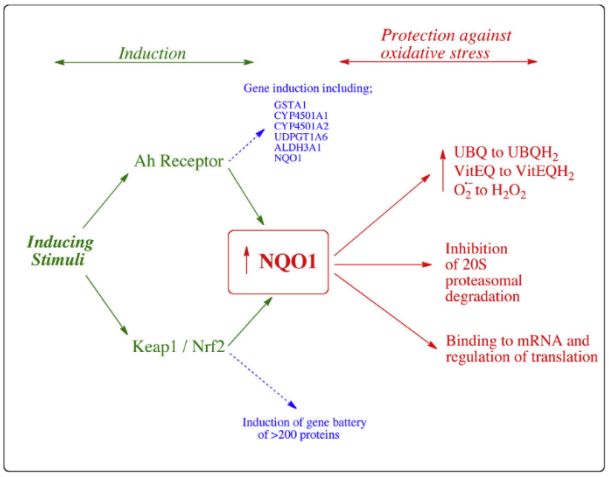

Obrázek 21. *Úloha NQO1 v ochraně buněk proti oxidativnímu stresu.(převzato z Ross, 2018)*[121]

Na druhou stranu, pro již transformované buňky, kterým NQO1 napomáhá vyrovnat se s oxidativní zátěží, byla pozorována spojitost zvýšené exprese NQO1 s horší prognózou stavu pacienta. V rakovinných buňkách v hypoxickém stavu NQO1 zároveň

nepřímo reguluje dostupnost kyslíku svým stabilizačním působením na transkripční faktor HIF-1α (*Obr. 22*), který je zde hlavním regulátorem homeostázy kyslíku[20].

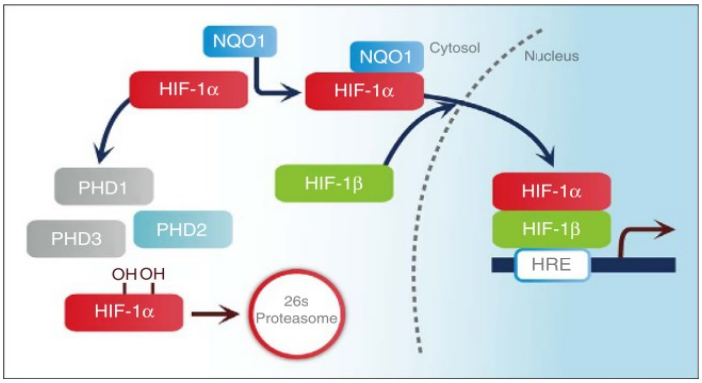

Obrázek 22. *Model znázorňující stabilizační působení NQO1 na HIF-1α v rakovinných buňkách. Při fyziologické hladině O_2 v buňkách je konstitutivně exprimovaný HIF-1α hydroxylován zástupci rodiny proteinů s prolyl-hydroxylasovou doménou (PHD). Hydroxylace je rozeznávána proteiny s E3-ligasovou aktivitou, HIF-1α je ubikvitinován a proteasomálně degradován (vlevo). Ve stavu hypoxie je mechanismus hydroxylace poškozený vlivem interakce HIF-1α s NQO1 a HIF-1α dimerizuje s HIF-1β za tvorby transkripčně aktivního komplexu, který se váže k HRE (z angl. Hypoxia response element) DNA-sekvenčnímu motivu v oblasti promotoru nebo enhanceru cílových genů (vpravo). (převzato z Oh, 2016)[20]*

1.7 Techniky strukturní hmotnostní spektrometrie

V průběhu uplynulých tří dekád se hmotnostní spektrometrie (MS; z angl. Mass Spectrometry) stala neoddělitelnou součástí strukturní biologie. Díky svým vlastnostem jako je vysoká citlivost, rychlost analýzy, přesnost a správnost určení hmotnosti a aplikovatelnost v nejrůznějších uspořádáních[175,176] poskytuje nezměrné množství informací o primární struktuře proteinů, jejich modifikacích, ale také o jejich strukturním upsořádání, dynamice a interakcích. Mezi hmotnostně spektrometrické techniky strukturní biologie se řadí pro tuto práci stěžejní vodík/deuteriová výměna (HDX-MS)[177], dále chemické zesítění proteinů (XL-MS)[178], nativní MS[179] nebo měření iontové mobility (IM-MS)[180]. Všechny tyto techniky, které poskytují informaci o struktuře s nižším rozlišením, lze využít pro získání komplementárních informací charakterizujících proteinová uspořádání. Velmi užitečné jsou zejména v případech, kdy není možné aplikovat klasické strukturní techniky s vysokým rozlišením. Strukturní MS tak nachází uplatnění v situacích, kdy je limitující množství proteinu, proteiny jsou dynamické, vnitřně neuspořádané, nedostatečně homogenní, příliš velké, případně když je klíčová rychlost analýzy a rychlost získání (ale i interpretace) dat[181].

Analýzu proteinů pomocí MS lze provádět na třech základních úrovních, které jsou označovány jako bottom-up, top-down a middle-down. V nejběžnějším bottom-up uspořádání je využívána proteolýza v kombinaci s následnou MS analýzou, nejčastěji LC-MS/MS. Jedinou limitací tohoto uspořádání, co se týče velikosti analyzovaného proteinu nebo komplexity vzorku, je rozlišovací schopnost daného LC-MS systému[182]. Další jeho limitací je ztráta informace o různých formách jednotlivých proteinů. Opačnou strategii, která právě vyniká schopností určit přítomnost proteoforem, je top-down. V top-down experimentu je v hmotnostním spektrometru analyzována intaktní forma proteinu, která je následně fragmentována v plynné fázi. Nejvyužívanější fragmentační technikou je kolizně indukovaná disociace (CID; z angl. Collision-induced dissociation). Tato technika často neposkytuje dostatečné množství fragmentových iontů a také vede k disociaci PTM (např. fosforylace[183,184]), což znemožňuje jejich lokalizaci v rámci proteinové sekvence. V tomto ohledu pak lze jako alternativní fragmentační techniky využít např. disociaci záchytem elektronu (ECD; z angl. Electron capture dissociation), disociaci přenosem elektronu (ETD; z angl. Electron transfer dissociation) nebo nově zavedenou fotodisociaci ultrafialovým zářením (UVPD; z angl. Ultraviolet photodissociation), které poskytují komplementární informaci, nevedou k disociaci PTM

a tak umožňují přiřazení místa modifikace[185]. Middle-down přístup kombinuje obě výše zmíněná uspořádání, kdy se s využitím omezené proteolýzy získavají delší fragmenty (3–15 kDa), které jsou následně fragmentovány v plynné fázi[186].

1.7.1 Vodík/deuteriová výměna kombinovaná s MS

V 50. letech minulého století Linderstrøm-Lang společně se svými kolegy popsal základní teorii pro analýzu kinetiky proteinů pomocí vodík/deuteriové výměny (HDX; z angl. Hydrogen/deuterium exchange)[187]. S využitím této techniky je sledována konformační dynamika proteinu v roztoku skrze rychlost výměny amidických vodíků proteinové páteře za deuterium, čímž je reflektována jejich dostupnost rozpouštědlu. Ta je funkcí dvou vlastností konkrétních aminokyselinových zbytků – jejich zapojení v tvorbě prvků sekundární struktury (vodíkové vazby) a přístupnosti solventu[188]. Schopnost HDX zachytit lokální konformační změny proteinové molekuly může být využita pro charakterizaci protein-proteinových/ligandových interakcí, jejich alosterického chování, událostí doprovázejících sbalování nebo denaturaci proteinu, nebo jejich odpovědi na přítomnost nejrůznějších prvků, jakými jsou např. přítomnost mutace nebo PTM. Až do 90. let 20. století byla nejvyužívanější metodou pro analýzu HDX NMR[189,190,191]. Následně díky rozvoji měkkých ionizačních technik, ESI (ionizace elektrosprejem; z angl. Electrospray ionization) a MALDI (ionizace laserem za přítomnosti matrice; z angl. Matrix-assisted laser desorption/ionization) začala narůstat role detekce prostřednictvím MS[192,193] (HDX-MS).

Základní model kinetické teorie HDX předpokládá, že se amidické vodíky mohou vyskytovat ve dvou různých stavech, ve stavu nekompetentním pro výměnu (NH_{cl}) – když jsou nepřístupné solventu nebo zapojené v tvorbě sekundární struktury – nebo kompetentním (NH_{op}) pro výměnu za deuterium. Protože struktura proteinu je dynamická, NH_{cl} se stávají NH_{op} a naopak. HDX kinetiku pro sbalený protein lze popsat následovně vztahem (1):

$$NH_{cl} \underset{k_{cl}}{\overset{k_{op}}{\rightleftharpoons}} NH_{op} \xrightarrow{k_{ch}} ND_{op} \underset{k_{op}}{\overset{k_{cl}}{\rightleftharpoons}} ND_{cl} \qquad (1)$$

k_{op} a k_{cl} jsou rychlostní konstanty pro strukturní změny proteinu (relaxace/stabilizace struktury), k_{ch} je vnitřní („chemická“) rychlost HDX.

Rychlost výměny isotopů je vysoce závislá na pH prostředí (*Obr. 23a*) a mechanismus výměny může být katalyzovaný bazicky, kysele nebo vodou[194,195,196]. Za fyziologického pH (7,0–7,4) jde predominantně o bazicky katalyzovanou reakci.

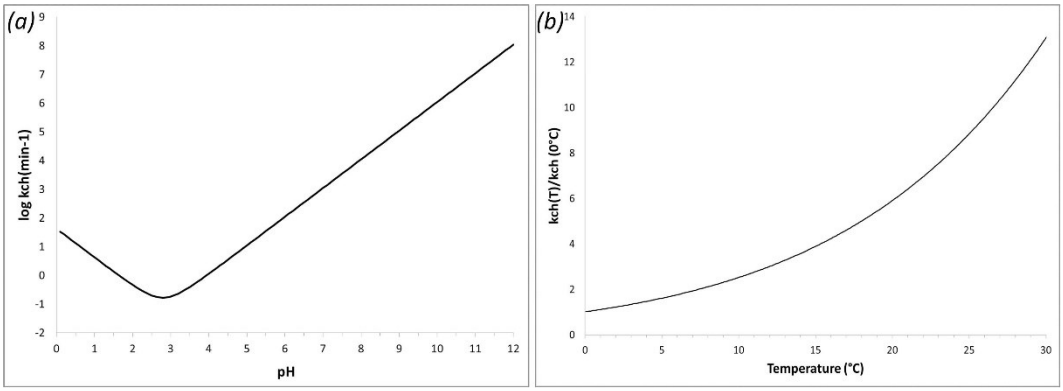

Obrázek 23. *Vliv pH a teploty na rychlost HDX. (a) Graf závislosti rychlosti chemické výměny, logk_{ch}, amidických vodíků za deuterium při 25 °C jako funkce pH. (b) Rychlost chemické výměny, k_{ch}, jako funkce teploty (°C) pro bazicky katalyzovanou reakci. k_{ch} byla pro teploty 0–30 °C vypočtena z rovnice (2) a normalizována na k_{ch} při 0 °C. (převzato z Oganesyan, 2018)*[177]

Při ní je každá změna pH o jednotku doprovázena desetinásobnou změnou reakční rychlosti. Dalším faktorem, kterým je rychlost výměny silně ovlivňována, je teplota[195] (*Obr. 23b*), kdy zvýšení teploty o 10 °C znamená přibližně trojnásobné zvýšení rychlosti reakce[189]. Teoretická rychlost HDX, k_{ch}, v závislosti na teplotě, *T,* může být vypočtena z modifikované Arrheniovy rovnice (2):

$$k_{ch} = k_{rc}(293)\exp\left[-\frac{E_A}{R}\left(\frac{1}{T}-\frac{1}{293}\right)\right] \qquad (2)$$

$k_{rc}(293)$ je referenční rychlostní konstanta $k_{int,H}$, $k_{int,OH}$ nebo $k_{int,H2O}$ (rychlostní konstanty pro kysele, bazicky nebo vodou katalyzovanou reakci) v závislosti na pH při 20 °C.; E_A je aktivační energie pro kysele, bazicky nebo vodou katalyzovanou reakci – $E_A(k_H)$ = 14 kcal.mol^{-1}, $E_A(k_{OH})$ = 17 kcal.mol^{-1}, $E_A(k_{H2O})$ = 19 kcal.mol^{-1}; R je univerzální plynová konstanta (8,314 J.mol^{-1}.K^{-1})[195].

Pro HDX existují dva způsoby experimentálního uspořádání – převládající kontinuální značení, které poskytuje informaci o HDX kinetice proteinu, který je v nativním stavu deuterován v časovém rozpětí sekund až hodin; nebo méně obvyklé pulsní značení, kdy je protein podroben konkrétnímu podnětu (např. denaturaci) a po určité době je pulsně (10–20 s) deuterován[197], poskytujíc tak informaci o kinetice procesu iniciovaném daným podnětem (*Obr. 24* na s. 44).

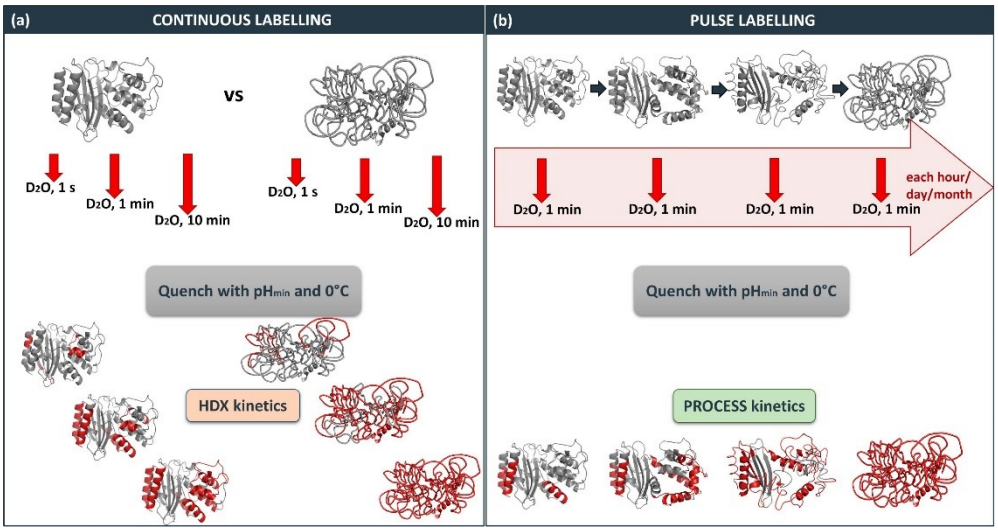

Obrázek 24. *Kontinuální vs. pulsní uspořádání HDX experimentu. (a) Při kontinuálním značení je protein inkubován s deuteriem po různě dlouhé časové intervaly, což nám poskytuje informaci o kintetice HDX daného proteinového systému v čase. (b) V pulsním uspořádání je protein v počátečním čase t_0 podroben podnětu iniciujícímu strukturní změnu (např. přídavek denaturantu), v následujících časech t_{1-x} je přidána deuteriová značka a pulsní HDX reakce je vždy po stejném definovaném krátkém časovém úseku zastavena, poskytujíc tak informaci o průběhu konformační změny vyvolané inicializačním podnětem. (převzato z Oganesyan, 2018)*[177]

Typické uspořádání kontinuálního HDX-MS experimentu je reprezentováno *Obr. 25* na s. 45. Proteinový systém je za podmínek s různými proměnnými, jež proti sobě srovnáváme, po definovaný časový úsek inkubován v pufru obsaujícím deuterium, načež je rychlost HDX reakce téměř zastavena snížením pH na hodnotu 2,5 a prudkým ochlazením na 0 °C nebo zamražením v kapalném dusíku. Při měření MS převládá bottom-up přístup a protein je při 0 °C, kdy je minimalizována zpětná výměna, s využitím nespecifických aspartátových proteas proteolyticky štěpen v LC-systému. Vzniklé peptidy jsou odsoleny na reverzní fázi a před tím, než vstoupí do hmotnostního spektrometru, jsou rovněž při 0 °C s využitím lineárního gradientu acetonitrilu chromatograficky separovány na analytické koloně s reverzní fází. Naměřená data jsou posléze analyzována s využitím softwaru pro HDX. Protože lze pouze spekulovat o tom, jakou velikost změny v deuteraci mezi dvěma různými podmínkami už je možné považovat za signifikantní, doporučuje se experiment provést v sérii dvou až tří technických replikátů. Dále je pak doporučeno provést korekci na rozsah zpětné výměny pro každý peptid[198]. To je nezbytné zejména v případě porovnávání vlivu zanesení mutace do sekvence proteinu, neboť různá velikost postranního řetězce aminokyselin může stericky ovlivnit přístupnost amidických vodíků proteinové páteře rozpouštědlu.

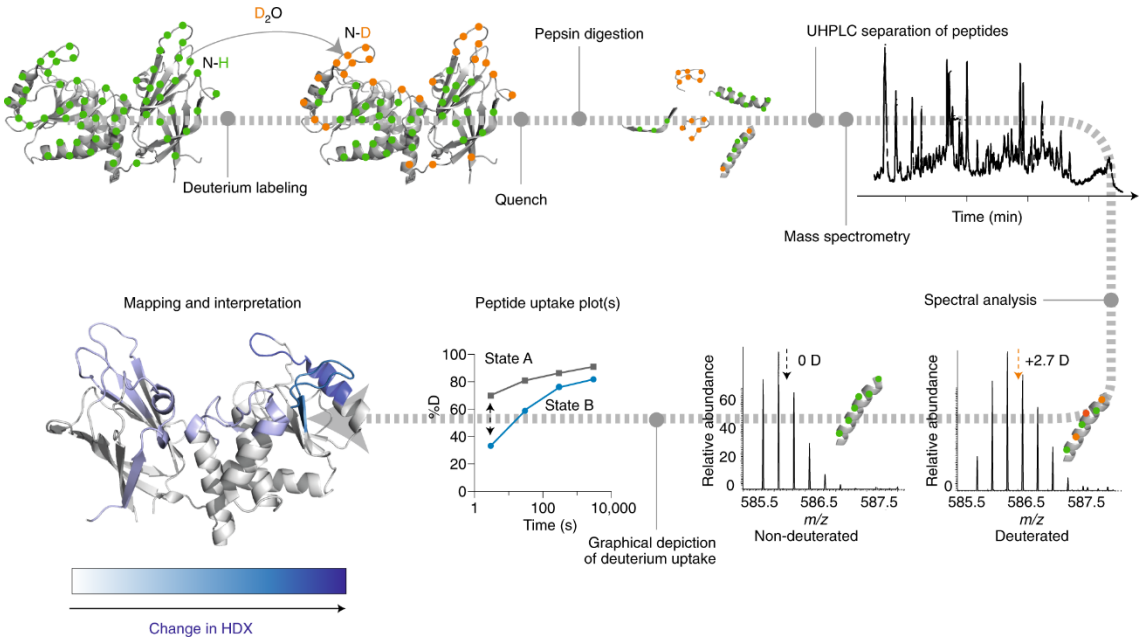

Obrázek 25. *Sekvenční schéma jednotlivých kroků HDX experimentu. Poté, co proběhne značení proteinu deuteriem (v kontinuálním nebo pulsním uspořádání) a HDX reakce je minimalizována snížením pH na hodnotu 2,5 a prudkým snížením teploty, protein je s využitím kyselých aspartátových proteas štěpen, buď v roztoku, nebo s využitím proteasové kolony naplněné imobilizovanou proteasou zapojenou on-line v LC-systému, kde jsou vzniklé peptidy před vstupem do MS odsoleny a separovány s využitím analytické kolony na principu reverzní fáze. Naměřená data jsou následně procesována pomocí specializovaného softwaru pro HDX, který poskytne informaci o úrovni deuterace jednotlivých peptidů. Získané informace mohou být následně aplikovány na strukturní model. (převzato z Masson, 2019)*[198]

K navýšení peptidové redundance a rozlišení až na jednotlivé aminokyseliny, alespoň v určitých segmentech proteinu, může napomoci vhodná volba proteasy. Běžnější je vedle štěpení v roztoku využívat štěpení proteinu pomocí kolon s imobilizovanou proteasou zapojených v uspořádání on-line v temperovaném LC-systému[199]. Pro každý protein se zvlášť testují nejvhodnější podmínky štěpení těmito nespecifickými proteasami, kdy nejběžněji využívanou aspartátovou proteasou je pepsin. Dále se využívají nepenthesinové proteasy nepenthesin-I[199,200] a nepenthesin-II[201], nebo aspergillo- a rhizopuspepsin, známé jako proteasy typu XIII a XVIII[202]. Pro každý protein je optimalizována nejvhodnější průtoková rychlost přes danou proteasu, kdy vyšší průtoková rychlost znamená kratší setrvání proteinu na proteasové koloně a poskytuje delší peptidy a naopak. V případě hůře štěpitelných proteinů, kterými jsou např. transmembránové proteiny obklopené detergentem, je možné využít volbu různých aditiv v pufru okyselujícím HDX reakci a minimalizujícím tak její rychlost – jimi jsou nejčastěji urea, TCEP (tris(2-karboxyethyl)fosfin) nebo hydrochlorid guanidinu. Jinou možností je zahřátí proteasové kolony, které rovněž zvyšuje efektivitu štěpení[203]. Proteasové kolony lze zapojit do LC-systému samostatně nebo použít jejich kombinaci.

Pro dosažení rozlišení na úrovni jednotlivých aminokyselinových zbytků je vedle bottom-up přístupu v mnohem menším rozsahu využíváno top-down HDX uspořádání s technikou fragmentace ECD nebo ETD v plynné fázi, které nejsou na rozdíl od CID fragmentace doprovázeny migrací labilních protonů a deuterií mezi atomy dusíku, síry a kyslíku v rámci jednoho peptidu[204], tzv. scramblingem deuteriové značky.

Průměrnou úroveň deuterace pro každý peptid lze určit na základě distribuce izotopů, která odráží rychlost strukturní změny. V případě, kdy v dané části proteinu dochází k pomalejším změnám struktury než je rychlost HDX, jedná se o tzv. EX1 kinetiku, která je v hmotnostním spektru demonstrována bimodální distribucí isotopových obálek. Pokud je naopak strukturní změna rychlejší než HDX, jde o tzv. EX2 kinetiku charakterizovanou unimodální isotopovou obálkou. Stále častěji se však objevují publikace zmiňující tzv. EXX kinetiku, kdy jsou rychlosti změny struktury a HDX přibližně stejné.[177] Pro EX1, EX2 a EXX charakteristické isotopové obálky jsou znázorněny v *Obr. 26*.

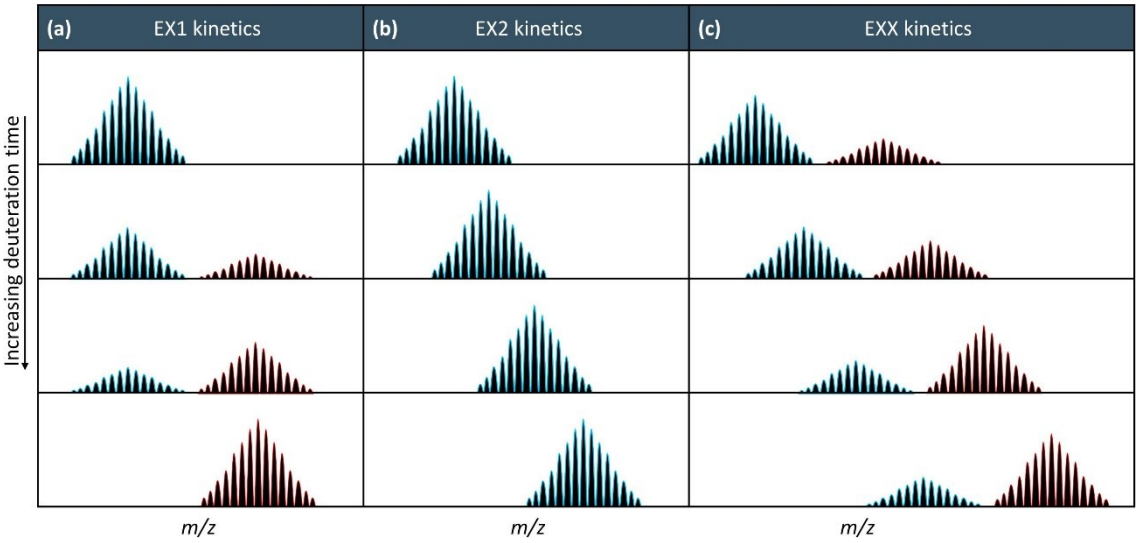

Obrázek 26. *Schematická reprezentace isotopových obálek charakteristických pro kinetiku EX1, EX2 a EXX. (převzato z Oganesyan, 2018)[177]*

1.7.2 Chemické zesítění kombinované s MS

Chemické zesítění proteinové struktury v kombinaci s MS (XL-MS) je další velmi rozšířenou strukturní MS technikou. Ke studiu proteinu je využito kovalentní modifikace s následným propojením snadno přístupných/reaktivních postranních řetězců aminokyselin bifunkčními činidly o známé délce, na základě čehož lze odvodit informace o jejich přibližné vzdálenosti[205,206], ať už v rámci struktury proteinu nebo proteinového

komplexu. Technikou chemického zesítění tak mohou být zachyceny různé přechodné stavy proteinů, interakce mezi podjednotkami, jejich topologie a dynamika.

K dispozici je široké spektrum síťovacích činidel s různou reaktivitou, délkou nebo rozpustností. Původně ke snížení komplexity získávaných dat byla navržena isotopově značená činidla, která lze využít i pro kvantifikaci strukturních změn v rámci různých stavů proteinu[207,208]. Dále lze využít činidel štěpitelných za podmínek fragmentace CID, činidel obsahujících fluorofory nebo nesoucích afinitní značku[178,209]. Nejvyužívanější skupinou síťovacích činidel jsou homobifunkční vysoce aminoreaktivní estery N-hydroxysukcinimidu síťující mezi sebou postranní řetězce lysinů nebo N-terminus proteinu.

Před samotným provedením síťovací reakce je nezbytné nalézt optimální experimentální podmínky. Proměnnými jsou zde molární nadbytek síťovacího činidla vůči proteinu, délka reakce a teplota. Koncentraci analyzovaného proteinu je běžné držet co nejnižší v rozmezí 0,5–1,5 $g.l^{-1}$, aby byly minimalizovány nespecifické interakce. Rovněž pufr v němž bude reakce probíhat musí být zvolen takový, aby neobsahoval složky interferující s reaktivními skupinami síťovaných aminokyselin. Produkty síťovací reakce lze ověřit pomocí SDS-PAGE, kdy pak z gelu můžeme izolovat konkrétní zesíťovaný stav, který je podroben proteolytickému štěpení a vzniklé peptidy analyzovány s využitím vysokoúčinné kapalinové chromatografie v tandemu s MS (HPLC/UHPLC-MS; z angl. High-peformance/Ultra-high performance liquid chromatography). Produkty síťovací reakce lze tímto přístupem analyzovat rovněž přímo z roztoku, čímž mizí limitace velikostí síťovaného systému (*Obr. 27*).

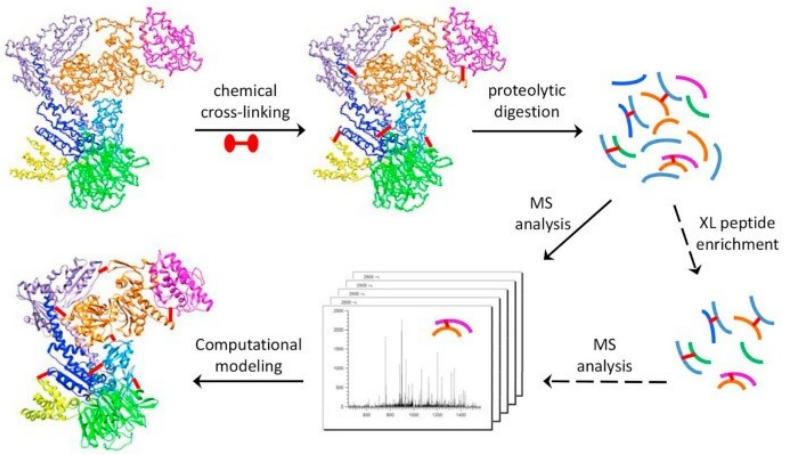

Obrázek 27. *Reprezentace průběhu typického XL-MS experimentu. Zesíťovaný protein je proteolyticky štěpen. Peptidy jsou následně podrobeny MS analýze a identifikovaná propojení poskytnou informaci o maximálních vzdálenostech mezi zesíťovanými zbytky v rámci proteinového uspořádání. (převzato z Chu, 2018)*[178]

1.7.3 Nativní MS

Technika nativní MS, kdy je protein sprejován pomocí nanoESI (nESI) z vodného roztoku přímo do hmotnostního analyzátoru, umožňuje monitorování nativní konformace proteinů i nekovalentně asociovaných biomolekul v plynné fázi. Oproti proteinovým molekulám sprejovaným z organických solventů mají tyto proteiny sprejované za nativních podmínek mnohem užší distribuci nábojových stavů, která je úměrná množství přístupných bazických aminokyselinových zbytků, které mohou být protonizovány (*Obr. 28*)[179].

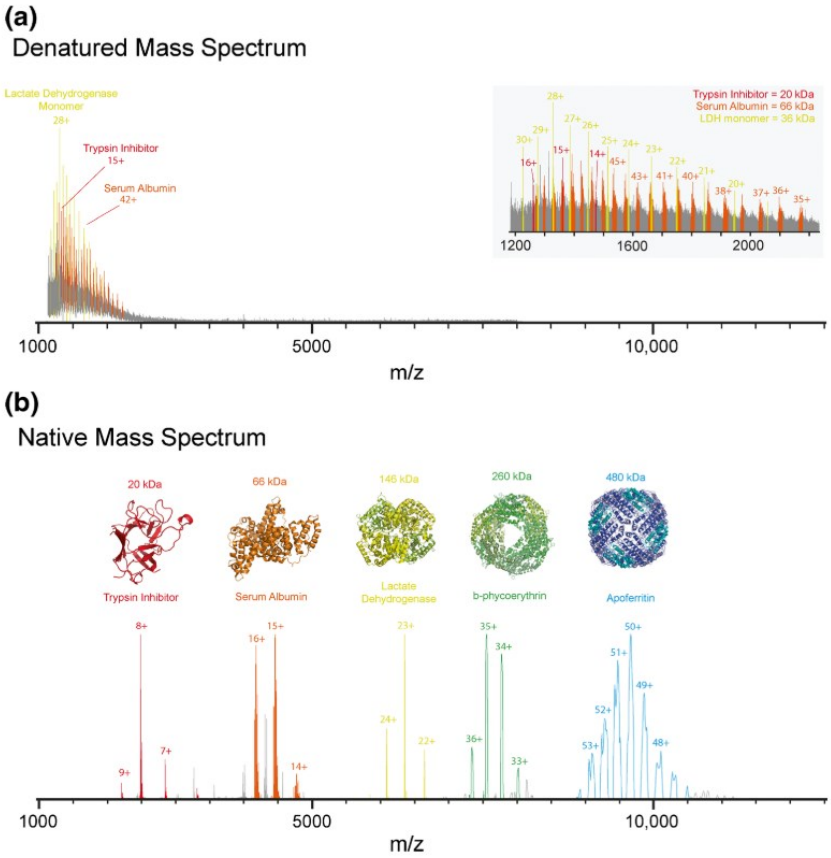

***Obrázek 28**. Srovnání MS analýzy identické směsi proteinů za denaturujících podmínek (a) a podmínek nativní MS (b). (převzato z Leney, 2017)[179]*

Schopnost nativní MS zachovat nekovalentní interakce nám může poskytnout informace ohledně složení, stechiometrie a topologie proteinových komplexů, určit afinitu malých ligandů vůči proteinu a rovnovážnou disociační konstantu celého komplexu (K_d)[179]. Pokud jsou podjednotky komplexu přidávány postupně, nESI může ukázat jak je komplex formován[210] – umožňuje identifikovat přímé interakce mezi podjednotkami, napomáhá přiřadit jejich relativní pozice a určit stabilní jádro komplexu. Zásluhou neustále se rozvíjející instrumentace lze získat náhled do struktury čím dál

větších a komplexnějších proteinových uspořádání jako jsou mega-Da ribozomy[211] nebo virové kapsidy[212].

Před samotným MS měřením je obvykle protein převeden do pufru obsahujícího acetát amonný, jehož iontovou sílu a pH je nutno striktně kontrolovat, aby byly dodrženy podmínky zajišťující dosažení nativní konformace analyzovaného proteinu. V typickém uspořádání se využívá ionizace nESI, kdy je vzorek sprejován skrze kapiláru s otvorem o průměru 0,5–10 µm, což umožňuje použít nízkou průtokovou rychlost (20–200 nl.min^{-1}) a minimalizovat tak spotřebu vzorku.

1.7.4 Iontová mobilitní spektrometrie kombinovaná s MS

Pro charakterizaci proteinů nebo proteinových komplexů, které je obtížné pozorovat vysoce rozlišenými strukturními technikami, je rovněž široce uplatňována iontová mobilitní spektrometrie nebo také iontová mobilita (IM) v kombinaci s MS (IM-MS) (*Obr. 29*). IM umožňuje narozdíl od MS, kdy jsou molekulové ionty separovány podle poměru hmoty a náboje, separovat částice v plynné fázi podle poměru velikosti/tvaru a náboje. Děje se tak v mobilitní cele vlivem srážek molekulových iontů

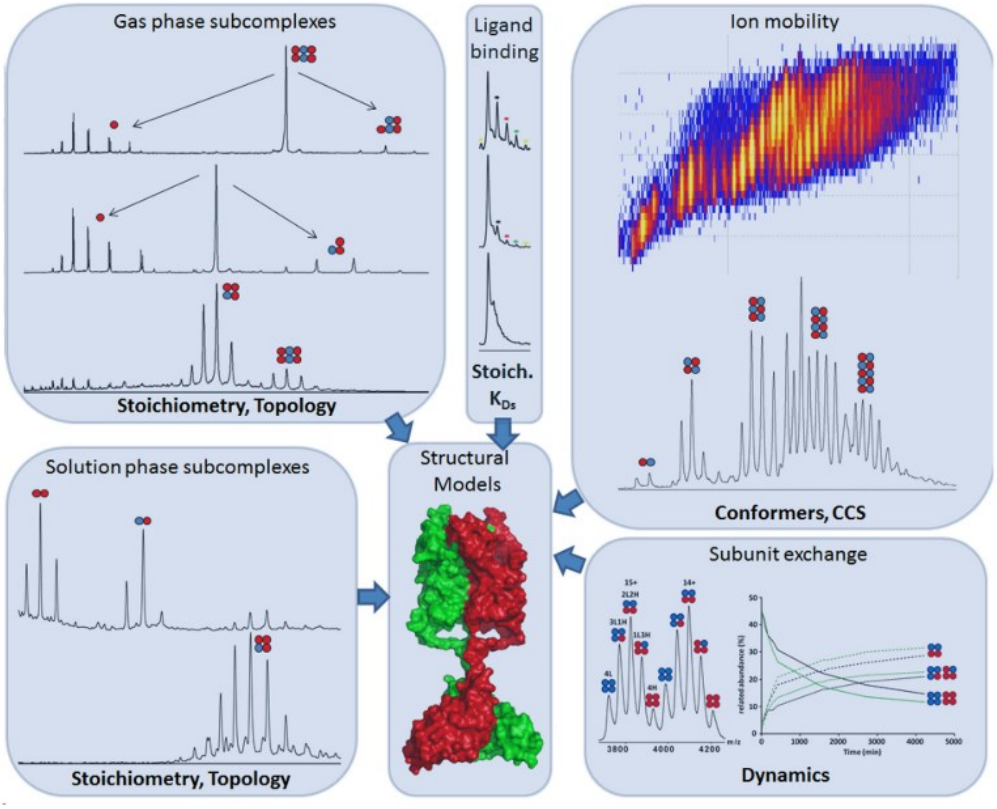

Obrázek 29. *Schematická reprezentace informací o proteinovém uspořádání, jež mohou být získány měřením nativní MS v kombinaci s IM. (převzato z Marcoux, 2015)*[175]

za atmosferického tlaku ve statickém elektrickém poli s inertním tlumivým plynem (nejčastěji dusík nebo helium) majícím opačný směr proudění[213]. Měřením času potřebného k průchodu iontu průletovou mobilitní celou (v angl. Drift time) a po kalibraci pomocí proteinů se známou strukturou (mj. cytochrom c, ubikvitin, myoglobin) může být získán jejich kolizní průřez (CCS; z angl. Collisional cross-section) udávaný v jednotkách $Å^2$. Větší molekulové ionty s vyšším CCS podstupují vyšší množství srážek s tlumivým plynem a jejich pohyblivost mobilitní celou je tak oproti menším částicím pomalejší[180].

Předřazením IM cely hmotnostnímu analyzátoru tak dochází k navýšení separační dimenzionality klasického hmotnostně spektrometrického uspořádání a je tak možné od sebe odlišit různé konformační stavy molekul o stejné hmotnosti. Jedním z přístupů IM-MS jak studovat proteinové molekuly je metoda kolizně indukované postupné destabilizace terciární struktury (CIU; z angl Collision induced unfolding)[214] (*Obr. 30*). V typickém CIU experimentu jsou izolované molekulové ionty v plynné fázi těsně před vstupem do IM cely postupně aktivovány postupně se zvyšujícím množstvím srážek s inertním plynem (např. argon, helium nebo dusík). Tím narůstá jejich vnitřní energie, vlivem čehož dochází k destabilizaci struktury, což se následně projeví na jejich pohyblivosti skrze IM celu. Je tak možné posoudit stabilitu proteinových uspořádání nebo jejich interakci s ligandy. Získané CCS jsou dále hojně využívány pro molekulové modelování[175].

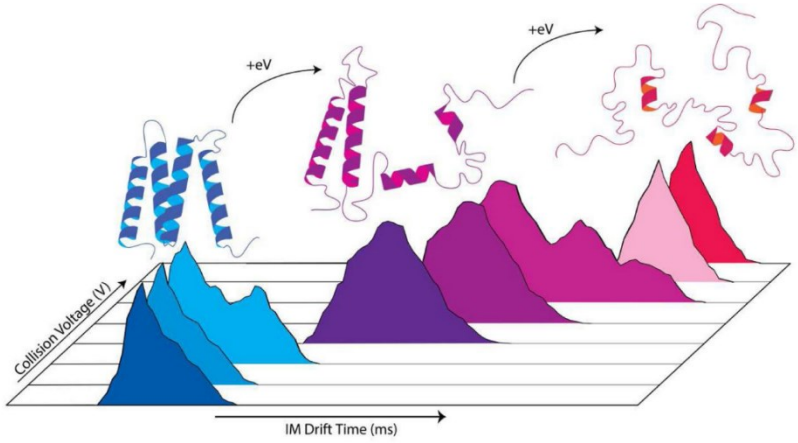

Obrázek 30. *Princip IM CIU experimentu. Postupným zvyšováním kolizního napětí dochází k destabilizaci prvků sekundární struktury, což se projeví na jeho zpožděném průchodu IM celou. (převzato z Dixit, 2018)[214]*

2 CÍLE PRÁCE

Cílem této disertační práce bylo strukturně charakterizovat dynamická proteinová uspořádání, která se podílejí na udržování proteostasy. Jejich chování v roztoku bylo pozorováno technikami strukturní hmotnostní spektrometrie, zejména s využitím vodík/deuteriové výměny. Pokud je funkce těchto proteinů jakkoli narušena, ať už vlivem modifikací nebo deregulací hladiny jejich exprese, jsou tyto disbalance demonstrovány na úrovni celého buněčného proteomu a velmi často se pojí s různými patologickými stavy jako je karcinogeneze, Alzheimerova choroba, Parkinsonova choroba, Huntingtonova nemoc, roztroušená skleróza nebo schizofrenie. Znalost struktury, interakčních partnerů a interakčních mechanismů těchto dynamických molekulárních chaperonů může významně napomoci při vývoji terapie vůči výše jmenovaným patologickým stavům.

Specifické cíle byly:

- Charakterizovat ATP-dependentní dimerizační rozhraní inducibilní formy Hsp70 (HSPA1A)
- Charakterizovat aminokyselinové zbytky tvořící stabilizační jednotky v kontextu alosterických přeměn inducibilní formy Hsp70 (HSPA1A)
- Popsat strukturní vliv vazby proteinu 14-3-3 na fosforylovaný ko-chaperon Tomm34 a dále strukturně charakterizovat dopad fosforylace na jeho interakci s chaperony Hsp70 a Hsp90
- Poskytnout strukturně rozlišenou informaci pro dynamickou apoformu enzymu NQO1 a následně porovnat rozdíly v dynamice NQO1 s navázaným kofaktorem nebo inhibitorem

3 METODY

Publikace zahrnuté v této práci obsahují popis veškerých použitých metod v plném rozsahu, včetně všech technických detailů nezbytných pro jejich reprodukovatelnost. V následujících řádcích je proto prezentován pouze stručný výčet technik využitých napříč touto prací.

Seznam použitých metod

- Vodík/deuteriová výměna v kombinaci s MS (HDX-MS)
- Nativní nESI-MS
- MS analýza primární struktury proteinů a posttranslačních modifikací (ESI-FT-ICR, aplikace přímým nástřikem nebo v LC-MS a LC-MS/MS uspořádání)
- Chemické zesítění proteinů (XL-MS)
- Příprava proteinového vzorku pro MS analýzu
- *In vitro* fosforylace proteinů

4 VÝSLEDKY A DISKUZE

Cílem této práce bylo strukturně charakterizovat dynamické chování proteinů a jejich komplexů zejména technikou vodík/deuteriové výměny. Společným jmenovatelem všech proteinů zahrnutých v této práci je jejich široké zapojení v proteostatických procesech.

4.1 Publikace I

Na základě výsledků, které dříve obdrželi Ďurech a kol. při charakterizaci interakce Hsp70 s ko-chaperonem Tomm34, kdy byla pomocí měření isotermální titrační kalorimetrie (ITC; z angl. Isothermal titration calorimetry) stanovena stechiometrie ATP-dependentně vznikajícího komplexu 2:1 ($Hsp70_2$:Tomm34)[117], je v tomto článku strukturně a funkčně charakterizován ATP-dependentní dimer lidské inducibilní formy Hsp70 v kontextu dalších Hsp70 homologů (*Obr. 31a*) – jmenovitě konstitutivně exprimovaná isoforma Hsc70, BiP z ER a prokaryotický homolog DnaK.

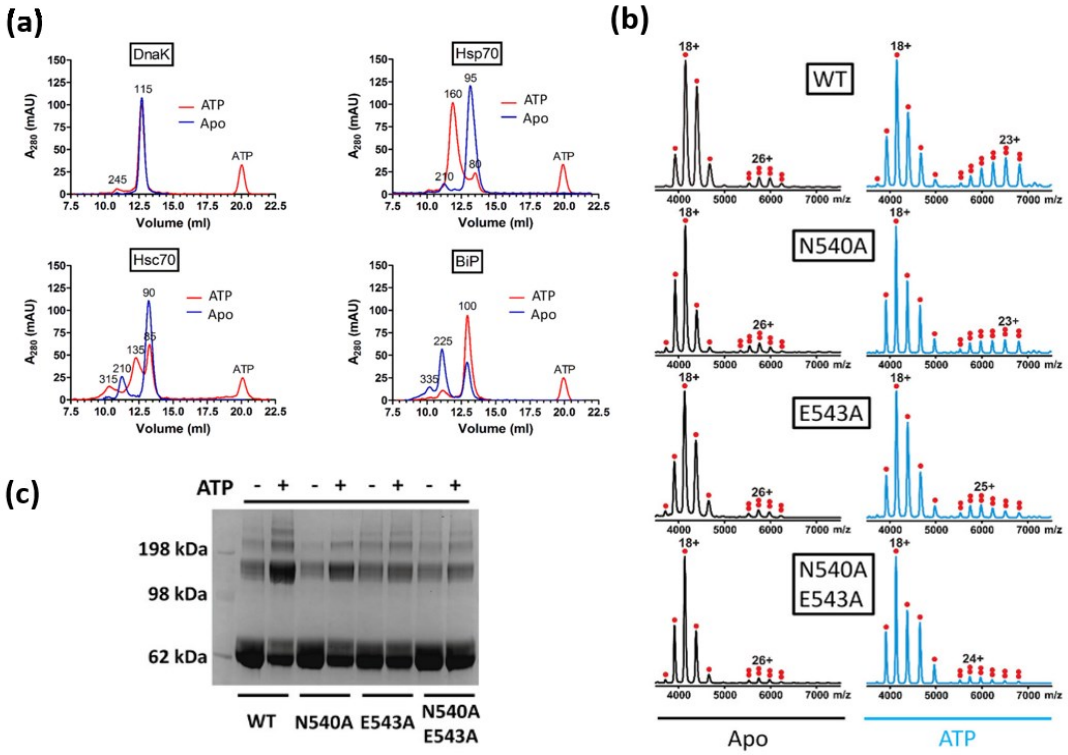

Obrázek 31. *Hsp70 a jeho schopnost dimerizace. (a) Před samotnou SEC byly v bakteriálních buňkách produkované homology DnaK, Hsp70, Hsc70 a Bip (40μM) inkubovány 20 min při RT v přítomnosti nebo absenci ATP (0,2mM). V každém chromatogramu je jednotlivým elučním píkům přiřazena experimentálně získaná molekulová hmotnost. (b) Hmotnostní spektra změřená nativní nESI-MS dimerizačních mutantů Hsp70 vs. WT (20μM) v přítomnosti a absenci ATP (inkubace 20 min/RT se 100mM ATP), před měřením byly proteiny převedeny do 200mM octanu amonného. (c) Schopnost jednotlivých dimerizačních mutantů Hsp70 vs. WT (40μM) tvořit ATP-dependentní dimer (20 min inkubace s 0,2mM ATP) je stabilizována chemickým zesítěním 10M nadbytkem DSA. (převzato z Publikace I – Trčka, 2019)*

Mimo práce Ďurecha a kol. byla přítomnost pro chaperonový cyklus relevantního dimeru Hsp70 formovaného v přítomnosti ATP popsána v poslední době v několika dalších publikacích[39,50,51,52,215].

S využitím gelové permeační chromatografie (SEC; z angl. Size exclusion chromatography) a chemického zesítění jednotlivých výše jmenovaných homologů pomocí aminoreaktivního činidla di-(N-sukcinimidyl) adipátu (DSA) bylo stanoveno, že Hsp70 a Hsc70 mají z testovaných Hsp70 forem největší sklon tvořit ATP-dependentní dimery. Ačkoli pro bakteriální homolog DnaK bylo již dříve v roztoku pozorováno velmi nízké zastoupení ATP-dependentního dimeru[50] stejně jako v elučním profilu, který jsme pro ni obdrželi separací SEC, ověřili jsme u všech námi produkovaných homologů měřením jejich schopnosti uvolnit navázaný substrát v přítomnosti ATP, že jsou alostericky aktivní.

Přítomnost Hsp70-ATP ve formě dimeru byla následně potvrzena i měřením nESI-MS (*Obr. 31b* na s. 53). Při použití vyššího napětí 70 V, které poskytlo dobré hmotnostní rozlišení, byl však poměr dimer/monomer v porovnání s SEC snížen, což by mohlo poukazovat na nestabilitu dimerního uspořádání v plynné fázi. Ze strukturního a biochemického hlediska byla dále charakterizována pouze inducibilní isoforma Hsp70 a její varianty nesoucí jedno-, dvou- nebo tříbodové mutace. Pro ni bylo analýzou pomocí SEC pozorováno, že se v případě dimerizace závislé na ATP jedná o časově a koncentračně podmíněný proces, kdy bylo při konstantní 200μM koncentraci ATP dosaženo nejvyššího podílu dimeru vůči monomeru při 40μM koncentraci Hsp70. Zároveň bylo možné s narůstajícím časem inkubace Hsp70 s ATP pozorovat postupný přechod od velmi intenzivního chromatografického píku náležejícího extendovanému monomeru v Apo/ADP stavu s molekulovou hmotností (M_m) odpovídající 95 kDa po 2 minutách, přes kompaktní monomerní ATP-vázající konformaci odpovídající zdánlivě 85 kDa po 10 minutách inkubace, až k jednoznačné převaze ATP-dependentního dimeru se zdánlivou M_m 160 kDa po 20 minutách. S využitím varianty nesoucí mutaci I164D, která ačkoli váže ATP, nenabývá plně otevřené konformace Hsp70, kdy by se utvářelo nové interakční rozhraní NBD-SBD, bylo stanoveno, že se Hsp70 musí nacházet ve své ATP-indukované konformaci, aby mohlo dojít k dimerizaci. Eluční profil byl sledován i z pohledu ATP-dependentní interakce s ko-chaperonem z rodiny J-proteinů Hsp40, který zvyšuje ATPasovou aktivitu Hsp70 a zpětnou konverzi chaperonu do monomerního stavu. Na jeho základě lze usuzovat, že nedochází k aktivaci ATPasové aktivity obou protomerů Hsp70 zároveň a interakce $Hsp70_2$:$Hsp40_2$ tedy není symetrická.

Rovněž s využitím SEC, XL-MS a nESI-MS (*Obr. 31b,c* na s. 53) pak byly v přítomnosti a absenci ATP charakterizovány další varianty Hsp70 – T204A s velmi nízkou bazální ATPasovou aktivitou, dále N540A, E543A a N540A-E543A, jež mají narušenu schopnost dimerizovat, neboť se nacházejí na dimerizačním rozhraní popsaném již dříve pro DnaK[50], a jejich kombinace T204A-N540A-E543A. Měřením HDX-MS v přítomnosti a absenci ATP bylo ověřeno, že u jednotlivých výše zmíněných variant Hsp70 nedochází vložením mutace ke ztrátě jejich alosterické aktivity. Dále byla s využitím technik molekulární biologie prošetřena schopnost dimerizačních mutantů N540A, E543A a N540A-E543A podílet se na opětovném sbalení denaturované luciferasy, kinetika vazby substrátu nebo jejich ATPasová aktivta, kdy byla ve všech případech zjištěna narušená funkční kooperace s Hsp40. Jejich přímá interakce s Hsp40 byla měřena technikou povrchové plasmonové resonance (SPR; z angl. Surface plasmon resonance). Získané výsledky naznačují, že je stejně jako v případě asociace DnaK s DnaJ[50] pro interakci s Hsp40 vyžadována přítomnost funkčního dimeru. Relevance dimerizace Hsp70 byla sledována i *ex vivo*, kdy byla popsána přítomnost oligomerních forem Hsp70 v rámci vysokomolekulárních proteinových komplexů. Technikou SAXS (z angl. Small-angle X-ray scattering; maloúhlový rozptyl rentgenového záření), kdy pro analýzu tvaru proteinové obálky homodimeru v roztoku byla použita varianta Hsp70 T204A jako prevence proti rychlé hydrolýze při manipulaci se vzorkem, byla potvrzena jeho antiparalelní orientace.

Dimer Hsp70 byl pak pozorován i z pohledu interakce s ko-chaperony CHIP a Tomm34. Ze separace komplexů Tomm34-Hsp70 a CHIP-Hsp70 pomocí SEC, a na základě měření nESI-MS, bylo pozorováno, že zatímco CHIP se váže k intaktnímu Hsp70 dimeru se stechiometrií 2:2 ($Hsp70_2$:$CHIP_2$), Tomm34 vyžaduje ATP indukovanou konformaci Hsp70, ale dimer rozrušuje s výslednou stechiometrií interakce 1:1 (Hsp70:Tomm34). Zároveň bylo zjištěno, že na ATP závislá vazba Tomm34 nevyžaduje přítomnost Hsp70 ve formě dimeru, neboť je schopen vázat se i na dimerizační mutanty N540A, E543A a N540A-E543A. Možným vysvětlením tohoto rozkolu s předchozí analýzou ITC, kdy byla stechiometrie komplexu stanovena v poměru 2:1 ($Hsp70_2$:Tomm34)[117], může být hypotéza, že asociace Tomm34 s jedním protomerem Hsp70 činí druhý protomer opouštějící dimer nezpůsobilým další interakce s Tomm34.

Bližší strukturní charakterizace poskytující strukturní informaci s vyšším rozlišením byla provedena na základě analýzy dat získaných měřením HDX-MS dimerizačních mutantů N540A, E543A a N540A-E543A proti WT Hsp70

v absenci (Apo stav) a přítomnosti ATP. Z charakterizace Apo stavu je patrné, že v případě variant N540A a N540A-E543A dochází vlivem inkorporace mutace do struktury Hsp70 v počátečních časových bodech k destabilizaci v oblasti SBDα helixů αA/αB pokryté peptidy 519–529, 530–542 a 533–542, přičemž N540A-E543A má výraznější vliv. Tato destabilizace se však nijak nepodepisuje na povaze jejich alosterického chování, kdy lze ve všech variantách v ATP stavu pozorovat protekci v místech, kde se utváří nové ATP-indukované rozhraní NBD-SBDβ, pro NBD charakterizované peptidy 143–150, 150–167 a 168–180 a pro SBDβ 413–427 a 478–486. Dále je znatelná protekce v oblasti flexibilního linkeru pokryté peptidem 394–401, u nějž dochází k zanoření do spodní části NBD. V úseku destabilizovaném vlivem zanesení mutací pak v přítomnosti ATP dochází k dalšímu nárůstu deuterace oproti WT. Navzdory tomu, že tento nárůst není nikterak výrazný, což je pravděpodobně způsobeno nízkou stabilitou ATP-dependentního dimeru s velmi rychlou hydrolýzou ATP, kdy můžeme ATP-dependentní změny pozorovat zejména v řádu sekund až jednotek minut, je tato deprotekce přičítána absenci dimerizačního rozhraní, které bylo v této oblasti již dříve identifikováno v případě antiparalelních homodimerů DnaK[51] a BiP[42]. Vzhledem k vysoké evoluční konzervovanosti aminokyselinových zbytků zapojených v těchto homolozích v procesu dimerizace lze předpokládat analogický mechanismus i u ostatních forem Hsp70. Další v přítomnosti ATP deprotektovaný region E543A a N540A-E543A mutantních forem reprezentovaný peptidy NBD (48–68, 268–282 a 294–302) a SBDα (519–529 a 530–542), odpovídá oblasti účastnící se tvorby dimerizačního rozhraní v případě DnaK, BiP nebo heterodimeru Hsc70:Sse1[216] (Sse1 je zástupcem rodiny NEF Hsp110 u kvasinek, který má strukturu homologní s Hsp70[217]). Toto rozhraní není kompatibilní s krystalovou strukturou homodimeru Sse1[218], na niž však lze naopak projektovat jiné v přítomnosti ATP deprotektované oblasti E543A a N540A-E543A variant zastoupené peptidy 353–368 z NBD a 547–564/550–576 z SBDα vzájemně tvořící ve WT další dimerizační rozhraní, které kromě homodimeru Sse1 nelze aplikovat žádné z výše uvedených dimerů isoforem Hsp70. Tyto výsledky naznačují, že antiparalelní dimer Hsp70 může nabývat konformace fluktuující mezi dvěma krajními strukturami popsanými pro homodimery BiP[42] a Sse1[218]. Námi identifikované regiony

zapojené v tvorbě dimerizačního rozhraní jsou vyznačeny v krystalové struktuře v *Obr. 32.*

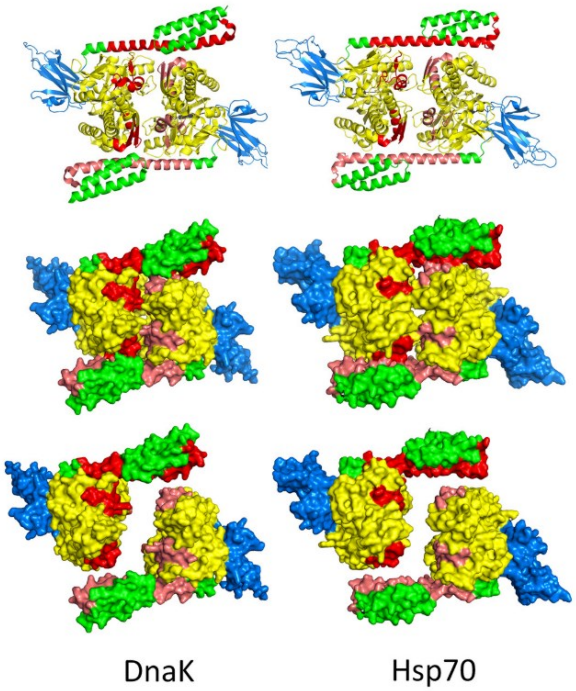

Obrázek 32. *Námi identifikované regiony ATP-dependentního dimerizačního rozhraní aplikované na model DnaK[39](PDB kód: 4JNE) nebo homologně vytvořený model Hsp70. Odstíny červené jsou zvýrazněny peptidy 48–68, 268–282, 294–302, 519–529 a 530–542 nalézající se na dimerizačním rozhraní NBD-NBD (žlutá) a NBD-SBDα (zelená). Modře je vyznačena SBDβ. (převzato z Publikace I – Trčka, 2019)*

Na základě znalosti strukturních modelů pak mohly být identifikovány aminokyselinové zbytky zprostředkující inter- a intramolekulární iontové interakce. Jejich porovnáním bylo zjištěno, že aminokyselinové zbytky zprostředkující intermolekulární interakce NBD-NBD v rámci dimerů isoforem Hsp70 (Hsp70, DnaK, BiP, Sse1, Hsc70(NBD)-Sse1) se různí, což by mohlo zodpovídat za jejich různé dimerizační vlastnosti. Naopak vysoce konzervovaný aminokyselinový zbytek D529 z αB helixu SBDα je součástí sítě intramolekulárních elektrostatických interakcí utvářených mezi SBDα-NBD ve všech isoformách Hsp70. Proto jsme prostřednictvím SEC a měření nESI-MS a HDX-MS ověřovali jeho význam v kontextu dimerizace s využitím mutantní formy Hsp70 D529A porovnávané vůči WT za Apo a ATP podmínek. Ačkoliv bylo pozorováno, že D529A forma je schopna dimerizace, z Apo podmínek získaných měřením HDX je patrné, že vlivem mutace dochází k výrazné destabilizaci struktury v oblasti helixu αA/αB SBDα, kam spadají právě pro dimerizaci kritická residua N540 a E543, což je patrně příčinou vzniku nižšího množství D529A dimeru oproti WT, jak lze číst z elučního profilu SEC.

Kromě analýzy dimerizačních mutantů N540A, E543A a N540A-E543A byla měřena rychlost HDX v přítomnosti a nepřítomnosti ATP i pro variantu s minimalizovanou rychlostí hydrolýzy T204A včetně jejích kombinací s dimerizačními mutanty, T204A-N540A, T204A-E543A a T204A-N540A-E543A. Protože však data získaná pro tyto varianty neposkytovala oproti prezentovaným dimerizačním mutantům N540A, E543A a N540A-E543A, žádnou informaci nad jejich rámec a vnášela nadbytečnou míru komplexity do jejich interpretace, rozhodli jsme se je nakonec nevyužít.

Pro stabilizaci dimerizačního rozhraní jsme se nedávno rozhodli využít přístupu, kdy byl protein v přítomnosti ATP stabilizován 10M a 50M nadbytkem homobifunkčního aminoreaktivního síťovacího činidla, bis-(sulfosukcinimidyl) glutarátu (BS2G). U takto zesíťovaných proteinů byla měřena rychlost HDX oproti jejich nezesíťovaným protějškům za podmínek analogických předchozím HDX-MS experimentům. Po přídavku 50M nadbytku BS2G, který byl použit jako kontrola pro zobrazení efektu nespecifických síťovacích interakcí, byl pozorován jeho globální vliv vyvolávající celkovou změnu struktury Hsp70, zatímco stabilizace 10M nadbytkem BS2G je specifická, pozorovatelná pouze v úsecích konzistentních se strukturním modelem Hsp70 v jeho ATP nebo ADP vázajícím stavu. Pro ATP-indukovaný stav WT proteinu byla pozorována ATP specifická stabilizace po přídavku 10M nadbytku síťovacího činidla pouze v oblasti peptidů pokrývajících výše definované dimerizační rozhraní 519–529, 530–542 a 533–542, a která nenastala v případě mutantu N540A-E543A. Tento rozdíl však není oproti nezesíťovanému WT příliš výrazný, proto by bylo do budoucna dobré provést měření s replikací, případně s využitím varianty T204A, která má nižší hydrolytickou aktivitu, a rozdíl by tak mohl být výraznější.

Tato strukturní a funkční charakterizace ATP-dependentního dimeru HSPA1A odhalila různé dimerizační vlastnosti homologů Hsp70, které mohou být zapříčiněny vlivem různých intermolekulárních interakcí v rámci NBD-NBD dimerizačních rozhraní. Dále bylo pozorováno, že ATP závislá dimerizace slouží jako důležitý regulační prvek chaperonového cyklu, kdy je nezbytná pro interakci s ko-chaperonem Hsp40 následovanou sbalením přenášeného substrátu. Naopak vlivem interakce ATP-vázajícího dimeru Hsp70 s TPR ko-chaperonem Tomm34 je dimerní uspořádání rozrušeno, což podporuje model, kdy je substrátový protein transportovaný do mitochondrie v cytoplasmě předáván mezi Hsp70 a Hsp90 chaperony a tím udržován v neagregovaném a pro transport kompetentním stavu, namísto toho, aby byl pomocí Hsp70 sbalen

do nativní konformace[117] (*Obr. 13* na s. 30, kap. 1.4.1.3). Schematické znázornění významu dimerního uspořádání Hsp70 pro ATPasový cyklus je znázorněno v *Obr. 33*.

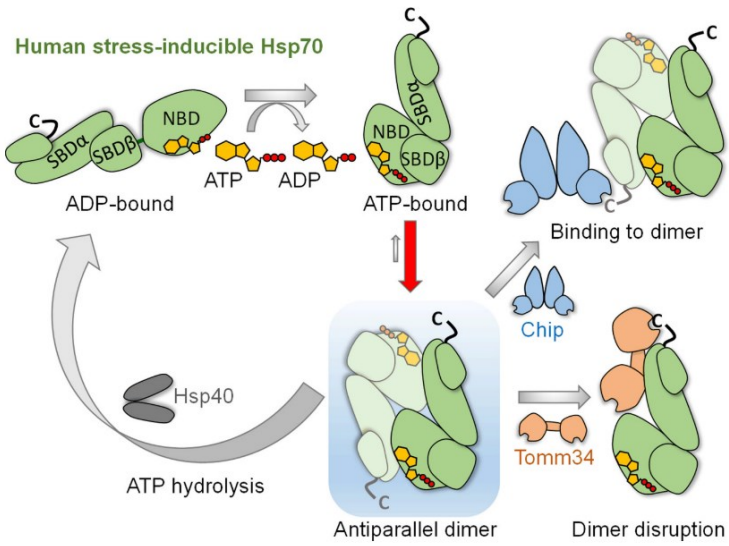

Obrázek 33. *Schematické znázornění významu dimeru v průběhu ATPasového cyklu a v kontextu interakce s ko-chaperony CHIP a Tomm34. ATP-dependentní antiparalelní dimer je nezbytný pro interakci s Hsp40, který na něj přenáší substrát a urychluje ATPasovou aktivitu Hsp70 ve prospěch sbalení substrátu. TPR ko-chaperon Tomm34 dimerní uspořádání ruší, naopak ko-chaperon CHIP zanechává dimer intaktní. (převzato z Publikace I – Trčka, 2019)*

4.2 Publikace II

Různorodé proteostatické funkce zajišťované chaperonem Hsp70 mohou být vykonávany díky jeho alosterickému chování. Vlivem vazby ATP do NBD dojde ke vzájemné rotaci obou jejích podjednotek, čímž mezi nimi vzniká štěrbina, kam je zanořen flexibilní linker. Strukturní změna je dále přenášena do SBD, kde SBDβ a SBDα disociují a utvářejí nová interakční rozhraní s ramenem NBD-I. Vazbou substrátu do široce otevřené hydrofobní kapsy v SBDβ je pak reverzním procesem, kdy dojde k opětovné asociaci SBDβ-SBDα a uvolnění linkeru, umožněna zpětná rotace ramen NBD, čímž se její katalytické zbytky dostanou do pozice optimální pro hydrolýzu γ–fosfátu ATP. Celý proces hydrolýzy ATP je dále amplifikován působením ko-chaperonů z rodiny J-proteinů, čímž je zajištěn další nárůst afinity SBD vůči substrátu a tento nerovnovážný stav je označován jako ultraafinitní[219]. Ačkoli aminokyselinové zbytky zahrnuté v procesu alosterie byly pomocí strukturních studií jednotlivých domén nebo ADP-vázající uzavřené konformace identifikovány již dříve (*Obr. 34a*), teprve nedávné objasnění ATP-vázající otevřené konformace (*Obr. 34b*) krystalu DnaK[39,41] umožnilo tyto poznatky aplikovat v kontextu výše popsaných strukturních změn. Navzdory tomu však stále není znám přesný mechanismus, jímž dochází při vazbě ATP k disociaci SBDβ-SBDα a jejich následné asociaci s NBD.

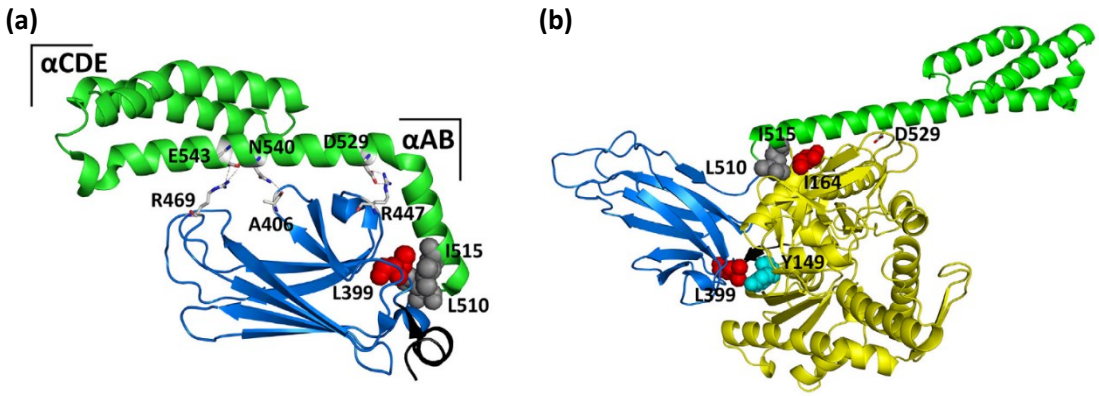

Obrázek 34. *Evolučně konzervované aminokyseliny stabilizující strukturu Hsp70 ve vysoko- i nízkoafinitním stavu. (a) Ve struktuře izolované SBD (HSPA1A; PDB kód: 4PO2) jsou vyznačeny aminokyseliny helixu αB, které sítí elektrostatických interakcí s SBDβ stabilizují pozici SBDα ve prospěch vysokoafinitní konformace, která je dále stabilizována za přispění hydrofobních kontaktů na rozhraní SBDβ-αA – L399 (červená), L510 a I515 (šedá). (b) V nízkoafinitní konformaci Hsp70 interakční rozhraní SBDβ-SBDα zaniká, nicméně ty samé hydrofobní aminokyseliny jsou zapojeny v tvorbě nového interakčního rozhraní mezi SBDβ-NBD (L399-Y149 (tyrkysová)) a SBDα-NBD (L510,I515-I164(červená)). (převzato z Publikace II – Vandová, 2020)*

Výsledky HDX-MS analýzy interakce Hsp70 s ko-chaperonem Tomm34[117] odhalily potenciální roli aminokyselinového zbytku D529 z helixu αB SBDα ve stabilizaci hydrofobní substrát-vázající kapsy skrze jeho elektrostatickou interakci s R447 uvnitř SBDβ v Apo stavu. Tato hydrofobní kapsa je dále tvořena aminokyselinami L399, L510, I515, M518 a V519, které se pak v ATP-vázajícím stavu účastní tvorby nové sítě hydrofobních kontaktů – L510, I515, M518 a V519 s I164 na interakčním rozhraní NBD-SBDα, zatímco L399 kontaktuje Y149 na rozhraní NBD-SBDβ (*Obr. 34* na s. 60). To poukazovalo na jejich možný podíl při stabilizaci obou konformačních stavů Hsp70, proto jsme měřením HDX-MS variant těchto zbytků s jednobodovou mutací L399A/D/F, L510A/D, I515A/D, M518A/D, V519A/D a D529A oproti WT za podmínek absence a přítomnosti ATP ověřili jejich schopnost zachovat si alosterické chování a tedy jejich angažovanost v síti alosterických interakcí. Z naměřených dat vyplynulo, že největší vliv na destabilizaci alosterické povahy Hsp70 mají varianty L399A/D, L510A/D, I515A/D a D529A. Naopak varianty L399F, M518A/D a V519A/D vykazovaly znaky alosterického chování obdobné WT, proto nebyly zahrnuty do dalších experimentů (*Obr. 35*).

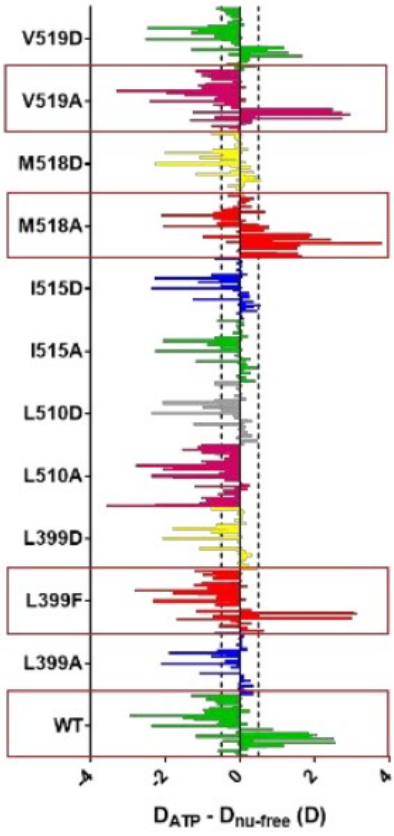

Obrázek 35. *Varianty Hsp70 a jim odpovídající rozdíl v deuteraci mezi stavy s ATP a bez nukleotidu pro jednotlivé peptidy. Mutanti L399F, M518A a V519A vykazují profil téměř totožný s WT, což poukazuje na jejich neporušenou schopnost alosterie.*

Detailní analýzou HDX-MS dat, která jsme obdrželi pro jednotlivé L399A/D, L510A/D, I515A/D a D529A varianty ve srovnání s WT v Apo stavu, bylo dále zjištěno, že mutace L399D, I515D a D529A mají velmi podobný dopad na destabilizaci struktury Hsp70. Jednak dochází k výrazné deprotekci SBDα v oblasti pokryté peptidy 513–546 již v počátečních časech deuterace a dále k destabilizaci C-terminální oblasti linkeru 394–402 ($L_{L,1}$ smyčka), která pokračuje přes oblast SBDβ charakterizovanou peptidy 402–410 ($L_{1,2}$ smyčka), 413–427 ($L_{2,3}$ smyčka a β3-list), 428–439 ($L_{3,4}$ smyčka; stabilní ve variantě I515D) a 440–455 (β4-list a $L_{4,5}$ smyčka). Naopak varianty L399A, L510D a I515A vykazují pouze lehkou destabilizaci v oblasti helixů αA/αB SBDα a mají zřejmě

částečně zachovanou schopnost asociace mezi SBDβ-SBDα. Kvůli destabilizaci podjednotky SBDα v Apo stavu způsobené mutacemi L399D, I515D a D529A je vysoce pravděpodobné, že bude poškozen mechanismus vazby substrátu. Tato hypotéza byla ověřována a později potvrzena měřením vazebné kinetiky peptidového substrátu fluorescenční polarizací. V přítomnosti ATP byla schopna dosáhnout ATP-indukovaného stavu analogického WT pouze varianta D529A. ATP-indukovaný stav je charakterizován protekcí v oblasti interakčního rozhraní NBD-SBDβ, která zahrnuje peptidy pokrývající podjednotku NBD-IA (aminokyseliny 143–180), flexibilní linker (386–392, 394–401) a smyčky z SBDβ $L_{2,3}$ (413–427) a $L_{6,7}$ (479–486). Na základě získaných výsledků lze konstatovat, že zatímco v Apo stavu L399-L510-I515-D529 tvoří strukturní jednotku, která sérií hydrofobních a elektrostatických kontaktů stabilizuje oblast linkeru a helixy αA/αB SBDα, pro stabilizaci ATP-indukovaného stavu jsou stěžejními residui L399-L510-I515.

Schopnost mutovaných Hsp70 forem L399A/D/F, L510A/D, I515A/D a D529A dosáhnout ATP-indukované konformace byla dále ověřena pomocí afinitní precipitace na streptavidinové matrici v kontextu interakce s ko–chaperony Hip a Tomm34. Hip, který interaguje s NBD v Apo konformaci, interagoval v přítomnosti ADP se všemi variantami Hsp70, v přítomnosti ATP pak neinteragoval pouze s WT, D529A a L399F, což odkazuje na jejich neporušenou schopnost nabývat ATP-indukované konformace. To bylo potvrzeno i v případě interakce s Tomm34 selektivně interagujícího pouze s ATP-indukovaným stavem Hsp70, kdy byla opět pozorována interakce s WT, D529A a L399F. Toto pozorování vyzdvihuje vliv nejen náboje, ale i velikosti postranního řetězce hydrofobní aminokyseliny pro konstruktivní interakci mezi NBD-SBDβ (L399) a NBD-SBDα (L510, I515), jak je patrné zejména z neporušené alosterie v případě L399F oproti substituci L399A.

Abychom funkčně charakterizovali míru poškození alosterického chování u variant L399A/D, L510A/D, I515A/D a D529A, byla dále měřením fluorescenční polarizace posuzována jejich schopnost po vazbě ATP do NBD uvolnit navázaný peptid. Komplementární výsledky byly získány měřením jejich ATPasové aktivity v reakci na přítomnost vazby peptidového substrátu, proteinového substrátu p53 nebo ko-chaperonu Hsp40. Interakcí variant Hsp70 s ko-chaperonem Hsp40 byla posléze testována i schopnost jednotlivých mutantních forem opětovně sbalit termálně denaturovanou luciferasu a následným měřením fyzické kooperace Hsp70 variant s Hsp40 technikou SPR bylo ověřeno, že ke ztrátě chaperonové aktivity konkrétních

variant Hsp70 nedochází vlivem neschopnosti fyzické interakce s ko-chaperonem Hsp40. Veškeré atributy charakterizující strukturní a funkční vlastnosti jednotlivých mutantních variant inducibilního Hsp70 jsou shrnuty v *Tab. 3*.

Tabulka 3: *Přehled strukturních, alosterických a chaperonových charakteristik mutantů HSPA1A.*

		WT	D529A	L399A	L399D	L510A	L510D	I515A	I515D
Structure and binding activity of the SBD in the Apo state	SBDα subdomain destabilization	-	High	Intermediate	High	Low	Low	Low	High
	SBDβ destabilization	-	High	Low	High	Low	Low	Low	High
	Interdomain linker destabilization	-	High	Low	High	Low	Low	Low	High
	Substrate peptide binding kinetics	Slow	Fast	Slow	Fast	Slow	Slow	Slow	Fast
Allostery	ATP-dependent interaction with Tomm34 co-chaperone	Yes	Yes	Decreased	Decreased	No	No	No	No
	ATP-induced domain-docking	Yes	Yes	No	No	No	No	No	No
	ATP-induced SBDβ destabilization	High	High	Low	Low	Low	Low	Low	Low
	ATP-induced substrate release (% of WT)	100%	54%	68%	11%	82%	46%	29%	14%
	Peptide-induced ATPase activity	No	No	No	Yes	No	No	No	Yes
	Interaction with Hsp40	Yes	Yes	Yes	Yes	Yes	Yes	Yes	Yes
Chaperone activities	Basal ATPase activity (pmol ATP / μM Hsp70 / min)	0.436±0.004	0.482±0.023	1.563±0.058	1.921±0.062	1.373±0.005	1.647±0.035	1.601±0.189	1.381±0.069
	Luciferase refolding activity (%)	45.53±0.93	16.35±0.78	37.02±0.31	18.05±1.90	48.88±5.12	25.66±.4.44	28.41±3.02	16.81±0.45

(převzato z Publikace II – Vandová, 2020; upraveno)

Na základě nedávno identifikovaného mechanismu interakce alosterických inhibitorů Hsp70, novolaktonu a PET-16 (z angl. triphenyl(phenylethynyl)phosphonium bromide), jsme testovali vliv variant nesoucích mutaci na popsaném interakčním rozhraní – L399D, L510D, I515D a D529A – na vazbu inhibitoru PES (z angl. phenyl-ethynesulfonamide). PES je derivátem PET-16 a *in vivo* vykazuje obdobné biologické účinky[220,221]. Pro tyto inhibitory byla navržena vazba prostřednictvím sítě kontaktů mezi L399 a smyčkami $L_{L,1}$-$L_{\alpha,\beta}$ tak, že jsou nejdříve koordinovány do vazebného místa mezi podjednotkami SBDα-SBDβ[220,222]. S využitím afinitní precipitace bylo pozorováno, že vybraní mutanti mají pravděpodobně vlivem destabilizace rozhraní SBDα-SBDβ poškozenou strukturu vazebného místa pro PES.

Charakterizací jednobodových mutantních variant inducibilního chaperonu Hsp70 byla pro Apo/ADP-vázající stav popsána hydrofobní stabilizační jednotka SBD (*Obr. 36* na s. 64). Ta sestává ze sítě hydrofobních kontaktů mezi L399 tvořícím střed kapsy vázající substrát v SBDβ a L510 spolu s I515 z podjednotky SBDα. Dále je pozice SBDα vůči SBDβ stabilizována D529, který je součástí sítě elektrostatických interakcí. V ATP indukované konformaci pak dojde k alosterickému přeuspořádání SBDα/SBDβ podjednotek, které utvoří nová interakční rozhraní v rámci SBD-NBD. Tato rozhraní jsou opět stabilizována s využitím vysoce konzervovaných aminokyselin L399-L510-I515-D529. Regulace aktivity Hsp70 skrze alosterické vlastnosti specifické pro tuto isoformu může být využita při léčbě patologických stavů souvisejících s Hsp70.

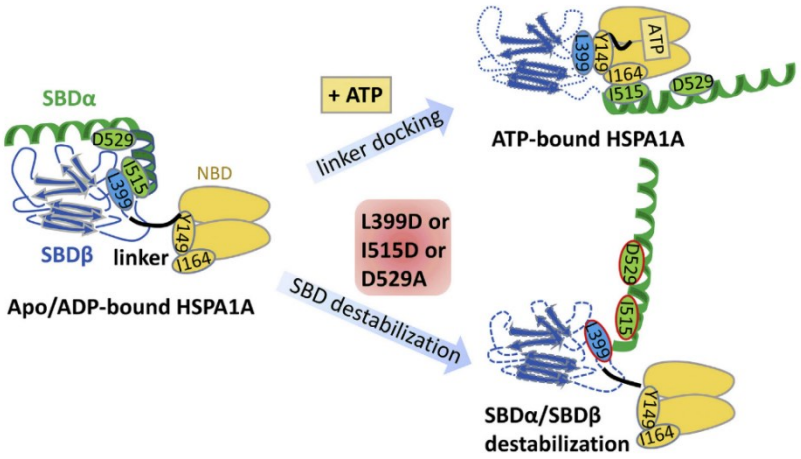

Obrázek 36. *Schéma reprezentující závěry Publikace II. Konzervované aminokyseliny tvořící stabilizační jednotku na rozhraní SBDβ-SBDα utvářejí v nízkoafinitním konformačním stavu s navázaným ATP nová interakční rozhraní SBDβ-NBD a SBDα-NBD. Pokud je některý z těchto kontaktů porušen přítomností mutace, dochází k výrazné destabilizaci SBDα a SBDβ a protein přestává být alostericky aktivní. (převzato z Publikace II – Vandová, 2020)*

4.3 Publikace III

Nedávno byla strukturně a funkčně charakterizována interakce ko-chaperonu Tomm34 účastnícího se transportu mitochondriálních prekurzorů v cytoplasmě s chaperony Hsp70 a Hsp90[116,117]. Zatímco v případě Hsp90 interaguje Tomm34 prostřednictvím své TPR2 domény s jeho C-terminálním motivem MEEVD, s Hsp70 Tomm34 kooperuje rozsáhleji – jednak prostřednictvím TPR1 domény s C-koncovým motivem Hsp70 IEEVD, další kontakty s Hsp70 pak tvoří skrze svůj flexibilní linker. Z funkčního hlediska bylo pozorováno, že je interakce Tomm34 s Hsp70 ATP-dependentní a inhibuje proces sbalování substrátu zprostředkovaný Hsp70 ve spolupráci s ko-chaperonem Hsp40[117]. Na základě prací popisujících vliv fosforylace jednotlivých složek aparátu transportu mitochondriálních preproteinů v cytoplasmě na tento proces[166,167] jsme se rozhodli prošetřit, zda je tato PTM relevantní i z pohledu interakce Tomm34 s Hsp70.

V sekvenci Tomm34 byla identifikována dvě místa vysoce potenciálně fosforylovatelná PKA[168] – S93, který je součástí TPR1, a S160 nacházející se ve flexibilním linkeru (aminokyselinové zbytky 140–190) – a jejichž fosforylace byla pozorována *in vivo*[223]. Obě tato místa zároveň tvoří interakční rozhraní s Hsp70. V souvislosti s mitochondriálním transportem je zmiňován i dimerní adaptorový protein 14-3-3[171,172], který interaguje s fosforylovanými úseky svých vazebných partnerů. Ačkoli se S160 (RWNS[160]LP) nalézá v oblasti charakteristického vazebného motivu

RXX[pS/pT]X[P/G] pro interakci se 14-3-3 proteiny[169,224,225], S93 (RRAS^{93}AY) se s ním rozchází v pozici +2, kde postrádá prolin. Avšak již v minulosti byla pozorována interakce 14-3-3 s atypickým fosforylovaným vazebným motivem[225]. Vliv fosforylace byl proto pozorován i v kontextu interakce Tomm34 se 14-3-3 proteinem.

Poté, co byly připraveny varianty Tomm34 nesoucí mutace v místech fosforylace (S93A, S160A a S93A-S160A) a měřením HDX-MS ve srovnání s WT bylo ověřeno, že vnesením mutace nedochází k ovlivnění sekundární struktury, byla pro ně optimalizována *in vitro* fosforylace s využitím PKA. Úroveň modifikace jednotlivých proteoforem byla ověřena měřením hmotnosti intaktního proteinu přímým nástřikem do MS. Konkrétní místa modifikace pak byla přiřazena a relativně kvantifikována na základě bottom-up analýzy LC-MS/MS. Kromě S93 a S160, které byly v Tomm34 WT PKA fosforylovány z 94 % a 65 %, byla identifikována 24% fosforylace na S280 a další tři minoritní (S186 – 8 %, S146 – 4 %, S1 – 3 %).

S využitím SEC byla ověřena schopnost fosforylovaného (-P) Tomm34 WT-P interagovat s šesti různými isoformami 14-3-3 proteinu, β, γ, ε, ζ, σ, τ. Kooperace proteinkinasou fosforylovaného Tomm34 se všemi šesti isoformami 14-3-3 byla s využitím afinitní precipitace pozorována i *ex vivo* v Tomm34$^{-/-}$ MCF-7 buněčné linii. Pro následující experimenty byla využívána pouze isoforma 14-3-3γ, která byla co se týče formace komplexu s T34 WT-P nejefektivnější. Jednotlivé frakce SEC všech ostatních variant Tomm34 (WT, S93A-P/S93A, S160A-P/S160A a S93A-S160A-P/S93A-S160A) se 14-3-3γ, byly analyzovány s využitím SDS-PAGE, kdy gel obsahoval složky koordinující bivalentní ionty Mn^{2+} nebo Zn^{2+}, které jsou schopné specificky kooperovat s fosforylovaným serinem a napomáhají tak separovat jednotlivé fosforylované formy proteinu (tzv. Phos-tag gel)[226]. Tato separace společně s následným měřením LC-MS/MS poskytujícím procentuální zastoupení fosforylovaných forem v konkrétních eluovaných frakcích dále odhalily, že pro tvorbu komplexu je stěžejní a dostačující fosforylace na S160 v oblasti flexibilního linkeru. Nicméně přítomnost fosfátu na obou S93 a S160 zároveň urychlila průchod vzniklého komplexu chromatografickou kolonou oproti komplexu, kde byl Tomm34 fosforylován pouze na S160, což poukazuje na jejich různou konformaci. Zároveň bylo zjištěno, že fosforylace S280 nemá na tvorbu komplexu vliv. Měřením nESI-MS byla stanovena výsledná stechiometrie komplexu utvořeného mezi Tomm34 WT-P a 14-3-3γ 1:2. Tato technika také jednoznačně potvrdila, že pro tvorbu komplexu je nejdůležitější fosforylace na S160 (*Obr. 37* na s. 66)

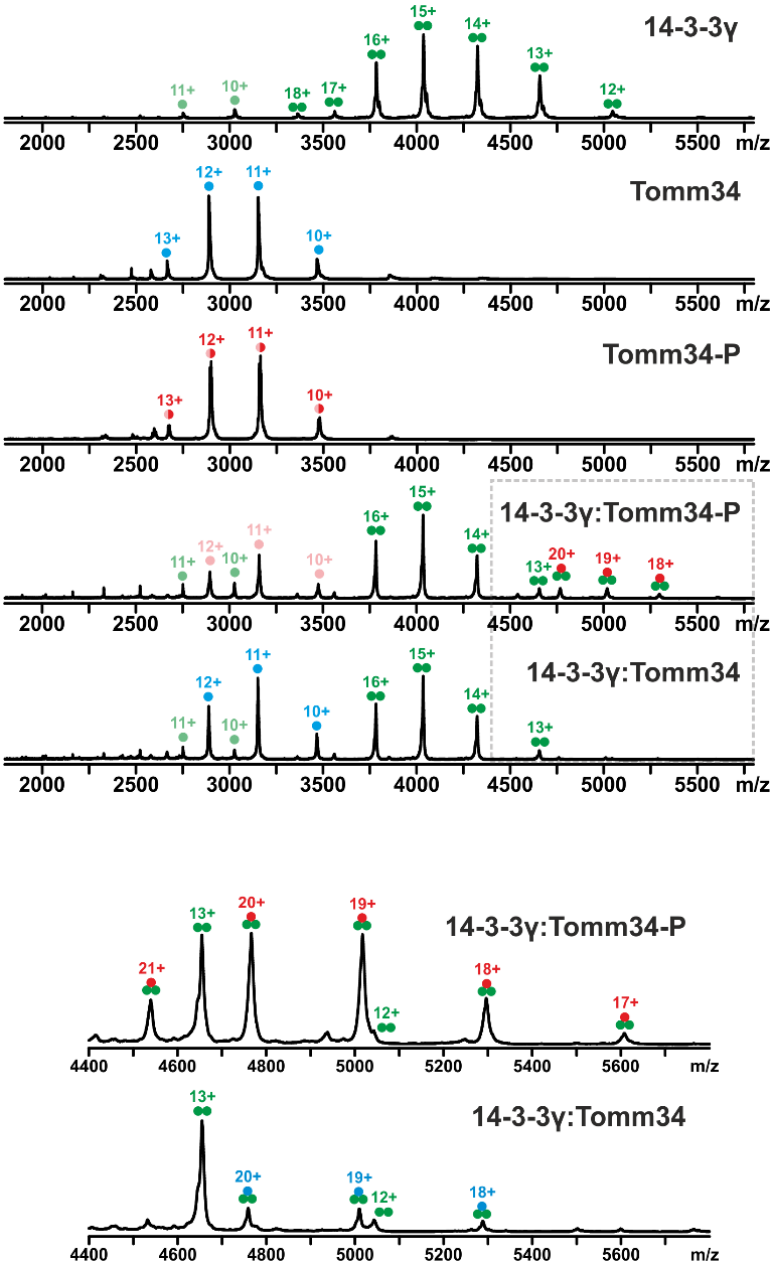

Obrázek 37. *Nativní ESI-MS spektra 14-3-3γ (zelená) a nefosforylovaného (modrá) a fosforylovaného (červená) Tomm34. Nad každým píkem hmotnostního spektra je vyznačen jeho nábojový stav a přiřazena odpovídající barvami reprezentovaná stechiometrie. V případě fosforylovaného Tomm34 je značka nad píky půlená – světlá barva odpovídá Tomm34 s S93-P, intenzivní zabarvení reprezentuje formu forsforylovanou na obou serinech, S93-P a S160-P. Z hmotnostního spektra lze pozorovat, že vzniklý komplex mezi 14-3-3γ:Tomm34-P (2:1) se ustavuje pouze s dvakrát forsforylovaným Tomm34 (S93-P a S160-P) a že modifikace na samotném S93-P není dostačující. (převzato z Publikace III – Trčka, 2020)*

Vliv fosforylace na strukturu Tomm34 byl sledován s využitím techniky HDX-MS (*Obr. 38a* na s. 68). Srovnáním fosforylovaného a nefosforylovaného WT bylo pozorováno, že již v počátečních časech inkubace 20 s a 2 min dochází k destabilizaci v oblasti TPR2, která je při delší inkubaci 20 min a 2 h následována destabilizací v oblasti TPR1. Na základě analýzy ostatních fosforylovaných variant S93A-P, S160A-P a S93A-S160A-P bylo odvozeno, že za destabilizaci TPR1 zodpovídá fosforylace v pozici

S93, neboť na rozdíl od varianty S160A mají varianty postrádající S93-P, S93A a S93A-S160A, velmi podobný profil deuterace, kdy nedochází k destabilizaci TPR1 a zároveň není tak výrazná destabilizace v TPR2. Naopak zvýšení přístupnosti TPR2 rozpouštědlu v blízkosti S280 je pozorováno ve všech fosforylovaných formách a je tedy přičítáno na vrub S280-P. Pro fosforylaci S160 nebylo pozorovano, že by ovlivňovala strukturu Tomm34 ani lokálně, zřejmě kvůli jejímu umístění ve flexibilní nestrukturované oblasti.

Technikou HDX-MS byl dále charakterizován strukturní dopad interakce mezi 14-3-3γ a Tomm34-P, kdy byla míra deuterace sledována v přítomnosti a absenci 14-3-3γ pro všechny fosforylované varianty Tomm34 – WT-P, S93A-P, S160A-P a S93A-S160A-P (*Obr. 38b* na s. 68). Vlivem asociace 14-3-3γ s WT-P dochází k další destabilizaci v oblastech TPR1 a TPR2 oproti samotnému WT-P. Stejný efekt lze pozorovat i v případě mutantní formy S93A nesoucí S160-P, kde však TPR1 není destabilizována v takové míře. To je v souladu s elučním profilem získaným SEC, kdy je deklarována kompaktnější architektura v případě komplexu 14-3-3γ s Tomm34 nesoucím pouze S160-P v porovnání s komplexem zahrnujícím Tomm34 fosforylovaný na obou serinech. Lehká destabilizace TPR2 byla pozorována i pro interakci nefosforylovaného WT se 14-3-3γ, naznačující jejich přechodnou interakci. Stejně jako v případě SEC bylo dále pozorováno, že stěžejní pro interakci se 14-3-3γ je S160-P, neboť varianty postrádající tuto fosforylaci, S160A-P a S93A-S160A-P, vykazovaly minimální míru destabilizace oproti WT-P. Na základě těchto dat lze usuzovat, že zatímco S160-P je zásadní a dostačující pro interakci se 14-3-3γ, díky S93-P způsobené destabilizaci v oblasti TPR1 dochází k pevnějšímu ukotvení 14-3-3.

Z pohledu strukturních změn vyvolaných ve strukturně rigidním proteinu 14-3-3γ interakcí s fosforylovanými variantami Tomm34 (*Obr. 38c,d* na s. 68) byla zaznamenána protekce v oblasti helixů H3, H5 a H7, které tvoří žlábek vázající fosfopeptidy. Protekce v oblasti helixu H8 indikuje, že se pravděpodobně jedná o další interakční rozhraní mezi Tomm34 a 14-3-3γ. Dále byla pozorována na fosforylaci nezávislá deprotekce v oblasti helixu H9, která byla mírně zvýšená v přítomnosti fosforylovaného Tomm34, což bylo již v minulosti pro 14-3-3 pozorováno[227], a může jít o region přechodně interagující s TPR2 nefosforylovaného Tomm34, jak bylo zmíněno výše.

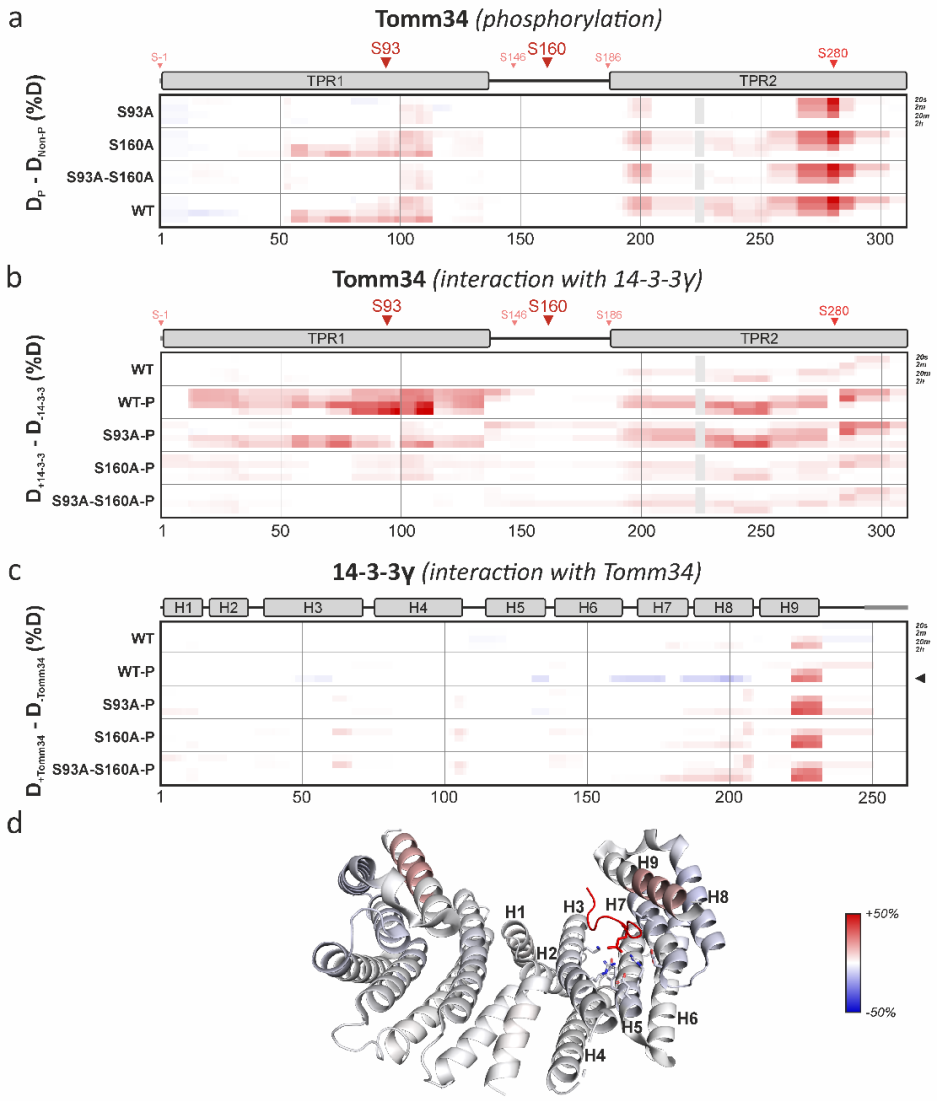

Obrázek 38. *Diferenční grafy znázornňující rozdíl v deuteraci a její vývoj v čase pro podmínky vyznačené v levé části. Fosforylací S93 a S280 vyvolaná destabilizace sekundární struktury Tomm34 (a) je dále amplifikována interakcí se 14-3-3γ, která je podmíněna přítomností fosforylace na S160 (b). Destabilizace struktury vlivem přítomnosti fosforylace na S160 není pozorována, neboť se nachází ve flexibilní oblasti linkeru. Ve struktuře dimeru 14-3-3γ je pozorována pouze na interakci nezávislá destabilizace helixu H9 a pak na interakci závislá protekce v oblasti helixů H3, H5 a H7 (c), které tvoří žlábek koordinující fosfopeptidy,vyznačený v dimerní krystalové struktuře 14-3-3γ (d). Protektovaný H8 pravděpodobně tvoří další interakční rozhraní s Tomm34-P. Nad diferenčními grafy je vyznačeno doménové uspořádání charakterizovaných proteinů. (převzato z Publikace III – Trčka, 2020)*

S využitím HDX jsme dále sledovali interakci Tomm34 WT/WT-P a S93A-S160A/S93A-S160A-P s C-terminálním motivem EEVD peptidů Hsp70 (GGSGSGPTIEEVD) a Hsp90 (GDDDTSRMEEVD) v přítomnosti a nepřítomnosti 14-3-3γ (*Obr. 39*). Zatímco peptid reprezentující C-terminus Hsp90 se k TPR2 váže nezávisle na fosforylaci S280, vlivem S93-P dochází k oslabení kooperace mezi TPR1 a Hsp70 peptidem. Přítomnost 14-3-3γ a jím indukované změny deuterace byly zanedbatelné. Totožný výsledek byl získán měřením fluorescenční polarizace fluorescenčně značených C-terminálních peptidů Hsp70 a Hsp90 v přítomnosti fosforylovaných a nefosforylovaných variant Tomm34 (WT/WT-P, S93A/S93A-P, S160A/S160A-P, S93A-S160A/S93A-S160A-P) v přítomnosti a nepřítomnosti 14-3-3γ. Tato interakce byla dále testována s využitím intaktních proteinů Hsp70 a Hsp90 a následně analyzována s využitím afinitní precipitace. Zatímco výsledky pro interakci s Hsp90 proteinem byly analogické závěrům pro Hsp90 peptid a byla pozorována přítomnost komplexu Hsp90:WT-P:14-3-3γ, protein Hsp70 vykazoval sníženou afinitu k Tomm34 WT-P korelující s přítomností S160-P, spíše než S93-P jak bylo pozorováno pro peptid. Dále bylo pozorováno, že Hsp70 ATP-dependentní dimer není součástí komplexu tvořeného Tomm34 WT-P:14-3-3γ proteiny. Přítomnost adaptorového proteinu 14-3-3γ interagujícího s fosforylovaným Tomm34 tedy působí jako prevence rozkladu ATP-dependentního Hsp70 dimeru. Stejný výsledek byl získán i analýzou pomocí SEC, kdy není potřeba imobilizace proteinů. Při ní bylo zároveň pozorováno, že v případě nepřítomnosti 14-3-3γ Tomm34 WT-P přechodně kontaktuje ATP-dependentní Hsp70 dimer který destabilizuje, ale netvoří s ním stabilní komplex, jako je tomu u nefosforylovaného Tomm34. Tento přechodný komplex mezi Tomm34 WT-P:Hsp70 (1:1) se podařilo zachytit pomocí glutaraldehydové síťovací reakce, jíž byla potvrzena i všechna ostatní předchozí pozorování co se týče interakce mezi fosforylovaným Tomm34 a ATP-dependentním dimerem Hsp70 a jejího ovlivnění přítomností dimeru

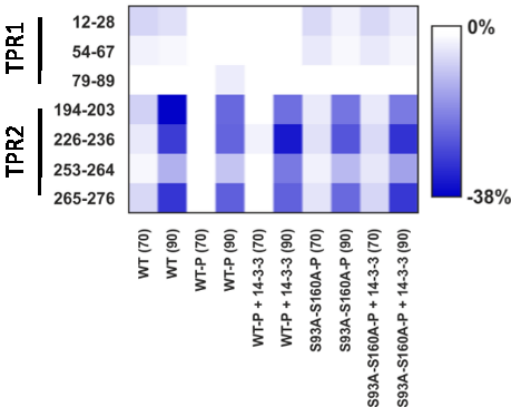

Obrázek 39. *Diferenční výnos rozdílů v deuteraci konkrétních forem Tomm34/Tomm34-P po interakci s Hsp70 a Hsp90 peptidy. Ve výnosu jsou zohledněny pouze pro vazbu EEVD motivu peptidů relevantní segmenty Tomm34 – TPR1 a TPR2. Z grafu lze pozorovat pokles interakce Hsp70 peptidu s fosforylovanou TPR1 doménou nesoucí S93-P. Naopak vazba peptidu Hsp90 k TPR2 není ovlivněna fosforylací na S280. (převzato z Publikace III – Trčka, 2020)*

14-3-3γ. Funkčně pak byl efekt proteinu 14-3-3 na regulaci interakce mezi fosforylovaným Tomm34 a Hsp70 při transportu mitochondriálních prekurzorů prokázán tak, že v přítomnosti fosforylovaného Tomm34 a 14-3-3γ byla zachována schopnost ATP-dependentního dimeru interagovat s JDP ko-chaperonem Hsp40 a podílet se na úspěšném sbalení denaturované luciferasy.

Nově identifikovaná interakce mezi adaptorovým proteinem 14-3-3 a PKA-fosforylovaným ko-chaperonem Tomm34 ustavená skrze S93-P a S160-P příznivě ovlivňuje sbalení substrátu Hsp70 do nativní konformace, neboť je tak Tomm34 vyloučen z vazby na ATP-dependentní dimer Hsp70, jejž jinak rozrušuje. To poukazuje na další prvek regulace transportu mitochondriálních prekurzorů v cytoplasmě a potvrzuje významnou roli ko-chaperonu Tomm34 v tomto procesu. Různé podmínky interakce Tomm34 s ATP dimerem Hsp70 a jejich efekt na zpracování substrátu jsou shrnuty v *Obr. 40*.

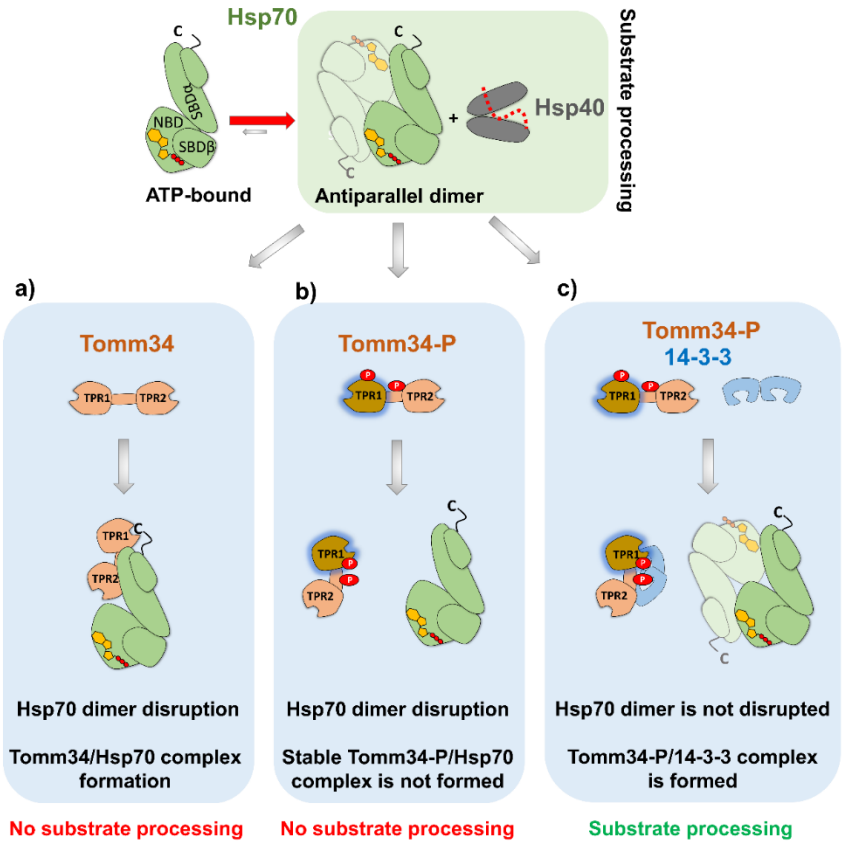

Obrázek 40. *Regulace ATP-dependentní interakce Hsp70 s Tomm34 skrze jeho fosforylaci a vazbu 14-3-3. ATP závislý Hsp70 dimer kooperuje za účelem zpracování substrátu s ko-chaperonem Hsp40. (a) Nefosforylovaný Tomm34 interaguje skrze svou TPR1 doménu s C-terminálním motivem EEVD Hsp70, čímž rozrušuje dimer Hsp70 a předchází zpracování substrátu. (b) PKA fosforylovaný Tomm34 (Tomm34-P) má vlivem přítomnosti S93-P destabilizovanou TPR1, čímž je narušeno interakční rozhraní s Hsp70-ATP. Navzdory tomu ho přechodně kontaktuje a rovněž ruší dimerní uspořádání s následným zpracováním substrátu. (c) Pokud je přítomen protein 14-3-3, interaguje s Tomm34-P, čímž je zachován Hsp70-ATP dimer a následně může dojít ke sbalení substrátu. (převzato z Publikace III – Trčka, 2020)*

4.4 Publikace IV

Enzymatická cytoprotektivní i chaperonová stabilizační funkce homodimerního flavoproteinu NQO1 je z velké části podmíněna jeho konkrétním ligačním stavem, kdy může vázat FAD, NAD(P)H, substráty nebo inhibitory, a který se odráží v jeho strukturním uspořádání. Ačkoli je k dispozici krystalová struktura pro holoformu s navázaným FAD ($NQO1_{HOLO}$) a formu s navázaným dikumarolem ($NQO1_{DIC}$) (*Obr. 41*), doposud nebyla k dispozici žádná vysoce rozlišená strukturní informace pro apostav ($NQO1_{APO}$) vzhledem k jeho dynamické povaze. Tuto strukturu a její dynamické chování jsme se proto rozhodli charakterizovat s využitím HDX-MS a srovnat se stavy $NQO1_{HOLO}$ a $NQO1_{DIC}$.

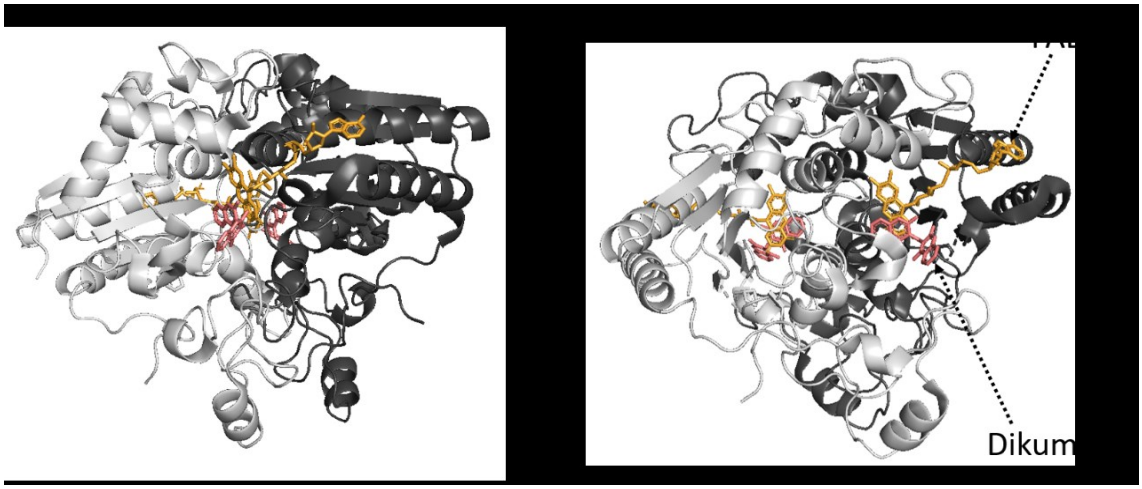

Obrázek 41. *Krystalová struktura dimeru NQO1 s navázaným FAD a dikumarolem. Ze strukturního modelu v levé části lze pozorovat lokalizaci aktivního centra s navázaným FAD (žlutá) a dikumarolem (růžová) na rozhraní obou protomerů NQO1 (různé odstíny šedé). V pravé části pak je vidět vazbu dikumarolu k isoalloxazinovému kruhu FAD skrze patrové interakce[127]. (PDB kód: 2F1O) (vytvořeno v PyMOLu)*

Před samotným provedením HDX-MS byla čistota purifikovaného proteinu ověřena separací pomocí SDS-PAGE a jeho specifická aktivita detekována spektrofotometricky po interakci s 2,6-dichlorfenolindofenolem (DCPIP; z angl. 2,6-dichlorophenolindophenol)[125]. Přímým nástřikem odsoleného NQO1 do MS byla následně změřena jeho intaktní monoisotopická hmotnost 32 428,6843 kDa (± 0,5 ppm) odpovídající hmotnosti konstruktu bez N-terminálního methioninu. Následně byla měřením nESI v apo- a holostavu potvrzena přítomnost dimeru.

S využitím techniky HDX-MS byla porovnávána míra deuterace pro NQO1 v apo- a holoformě a s navázaným dikumarolem. Analýzou profilů isotopových obálek jednotlivých peptidů bylo zjištěno, že téměř celý protein odpovídá kinetickému chování EX2, kdy je rychlost strukturní změny (k_{cl}) vyšší než rychlost HDX (k_{ch})

(viz Linderstrøm-Langův kinetický model (1), kap. 1.7.1, s. 42). Za předpokladu čisté EX2 kinetiky lze konstatovat, že velikost experimentální rychlostní konstanty pro HDX do určité míry odráží lokální stabilitu sekundární struktury proteinu. Nespadají sem pouze dvě oblasti vykazující velmi slabou úroveň smíšené kinetiky EXX zahrnující aminokyselinové zbytky 75–92 a 249–271.

Na základě znalosti krystalové struktury pro $NQO1_{DIC}$ (PDB kód: 2F1O[127]), která je téměř totožná s $NQO1_{HOLO}$ (PDB kód: 1DXQ[132]), jsme následně pozorovali úroveň deuterace v oblastech definujících vazebná místa pro FAD (FBS; z angl. FAD binding site) a dikumarol (DBS; z angl. Dicoumarol binding site) a rozhraní dimeru (MMI; z angl. Monomer:monomer interface). V rámci monomeru se FBS a DBS částečně překrývají a nacházejí se v bezprostřední blízkosti MMI. Analýzou míry inkorporace deuteria do varianty $NQO1_{APO}$ (*Obr. 42a* na s. 73) bylo po 3 hodinách inkubace pozorováno, že u většiny peptidů náležejících do klíčových oblastí FBS, DBS a MMI došlo k výměně více než 20 % amidických vodíků za deuterium, což poukazuje na vysoce dynamické uspořádání $NQO1_{APO}$, které není uzpůsobeno pro vazbu kofaktoru nebo inhibitoru. Zároveň byly identifikovány oblasti vykazující minimální úroveň inkorporace deuteria (méně než 20%), které jsou v rámci krystalu 2F1O lokalizovány hluboko uvnitř struktury a zahrnují helixy α1, α3 a α4 a β-listy β1, β3, β4 a β5. Lze tedy předpokládat, že právě tyto segmenty jsou zodpovědné za soudržnost dimerního uspořádání NQO1 v apostavu a tvoří tzv. minimální stabilní jádro dimeru $NQO1_{APO}$. Pro něj bylo již dříve v roztoku popsáno flexibilnější a extendované strukturní uspořádání oproti dimeru $NQO1_{HOLO}$[125,129].

Po vazbě FAD byla srovnáním $NQO1_{HOLO}$ vůči apoformě pozorována celková stabilizace struktury $NQO1_{HOLO}$ i v našem případě (*Obr. 42* na s. 73). Ta byla po 3 hodinách inkubace nejvýraznější právě v oblastech zahrnujících zbytky FBS – oblast smyček L1 (zahrnutá mimo FBS, také v MMI), L4 (kromě FBS je součástí i DBS a MMI) a helixu α5 (pouze součástí FBS). Dále pak k výrazné stabilizaci již v počátečních časech inkubace dochází i v oblastech β-listu β6, helixu α7 a smyčky L3, kdy regiony β6 a α7 nejsou součástí MMI, FBS ani DBS, zatímco L3 spoluutváří MMI. Srovnání rozdílu deuterace mezi $NQO1_{DIC}$ a $NQO1_{APO}$ (*Obr. 42* na s. 73) dále odhalilo, že inkorporace dikumarolu do $NQO1_{HOLO}$ vnesla do struktury ještě vyšší stupeň uspořádanosti. Kromě zvýšení úrovně stabilizace oblastí popsaných již v případě $NQO1_{HOLO}$, s výjimkou helixu α5, kde byl rozdíl v deuteraci oproti $NQO1_{APO}$ stejný jako v případě $NQO1_{HOLO}$, došlo

vlivem vazby dikumarolu dále k výrazné protekci v oblastech β-listu β4 a smyčky L5 (je součástí DBS i MMI).

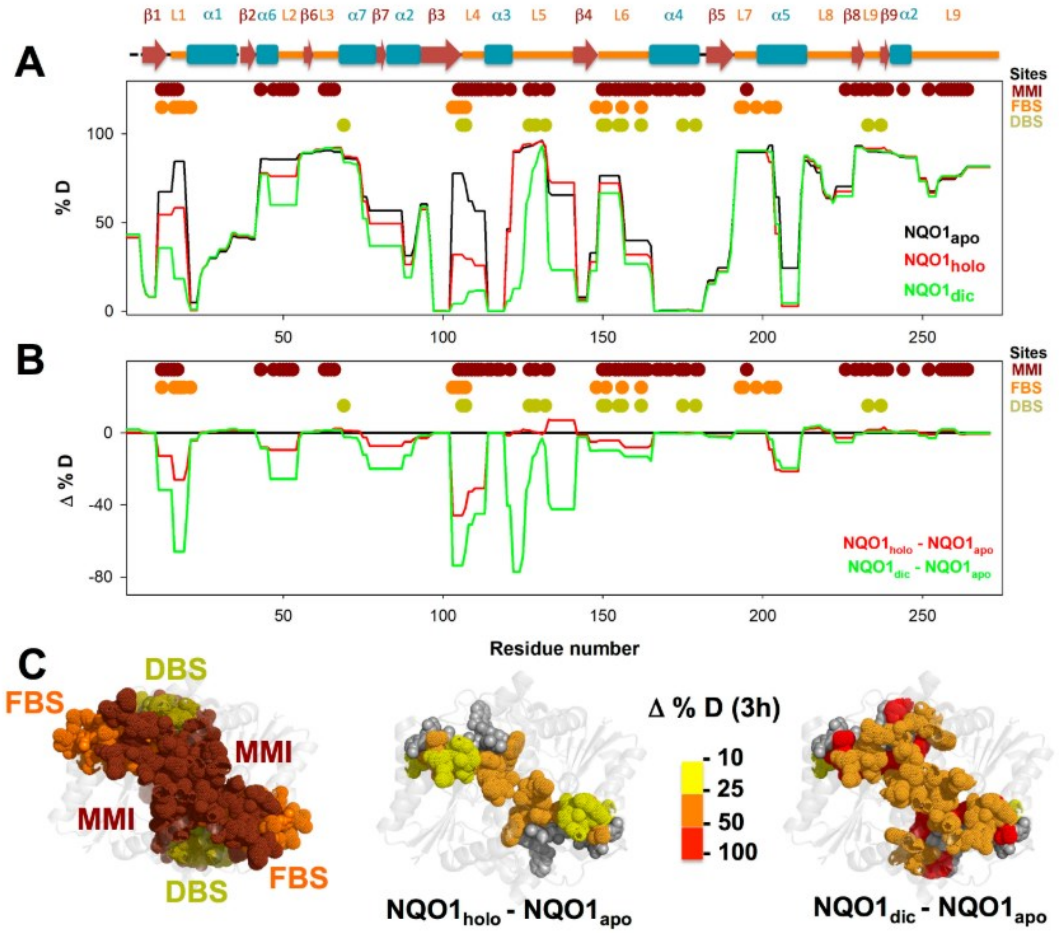

Obrázek 42. *Strukturní změny v různých ligačních stavech NQO1. (a) Graf znázorňující úroveň inkorporace deuteria (%D) (osa y) do konkrétních segmentů (osa x) NQO1 forem. Barevnými body jsou v horní části vyznačeny pozice vazebných míst pro FAD (FBS) a dikumarol (DBS) a aminokyseliny zahrnuté v tvorbě dimerizačního rozhraní (MMI). Nad grafem je vyznačena sekundární struktura NQO1. (b) Kvantifikace rozdíné deuterace segmentů (Δ%D) mezi $NQO1_{HOLO}$/$NQO1_{DIC}$ vs. $NQO1_{APO}$ odrážející jejich stabilizaci vlivem vazby FAD a dikumarolu. (c) V levé části jsou na struktuře NQO1 vyznačeny aminokyseliny tvořící FBS, DBS a MMI. Vprostřed a vpravo je pak barevným škálováním naznačena úroveň protekce těchto míst pro $NQO1_{HOLO}$/$NQO1_{DIC}$ vs. $NQO1_{APO}$. (převzato z Publikace IV – Vaňková, 2019)*

Abychom získali lepší představu o dynamice NQO1, provedli jsme výpočet rychlostní konstanty HDX (k_{slow}) pro jednotlivé segmenty proteinu vyjádřením ze vztahu (3):

$$\%\, D(t) = A_{burst} + A_{slow}.(1 - e^{-k_{slow}.t}) \qquad (3)$$

který popisuje kinetiku HDX reakce pomocí jednoduché funkce se dvěma kinetickými fázemi – velmi rychlou počáteční fází odehrávající se bezprostředně po iniciaci HDX reakce a charakterizovanou amplitudou A_{burst}, a pomalou fází ustavující

se po několika sekundách až minutách HDX reakce a charakterizovanou amplitudou A_{slow} a rychlostní konstantou I. řádu, k_{slow}. *%D(t)* je celkové procentuální množství vyměněných amidických vodíků za deuterium v daném čase, *t*. Na základě této kinetické analýzy bylo pro $NQO1_{APO}$ znovu pozorováno, že proteinové segmenty, které tvoří FBS, DBS a MMI a nejsou součástí tzv. minimálního jádra, mají oproti němu mnohem vyšší rychlost HDX s k_{slow} v řádech 10^{-1}–10^{-2} s^{-1}. Pro $NQO1_{HOLO}$ je rychlost HDX ve výše jmenovaných vazbou FAD stabilizovaných oblastech podílejících se na tvorbě MMI, FBS a DBS snížena 3–5×, pro $NQO1_{DIC}$ je toto snížení po vazbě dikumarolu ještě výraznější a to o 1–2 řády.

Rozdíly v kinetice jednotlivých segmentů po vazbě ligandu pro $NQO1_{HOLO}$ a $NQO1_{DIC}$ vůči $NQO1_{APO}$ byly kvantifikovány skrze parametr průměrné změny deuterace $\Delta\%D_{av}$, která byla vypočtena ze tří největších rozdílů mezi podmínkami v daném segmentu napříč všemi časovými body. Tato analýza dále přiblížila stabilizační vliv FAD a dikumarolu v dynamických regionech $NQO1_{APO}$, které spadají do MMI, FBS nebo DBS. Konkrétně se jedná o regiony 11–20 (smyčka L1, helix α1), 46–76 (smyčky L2 a L3, helix α7, β-list β6), 103–113 (β-list β3, smyčka L4), 149–165 (smyčka L6) a 191–211 (smyčka L7, helix α5). Pro dikumarol sem navíc spadají další dvě oblasti – 120–141 (smyčka L5) a 223–240 (smyčky L8 a L9, β-listy β8 a β9).

Strukturní charakterizace NQO1 proteinu s využitím HDX-MS v apo- a holostavu nebo s navázaným dikumarolem potvrdila dynamickou povahu $NOQ1_{APO}$ v roztoku a napomohla identifikovat stabilní jádro tohoto flexibilního uspořádání. Dále z porovnání s $NQO1_{HOLO}$ bylo definováno, jaké segmenty $NQO1_{APO}$ jsou vazbou FAD stabilizovány. Ještě výraznější stupeň stabilizace struktury NQO1 byl pozorován vlivem vazby inhibitoru, což nelze pozorovat z dostupných krystalografických modelů. Bylo pozorováno, že vazbou dikumarolu stabilizované oblasti se z velké části nacházejí na povrchu struktury proteinu a daleko od DBS, což by mohlo mít vliv na interakci s vazebnými partnery, kteří by mohli být stabilizováni skrze interakci s těmito povrchovými aminokyselinami v $NQO1_{HOLO}$. Zároveň tento náhled do dynamiky jednotlivých forem NQO1 a identifikace stabilního jádra proteinu napomáhá pochopit dopad mutací spojených s patologickými stavy nositele, jako např. v případě nejběžnějšího polymorfismu P187S, kdy se P187 nachází v oblasti β-listu β5, který je součástí minimálního jádra v $NQO1_{APO}$ a jeho mutace tak může mít dalekosáhlý strukturní dopad.

5 ZÁVĚREČNÉ SHRNUTÍ

Cílem této práce bylo s využitím metod strukturní hmotnostní spektrometrie, zejména HDX-MS, strukturně charakterizovat dynamická proteinová uspořádání podílející se na udržování proteostasy. Následující výsledky prezentované ve čtyřech publikacích, byly získány strukturní charakterizací inducibilní formy Hsp70 (HSPA1A), ko-chaperonu Tomm34 a proteinu NQO1:

- S využitím HDX-MS bylo charakterizováno evolučně konzervované dimerizační rozhraní ATP-dependentního dimeru HSPA1A a dále biofyzikálními a molekulárně biologickými technikami potvrzen význam dimerizace pro efektivní zpracování substrátu

- Analýzou mutačních variant HSPA1A byly s využitím HDX-MS identifikovány konzervované aminokyselinové zbytky podílející se zároveň na stabilizaci vysoko- i nízkoafinitní konformace HSPA1A a tudíž nepostradatelné pro zachování schopnosti alosterie

- S využitím HDX-MS byla popsána fosforylačně-dependentní destabilizace struktury Tomm34 narušující interakční rozhraní mezi Tomm34-P/Hsp70-ATP

- Strukturně byla charakterizována interakce mezi Tomm34-P/14-3-3γ, pro niž bylo pozorováno, že zamezuje interakci Tomm34-P/Hsp70-ATP a předchází tak rozrušení Hsp70-ATP dimeru, kterému je následně umožněno zpracovat substrát

- S pomocí HDX-MS byla charakterizována dynamika struktury $NQO1_{APO}$, informace v tomto rozlišení dříve nedostupná právě díky jeho vysoké flexibilitě

- Technikou HDX-MS byl pozorován stabilizační vliv vazby FAD ve struktuře $NQO1_{HOLO}$ a další stabilizace struktury po vazbě inhibitoru

SEZNAM PUBLIKACÍ

Publikace zahrnuté v této práci:

Trčka, F., Ďurech, M., **Vaňková, P.**, Chmelík, J., Martinková, V., Hausner, J., Kádek, A., Marcoux, J., Klumpler, T., Vojtěšek, B., Müller, P. & Man, P. Human Stress-inducible Hsp70 Has a High Propensity to Form ATP-dependent Antiparallel Dimers That Are Differentially Regulated by Cochaperone Binding. *Mol. Cell. Proteomics* **18**, 320–337 (2019). doi: 10.1074/mcp.RA118.001044

Vandová, V. & **Vaňková, P.**, Ďurech, M., Houser, J., Kavan, D., Man, P., Müller, P. & Trčka, F. HSPA1A conformational mutants reveal a conserved structural unit in Hsp70 proteins. *Biochim. Biophys. Acta - Gen. Subj.* **1864**, 129458 (2020). doi: 10.1016/j.bbagen.2019.129458

Trčka, F., Ďurech, M., **Vaňková, P.**, Vandová, V., Šimončík, O., Kavan, D., Vojtěšek, B., Müller, P. & Man, P. The interaction of the mitochondrial protein importer TOMM34 with HSP70 is regulated by TOMM34 phosphorylation and binding to 14-3-3 adaptors. *J. Biol. Chem.* **295**, 8928–8944 (2020). doi: 10.1074/jbc.RA120.012624

Vaňková, P., Salido, E., Timson, D. J., Man, P. & Pey, A. L. A Dynamic Core in Human NQO1 Controls the Functional and Stability Effects of Ligand Binding and Their Communication across the Enzyme Dimer. *Biomolecules* **9**, 1–17 (2019). doi: 10.3390/biom9110728

Ostatní publikace:

Ferofontov, A., **Vaňková, P.**, Man, P., Giladi, M. & Haitin, Y. Conserved cysteine dioxidation enhances membrane interaction of human Cl − intracellular channel 5. *FASEB J.* **34**, 9925–9940 (2020). doi: 10.1096/fj.202000399R

Lysniansky Bar-El, M., **Vaňková, P.**, Man, P., Haitin, Y. & Giladi, M. Structural basis of heterotetrameric assembly and disease mutations in the human cis-prenyltransferase complex. *Nat. Commun.* – akceptováno pro tisk

SEZNAM CITOVANÉ LITERATURY

1. Dill, K. A. & Chan, H. S. From Levinthal to pathways to funnels. *Nat. Struct. Mol. Biol.* **4**, 10–19 (1997).
2. Anfinsen, C. B. Principles that govern the folding of protein chains. *Science* **181**, 223–30 (1973).
3. Levinthal, C. Are there pathways for protein folding? *J. Chim. Phys.* **65**, 44–45 (1968).
4. Dill, K. A. & MacCallum, J. L. The protein-folding problem, 50 years on. *Science* **338**, 1042–6 (2012).
5. Zhou, H.-X., Rivas, G. & Minton, A. P. Macromolecular Crowding and Confinement: Biochemical, Biophysical, and Potential Physiological Consequences. *Annu. Rev. Biophys.* **37**, 375–397 (2008).
6. Rothman, J. E. Polypeptide chain binding proteins: Catalysts of protein folding and related processes in cells. *Cell* **59**, 591–601 (1989).
7. Kim, Y. E., Hipp, M. S., Bracher, A., Hayer-Hartl, M. & Ulrich Hartl, F. Molecular Chaperone Functions in Protein Folding and Proteostasis. *Annu. Rev. Biochem.* **82**, 323–355 (2013).
8. Ritossa, F. M. & Vonborstel, R. C. Chromosome Puffs in Drosophila Induced by Ribonuclease. *Science* **145**, 513–4 (1964).
9. Mirault, M. E., Goldschmidt-Clermont, M., Moran, L., Arrigo, A. P. & Tissières, A. The effect of heat shock on gene expression in Drosophila melanogaster. *Cold Spring Harb. Symp. Quant. Biol.* **42 Pt 2**, 819–27 (1978).
10. Yan, W., Schilke, B., Pfund, C., Walter, W., Kim, S. & Craig, E. A. Zuotin, a ribosome-associated DnaJ molecular chaperone. *EMBO J.* **17**, 4809–17 (1998).
11. Hundley, H. A.; Walter, W.; Bairstow, S. & Craig, E. A. Human Mpp11 J Protein: Ribosome-Tethered Molecular Chaperones Are Ubiquitous. *Science* **308**, 1032–1034 (2005).
12. Dudek, J., Pfeffer, S., Lee, P., Jung, M., Cavalié, A., Helms, V., Förster, F. & Zimmermann, R. Protein Transport into the Human Endoplasmic Reticulum. *J. Mol. Biol.* **427**, 1159–1175 (2015).
13. Schulz, C., Schendzielorz, A. & Rehling, P. Unlocking the presequence import pathway. *Trends Cell Biol.* **25**, 265–275 (2015).
14. Nillegoda, N. B., Kirstein, J., Szlachcic, A., Berynskyy, M., Stank, A., Stengel, F., Arnsburg, K., Gao, X., Scior, A., Aebersold, R., Guilbride, D. L., Wade, R. C., Morimoto, R. I., Mayer, M. P. & Bukau, B. Crucial HSP70 co-chaperone complex unlocks metazoan protein disaggregation. *Nature* **524**, 247–251 (2015).
15. Mayer, M. P. Hsp70 chaperone dynamics and molecular mechanism. *Trends Biochem. Sci.* **38**, 507–514 (2013).
16. Schulte, J. & Littleton, J. T. The biological function of the Huntingtin protein and its relevance to Huntington's Disease pathology. *Curr. Trends Neurol.* **5**, 65–78 (2011).
17. Radons, J. The human HSP70 family of chaperones: where do we stand? *Cell Stress Chaperones* **21**, 379–404 (2016).
18. Semenza, G. L. Hypoxia-Inducible Factors in Physiology and Medicine. *Cell* **148**, 399–408 (2012).
19. O'Dwyer, P. J., Yao, K. S., Ford, P., Godwin, A. K. & Clayton, M. Effects of hypoxia on detoxicating enzyme activity and expression in HT29 colon adenocarcinoma cells. *Cancer Res.* **54**, 3082–7 (1994).
20. Oh, E-T., Kim, J-W., Kim, J. M., Kim, S. J., Lee, J-S., Hong, S-S., Goodwin, J., Ruthenborg, R. J., Jung, M. G., Lee, H-J.,Lee, C-H., Park, E. S., Kim, C. & Park, H. J. NQO1 inhibits proteasome-mediated degradation of HIF-1α. *Nat. Commun.* **7**, 13593 (2016).
21. Beaver, S. K., Mesa-Torres, N., Pey, A. L. & Timson, D. J. NQO1: A target for the treatment of cancer and neurological diseases, and a model to understand loss of function disease mechanisms. *Biochim. Biophys. Acta - Proteins Proteomics* **1867**, 663–676 (2019).
22. Daugaard, M., Rohde, M. & Jäättelä, M. The heat shock protein 70 family: Highly homologous proteins with overlapping and distinct functions. *FEBS Lett.* **581**, 3702–3710 (2007).
23. Rosenzweig, R., Nillegoda, N. B., Mayer, M. P. & Bukau, B. The Hsp70 chaperone network. *Nat. Rev. Mol. Cell Biol.* **20**, 665–680 (2019).

24. Gupta, R. S. & Singh, B. Phylogenetic analysis of 70 kD heat shock protein sequences suggests a chimeric origin for the eukaryotic cell nucleus. *Curr. Biol.* **4**, 1104–1114 (1994).

25. Craig, E. A. & Marszalek, J. How Do J-Proteins Get Hsp70 to Do So Many Different Things? *Trends Biochem. Sci.* **42**, 355–368 (2017).

26. Fernández-Fernández, M. R., Gragera, M., Ochoa-Ibarrola, L., Quintana-Gallardo, L. & Valpuesta, J. M. Hsp70 - a master regulator in protein degradation. *FEBS Lett.* **591**, 2648–2660 (2017).

27. Kampinga, H. H., Hageman, J., Vos, M. J., Kubota, H., Tanguay, R. M., Bruford, E. A., Cheetham, M. E., Chen, B. & Hightower, L. E. Guidelines for the nomenclature of the human heat shock proteins. *Cell Stress Chaperones* **14**, 105–11 (2009).

28. Nylandsted, J., Gyrd-Hansen, M., Danielewicz, A., Fehrenbacher, N., Lademann, U., Høyer-Hansen, M., Weber, E., Multhoff, G., Rohde, M. & Jäättelä, M. Heat Shock Protein 70 Promotes Cell Survival by Inhibiting Lysosomal Membrane Permeabilization. *J. Exp. Med.* **200**, 425–435 (2004).

29. Yang, X., Wang, J., Zhou, Y., Wang,Y., Wang, S. & Zhang, W. Hsp70 promotes chemoresistance by blocking Bax mitochondrial translocation in ovarian cancer cells. *Cancer Lett.* **321**, 137–143 (2012).

30. Gao, Y., Han, C., Huang, H., Xin, Y., Xu, Y., Luo, L. & Yin, Z. Heat shock protein 70 together with its co-chaperone CHIP inhibits TNF-α induced apoptosis by promoting proteasomal degradation of apoptosis signal-regulating kinase1. *Apoptosis* **15**, 822–833 (2010).

31. Gunther, S., Ostheimer, C., Stangl, S., Specht, H. M., Mozes, P., Jesinghaus, M., Vordermark, D., Combs, S. E., Peltz, F., Jung, M. P. & Multhoff, G. Correlation of Hsp70 Serum Levels with Gross Tumor Volume and Composition of Lymphocyte Subpopulations in Patients with Squamous Cell and Adeno Non-Small Cell Lung Cancer. *Front. Immunol.* **6**, 556 (2015).

32. Rüdiger, S., Germeroth, L., Schneider-Mergener, J. & Bukau, B. Substrate specificity of the DnaK chaperone determined by screening cellulose-bound peptide libraries. *EMBO J.* **16**, 1501–7 (1997).

33. Flaherty, K. M., McKay, D. B., Kabsch, W. & Holmes, K. C. Similarity of the three-dimensional structures of actin and the ATPase fragment of a 70-kDa heat shock cognate protein. *Proc. Natl. Acad. Sci. U. S. A.* **88**, 5041–5 (1991).

34. Mayer, M. P. Intra-molecular pathways of allosteric control in Hsp70s. *Philos. Trans. R. Soc. Lond. B. Biol. Sci.* **373**, 20170183 (2018).

35. Zhu, X., Zhao, X., Burkholder, W. F., Gragerov, A., Ogata, C. M., Gottesman, M. E. & Hendrickson, W. A. Structural analysis of substrate binding by the molecular chaperone DnaK. *Science* **272**, 1606–14 (1996).

36. Schlecht, R., Erbse, A. H., Bukau, B. & Mayer, M. P. Mechanics of Hsp70 chaperones enables differential interaction with client proteins. *Nat. Struct. Mol. Biol.* **18**, 345–351 (2011).

37. Assimon, V. A., Southworth, D. R. & Gestwicki, J. E. Specific Binding of Tetratricopeptide Repeat Proteins to Heat Shock Protein 70 (Hsp70) and Heat Shock Protein 90 (Hsp90) Is Regulated by Affinity and Phosphorylation. *Biochemistry* **54**, 7120–31 (2015).

38. Schmid, D., Baici, A., Gehring, H. & Christen, P. Kinetics of molecular chaperone action. *Science* **263**, 971–3 (1994).

39. Qi, R., Sarbeng, E. B., Liu, Q., Le, K. Q., Xu, X., Xu, H., Yang, J., Wong, J. L., Vorvis, C., Hendrickson, W. A., Zhou, L. & Liu, Q. Allosteric opening of the polypeptide-binding site when an Hsp70 binds ATP. *Nat. Struct. Mol. Biol.* **20**, 900–7 (2013).

40. Kityk, R., Vogel, M., Schlecht, R., Bukau, B. & Mayer, M. P. Pathways of allosteric regulation in Hsp70 chaperones. *Nat. Commun.* **6**, 8308 (2015).

41. Kityk, R., Kopp, J., Sinning, I. & Mayer, M. P. Structure and Dynamics of the ATP-Bound Open Conformation of Hsp70 Chaperones. *Mol. Cell* **48**, 863–874 (2012).

42. Yang, J., Nune, M., Zong, Y., Zhou, L. & Liu, Q. Close and Allosteric Opening of the Polypeptide-Binding Site in a Human Hsp70 Chaperone BiP. *Structure* **23**, 2191–2203 (2015).

43. Yang, J., Zong, Y., Su, J., Li, H., Zhu, H., Columbus, L., Zhou, L. & Liu, Q. Conformation transitions of the polypeptide-binding pocket support an active substrate release from Hsp70s. *Nat. Commun.* **8**, 1201 (2017).

44. Liberek, K., Marszalek, J., Ang, D., Georgopoulos, C. & Zylicz, M. Escherichia coli DnaJ and GrpE heat shock proteins jointly stimulate ATPase activity of DnaK. *Proc. Natl. Acad. Sci. U. S. A.* **88**, 2874–8 (1991).
45. Buchberger, A., Valencia, A., McMacken, R., Sander, C. & Bukau, B. The chaperone function of DnaK requires the coupling of ATPase activity with substrate binding through residue E171. *EMBO J.* **13**, 1687–95 (1994).
46. Kampinga, H. H. & Craig, E. A. The HSP70 chaperone machinery: J proteins as drivers of functional specificity. *Nat. Rev. Mol. Cell Biol.* **11**, 579–92 (2010).
47. Rudiger, S.; Schneider-Mergner, J.; Bukau, B. Its substrate specificity characterizes the DnaJ co-chaperone as a scanning factor for the DnaK chaperone. *EMBO J.* **20**, 1042–1050 (2001).
48. Kityk, R., Kopp, J. & Mayer, M. P. Molecular Mechanism of J-Domain-Triggered ATP Hydrolysis by Hsp70 Chaperones. *Mol. Cell* **69**, 227-237.e4 (2018).
49. Vogel, M., Mayer, M. P. & Bukau, B. Allosteric regulation of Hsp70 chaperones involves a conserved interdomain linker. *J. Biol. Chem.* **281**, 38705–11 (2006).
50. Sarbeng, E. B., Liu, Q., Tian, X., Yang, J., Li, H., Wong, J. L., Zhou, L. & Liu, Q. A Functional DnaK Dimer Is Essential for the Efficient Interaction with Hsp40 Heat Shock Protein. *J. Biol. Chem.* **290**, 8849–8862 (2015).
51. Liu, Q., Li, H., Yang, Y., Tian, X., Su, J., Zhou, L. & Liu, Q. A disulfide-bonded DnaK dimer is maintained in an ATP-bound state. *Cell Stress Chaperones* **22**, 201–212 (2017).
52. Morgner, N., Schmidt, C., Beilsten-Edmands, V., Ebong, I., Patel, N. A., Clerico, E. M., Kirschke, E., Daturpalli, S., Jackson, S. E., Agard, D., & Robinson, C. V. Hsp70 Forms Antiparallel Dimers Stabilized by Post-translational Modifications to Position Clients for Transfer to Hsp90. *Cell Rep.* **11**, 759–769 (2015).
53. Zhuravleva, A., Clerico, E. M. & Gierasch, L. M. An interdomain energetic tug-of-war creates the allosterically active state in Hsp70 molecular chaperones. *Cell* **151**, 1296–307 (2012).
54. Liu, Q., Liang, C. & Zhou, L. Structural and functional analysis of the Hsp70/Hsp40 chaperone system. *Protein Sci.* **29**, 378–390 (2020).
55. Mayer, M. P. & Gierasch, L. M. Recent advances in the structural and mechanistic aspects of Hsp70 molecular chaperones. *J. Biol. Chem.* **294**, 2085–2097 (2019).
56. Li, Z., Hartl, F. U. & Bracher, A. Structure and function of Hip, an attenuator of the Hsp70 chaperone cycle. *Nat. Struct. Mol. Biol.* **20**, 929–935 (2013).
57. Velasco, L., Dublang, L., Moro, F. & Muga, A. The Complex Phosphorylation Patterns that Regulate the Activity of Hsp70 and Its Cochaperones. *Int. J. Mol. Sci.* **20**, 4122 (2019).
58. Biebl, M. M. & Buchner, J. Structure, Function, and Regulation of the Hsp90 Machinery. *Cold Spring Harb. Perspect. Biol.* **11**, a034017 (2019).
59. Chen, B., Zhong, D. & Monteiro, A. Comparative genomics and evolution of the HSP90 family of genes across all kingdoms of organisms. *BMC Genomics* **7**, 156 (2006).
60. Csermely, P., Schnaider, T., Soti, C., Prohászka, Z. & Nardai, G. The 90-kDa Molecular Chaperone Family. *Pharmacol. Ther.* **79**, 129–168 (1998).
61. Bardwell, J. C. & Craig, E. A. Ancient heat shock gene is dispensable. *J. Bacteriol.* **170**, 2977–83 (1988).
62. Tanaka, N. & Nakamoto, H. HtpG is essential for the thermal stress management in cyanobacteria. *FEBS Lett.* **458**, 117–123 (1999).
63. Honoré, F. A., Méjean, V. & Genest, O. Hsp90 Is Essential under Heat Stress in the Bacterium Shewanella oneidensis. *Cell Rep.* **19**, 680–687 (2017).
64. Taipale, M., Krykbaeva, I., Koeva, M., Kayatekin, C., Westover, K. D., Karras, G. I. & Lindquist, S. Quantitative analysis of HSP90-client interactions reveals principles of substrate recognition. *Cell* **150**, 987–1001 (2012).
65. Alexandrova, E. M., Yallowitz, A. R., Li, D., Xu, S., Schulz, R., Proia, D. A., Lozano, G., Dobbelstein, M. & Moll, U. M. Improving survival by exploiting tumour dependence on stabilized mutant p53 for treatment. *Nature* **523**, 352–356 (2015).
66. Scherrer, L. C, Dalman, F. C, Massa, E., Meshinchi, S. & Pratt, W. B. Structural and functional reconstitution of the glucocorticoid receptor-hsp90 complex. *J Biol Chem.* **265**, 21397-21400 (1990).

67. Pratt, W. B., Gehring, U. & Toft, D. O. Molecular chaperoning of steroid hormone receptors. *EXS.* **77**, 79–95 (Birkhäuser Basel, 1996).

68. Park, S. J., Suetsugu, S., Sagara, H. & Takenawa, T. HSP90 cross-links branched actin filaments induced by N-WASP and the Arp2/3 complex. *Genes to Cells* **12**, 611–622 (2007).

69. Weis, F., Moullintraffort, L., Heichette, C., Chrétien, D. & Garnier, C. The 90-kDa Heat Shock Protein Hsp90 Protects Tubulin against Thermal Denaturation. *J. Biol. Chem.* **285**, 9525–9534 (2010).

70. Krtková, J., Zimmermann, A., Schwarzerová, K. & Nick, P. Hsp90 binds microtubules and is involved in the reorganization of the microtubular network in angiosperms. *J. Plant Physiol.* **169**, 1329–1339 (2012).

71. Savitski, M. M., Zinn, N., Faelth-Savitski, M., Poeckel, D., Gade, S., Becher, I., Muelbaier, M., Wagner, A. J., Strohmer, K., Werner, T., Melchert, S., Petretich, M., Rutkowska, A., Vappiani, J., Franken, H., Steidel, M., Sweetman, G. M., Gilan, O., Lam, E. Y. N., Dawson, M. A., Prinjha, R. K., Grandi, P., Bergamini, G. & Bantscheff, M. Multiplexed Proteome Dynamics Profiling Reveals Mechanisms Controlling Protein Homeostasis. *Cell* **173**, 260-274 (2018).

72. Sima, S. & Richter, K. Regulation of the Hsp90 system. *Biochim. Biophys. Acta - Mol. Cell Res.* **1865**, 889–897 (2018).

73. Genest, O., Wickner, S. & Doyle, S. M. Hsp90 and Hsp70 chaperones: Collaborators in protein remodeling. *J. Biol. Chem.* **294**, 2109–2120 (2019).

74. Radli, M. & Rüdiger, S. G. D. Dancing with the Diva: Hsp90–Client Interactions. *J. Mol. Biol.* **430**, 3029–3040 (2018).

75. Tsutsumi, S., Mollapour, M., Prodromou, C., Lee, C.-T., Panaretou, B., Yoshida, S., Mayer, M. P. & Neckers, L. M. Charged linker sequence modulates eukaryotic heat shock protein 90 (Hsp90) chaperone activity. *Proc. Natl. Acad. Sci.* **109**, 2937–2942 (2012).

76. Daturpalli, S., Knieß, R. A., Lee, C.-T. & Mayer, M. P. Large Rotation of the N-terminal Domain of Hsp90 Is Important for Interaction with Some but Not All Client Proteins. *J. Mol. Biol.* **429**, 1406–1423 (2017).

77. Krukenberg, K. A., Förster, F., Rice, L. M., Sali, A. & Agard, D. A. Multiple Conformations of E. coli Hsp90 in Solution: Insights into the Conformational Dynamics of Hsp90. *Structure* **16**, 755–765 (2008).

78. Saibil, H. Chaperone machines for protein folding, unfolding and disaggregation. *Nat. Rev. Mol. Cell Biol.* **14**, 630–642 (2013).

79. Shiau, A. K., Harris, S. F., Southworth, D. R. & Agard, D. A. Structural Analysis of E. coli hsp90 Reveals Dramatic Nucleotide-Dependent Conformational Rearrangements. *Cell* **127**, 329–340 (2006).

80. Richter, K., Muschler, P., Hainzl, O. & Buchner, J. Coordinated ATP Hydrolysis by the Hsp90 Dimer. *J. Biol. Chem.* **276**, 33689–33696 (2001).

81. Ali, M. M. U., Roe, S. M., Vaughan, C. K., Meyer, P., Panaretou, B., Piper, P. W., Prodromou, C. & Pearl, L. H. Crystal structure of an Hsp90–nucleotide–p23/Sba1 closed chaperone complex. *Nature* **440**, 1013–1017 (2006).

82. Dollins, D. E., Warren, J. J., Immormino, R. M. & Gewirth, D. T. Structures of GRP94-Nucleotide Complexes Reveal Mechanistic Differences between the hsp90 Chaperones. *Mol. Cell* **28**, 41–56 (2007).

83. Lavery, L. A., Partridge, J. R., Ramelot, T. A., Elnatan, D., Kennedy, M. A. & Agard, D. A. Structural Asymmetry in the Closed State of Mitochondrial Hsp90 (TRAP1) Supports a Two-Step ATP Hydrolysis Mechanism. *Mol. Cell* **53**, 330–343 (2014).

84. Mishra, P. & Bolon, D. N. A. Designed Hsp90 Heterodimers Reveal an Asymmetric ATPase-Driven Mechanism In Vivo. *Mol. Cell* **53**, 344–350 (2014).

85. Mayer, M. P. & Le Breton, L. Hsp90: Breaking the Symmetry. *Mol. Cell* **58**, 8–20 (2015).

86. Li, J., Soroka, J. & Buchner, J. The Hsp90 chaperone machinery: Conformational dynamics and regulation by co-chaperones. *Biochim. Biophys. Acta - Mol. Cell Res.* **1823**, 624–635 (2012).

87. Sahasrabudhe, P., Rohrberg, J., Biebl, M. M., Rutz, D. A. & Buchner, J. The Plasticity of the Hsp90 Co-chaperone System. *Mol. Cell* **67**, 947-961.e5 (2017).

88. Richter, K., Muschler, P., Hainzl, O., Reinstein, J. & Buchner, J. Sti1 is a non-competitive inhibitor of the Hsp90 ATPase. Binding prevents the N-terminal dimerization reaction during the atpase cycle. *J. Biol. Chem.* **278**, 10328–33 (2003).

89. Röhl, A., Wengler, D., Madl, T., Lagleder, S., Tippel, F., Hermann, M., Hendrix, J., Richter, K., Hack, G., Schmid, A. B., Kessler, H., Lamb, D. C. & Buchner, J. Hsp90 regulates the dynamics of its cochaperone Sti1 and the transfer of Hsp70 between modules. *Nat. Commun.* **6**, 6655 (2015).

90. Silverstein, A. M., Galigniana, M. D., Chen, M.-S., Owens-Grillo, J. K., Chinkers, M. & Pratt, W. B. Protein Phosphatase 5 Is a Major Component of Glucocorticoid Receptor·hsp90 Complexes with Properties of an FK506-binding Immunophilin. *J. Biol. Chem.* **272**, 16224–16230 (1997).

91. Stepanova, L., Leng, X., Parker, S. B. & Harper, J. W. Mammalian p50Cdc37 is a protein kinase-targeting subunit of Hsp90 that binds and stabilizes Cdk4. *Genes Dev.* **10**, 1491–1502 (1996).

92. Li, J., Richter, K., Reinstein, J. & Buchner, J. Integration of the accelerator Aha1 in the Hsp90 co-chaperone cycle. *Nat. Struct. Mol. Biol.* **20**, 326–31 (2013).

93. Halpin, J. C., Huang, B., Sun, M. & Street, T. O. Crowding activates heat shock protein 90. *J. Biol. Chem.* **291**, 6447–6455 (2016).

94. Meyer, P., Prodromou, C., Liao, C., Hu, B., Roe, S. M., Vaughan, C. K., Vlasic, I., Panaretou, B., Piper, P. W. & Pearl, L. H. Structural basis for recruitment of the ATPase activator Aha1 to the Hsp90 chaperone machinery. *EMBO J.* **23**, 511–9 (2004).

95. Didenko, T., Duarte, A. M. S., Karagöz, G. E. & Rüdiger, S. G. D. Hsp90 structure and function studied by NMR spectroscopy. *Biochim. Biophys. Acta* **1823**, 636–47 (2012).

96. Retzlaff, M., Hagn, F., Mitschke, L., Hessling, M., Gugel, F., Kessler, H., Richter, K. & Buchner, J. Asymmetric Activation of the Hsp90 Dimer by Its Cochaperone Aha1. *Mol. Cell* **37**, 344–354 (2010).

97. Brehme, M., Voisine, C., Rolland, T., Wachi, S., Soper, J. H., Zhu, Y., Orton, K., Villella, A., Garza, D., Vidal, M., Ge, H. & Morimoto, R. I. A Chaperome Subnetwork Safeguards Proteostasis in Aging and Neurodegenerative Disease. *Cell Rep.* **9**, 1135–1150 (2014).

98. Graham, J. B., Canniff, N. P. & Hebert, D. N. TPR-containing proteins control protein organization and homeostasis for the endoplasmic reticulum. *Crit. Rev. Biochem. Mol. Biol.* **54**, 103–118 (2019).

99. D'Andrea, L. D. & Regan, L. TPR proteins: the versatile helix. *Trends Biochem. Sci.* **28**, 655–62 (2003).

100. Scheufler, C., Brinker, A., Bourenkov, G., Pegoraro, S., Moroder, L., Bartunik, H., Hartl, F. U. & Moarefi, I. Structure of TPR domain-peptide complexes: critical elements in the assembly of the Hsp70-Hsp90 multichaperone machine. *Cell* **101**, 199–210 (2000).

101. Brinker, A., Scheufler, C., von der Mülbe, F., Fleckenstein, B., Herrmann, C., Jung, G., Moarefi, I. & Hartl, F. U. Ligand discrimination by TPR domains. Relevance and selectivity of EEVD-recognition in Hsp70 x Hop x Hsp90 complexes. *J. Biol. Chem.* **277**, 19265–75 (2002).

102. Röhl, A., Tippel, F., Bender, E., Schmid, A. B., Richter, K., Madl, T. & Buchner, J. Hop/Sti1 phosphorylation inhibits its co-chaperone function. *EMBO Rep.* **16**, 240–249 (2015).

103. Müller, P., Ruckova, E., Halada, P., Coates, P. J., Hrstka, R., Lane, D. P. & Vojtesek, B. C-terminal phosphorylation of Hsp70 and Hsp90 regulates alternate binding to co-chaperones CHIP and HOP to determine cellular protein folding/degradation balances. *Oncogene* **32**, 3101–10 (2013).

104. Schmid, A. B., Lagleder, S., Gräwert, M. A., Röhl, A., Hagn, F., Wandinger, S. K., Cox, M. B., Demmer, O., Richter, K., Groll, M., Kessler, H. & Buchner, J. The architecture of functional modules in the Hsp90 co-chaperone Sti1/Hop. *EMBO J.* **31**, 1506–1517 (2012).

105. Southworth, D. R. & Agard, D. A. Client-Loading Conformation of the Hsp90 Molecular Chaperone Revealed in the Cryo-EM Structure of the Human Hsp90:Hop Complex. *Mol. Cell* **42**, 771–781 (2011).

106. Richter, K., Muschler, P., Hainzl, O., Reinstein, J. & Buchner, J. Sti1 Is a Non-competitive Inhibitor of the Hsp90 ATPase. *J. Biol. Chem.* **278**, 10328–10333 (2003).

107. Kajiro, M., Hirota, R., Nakajima, Y., Kawanowa, K., So-ma, K., Ito, I., Yamaguchi, Y., Ohie, S., Kobayashi, Y., Seino, Y., Kawano, M., Kawabe, Y., Takei, H., Hayashi, S., Kurosumi, M., Murayama, A., Kimura, K. & Yanagisawa, J. The ubiquitin ligase CHIP acts as an upstream regulator of oncogenic pathways. *Nat. Cell Biol.* **11**, 312–9 (2009).

108. Soss, S. E., Yue, Y., Dhe-Paganon, S. & Chazin, W. J. E2 conjugating enzyme selectivity and requirements for function of the E3 ubiquitin ligase CHIP. *J. Biol. Chem.* **286**, 21277–86 (2011).

109. McDonough, H. & Patterson, C. CHIP: a link between the chaperone and proteasome systems. *Cell Stress Chaperones* **8**, 303 (2003).

110. Edkins, A. L. CHIP: A Co-chaperone for Degradation by the Proteasome. in *The Networking of Chaperones by Co-chaperones* vol. 78 219–242 (2015).

111. Zhang, M., Windheim, M., Roe, M. S., Peggie, M., Cohen, P., Prodromou, C. & Pearl, L. H. Chaperoned ubiquitylation--crystal structures of the CHIP U box E3 ubiquitin ligase and a CHIP-Ubc13-Uev1a complex. *Mol. Cell* **20**, 525–38 (2005).

112. Xu, Z., Kohli, E., Devlin, K. I., Bold, M., Nix, J. C. & Misra, S. Interactions between the quality control ubiquitin ligase CHIP and ubiquitin conjugating enzymes. *BMC Struct. Biol.* **8**, 26 (2008).

113. Graf, C., Stankiewicz, M., Nikolay, R. & Mayer, M. P. Insights into the Conformational Dynamics of the E3 Ubiquitin Ligase CHIP in Complex with Chaperones and E2 Enzymes. *Biochemistry* **49**, 2121–2129 (2010).

114. VanPelt, J. & Page, R. C. Unraveling the CHIP:Hsp70 complex as an information processor for protein quality control. *Biochim. Biophys. acta. Proteins proteomics* **1865**, 133–141 (2017).

115. Faou, P. & Hoogenraad, N. J. Tom34: a cytosolic cochaperone of the Hsp90/Hsp70 protein complex involved in mitochondrial protein import. *Biochim. Biophys. Acta* **1823**, 348–57 (2012).

116. Trcka, F., Durech, M., Man, P., Hernychova, L., Müller, P. & Vojtesek, B. The assembly and intermolecular properties of the Hsp70-Tomm34-Hsp90 molecular chaperone complex. *J. Biol. Chem.* **289**, 9887–901 (2014).

117. Durech, M., Trcka, F., Man, P., Blackburn, E. A., Hernychova, L., Dvorakova, P., Coufalova, D., Kavan, D., Vojtesek, B. & Müller, P. Novel Entropically Driven Conformation-specific Interactions with Tomm34 Protein Modulate Hsp70 Protein Folding and ATPase Activities. *Mol. Cell. Proteomics* **15**, 1710–27 (2016).

118. Siegel, D., Dehn, D. D., Bokatzian, S. S., Quinn, K., Backos, D. S., Di Francesco, A., Bernier, M., Reisdorph, N., de Cabo, R. & Ross, D. Redox modulation of NQO1. *PLoS One* **13**, e0190717 (2018).

119. Tedeschi, G., Chen, S. & Massey, V. DT-diaphorase. *J. Biol. Chem.* **270**, 1198–1204 (1995).

120. Jaiswal, A. K. Regulation of genes encoding NAD(P)H:quinone oxidoreductases. *Free Radic. Biol. Med.* **29**, 254–262 (2000).

121. Ross, D. & Siegel, D. NQO1 in protection against oxidative stress. *Curr. Opin. Toxicol.* **7**, 67–72 (2018).

122. Waleh, N., Calaoagan, J., Murphy, B. J., Knapp, A. M., Sutherland, R. M. & Laderoute, K. R. The redox-sensitive human antioxidant responsive element induces gene expression under low oxygen conditions. *Carcinogenesis* **19**, 1333–1337 (1998).

123. Moscovitz, O., Tsvetkov, P., Hazan, N., Michaelevski, I., Keisar, H., Ben-Nissan, G., Shaul, Y. & Sharon, M. A mutually inhibitory feedback loop between the 20S proteasome and its regulator, NQO1. *Mol. Cell* **47**, 76–86 (2012).

124. Lata, S., Ali, A., Sood, V., Raja, R. & Banerjea, A. C. HIV-1 Rev downregulates Tat expression and viral replication via modulation of NAD(P)H:quinine oxidoreductase 1 (NQO1). *Nat. Commun.* **6**, 7244 (2015).

125. Medina-Carmona, E., Neira, J. L., Salido, E., Fuchs, J. E., Palomino-Morales, R., Timson, D. J. & Pey, A. L. Site-to-site interdomain communication may mediate different loss-of-function mechanisms in a cancer-associated NQO1 polymorphism. *Sci. Rep.* **7**, 44532 (2017).

126. Cullen, J. J., Hinkhouse, M. M., Grady, M., Gaut, A. W., Liu, J., Zhang, Y. P., Weydert, C. J. D., Domann, F. E. & Oberley, L. W. Dicumarol inhibition of NADPH:quinone oxidoreductase induces growth inhibition of pancreatic cancer via a superoxide-mediated mechanism. *Cancer Res.* **63**, 5513–20 (2003).

127. Asher, G., Dym, O., Tsvetkov, P., Adler, J. & Shaul, Y. The crystal structure of NAD(P)H quinone oxidoreductase 1 in complex with its potent inhibitor dicoumarol. *Biochemistry* **45**, 6372–8 (2006).

128. Li, R., Bianchet, M. A., Talalay, P. & Amzel, L. M. The three-dimensional structure of NAD(P)H:quinone reductase, a flavoprotein involved in cancer chemoprotection and chemotherapy: mechanism of the two-electron reduction. *Proc. Natl. Acad. Sci. U. S. A.* **92**, 8846–50 (1995).

129. Medina-Carmona, E., Palomino-Morales, R. J., Fuchs, J. E., Padin-Gonzalez, E., Mesa-Torres, N., Salido, E., Timson, D. J. & Pey, A. L. Conformational dynamics is key to understanding loss-of-function of NQO1 cancer-associated polymorphisms and its correction by pharmacological ligands. *Sci. Rep.* **6**, 20331 (2016).

130. Medina-Carmona, E., Rizzuti, B., Martin-Escolano, R., Pacheco-Garcia, J. L., Mesa-Torres, N., Neira, J. L., Guzzi, R. & Pey, A. L. Phosphorylation compromises FAD binding and intracellular stability of wild-type and cancer-associated NQO1: Insights into flavo-proteome stability. *Int. J. Biol. Macromol.* **125**, 1275–1288 (2019).

131. Martínez-Limón, A., Alriquet, M., Lang, W.-H., Calloni, G., Wittig, I. & Vabulas, R. M. Recognition of enzymes lacking bound cofactor by protein quality control. *Proc. Natl. Acad. Sci.* **113**, 12156–12161 (2016).

132. Faig, M., Bianchet, M. A., Talay, P., Chen, S., Winski, S., Ross, D. & Amzel, L. M. Structures of recombinant human and mouse NAD(P)H:quinone oxidoreductases: species comparison and structural changes with substrate binding and release. *Proc. Natl. Acad. Sci. U. S. A.* **97**, 3177–82 (2000).

133. Lienhart, W.-D., Gudipati, V., Uhl, M. K., Binter, A., Pulido, S. A., Saf, R., Zangger, K., Gruber, K. & Macheroux, P. Collapse of the native structure caused by a single amino acid exchange in human NAD(P)H:quinone oxidoreductase(1.). *FEBS J.* **281**, 4691–4704 (2014).

134. Siegel, D., Anwar, A., Winski, S. L., Kepa, J. K., Zolman, K. L. & Ross, D. Rapid Polyubiquitination and Proteasomal Degradation of a Mutant Form of NAD(P)H:Quinone Oxidoreductase 1. *Mol. Pharmacol.* **59**, 263–268 (2001).

135. Lienhart, W.-D., Strandback, E., Gudipati, V., Koch, K., Binter, A., Uhl, M. K., Rantasa, D. M., Bourgeois, B., Madl, T., Zangger, K., Gruber, K. & Macheroux, P. Catalytic competence, structure and stability of the cancer-associated R139W variant of the human NAD(P)H:quinone oxidoreductase 1 (NQO1). *FEBS J.* **284**, 1233–1245 (2017).

136. Pey, A. L., Megarity, C. F. & Timson, D. J. NAD(P)H quinone oxidoreductase (NQO1): an enzyme which needs just enough mobility, in just the right places. *Biosci. Rep.* **39**, (2019).

137. Luo, S., Kang, S. S., Wang, Z.-H., Liu, X., Day, J. X., Wu, Z., Peng, J., Xiang, D., Springer, W. & Ye, K. Akt Phosphorylates NQO1 and Triggers its Degradation, Abolishing Its Antioxidative Activities in Parkinson's Disease. *J. Neurosci.* **39**, 7291–7305 (2019).

138. Verma, R., Chen, S., Feldman, R., Schieltz, D, Yates, J., Dohmen, J. & Deshaies, R. J. Proteasomal proteomics: identification of nucleotide-sensitive proteasome-interacting proteins by mass spectrometric analysis of affinity-purified proteasomes. *Mol. Biol. Cell* **11**, 3425–39 (2000).

139. Saeki, Y. & Tanaka, K. Assembly and function of the proteasome. *Methods Mol. Biol.* **832**, 315–37 (2012).

140. Ballinger, C. A., Connell, P., Wu, Y., Hu, Z., Thompson, L. J., Yin, L.-Y. & Patterson, C. Identification of CHIP, a Novel Tetratricopeptide Repeat-Containing Protein That Interacts with Heat Shock Proteins and Negatively Regulates Chaperone Functions. *Mol. Cell. Biol.* **19**, 4535–4545 (1999).

141. Seufert, W. & Jentsch, S. Ubiquitin-conjugating enzymes UBC4 and UBC5 mediate selective degradation of short-lived and abnormal proteins. *EMBO J.* **9**, 543–50 (1990).

142. Murata, S., Minami, Y., Minami, M., Chiba, T. & Tanaka, K. CHIP is a chaperone-dependent E3 ligase that ubiquitylates unfolded protein. *EMBO Rep.* **2**, 1133–8 (2001).

143. Jacobson, A. D., Zhang, N.-Y., Xu, P., Han, K.-J., Noone, S., Peng, J. & Liu, C.-W. The lysine 48 and lysine 63 ubiquitin conjugates are processed differently by the 26 s proteasome. *J. Biol. Chem.* **284**, 35485–94 (2009).

144. Lüders, J., Demand, J. & Höhfeld, J. The Ubiquitin-related BAG-1 Provides a Link between the Molecular Chaperones Hsc70/Hsp70 and the Proteasome. *J. Biol. Chem.* **275**, 4613–4617 (2000).

145. Demand, J., Alberti, S., Patterson, C. & Höhfeld, J. Cooperation of a ubiquitin domain protein and an E3 ubiquitin ligase during chaperone/proteasome coupling. *Curr. Biol.* **11**, 1569–77 (2001).

146. Alberti, S., Demand, J., Esser, C., Emmerich, N., Schild, H. & Hohfeld, J. Ubiquitylation of BAG-1 suggests a novel regulatory mechanism during the sorting of chaperone substrates to the proteasome. *J. Biol. Chem.* **277**, 45920–7 (2002).

147. Adler, J., Reuven, N., Kahana, C. & Shaul, Y. c-Fos Proteasomal Degradation Is Activated by a Default Mechanism, and Its Regulation by NAD(P)H:Quinone Oxidoreductase 1 Determines c-Fos Serum Response Kinetics. *Mol. Cell. Biol.* **30**, 3767–3778 (2010).

148. Gamerdinger, M., Hajieva, P., Kaya, A. M., Wolfrum, U., Hartl, F. U. & Behl, C. Protein quality control during aging involves recruitment of the macroautophagy pathway by BAG3. *EMBO J.* **28**, 889–901 (2009).

149. Cheng, X.-R., Zhou, W.-X., Zhang, Y.-X., Zhou, D.-S., Yang, R.-F. & Chen, L.-F. Differential gene expression profiles in the hippocampus of senescence-accelerated mouse. *Neurobiol. Aging* **28**, 497–506 (2007).

150. Tsvetkov, P., Adamovich, Y., Elliott, E. & Shaul, Y. E3 ligase STUB1/CHIP regulates NAD(P)H:quinone oxidoreductase 1 (NQO1) accumulation in aged brain, a process impaired in certain Alzheimer disease patients. *J. Biol. Chem.* **286**, 8839–45 (2011).

151. Friguet, B. Oxidized protein degradation and repair in ageing and oxidative stress. *FEBS Lett.* **580**, 2910–2916 (2006).

152. Tasset, I. & Cuervo, A. M. Role of chaperone-mediated autophagy in metabolism. *FEBS J.* **283**, 2403–2413 (2016).

153. Cuervo, A. M. & Dice, J. F. A Receptor for the Selective Uptake and Degradation of Proteins by Lysosomes. *Science (80-.).* **273**, 501–503 (1996).

154. Bandyopadhyay, U., Kaushik, S., Varticovski, L. & Cuervo, A. M. The Chaperone-Mediated Autophagy Receptor Organizes in Dynamic Protein Complexes at the Lysosomal Membrane. *Mol. Cell. Biol.* **28**, 5747–5763 (2008).

155. Bandyopadhyay, U., Sridhar, S., Kaushik, S., Kiffin, R. & Cuervo, A. M. Identification of Regulators of Chaperone-Mediated Autophagy. *Mol. Cell* **39**, 535–547 (2010).

156. Sahu, R., Kaushik, S., Clement, C. C., Cannizzo, E. S., Scharf, B., Follenzi, A., Potolicchio, I., Nieves, E., Cuervo, A. M. & Santambrogio, L. Microautophagy of Cytosolic Proteins by Late Endosomes. *Dev. Cell* **20**, 131–139 (2011).

157. Zhang, H. & Baehrecke, E. H. Eaten alive: novel insights into autophagy from multicellular model systems. *Trends Cell Biol.* **25**, 376–387 (2015).

158. Kraft, C., Peter, M. & Hofmann, K. Selective autophagy: ubiquitin-mediated recognition and beyond. *Nat. Cell Biol.* **12**, 836–841 (2010).

159. Rauch, J. N., Tse, E., Freilich, R., Mok, S.-A., Makley, L. N., Southworth, D. R. & Gestwicki, J. E. BAG3 Is a Modular, Scaffolding Protein that physically Links Heat Shock Protein 70 (Hsp70) to the Small Heat Shock Proteins. *J. Mol. Biol.* **429**, 128–141 (2017).

160. Aviram, N. & Schuldiner, M. Targeting and translocation of proteins to the endoplasmic reticulum at a glance. *J. Cell Sci.* **130**, 4079–4085 (2017).

161. Denks, K., Vogt, A., Sachelaru, I., Petriman, N.-A., Kudva, R. & Koch, H.-G. The Sec translocon mediated protein transport in prokaryotes and eukaryotes. *Mol. Membr. Biol.* **31**, 58–84 (2014).

162. Becker, T., Song, J. & Pfanner, N. Versatility of Preprotein Transfer from the Cytosol to Mitochondria. *Trends Cell Biol.* **29**, 534–548 (2019).

163. Ramage, L., Junne, T., Hahne, K., Lithgow, T. & Schatz, G. Functional cooperation of mitochondrial protein import receptors in yeast. *EMBO J.* **12**, 4115–23 (1993).

164. Avendaño-Monsalve, M. C., Ponce-Rojas, J. C. & Funes, S. From cytosol to mitochondria: the beginning of a protein journey. *Biol. Chem.* **401**, 645–661 (2020).

165. Harbauer, A. B., Zahedi, R. P., Sickmann, A., Pfanner, N. & Meisinger, C. The Protein Import Machinery of Mitochondria—A Regulatory Hub in Metabolism, Stress, and Disease. *Cell Metab.* **19**, 357–372 (2014).

166. Zemanovic, S., Ivanov, M. V., Ivanova, L. V., Bhatnagar, A., Michalkiewicz, T., Teng, R.-J., Kumar, S., Rathore, R., Pritchard, K. A., Konduri, G. G. & Afolayan, A. J. Dynamic Phosphorylation of the C Terminus of Hsp70 Regulates the Mitochondrial Import of SOD2 and

Redox Balance. *Cell Rep.* **25**, 2605-2616.e7 (2018).

167. Schmidt, O., Harbauer, A. B., Rao, S., Eyrich, B., Zahedi, R. P., Stojanovski, D., Schönfisch, B., Guiard, B., Sickmann, A., Pfanner, N. & Meisinger, C. Regulation of Mitochondrial Protein Import by Cytosolic Kinases. *Cell* **144**, 227–239 (2011).
168. Blom, N., Gammeltoft, S. & Brunak, S. Sequence and structure-based prediction of eukaryotic protein phosphorylation sites. *J. Mol. Biol.* **294**, 1351–62 (1999).
169. Gardino, A. K., Smerdon, S. J. & Yaffe, M. B. Structural determinants of 14-3-3 binding specificities and regulation of subcellular localization of 14-3-3-ligand complexes: a comparison of the X-ray crystal structures of all human 14-3-3 isoforms. *Semin. Cancer Biol.* **16**, 173–82 (2006).
170. Bustos, D. M. & Iglesias, A. A. Intrinsic disorder is a key characteristic in partners that bind 14-3-3 proteins. *Proteins* **63**, 35–42 (2006).
171. Hachiya, N., Alam, R., Sakasegawa, Y., Sakaguchi, M., Mihara, K. & Omura, T. A mitochondrial import factor purified from rat liver cytosol is an ATP-dependent conformational modulator for precursor proteins. *EMBO J.* **1**, 1–579 (1993).
172. Komiya, T., Hachiya, N., Sakaguchi, M., Omura, T. & Mihara, K. Recognition of mitochondria-targeting signals by a cytosolic import stimulation factor, MSF. *J. Biol. Chem.* **269**, 30893–7 (1994).
173. Anusevicius, Z., Sarlauskas, J. & Cenas, N. Two-electron reduction of quinones by rat liver NAD(P)H:quinone oxidoreductase: quantitative structure-activity relationships. *Arch. Biochem. Biophys.* **404**, 254–62 (2002).
174. Bolton, J. L., Trush, M. A., Penning, T. M., Dryhurst, G. & Monks, T. J. Role of quinones in toxicology. *Chem. Res. Toxicol.* **13**, 135–60 (2000).
175. Marcoux, J. & Cianférani, S. Towards integrative structural mass spectrometry: Benefits from hybrid approaches. *Methods* **89**, 4–12 (2015).
176. Politis, A. & Borysik, A. J. Assembling the pieces of macromolecular complexes: Hybrid structural biology approaches. *Proteomics* **15**, 2792–803 (2015).
177. Oganesyan, I., Lento, C. & Wilson, D. J. Contemporary hydrogen deuterium exchange mass spectrometry. *Methods* **144**, 27–42 (2018).
178. Chu, F., Thornton, D. T. & Nguyen, H. T. Chemical cross-linking in the structural analysis of protein assemblies. *Methods* **144**, 53–63 (2018).
179. Leney, A. C. & Heck, A. J. R. Native Mass Spectrometry: What is in the Name? *J. Am. Soc. Mass Spectrom.* **28**, 5–13 (2017).
180. Uetrecht, C., Rose, R. J., van Duijn, E., Lorenzen, K. & Heck, A. J. R. Ion mobility mass spectrometry of proteins and proteinassemblies. *Chem. Soc. Rev.* **39**, 1633–1655 (2010).
181. Inglis, A. J., Masson, G. R., Shao, S., Perisic, O., McLaughlin, S. H., Hegde, R. S. & Williams, R. L. Activation of GCN2 by the ribosomal P-stalk. *Proc. Natl. Acad. Sci.* **116**, 4946–4954 (2019).
182. Duong, V.-A., Park, J.-M. & Lee, H. Review of Three-Dimensional Liquid Chromatography Platforms for Bottom-Up Proteomics. *Int. J. Mol. Sci.* **21**, 1524 (2020).
183. Siuti, N. & Kelleher, N. L. Decoding protein modifications using top-down mass spectrometry. *Nat. Methods* **4**, 817–821 (2007).
184. Brodbelt, J. S. Ion Activation Methods for Peptides and Proteins. *Anal. Chem.* **88**, 30–51 (2016).
185. Mao, Y., Valeja, S. G., Rouse, J. C., Hendrickson, C. L. & Marshall, A. G. Top-Down Structural Analysis of an Intact Monoclonal Antibody by Electron Capture Dissociation-Fourier Transform Ion Cyclotron Resonance-Mass Spectrometry. *Anal. Chem.* **85**, 4239–4246 (2013).
186. Laskay, Ü. A., Lobas, A. A., Srzentić, K., Gorshkov, M. V & Tsybin, Y. O. Proteome Digestion Specificity Analysis for Rational Design of Extended Bottom-up and Middle-down Proteomics Experiments. *J. Proteome Res.* **12**, 5558–5569 (2013).
187. Englander, S. W., Mayne, L., Bai, Y. & Sosnick, T. R. Hydrogen exchange: The modem legacy of Linderstrom-Lang. *Protein Sci.* **6**, 1101–1109 (1997).
188. Englander, S. W. Hydrogen exchange and mass spectrometry: A historical perspective. *J. Am. Soc. Mass Spectrom.* **17**, 1481–1489 (2006).
189. Englander, S. W., Downer, N. W. & Teitelbaum, H. Hydrogen Exchange. *Annu. Rev. Biochem.* **41**, 903–924 (1972).

190. Rosa, J. J. & Richards, F. M. Hydrogen exchange from identified regions of the S-protein component of ribonuclease as a function of temperature, pH, and the binding of S-peptide. *J. Mol. Biol.* **145**, 835–851 (1981).

191. Englander, S. W. & Kallenbach, N. R. Hydrogen exchange and structural dynamics of proteins and nucleic acids. *Q. Rev. Biophys.* **16**, 521–655 (1983).

192. Katta, V., Chait, B. T. & Carr, S. Conformational changes in proteins probed by hydrogen-exchange electrospray-ionization mass spectrometry. *Rapid Commun. Mass Spectrom.* **5**, 214–217 (1991).

193. Zhang, Z. & Smith, D. L. Determination of amide hydrogen exchange by mass spectrometry: A new tool for protein structure elucidation. *Protein Sci.* **2**, 522–531 (1993).

194. Molday, R. S., Englander, S. W. & Kallen, R. G. Primary structure effects on peptide group hydrogen exchange. *Biochemistry* **11**, 150–158 (1972).

195. Bai, Y., Milne, J. S., Mayne, L. & Englander, S. W. Primary structure effects on peptide group hydrogen exchange. *Proteins Struct. Funct. Genet.* **17**, 75–86 (1993).

196. Eigen, M. Proton Transfer, Acid-Base Catalysis, and Enzymatic Hydrolysis. Part I: ELEMENTARY PROCESSES. *Angew. Chemie Int. Ed. English* **3**, 1–19 (1964).

197. Konermann, L., Tong, X. & Pan, Y. Protein structure and dynamics studied by mass spectrometry: H/D exchange, hydroxyl radical labeling, and related approaches. *J. Mass Spectrom.* **43**, 1021–1036 (2008).

198. Masson, G. R., Burke, J. E., Ahn, N. G., Anand, G. S., Borchers, C., Brier, S., Bou-Assaf, G. M., Engen, J. R., Englander, S. W., Faber, J., Garlish, R., Griffin, P. R., Gross, M. L., Guttman, M., Hamuro, Y., Heck, A. J. R., Houde, D., Iacob, R. E., Jorgensen, T. J. D., Kaltashov, I. A., Klinman, J. P., Konermann, L., Man, P., Mayne, L., Pascal, B. D., Reichmann, D., Skehel, M., Snijder, J., Strutzenberg, T. S., Underbakke, E. S., Wagner, C., Wales, T. E., Walters, B. T., Weis, D. D., Wilson, D. J., Wintrode, P. L., Zhang, Z., Zheng, J., Schriemer, D. C. & Rand, K. D. Recommendations for performing, interpreting and reporting hydrogen deuterium exchange mass spectrometry (HDX-MS) experiments. *Nat. Methods* **16**, 595–602 (2019).

199. Kadek, A., Mrazek, H., Halada, P., Rey, M., Schriemer, D. C. & Man, P. Aspartic Protease Nepenthesin-1 as a Tool for Digestion in Hydrogen/Deuterium Exchange Mass Spectrometry. *Anal. Chem.* **86**, 4287–4294 (2014).

200. Kadek, A., Tretyachenko, V., Mrazek, H., Ivanova, L., Halada, P., Rey, M., Schriemer, D. C. & Man, P. Expression and characterization of plant aspartic protease nepenthesin-1 from Nepenthes gracilis. *Protein Expr. Purif.* **95**, 121–8 (2014).

201. Yang, M., Hoeppner, M., Rey, M., Kadek, A., Man, P. & Schriemer, D. C. Recombinant Nepenthesin II for Hydrogen/Deuterium Exchange Mass Spectrometry. *Anal. Chem.* **87**, 6681–6687 (2015).

202. Cravello, L., Lascoux, D. & Forest, E. Use of different proteases working in acidic conditions to improve sequence coverage and resolution in hydrogen/deuterium exchange of large proteins. *Rapid Commun. Mass Spectrom.* **17**, 2387–2393 (2003).

203. Möller, I. R., Slivacka, M., Hausner, J., Nielsen, A. K., Pospisilova, E., Merkle, P. S., Liskova, R., Polak, M., Loland, C. J., Kadek, A., Man, P. & Rand, K. D. Improving the Sequence Coverage of Integral Membrane Proteins during Hydrogen/Deuterium Exchange Mass Spectrometry Experiments. *Anal. Chem.* **91**, 10970–10978 (2019).

204. Rand, K. D., Zehl, M. & Jørgensen, T. J. D. Measuring the hydrogen/deuterium exchange of proteins at high spatial resolution by mass spectrometry: overcoming gas-phase hydrogen/deuterium scrambling. *Acc. Chem. Res.* **47**, 3018–27 (2014).

205. Merkley, E. D., Rysavy, S., Kahraman, A., Hafen, R. P., Daggett, V. & Adkins, J. N. Distance restraints from crosslinking mass spectrometry: Mining a molecular dynamics simulation database to evaluate lysine-lysine distances. *Protein Sci.* **23**, 747–759 (2014).

206. Leitner, A., Joachimiak, L. A., Unverdorben, P., Waltzhoeni, T., Frydman, J., Förster, F. & Aebersold, R. Chemical cross-linking/mass spectrometry targeting acidic residues in proteins and protein complexes. *Proc. Natl. Acad. Sci.* **111**, 9455–9460 (2014).

207. Kukacka, Z., Rosulek, M., Strohalm, M., Kavan, D. & Novak, P. Mapping protein structural changes by quantitative cross-linking. *Methods* **89**, 112–20 (2015).

208. Walzthoeni, T., Joachimjak, L. A., Rosenberger, G., Röst, H. L., Malmström, L., Leitner, A., Frydman, J. & Aebersold, R. xTract: software for characterizing conformational changes of

protein complexes by quantitative cross-linking mass spectrometry. *Nat. Methods* **12**, 1185–1190 (2015).

209. Sinz, A. Chemical cross-linking and mass spectrometry to map three-dimensional protein structures and protein–protein interactions. *Mass Spectrom. Rev.* **25**, 663–682 (2006).
210. Schmidt, C., Beilsten-Edmands, V. & Robinson, C. V. The joining of the Hsp90 and Hsp70 chaperone cycles yields transient interactions and stable intermediates: insights from mass spectrometry. *Oncotarget* **6**, 18276–18281 (2015).
211. Deroo, S., Hyung, S.-J., Marcoux, J., Gordiyenko, Y., Koripella, R. K., Sanyal, S. & Robinson, C. V. Mechanism and rates of exchange of L7/L12 between ribosomes and the effects of binding EF-G. *ACS Chem. Biol.* **7**, 1120–7 (2012).
212. Snijder, J., Rose, R. J., Veesler, D., Johnson, J. E. & Heck, A. J. R. Studying 18 MDa virus assemblies with native mass spectrometry. *Angew. Chem. Int. Ed. Engl.* **52**, 4020–3 (2013).
213. Lanucara, F., Holman, S. W., Gray, C. J. & Eyers, C. E. The power of ion mobility-mass spectrometry for structural characterization and the study of conformational dynamics. *Nat. Chem.* **6**, 281–94 (2014).
214. Dixit, S. M., Polasky, D. A. & Ruotolo, B. T. Collision induced unfolding of isolated proteins in the gas phase: past, present, and future. *Curr. Opin. Chem. Biol.* **42**, 93–100 (2018).
215. Aprile, F. A., Dhulesia, A., Stengel, F., Roodveldt, C., Benesch, J. L. P., Tortora, P., Robinson, C. V., Salvatella, X., Dobson, C. M. & Cremades, N. Hsp70 oligomerization is mediated by an interaction between the interdomain linker and the substrate-binding domain. *PLoS One* **8**, e67961 (2013).
216. Schuermann, J. P., Jiang, J., Cuellar, J., Llorca, O., Wang, L., Gimenez, L. E., Jin, S., Taylor, A. B., Demeler, B., Morano, K. A., Hart, P. J., Valpuesta, J. M., Lafer, E. M. & Sousa, R. Structure of the Hsp110:Hsc70 Nucleotide Exchange Machine. *Mol. Cell* **31**, 232–243 (2008).
217. Bracher, A. & Verghese, J. The nucleotide exchange factors of Hsp70 molecular chaperones. *Front. Mol. Biosci.* **2**, 10 (2015).
218. Liu, Q. & Hendrickson, W. A. Insights into Hsp70 chaperone activity from a crystal structure of the yeast Hsp110 Sse1. *Cell* **131**, 106–20 (2007).
219. De Los Rios, P. & Barducci, A. Hsp70 chaperones are non-equilibrium machines that achieve ultra-affinity by energy consumption. *Elife* **3**, e02218 (2014).
220. Leu, J. I.-J., Zhang, P., Murphy, M. E., Marmorstein, R. & George, D. L. Structural basis for the inhibition of HSP70 and DnaK chaperones by small-molecule targeting of a C-terminal allosteric pocket. *ACS Chem. Biol.* **9**, 2508–16 (2014).
221. Leu, J. I.-J., Zhang, P., Murphy, M. E., Marmorstein, M. & George, D. L. Inhibition of stress-inducible HSP70 impairs mitochondrial proteostasis and function. *Oncotarget* **8**, 45656–45669 (2017).
222. Hassan, A. Q., Kirby, C. A., Zhou, W., Schuhmann, T., Kityk, R., Kipp, D. R., Baird, J., Chen, J., Chen, Y., Chung, F., Hoepfner, D., Movva, N. R., Pagliarini, R., Petersen, F., Quinn, C., Quinn, D., Riedl, R., Schmitt, E. K., Schitter, A., Stams, T., Studer, C., Fortin, P. D., Mayer, M. P. & Sadlish, H. The novolactone natural product disrupts the allosteric regulation of Hsp70. *Chem. Biol.* **22**, 87–97 (2015).
223. Hornbeck, P. V., Zhang, B., Murray, B., Kornhauser, J. M., Latham, V. & Skrzypek, E. PhosphoSitePlus, 2014: mutations, PTMs and recalibrations. *Nucleic Acids Res.* **43**, D512-20 (2015).
224. Madeira, F., Tinti, M., Murugesan, G., Berrett, E., Stafford, M., Toth, R., Cole, C., MacKintosh, C. & Barton, G. J. 14-3-3-Pred: improved methods to predict 14-3-3-binding phosphopeptides. *Bioinformatics* **31**, 2276–83 (2015).
225. Alblova, M., Smidova, A., Docekal, V., Vesely, J., Herman, P., Obsilova, V. & Obsil, T. Molecular basis of the 14-3-3 protein-dependent activation of yeast neutral trehalase Nth1. *Proc. Natl. Acad. Sci. U. S. A.* **114**, E9811–E9820 (2017).
226. Kinoshita, E., Kinoshita-Kikuta, E., Takiyama, K. & Koike, T. Phosphate-binding tag, a new tool to visualize phosphorylated proteins. *Mol. Cell. Proteomics* **5**, 749–57 (2006).
227. Kacirova, M., Kosek, D., Kadek, A., Man, P., Vecer, J., Herman, P., Obsilova, V. & Obsil, T. Structural Characterization of Phosducin and Its Complex with the 14-3-3 Protein. *J. Biol. Chem.* **290**, 16246–60 (2015).

PŘILOŽENÉ PUBLIKACE

Publikace I

Trčka, F., Ďurech, M., Vaňková, P., Chmelík, J., Martinková, V., Hausner, J., Kádek, A., Marcoux, J., Klumpler, T., Vojtěšek, B., Müller, P. & Man, P.

Stress-inducible Hsp70 Has a High Propensity to Form ATP-dependent Antiparallel Dimers That Are Differentially Regulated by Cochaperone Binding.

Mol. Cell. Proteomics **18**, 320–337 (2019)

Můj příspěvěk k práci: *provedení HDX-MS, nESI-MS a XL-MS experimentů s interpretací dat a jejich grafickou prezentací*

Human Stress-inducible Hsp70 Has a High Propensity to Form ATP-dependent Antiparallel Dimers That Are Differentially Regulated by Cochaperone Binding

Authors

Filip Trcka, Michal Durech, Pavla Vankova, Josef Chmelik, Veronika Martinkova, Jiri Hausner, Alan Kadek, Julien Marcoux, Tomas Klumpler, Borivoj Vojtesek, Petr Muller, and Petr Man

Correspondence

pman@biomed.cas.cz; muller@mou.cz

In Brief

The oligomerization (and particularly dimerization) of Hsp70 proteins plays an important role in their chaperoning activities. Here, we report that human stress-inducible Hsp70 possesses the highest propensity among analyzed Hsp70 homologs to form dimers in the presence of ATP. ATP-bound Hsp70 assembles in solution as an antiparallel dimer closely resembling the dimeric structures captured in DnaK and BiP crystals. ATP-dependent Hsp70 dimerization is necessary for efficient Hsp40 interaction and is differentially affected by TPR cochaperone binding.

Graphical Abstract

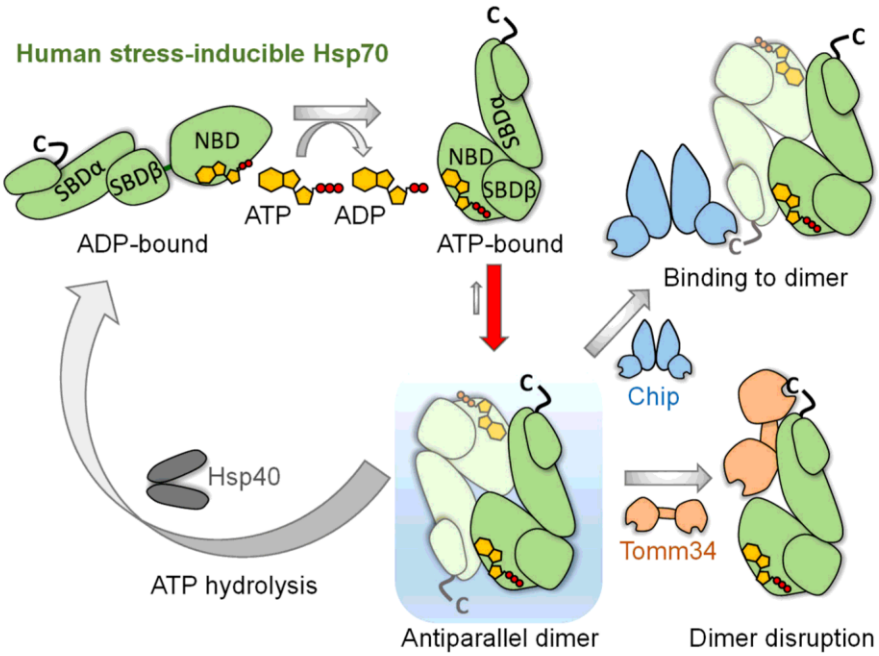

Highlights

- Hsp70 homologs differ in their oligomeric properties in the presence of ATP.
- Human inducible Hsp70 forms ATP-dependent anti-parallel dimers with high propensity.
- Dimerization of ATP-bound Hsp70 is required for effective Hsp70-Hsp40 interaction.
- ATP-dependent interaction with Tomm34 TPR cochaperone disrupts Hsp70 dimer.

Trcka et al., 2019, Molecular & Cellular Proteomics *18*, 320–337

https://doi.org/10.1074/mcp.RA118.001044

Human Stress-inducible Hsp70 Has a High Propensity to Form ATP-dependent Antiparallel Dimers That Are Differentially Regulated by Cochaperone Binding*[S]

Filip Trcka‡, Michal Durech‡, Pavla Vankova§¶, Josef Chmelik§¶, Veronika Martinkova‡, Jiri Hausner§¶, Alan Kadek§¶‡‡, Julien Marcoux‖, Tomas Klumpler, Borivoj Vojtesek‡, Petr Muller§§‡, and Petr Man§¶ ¶¶**

Eukaryotic protein homeostasis (proteostasis) is largely dependent on the action of highly conserved Hsp70 molecular chaperones. Recent evidence indicates that, apart from conserved molecular allostery, Hsp70 proteins have retained and adapted the ability to assemble as functionally relevant ATP-bound dimers throughout evolution. Here, we have compared the ATP-dependent dimerization of DnaK, human stress-inducible Hsp70, Hsc70 and BiP Hsp70 proteins, showing that their dimerization propensities differ, with stress-inducible Hsp70 being predominantly dimeric in the presence of ATP. Structural analyses using hydrogen/deuterium exchange mass spectrometry, native electrospray ionization mass spectrometry and small-angle X-ray scattering revealed that stress-inducible Hsp70 assembles in solution as an antiparallel dimer with the intermolecular interface closely resembling the ATP-bound dimer interfaces captured in DnaK and BiP crystal structures. ATP-dependent dimerization of stress-inducible Hsp70 is necessary for its efficient interaction with Hsp40, as shown by experiments with dimerization-deficient mutants. Moreover, dimerization of ATP-bound Hsp70 is required for its participation in high molecular weight protein complexes detected *ex vivo*, supporting its functional role *in vivo*. As human cytosolic Hsp70 can interact with tetratricopeptide repeat (TPR) domain containing cochaperones, we tested the interaction of Hsp70 ATP-dependent dimers with Chip and Tomm34 cochaperones. Although Chip associates with intact Hsp70 dimers to form a larger complex, binding of Tomm34 disrupts the Hsp70 dimer and this event plays an important role in Hsp70 activity regulation. In summary, this study provides structural evidence of robust ATP-dependent antiparallel dimerization of human inducible Hsp70 protein and suggests a novel role of TPR domain cochaperones in multichaperone complexes involving Hsp70 ATP-bound dimers. ***Molecular & Cellular Proteomics 18: 320–337, 2019. DOI: 10.1074/mcp.RA118.001044.***

Protein homeostasis, including *de novo* protein synthesis surveillance, preprotein transport, misfolded protein degradation and aggregate dissolving, relies on the coordinated actions of the abundant Hsp70 and Hsp90 molecular chaperones (1, 2). Hsp70 proteins exhibit remarkable sequence and structural conservation across all kingdoms of life, suggesting conserved molecular mechanics (3, 4). In eukaryotes, Hsp70s have diversified into organelle-specific species including cytosolic Hsc70 and Hsp70 isoforms, and the endoplasmic reticulum (ER)[1] isoform, BiP (5).

Hsp70 proteins contain two independent domains: an N-terminal nucleotide-binding domain (NBD) and a C-terminal substrate-binding domain (SBD). The SBDβ subdomain forms a substrate-binding pocket with preference for hydrophobic polypeptide sequences (6, 7), whereas SBDα forms an α-helical lid that covers SBDβ through ionic contacts and helps to stabilize substrate binding (8, 9). The NBD and SBD are connected by a highly conserved hydrophobic linker (10). ATP coordination into the nucleotide-binding pocket of NBD leads to dramatic allosteric changes in Hsp70, characterized by NBD-SBDβ docking stabilizing the interdomain linker, accompanied by SBDα detachment from SBDβ and its docking onto the NBD (6, 11–14). The SBDβ domain in the ATP-bound conformation of Hsp70 has unfavorable kinetics of substrate binding, which leads to substrate release (15, 16). ATP hydrolysis triggers rearrangements in SBDβ reducing substrate

From the ‡Regional Centre for Applied Molecular Oncology, Masaryk Memorial Cancer Institute, Zluty kopec 7, 656 53 Brno, Czech Republic; §BioCeV - Institute of Microbiology of the Czech Academy of Sciences, v.v.i., Prumyslova 595, 252 50 Vestec, Czech Republic; ¶Department of Biochemistry, Faculty of Science, Charles University in Prague, Hlavova 8, 128 43 Prague, Czech Republic; ‖Institut de Pharmacologie et de Biologie Structurale, Université de Toulouse, CNRS, UPS, Toulouse, France; **CEITEC–Central European Institute of Technology, Masaryk University, 625 00 Brno, Czech Republic

Received September 4, 2018, and in revised form, November 9, 2018
Published, MCP Papers in Press, November 20, 2018, DOI 10.1074/mcp.RA118.001044

on/off rates and therefore stabilizing substrate entrapment (17–19).

Two classes of cochaperones modulate the ATPase cycle of Hsp70 by accelerating ATP hydrolysis and ADP/ATP nucleotide exchange: Hsp40 homologs and nucleotide exchange factors (NEFs) (19, 20). Hsp40 proteins contain a J-domain (named after the bacterial Hsp40 protein DnaJ) that interacts with the Hsp70 interdomain linker at the NBD-SBDβ interface, stimulating the NBD catalytic center (18). The J-domain also helps to communicate the hydrolysis-stimulating role of the substrate, which is brought to Hsp70 by Hsp40 substrate-binding activity (17, 18). A structurally differing group of NEFs assists ADP to ATP exchange in the NBD of Hsp70 by convergent mechanics through opening of the nucleotide binding cleft (20). Interesting members of the NEF group are Hsp110 proteins, represented by yeast Sse1, which exhibit significant structural homology to the ATP-bound state of Hsp70 and mediate nucleotide exchange through heterodimerization with Hsp70 (14, 21).

Beside the ATPase regulating cochaperones, eukaryotes have evolved a large group of cochaperones containing tetratricopeptide repeat (TPR) domains that mediate their interaction with the conserved C-terminal EEVD motif of eukaryotic Hsp70 and Hsp90 (22). Apart from their TPR domains, these cochaperones bear additional domains with various functions diversifying molecular chaperones-mediated substrate processing (23).

Recently, dimerization and other oligomeric forms of Hsp70 family members in both conformational states, Apo/ADP- and ATP-bound, were described to play an important role in their chaperoning activities (24–28). Crystallographic studies revealed the presence of antiparallel ATP-bound dimers in the crystal structure of evolutionary distant Hsp70 orthologs DnaK (11, 13) and BiP (6, 12). The ATP-dependent dimerization of DnaK is necessary for its cooperation with DnaJ, however the dimeric state is very low in solution (25). In contrast, our previous isothermal titration calorimetry (ITC) analysis suggested that human inducible Hsp70 isoform exists predominantly as a dimer in an ATP supplemented buffer (29).

The aim of this work was to compare the levels of ATP-dependent dimerization in different Hsp70 proteins and to functionally and structurally characterize dimers of the human inducible Hsp70 isoform. Unlike DnaK and BiP, our data indicate that antiparallel dimerization of ATP-bound Hsp70 is highly pronounced in human Hsc70/Hsp70 cytosolic isoforms and is differentially regulated by interactions with Chip and Tomm34 TPR cochaperones.

EXPERIMENTAL PROCEDURES

Cloning and Protein Preparation—All coding sequences were cloned by Gateway recombination technology (Invitrogen, Carlsbad, CA). The full coding sequences of the *E. coli dnaK* (DnaK, P0A6Y8-1) and human *HSPA1A* (Hsp70, P0DMV8-1), *HSPA8* (Hsc70, P11142-1) and *HSPA5* (BiP, P11021-1, aa 19–654) genes and sequences coding for Hsp70 point mutants (I164D, T204A, D529A, N540A, E543A, N540A-E543A) were cloned into pDEST17 and pT7-SBP vectors containing an N-terminal His_6 or SBP tag, respectively. The Hsp70 point mutations were prepared using QuickChange Site-Directed Mutagenesis Kit (Agilent Technologies, Santa Clara, CA) according to the manufacturer's instructions. The full coding sequences of the human *DNAJB1* (Hsp40, P25685-1), *TOMM34* (Tomm34, Q15785-1), *BAG1* (Bag-1, Q99933-4) and *STUB1* (Chip, Q9UNE7-1) genes were cloned into pDEST15, containing an N-terminal His_6-GST tag cleavable by tobacco etch virus (TEV) protease. Genes were expressed in BL21(DE3) RIPL cells and purified as described (29). His_6-tagged Hsp70 proteins were purified on HisTrap columns (GE Healthcare, Piscataway, NJ), dialyzed against buffer A (20 mM Tris, pH 7.2, 100 mM KCl) for 24 h, applied to HiTrap Q columns (GE Healthcare) and eluted by a linear gradient of buffer B (20 mM Tris, pH 7.2, 1 M KCl). Fractions containing His_6-tagged proteins were concentrated and subjected to gel filtration using a HiPrep 16/60 Sephacryl S-100 HR column. An untagged stress-inducible Hsp70 protein was produced by TEV protease treatment of streptavidin matrix-bound SBP-tagged protein bearing TEV cleavage site between SBP tag and the protein sequence.

Cell Culture and Transfection—HEK293 cells were cultured in Dulbecco's modified Eagle's medium (DMEM) supplemented with 10% fetal bovine serum and 300 mg/l L-glutamine in a humidified atmosphere of 5% CO_2 at 37 °C. Transient transfections of cells with the plasmids pCMV-N-HA-Hsp70 and pCMV-N-HA-Hsp70-N540A-E543A were performed by polyethylenimine (PEI). Cells were collected 24 h after transfection, lysed in 25 mM Hepes, pH 7.5, 75 mM KCl, 75 mM KAc, 2 mM $MgCl_2$, and the lysates desalted by 7-kDa molecular mass cut-off Zeba spin desalting column (Thermo Fischer Scientific, Waltham, MA).

SBP Pull-down Assays—All proteins were exchanged into pull-down assay buffer (50 mM Hepes, pH 7.5, 0.1 M KAc, 2 mM $MgCl_2$) before mixing 70 pmol of various SBP-tagged Hsp70 constructs with streptavidin agarose beads for 30 min at 4 °C. After washing with assay buffer, 140 pmol of Tomm34 protein in buffer containing 0.2 mM ATP or no nucleotide was added to the beads for 1 h at 4 °C. Beads were washed before eluting with 2 mM biotin in assay buffer and analysis by SDS-PAGE.

Antibodies—Monoclonal antibodies to Tomm34, Hsp70 and Chip were previously prepared and characterized in-house. Blots were developed with rabbit anti-mouse IgG secondary antibody conjugated with horseradish peroxidase (Dako, Santa Clara, CA).

Luciferase Refolding Assay—Luciferase refolding assay was performed as described previously with some changes (29). The refolding protein mixture contained 1 μM Hsp70 WT or its mutants, 2 μM Hsp40, 0.5 μM Bag-1 and 8 nM denatured luciferase in 25 mM Hepes, pH 7.2, 50 mM KAc, 2 mM DTT, 2 mM $MgCl_2$. Luciferase activity was measured at 21 °C using an Infinite M1000 Pro (Tecan, Männedorf, Switzerland) at emission wavelengths of 560 nm and 100 ms integra-

[1] The abbreviations used are: ER, endoplasmic reticulum; ADP, adenosine diphosphate; ATP, adenosine triphosphate; Bag-1, Bcl2-associated athanogene 1; Chip, carboxyl terminus of Hsp70-interacting protein; ESI-MS, electrospray ionization mass spectrometry; GST, glutathione S-transferase; HDX, hydrogen/deuterium exchange; Hsc, heat shock cognate; Hsp, heat shock protein; NBD, nucleotide-binding domain; NEF, nucleotide exchange factor; PDB, protein data bank; SAXS, small-angle X-ray scattering; SBD, substrate-binding domain; SBP, streptavidin-binding peptide; SEC, size exclusion chromatography; SPR, surface plasmon resonance; TEV, tobacco etch virus; Tomm34, translocase of outer mitochondrial membrane 34; TPR, tetratricopeptide repeat; WT, wild type.

tion time. The signal from samples with native luciferase was set as 100%. Luciferase activity of denatured luciferase only and the refolding activity of chaperone mixture without Hsp70 acted as negative controls.

Malachite Green ATPase Assay—Experiments used published protocols (29, 30). Hsp70 WT or its mutants (2 μM) were titrated with Hsp40 protein in buffer containing 50 mM Hepes, pH 7.5, 0.15 M KAc, 2 mM $MgCl_2$, 2 mM ATP for 3 h at 37 °C. Malachite green reagent was added, and 34% sodium citrate was immediately added to halt the non-enzymatic hydrolysis of ATP. Samples were incubated for another 15 min before measuring absorbance at 620 nm. A phosphate standard curve was used to calculate pmol ATP/μM Hsp70/min.

Peptide Binding—Fluorescein-NRLLLTG peptide binding experiments were performed in 50 mM Hepes, pH 7.5, 0.15 M KAc, 2 mM $MgCl_2$, 0.01% Tween 20. To obtain equilibrium binding curves, mixtures containing 30 nM peptide were titrated with different concentrations of Hsp70 WT and mutant proteins and incubated overnight at 4 °C. Peptide binding kinetics and peptide release was analyzed using peptide and protein concentrations of 30 nM and 50 μM, respectively, where ATP (0.4 mM) was added after overnight incubation at 4 °C to measure release. To distinguish nonspecific binding, we used BSA with the same concentration as analyzed protein. All reactions were carried out in a total volume of 12 μl in 384-well black Nunc Plates (Thermo Fischer Scientific). Fluorescence polarization was measured at 21 °C using an Infinite M1000 Pro (Tecan) with excitation and emission wavelengths of 470 and 520 nm, respectively. Data were analyzed using GraphPad Prism version 5.03 for Windows (GraphPad Software, San Diego, CA).

Small-angle X-ray Scattering (SAXS)—The SAXS data sets were collected using the BioSAXS-1000, Rigaku at CEITEC (Brno, Czech Republic). Data were collected at 277 K with focused (confocal MaxFlux SAXS optic, Rigaku) Cu Kα X-ray (1.54 Å). Sample to detector (PILATUS 100K, Dectris) distance was 0.48 m covering a scattering vector ($q = 4\pi\sin(\theta)/\lambda$) range from 0.009 to 0.6 $Å^{-1}$. Size exclusion buffer was used for the blank measurement. Hsp70-T204A protein samples were measured at 2.5 and 1.5 mg/ml. Six separate two-dimensional images were collected for buffer and sample (10 min exposure per image). Radial averaging, data reduction and buffer subtractions were performed using SAXSLab3.0.0r1, Rigaku. Six individual scattering curves (10 min exposures) were compared with check the radiation damage and averaged.

Integral structural parameters (supplemental Table S1) were determined using PRIMUS/qt ATSAS v.2.8.3 (31). For molecular weight estimations, an *ab initio* model was reconstructed using DAMMIF ATSAS v.2.8.3, where the annealing mode was set to "fast," whereas all other parameters were kept at default. The *ab initio* modeling for superimposition with atomic models was performed by DAMMIN ATSAS v.2.8.3, where the computation mode was set to "slow," point symmetry of the particle to "P2" and all other parameters were kept at default. Evaluation of solution scattering and fitting to experimental scattering curves was performed using CRYSOL ATSAS v.2.8.3, where automatic constant subtraction was allowed; other parameters were kept at default. Superimposition of the atomic and *ab initio* models was performed by SUPCOMB ATSAS v.2.8.3. UCSF Chimera was used for graphical representation (32).

Surface Plasmon Resonance (SPR)—SPR was carried out on a Biacore T200 system (GE Healthcare). Biotinylated Hsp40 (EZ-Link™ Thermo Fischer Scientific) was immobilized on Series S Sensor chip SA (GE Healthcare) for about 460 response units. All measurements were performed at 21 °C in SPR buffer (25 mM Hepes, pH 7.5, 100 mM KAc, 2 mM $MgCl_2$, 0.005% Tween 20). Each Hsp70 protein (1 μM) was pre-incubated with or without 0.2 mM ATP and injected for 20 min at 10 μl/min. The first channel on the sensor was coated with biotin and used as a background control. The data were plotted after subtracting this background control.

Analytical Size Exclusion Chromatography (SEC)—Separations by SEC were carried out using Superdex 200 Increase 10/300 GL (GE Healthcare) pre-equilibrated with 25 mM Hepes, pH 7.5, 150 mM KAc, 2 mM $MgCl_2$. 75 μl of Hsp70 proteins (40 μM) pre-incubated with/without 0.2 mM ATP for 20 min at 21 °C was injected and isocratically eluted at 0.3 ml/min. In experiments testing the influence of Hsp40 on Hsp70 dimers, Hsp40 (10 μM) was added at the end of the Hsp70 incubation with ATP and incubated for 5 min. In experiments analyzing the effect of TPR domain cochaperones on Hsp70 dimerization, Tomm34 or Chip proteins were mixed with Hsp70 in equimolar ratio (40 μM each) in the presence/absence of 0.2 mM ATP. Incubation time, injection volume and flow rate were as described above. From each run, 300 μl fractions corresponding to protein peaks were collected and analyzed using gel electrophoresis and Coomassie staining. Apparent molecular weights of proteins and protein complexes were determined using calibration curves obtained from a mixture of Thyroglobulin, Apoferritin, Amylase, Alcohol Dehydrogenase, Albumin and Carbonic Anhydrase.

Desalted lysates of HEK293 cells with overexpressed HA-tagged Hsp70 WT or N540A-E543A mutant were incubated with/without 2 mM ATP for 20 min at 21 °C before loading on columns pre-equilibrated with cell lysis buffer 25 mM Hepes, pH 7.5, 75 mM KCl, 75 mM KAc, 2 mM $MgCl_2$. The injection volume was 200 μl. 500 μl fractions isocratically eluted at flow rate of 0.3 ml/min were collected and analyzed by gel electrophoresis and Western blotting. All analyses were performed at least three times.

Chemical Cross-linking—Chemical cross-linking was performed using disuccinimidyl adipate (DSA, Creative Molecules, Vancover, Canada). Hsp70, its dimerization mutants or homologs DnaK, Hsc70 and BiP (40 μM each) in 50 mM Hepes, pH 7.5, 150 mM KAc, 2 mM $MgCl_2$ were incubated in the presence or absence of ATP (0.2 mM) for 20 min at 21 °C. Ten molar excess of the cross-linking agent was added and incubated for 30 min at 21 °C. 5 μg protein samples were resolved by LDS-PAGE (pre-cast 4–12% gel, NuPage) and visualized by Coomassie staining.

For glutaraldehyde chemical cross-linking, Hsp70, Tomm34 or both (40 μM each) in 25 mM Hepes, pH 7.5, 150 mM KAc, 2 mM $MgCl_2$ were incubated for 20 min at 21 °C with or without ATP (0.2 mM). Glutaraldehyde was added (final concentration 0.5 mM) and the reactions stopped after 10 min with Tris, pH 8 (final concentration 80 mM). Samples were diluted 100x in 2× CSB loading buffer and 5 μl separated by SDS-PAGE, blotted and probed with Tomm34 or Hsp70 antibody. Lysates of HEK293 cells with overexpressed HA-tagged Hsp70 WT or N540A-E543A mutant were desalted into 25 mM Hepes, pH 7.5, 75 mM KCl, 75 mM KAc, 2 mM $MgCl_2$ and incubated with/without 2 mM ATP for 20 min at 21 °C before mixing with glutaraldehyde (final concentration 0.5 mM) for 10 min at 21 °C. The reactions were stopped by adding Tris, pH 8 (final concentration 80 mM), samples were supplemented with 2× CSB loading buffer and analyzed by SDS-PAGE and Western blotting with Hsp70 antibody. All electrophoresis-based experiments were performed at least three times.

Native Electrospray Ionization Mass Spectrometry (ESI-MS)—Hsp70 variants (40 μM) were incubated in 25 mM Hepes, pH 7.5, 150 mM KAc, 2 mM $MgCl_2$ with or without 0.2 mM ATP for 20 min, transferred into 200 mM ammonium acetate pH 7.5 using Zeba Spin columns (0.5 ml, 7-kDa cut off) and diluted to 20 μM protein concentration. To study Hsp70-cochaperone interactions, we pre-incubated Hsp70 with or without ATP as described above, mixed with the cochaperone in equimolar ratio, transferred into ammonium acetate and performed native ESI-MS analysis on Waters Synapt G2Si. Samples were electrosprayed from home-made gold-coated borosilicate

spraying tips. Two sets of parameters differing in the trap collision energy (1V and 70V) were used. Although low collisional activation led to better transmission of dimeric molecules, higher collisional activation provided better resolution and can be used for MW estimation. Other parameters were: sampling cone voltage 50V, source offset 20V, trap gas 4 ml/min and source temperature 30 °C. Data were analyzed in MassLynx 4.1.

Molecular Modeling—The homology model of dimeric human stress-inducible Hsp70 was built using Modeler 9.17 (33). The D and F chains of BiP (PDB code 5E84) with sequence identity 64% with human stress-inducible Hsp70, were used as template.

Experimental Design and Rationale for Hydrogen/Deuterium Exchange (HDX) Mass Spectrometry—Hsp70 and its point mutants N540A, E543A and N540A-E543A were pre-incubated in the presence or absence of 5-fold molar excess of ATP for 30 min in 50 mM Hepes, pH 7.5, 0.1 M KAc, 2 mM $MgCl_2$. Deuterium labeling was initiated by 5-fold dilution into D_2O-based 50 mM Hepes, pD 7.5, 0.1 M KAc, 2 mM $MgCl_2$. After 20 s to 2 h at 21 °C, exchange was quenched by 8-fold dilution in 1 M glycine, pH 2.3. Each sample was injected into LC-system and processed as described (34) with minor modifications: desalting lasted 3 min, analytical column used was ZORBAX 300SB-C18, 0.5 × 35 mm, 3.5 μm (Agilent Technologies) with flow rate 20 μl. Gradient was shortened to 7 min, finishing at 25% solvent B. MS used 15 T FT-ICR (SolariX XR, Bruker Daltonics, Bremen, Germany). Data were acquired with ftmsControl 2.1.0 and HyStar 4.0, processed in DataAnalysis 4.1 and analysis of deuterated samples used an in-house program Deutex (unpublished). Peptides arising from pepsin digestion were identified in a separate LC-MS/MS run, where the gradient elution was performed for 35 min. Each full MS scan was followed by six MS/MS scans of the top most intense ions. Mascot generic files were generated in Data Analysis 4.1 using two peak-picking algorithms - FTMS and SNAP. These data were searched by MASCOT 2.5 against a database containing Hsp70 WT and mutant sequences and against the pepsin sequence. Search parameters were: no enzyme specificity, no modification considered, precursor tolerance 3 ppm (although most hits were below 1 ppm), fragment ion tolerance 0.05-Da. All assignments were checked manually. Based on replicate measurements (wild-type in triplicate, mutants in duplicate, all independent preparations), the average standard deviation of deuterium determination was < 0.17-Da. Differences greater than 0.35-Da in deuterium incorporation between samples were considered significant (35). Fully deuterated controls were performed for all protein versions and the data were corrected for back-exchange as described (36).

Software—Multiple sequence alignments were performed using DNASTAR Lasergene Suite (www.dnastar.com). Molecular structures were rendered using PyMOL (www.pymol.org).

RESULTS

Hsp70 and Hsc70 Exhibit Increased Propensity to Form ATP-induced Oligomers/Dimers—To evaluate the propensity of different Hsp70 homologs to undergo ATP-specific oligomerization, we performed analytical size-exclusion chromatography (SEC) of DnaK, Hsp70, Hsc70 and BiP pre-incubated in the absence (Apo form) or presence of ATP (Fig. 1*A*). DnaK eluted as a predominant peak with an apparent molecular weight (MW, all SEC-derived MW are considered apparent, see Experimental Procedures) of 115 kDa under both conditions. In the presence of ATP, a small population of DnaK eluted earlier, with MW 245 kDa, which might represent ATP-bound DnaK dimers (25). Although Hsp70 eluted as a predominant peak with MW 95 kDa and a minor peak with MW 210 kDa in the Apo form, pre-incubation with ATP led to its redistribution to a predominant peak of MW 160 kDa and a minor peak at 80 kDa. Similarly, Hsc70 Apo form shifted from the dominant peak at MW 90 kDa and a minor peak of 210 kDa to two major peaks with MW of 135 and 85 kDa and an early peak of 315 kDa after ATP addition. BiP in the Apo form eluted in three peaks with MW 335, 225 and 100 kDa. Incubation with ATP decreased its oligomerization, evidenced by BiP redistribution to a dominant peak of MW 100 kDa. This behavior of BiP in SEC experiments was reported earlier (28). It is noteworthy that the low MW peaks of Hsp70, Hsc70 and BiP eluted slightly later in the presence of ATP. This observation reflects ATP-induced docking of NBD and SBD domains leading to protein compaction (10, 28). Surprisingly, similar behavior was not observed for ATP-bound DnaK. This might be explained by the insufficient SEC separation of the docked and undocked DnaK molecules, or by a more continuous distribution of DnaK molecules between docked/undocked/intermediate states in the presence of ATP (11, 37, 38). To verify whether our purified proteins are conformationally active, we tested their ability to release substrate peptide in the presence of ATP (supplemental Fig. S1*A*). All proteins exhibited decreased peptide binding after ATP addition, confirming their allosteric activity. These results show that these Hsp70 homologs have varying propensities to oligomerize in the Apo form (with BiP being the most oligomeric, Fig. 1*A*) and especially in the ATP-bound state, where Hsp70 and Hsc70 exhibited the most pronounced ability to self-oligomerize. To exclude the possibility that ATP-induced oligomerization of Hsp70 protein was caused by the affinity purification tag (His_6), we performed SEC after tag cleavage by TEV protease (supplemental Fig. S1*B*). The Apo form of tag-free Hsp70 shifted from MW 90 kDa to 130 kDa after ATP addition, indicating that oligomerization is His_6-independent. As the yield of the tag-free proteins is low, we used tagged proteins in the next experiments.

To explore the presence and the nature of the oligomers in the Apo and ATP state further, we performed chemical cross-linking (DSA) of Hsp70 proteins incubated with or without ATP and analyzed the resulting complexes by SDS-PAGE (Fig. 1*B*). In agreement with SEC profiles, we observed ATP-dependent assembly of Hsp70 and Hsc70 proteins. Conversely, ATP decreased the amount of BiP oligomeric structures. The MW of Hsp70 and Hsp70 ATP-induced oligomers is ~150 kDa, strongly suggesting dimer formation. As with SEC data, ATP-dependent dimers of DnaK were not detectable.

Next, we verified the molecular masses of Hsp70 and Hsc70 protein assemblies formed after incubation with ATP by native electrospray ionization mass spectrometry (24, 27, 39, 40). Here, we used a lower protein concentration (20 μM) than for SEC (40 μM) to avoid spray instability and subsequent irreproducibility of data (higher concentrations caused frequent plugging of the ESI emitters). A decrease in monomer/dimer ratio was observed between Apo- and ATP treated

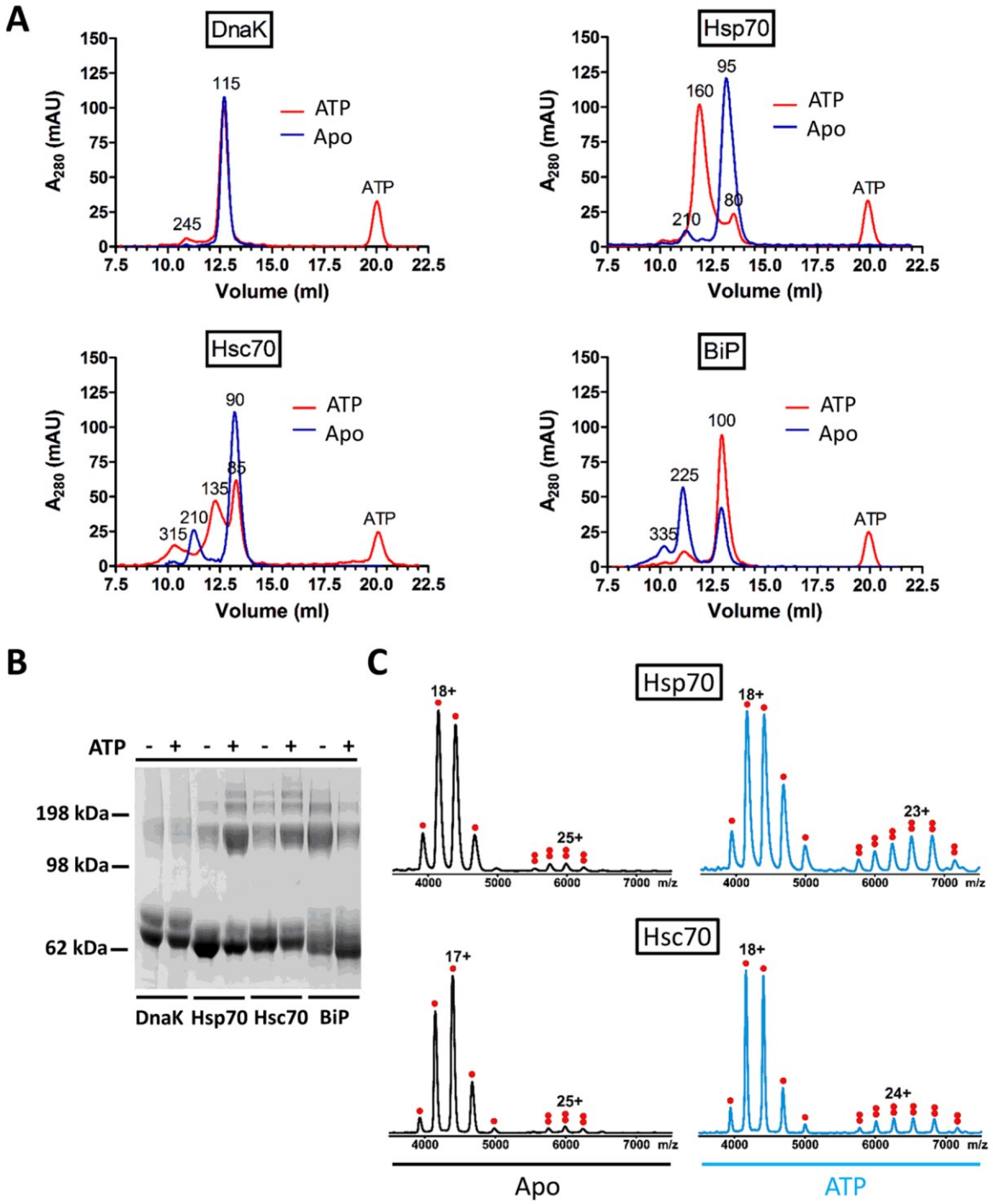

FIG. 1. **Homologs of Hsp70 differ in their propensity to dimerize in the presence of ATP.** *A,* Bacterially purified DnaK, Hsp70, Hsc70 and BiP proteins (40 μM) were pre-incubated with or without ATP (0.2 mM, 20 mins, 21 °C) before separation by analytical SEC. Apparent MW of eluting peaks is indicated (see Experimental procedures). *B,* Hsp70 homologs (40 μM) were pre-incubated with or without ATP for 20 mins before addition of chemical cross-linker (10 molar excess of DSA). The cross-linked complexes were separated by LDS-PAGE (pre-cast gradient (4–12%) gel, NuPage). The molecular weight standard is indicated. *C,* Native ESI-MS spectra of Hsp70 and Hsc70 proteins (20 μM) were acquired after their pre-incubation without (Apo) or with ATP (0.2 mM). The charged states corresponding to monomers and dimers are labeled with single and double dots, respectively.

Hsp70 (Fig. 1*C*), although the amount of dimer in the ATP state does not reflect ratios from SEC. This can be caused by lower gas-phase stability, poorer transmission of the dimer and/or by the lower protein concentration (20 μM) than used for SEC (40 μM). A similar picture was observed for Hsc70, corroborating the SEC results. The 315 kDa peak in Hsc70

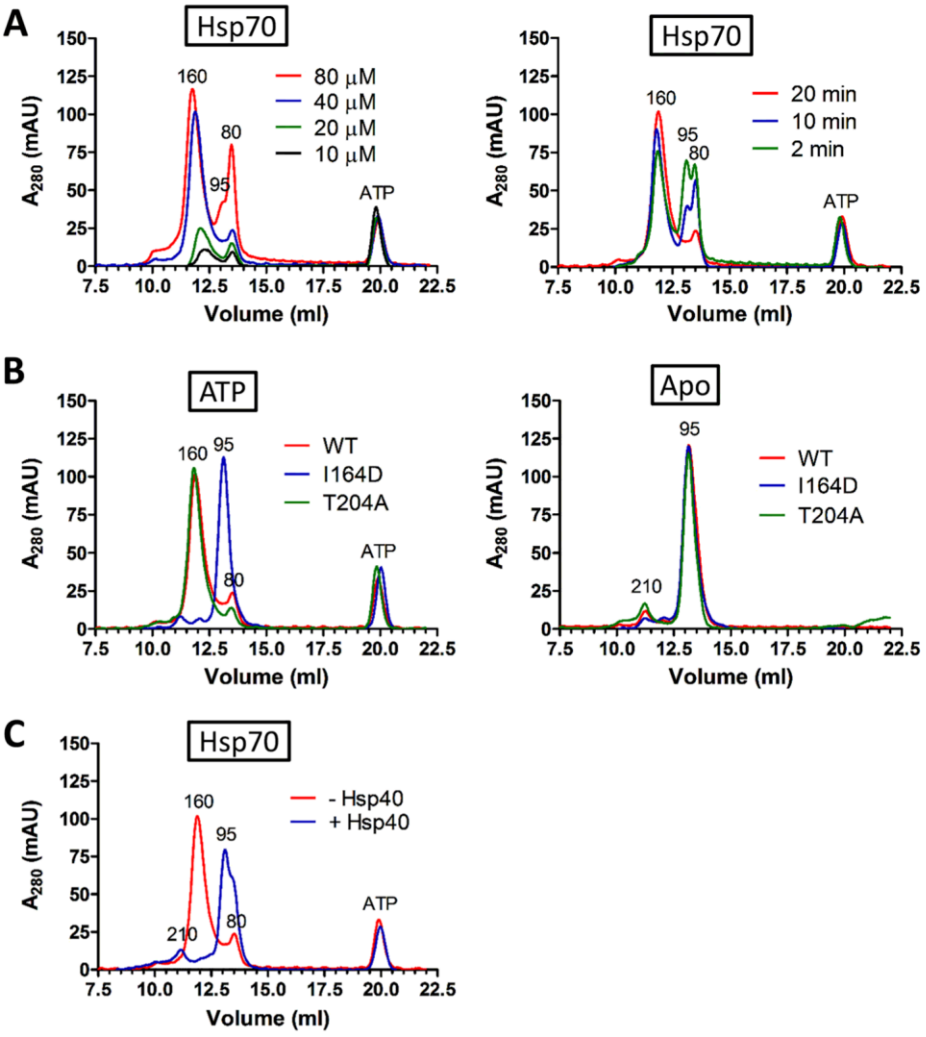

FIG. 2. **ATP-induced dimerization of Hsp70 requires its intact NBD-SBDβ docked conformation.** *A,* Hsp70 was mixed at different concentrations (10, 20, 40, 80 μM; 20 min incubation) or for different time intervals (2, 10, 20 min) with ATP (0.2 mM) at 21 °C before separation by SEC. *B,* Hsp70 and its mutant forms (I164D, T204A) (40 μM) were incubated without (Apo) or with ATP (0.2 mM, 20 min) at 21 °C before SEC. *C,* Hsp70 (40 μM) was incubated with ATP (0.2 mM, 21 °C) for 20 min. Hsp40 (10 μM) was added or not for 5 min and samples were separated by SEC. Apparent MW of eluting peaks is indicated (see Experimental procedures).

SEC analysis was not detected by native ESI-MS, possibly because of its gas-phase instability. These results indicate that Hsp70 homologs differ in their oligomeric properties in solution in the presence of ATP, with human stress-inducible Hsp70 predominantly forming a dimeric population.

ATP-induced Dimerization of the Human Stress-inducible Hsp70 Is a Time and Concentration Dependent Process Requiring Intact ATP-bound Conformation of the Protein—In these experiments we focused on the human inducible isoform of Hsp70. To characterize ATP-dependent dimerization, we measured the concentration and time dependence of this process by SEC (Fig. 2*A*). Under a constant ATP concentration (200 μM), Hsp70 dimers are detectable from 10 μM up to 80 μM protein concentration, with 40 μM showing the highest dimer to monomer peak intensities ratio. When incubated with ATP for increasing time intervals (2, 10, 20 min), Hsp70 dimers formed in a time-dependent manner, demonstrating that ATP-triggered Hsp70 dimer-monomer association/dissociation equilibrium is concentration- and time-dependent.

To evaluate whether the ATP-induced conformation of Hsp70 is necessary for its dimerization, we tested the behavior of the Hsp70 I164D mutant, which binds ATP but is not able to reach NBD-SBD docked conformation (Fig. 2*B*) (29). The elution profiles of I164D under both nucleotide conditions show a dominant peak at MW 95 kDa, indicating that this protein is not able to form ATP-dependent dimers and remains monomeric. Therefore, the ATP-dependent dimerization of Hsp70 requires its ATP-induced conformation. Next, we tested T204A mutant whose intrinsic ATPase activity is low, suggesting it might establish ATP-bound dimers with higher rate and/or stability (29, 41). The T204A mutant elution profile was almost identical to WT, with only a slight increase in dimer to monomer peak intensities, implying that dimerization is not affected by the intrinsic ATP conversion rate under our experimental setup. Finally, we probed the behavior of Hsp70 ATP-bound dimers in the presence of the ATPase-activating cochaperone, Hsp40 (Fig. 2*C*). A 5 min incubation of preformed Hsp70 dimers with substoichiometric amounts of Hsp40 led to the complete disappearance of the ATP-dependent dimer peak, with a concomitant increase of the 95 kDa peak belonging to the monomeric Apo/ADP state of Hsp70. A minor early eluting peak of Hsp70 Apo state dimer

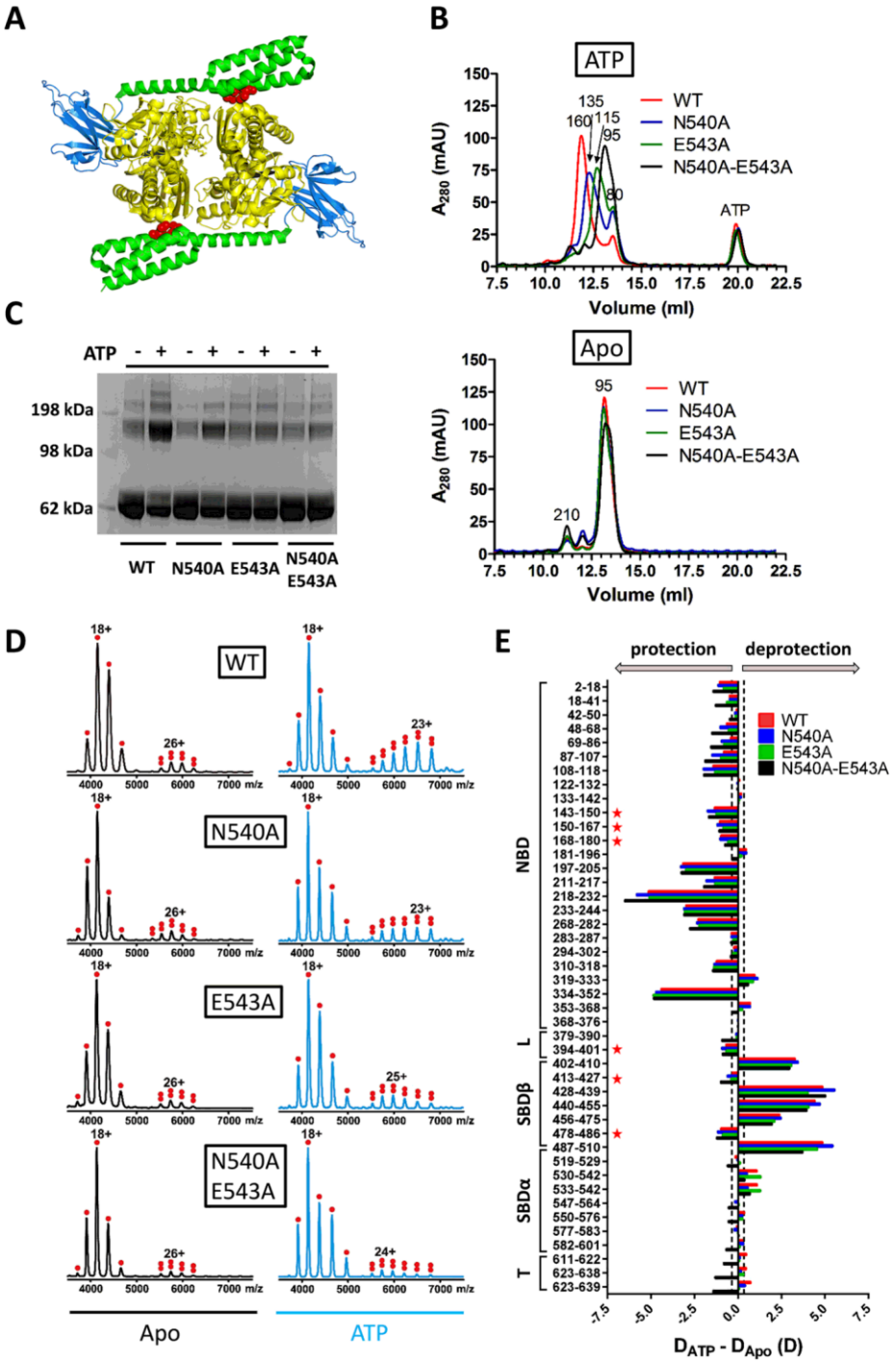

FIG. 3. **Conserved N540 and E543 residues are required for stable ATP-induced dimerization of Hsp70.** *A,* Crystal structure of DnaK ATP-bound dimer (PDB code 4jne) with N537 and E540 residues highlighted in red (N540, E543 numbering in human inducible Hsp70). The NBD domain is depicted in yellow, SBDβ in marine and SBDα in green. *B,* Hsp70 and N540A, E543A and N540A-E543A (40 μM) were incubated without (Apo) or with ATP (0.2 mM, 20 min) at 21 °C before SEC. *C,* Hsp70 WT, N540A, E543A and N540A-E543A proteins (40 μM) were pre-incubated with or without ATP for 20 min before addition of chemical cross-linker (10 molar excess of DSA). The cross-linked complexes were separated by LDS-PAGE (pre-cast gradient (4–12%) gel, NuPage). The molecular weight standard is indicated. *D,* Native ESI-MS spectra of Hsp70 WT, N540A, E543A and N540A-E543A proteins (20 μM) were acquired after their pre-incubation without (Apo) or with ATP. The charged states corresponding to monomers and dimers are labeled with single and double dots, respectively. *E*, Deuteration level (exchanged deuterons, *D*) differences of Hsp70 WT, N540A, E543A and N540A-E543A peptides in ATP-bound and nucleotide-free state (Apo) after 1200 s (for other incubation times see supplemental Fig. S2*B*) incubation in deuterated buffer. Numbers at the left indicate the Hsp70 peptide fragments; schematic representation at the left shows Hsp70 domain constitution; L, interdomain linker; T, C-terminal tail. The asterisks indicate peptides covering allosterically important regions of Hsp70 molecule. Dashed lines in the graph indicate significance level of 0.35 Da (see Experimental procedures).

(apparent MW 210 kDa) also appeared. These data support the requirement of ATP-induced Hsp70 conformation for dimerization and indicate that Hsp40 can recognize and stimulate the ATPase activity of dimeric Hsp70.

ATP-dependent Hsp70 Dimer Assembles In An Antiparallel Fashion Resembling the Dimers Captured In the Crystal Structures of DnaK and BiP—The conformational requirements for Hsp70 ATP-induced dimer formation suggest that the dimer might acquire a quaternary structure observed in the DnaK (11, 13) and BiP crystal packings (12), with two ATP-bound protomers assembled in an antiparallel orientation (Fig. 3*A*). Two residues (DnaK numbering N537, D540) in an α-helical bundle subdomain of DnaK are important for its ATP-dependent anti-parallel dimerization and are conserved in human Hsp70 (human numbering N540 and E543) (25). We rationalized that if these residues retained their role in human Hsp70 ATP-dependent dimerization, their mutation would disturb dimerization. Indeed, SEC of N540A, E543A and N540A-

E543A in Apo and ATP-bound state showed decreasing levels of dimeric forms in the order N540A>E543A>N540A-E543A, with the double mutant being unable to reach the dimeric structure (Fig. 3*B*). We saw a similar trend by chemical cross-linking and native ESI-MS (Fig. 3*C* and 3*D*). In native ESI-MS, the dimer of T204A mutant in ATP-bound state exhibited higher stability in the gas phase than WT and we therefore analyzed the dimerization interface mutant N540A-E543A also on the background of T204A mutation (T204A-N540A-E543A, supplemental Fig. S2*A*). This measurement further supported the importance of residues N540 and E543 for Hsp70 ATP-dependent dimerization. Additionally, we detected a minor population of Hsp70 dimers in Apo state, which is in concordance with current knowledge and our SEC data (Fig. 3*D*) (24). To exclude that diminished dimerization of mutants is caused by their impaired allosteric activity upon ATP binding, we analyzed WT and mutant proteins with or without ATP by HDX mass spectrometry (Fig. 3*E* and supplemental Fig. S2*B*). The ATP-induced deuteration changes are similar in WT and dimerization mutants, highlighted by protection of the NBD and opening of SBDβ. More precisely, the peptides covering allosterically important regions involved in linker-mediated domain docking (11–13, 29) are protected in all proteins in the presence of ATP: NBD docking interface (covered by peptides *143–150, 150–167* and *168–180*), SBDβ docking interface (*413–427, 478–486*) and linker region (*394–401*). These results indicate that the allosterically induced ATP-bound conformation is preserved in the N540A, E543A and N540A-E543A mutants. To independently verify the mutants' ability to reach the ATP-bound state, we tested their interaction with Tomm34, which we have shown to be ATP-dependent (supplemental Fig. S2*C*) (29). All proteins increasingly interacted with Tomm34 in the presence of ATP, supporting their conformational activity.

To evaluate the overall shape of Hsp70 ATP-dependent dimers in solution more closely, we performed small-angle X-ray scattering (SAXS) (Fig. 4 and supplemental Table S1), using T204A mutant to prevent ATP hydrolysis during sample preparation and handling. T204A protein was pre-incubated with ATP and its dimeric form was separated by SEC before SAXS at two protein concentrations (1.5 mg/ml, 2.5 mg/ml). The data were fitted to the theoretical scattering functions based on the atomic coordinates of various Hsp70 dimeric crystal structures or of our Hsp70 homology-based ATP-dependent dimer model (see Experimental Procedures). The best fit to the experimental data was obtained for Hsp70 dimer model (1.5 mg/ml, $\chi 2 = 1.2$; 2.5 mg/ml, $\chi 2 = 1.1$, Fig. 4*A* and 4*B*), supporting the proposed human Hsp70 ATP-dependent dimer model (Fig. 4*C*) over the crystal structures of DnaK and BiP dimers (PDB: 4b9q (chains AC), 5e84 (chains DF)). Taken together, these analyses suggest that the ATP-bound monomers of inducible human Hsp70 protein assemble in solution as an antiparallel dimer in a similar orientation as DnaK and BiP dimers in their crystal structures (11–13).

A

Concentration 1.5 mg/ml	$\chi 2$	Concentration 2.5 mg/ml	$\chi 2$
Hsp70 ATP dimer model	1.2	Hsp70 ATP dimer model	1.1
5e84 chains EF	1.5	4b9q chains AC	2.1
4b9q chains AC	1.8	5e84 chains EF	2.2
6ASY	1.9	6ASY	2.2
5e84 chains DF	2.1	5e84 chains DF	2.6
3c7n	2.4	3c7n	3.1
4jne	2.5	4jne	3.4
4b9q chains CD	2.7	4b9q chains CD	5.1
3d2f chains CD	3.9	3d2f chains CD	5.8
5e84 chains CA	7.6	5e84 chains CA	17.2
5e84 chains EA	16.3	5e84 chains EA	33.8
5e84 chain B	19.0	5e84 chain B	35.1

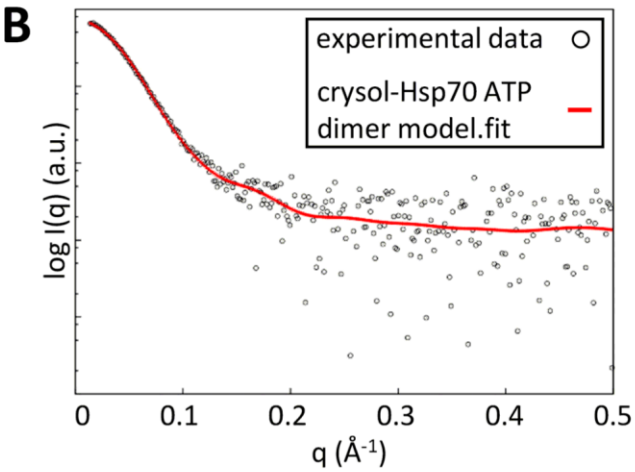

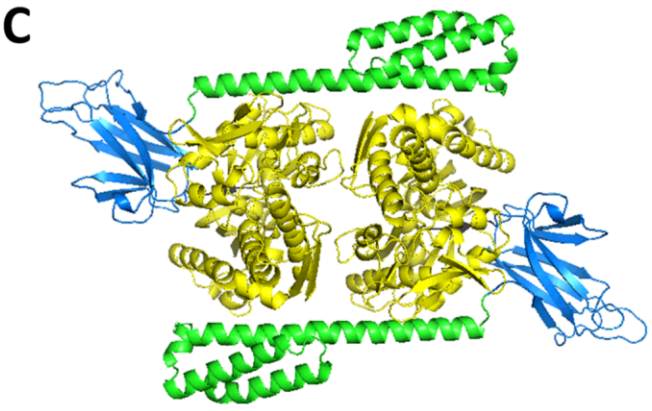

FIG. 4. **ATP-bound Hsp70 monomers assemble as antiparallel dimers in solution as determined by small-angle X-ray scattering.** *A*, $\chi 2$-ranked fitting of Hsp70 dimeric crystal structures (PDB codes with indicated chains) and homology-based Hsp70 dimer model (see Experimental Procedures) to the SAXS experimental data obtained for Hsp70-T204A mutant at two concentrations. Fitting to the experimental scattering curves was performed using CRYSOL ATSAS v.2.8.3. *B*, CRYSOL fit of Hsp70 ATP dimer atomic model. Simulated scattering data of dimeric Hsp70 atomic model (red) is fitted to experimentally obtained solution scattering showing overall good fit with $\chi 2 = 1.1$. *C*, Atomic model of Hsp70 ATP-dependent dimer, developed as described in Experimental Procedures. NBD is highlighted in yellow, SBDβ in marine and SBDα in green. N- and C-terminal unstructured regions of the model are omitted from the figure. The image was created in PyMOL.

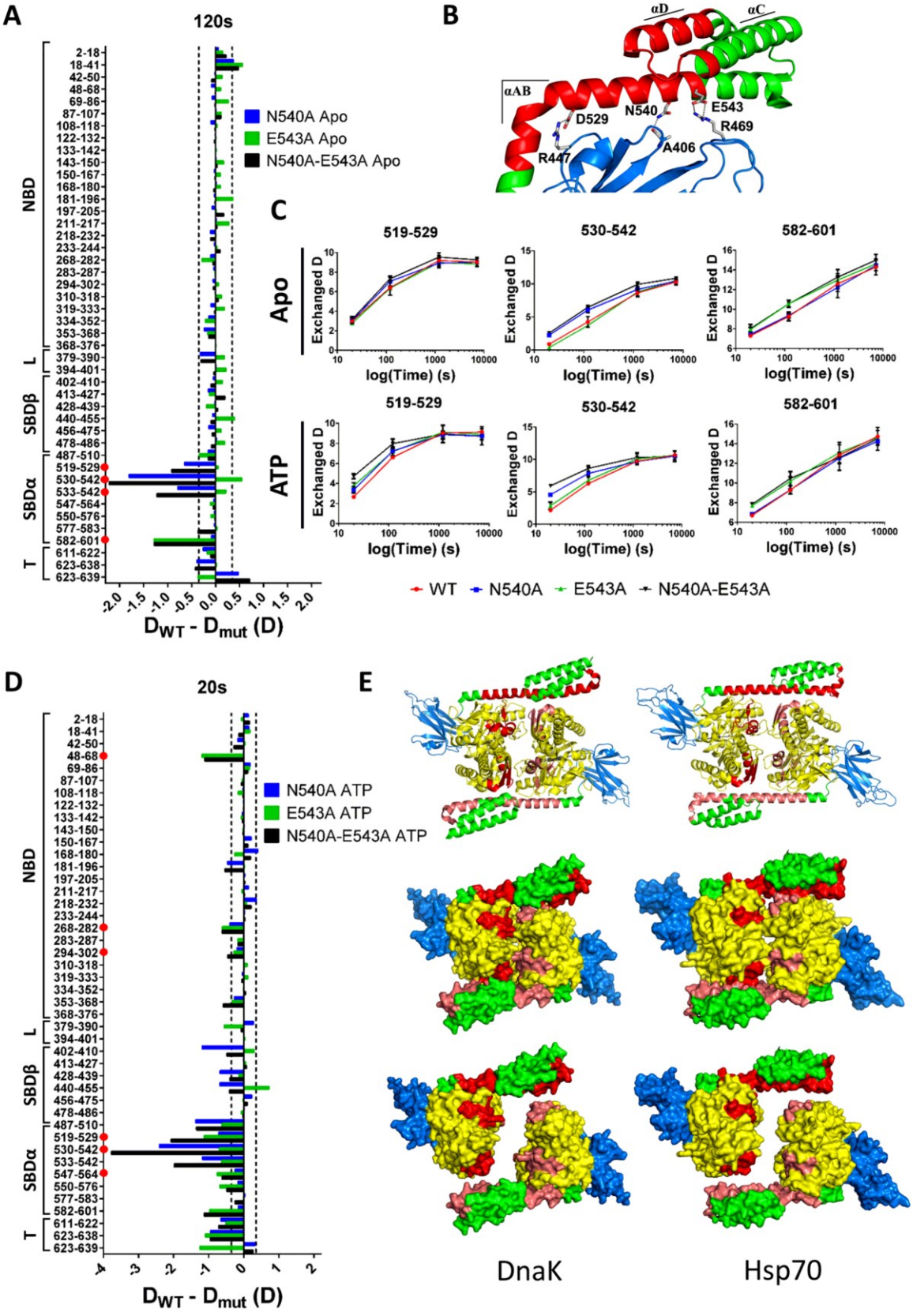

Hsp70 ATP-dependent Dimers Assemble Through Conserved Interfaces—To pinpoint the structural rearrangements introduced to the monomeric (Apo form) and dimeric (ATP-bound) Hsp70 states by N540A, E543A and N540A-E543A mutations, we compared the HDX rate of these mutants with the WT protein (Fig. 5 and supplemental Fig. S3), an approach that has been applied previously to study protein homodimerization (42–44). We observed significant destabilization of the SBD-αAB helices covered by peptides *519–529, 530–542, 533–542* in Apo N540A and N540A-E543A mutants, with the latter exhibiting more pronounced changes (Fig. 5*A* and 5*C,* and supplemental Fig. S3*B*). Because these peptides either contain or are in close vicinity to the substituted N540 and E543 residues, the detected structural changes are most likely because of local disturbances caused by the mutations, although the E543A mutation itself does not have an effect on this region. E543A and N540A-E543A showed increased deuterium incorporation in the loop connecting αC and αD helices and the αD helix (peptide *582–601*) under both nucleotide conditions (Fig. 5*A* and 5*C*), suggesting an important role of E543 in the stability of this region independently of conformation. As the αC/αD helices form a compact α-helical structural unit together with the αB helix (Fig. 5*B*), the loosening of the αD helix might explain the additive effect of E543A in destabilizing the αA/αB helices in the N540A-E543A mutant (Fig. 5*A*) (9). Because N540 and E543 together with D529 are involved in positioning the α-helical lid-SBDβ (Fig. 5*B*) (8, 9, 16) and D529 is present in the region destabilized by N540A and N540A-E543A substitutions (peptide *519–529*), we expect the mutants to have defects in the kinetics of substrate binding (see below, Fig. 6*B*).

Inspection of the ATP-bound state of Hsp70 dimerization mutants revealed several peptides with differential deuteration levels at early incubation times of the experiment (Fig. 5*D* 5*E,* and supplemental Fig. S3). These peptides can be divided into four groups according to deuteration rate under nucleotide-free and ATP-bound conditions: i) peptides with similarly increased deuteration under both nucleotide conditions, indicating ATP-independent structural changes; ii) peptides exhibiting elevated deuteration in the Apo state with further increased deuteration upon ATP addition; iii) peptides with increased deuteration only in the ATP-bound state with no correlation to the degree of dimerization deficiency introduced by N540A, E543A and N540A-E543A mutations; iv) peptides increasingly deuterated only in the presence of ATP, with E543A and N540A-E543A mutants being more affected than N540A mutant. Group i) is represented by the single peptide *582–601*, whose role has been described above. Group ii) encompasses peptides *519–529, 530–542* and *533–542*. Peptide *519–529* covers a region that does not show detectable ATP-induced changes in WT protein (supplemental Fig. S3*A*). The presence of ATP increases the degree of destabilization induced in this site only in the N540A-E543A mutant (Fig. 5*C* and supplemental Fig. S3*A*). Moreover, the E543A mutation does not affect deuteration of the *519–529* peptide in the Apo form but leads to elevated deuteration in the ATP-bound state (Fig. 5*C* and supplemental Fig. S3*A*). That the E543A and N540A-E543A mutations are more deleterious for Hsp70 ATP-dependent dimerization than N540A (Fig. 3*B*, 3*C* and 3*D*) indicates a role for the *519–529* region in dimerization. The αB helix covered by peptides *530–542* and *533–542* reacts to ATP addition by increased deuterium uptake in WT protein (supplemental Fig. S3*A*). Destabilization of this part of the protein detected in the Apo forms of N540A and N540A-E543A mutants is more pronounced in their ATP-bound states, particularly for N540A-E543A (Fig. 5*C* and supplemental Fig. S3*A*). Like *519–529,* deuteration of *530–542* and *533–542* peptides in E543A is elevated only in its NBD-SBDβ docked conformation (Fig. 5*C* and supplemental Fig. S3*A*). As the quaternary structure of Hsp70 ATP-dependent dimers in solution resembles the crystal packing of BiP ATP-bound dimers (Fig. 4) (12), we assume that increased deuteration rates of *530–542* and *533–542* peptides in the ATP-bound conformation of dimerization mutants reflect both mutation-induced loosening of the α-helical region structure (Fig. 5*B*) and dimer destabilization because of elimination of the conserved N540 and E543A residues mediating the intermolecular NBD-SBDα contacts (Fig. 3*A*) (12). Group (iii) is represented by *487–510* peptide (supplemental Fig. S3*A*). The deuteration profile of this peptide probably reflects N540A-

FIG. 5. **Hsp70 ATP-dependent dimers assemble through NBD-NBD and NBD-SBDα interfaces.** *A,* Deuteration level (exchanged deuterons, D) differences between Hsp70 WT and N540A, E543A and N540A-E543A peptides in nucleotide-free state (Apo) measured after 120 s (for other incubation times see supplemental Fig. S3*B*) incubation in deuterated buffer. The graph is labeled as in Fig. 3*E*. Red dots indicate peptides highlighted in part *B* and *C* of this figure. *B*, Crystal structure of human SBD (PDB code 4po2). SBDα (lid) helices and the lid-SBDβ positioning ionic/polar contacts are indicated. SBDβ is labeled in marine and SBDα in green. Regions covered by peptides highlighted by red dots in *A* are red. *C*, Deuteration kinetics of indicated peptides from Apo and ATP-bound Hsp70 proteins. *D,* Deuteration level (exchanged deuterons, D) differences between Hsp70 WT and N540A, E543A and N540A-E543A in ATP-bound state measured after 20 s (for other incubation times see supplemental Fig. S3*B*) incubation in deuterated buffer. The graph is labeled similarly as in Fig. 3*E*. Red dots indicate peptides highlighted (red/pink) on the atomic structures in *E*, *E. 48–68, 268–282, 294–302, 519–529 and 530–542* peptides highlighted in *D* were projected onto the homology-based Hsp70 ATP-bound dimer atomic model (see Experimental Procedures) and the corresponding peptides (see supplemental Fig. S4*C*) in DnaK were projected onto the crystal structure of DnaK ATP-bound dimer (PDB code 4jne). The peptides are colored in red or pink in the respective protomer. The atomic structures are shown in both ribbon and surface representations. Surface representation was also manually separated for clarity (bottom structures). NBD is highlighted in yellow, SBDβ in marine and SBDα in green. N- and C-terminal unstructured regions of the model are omitted from the figure. The image was created in PyMOL.

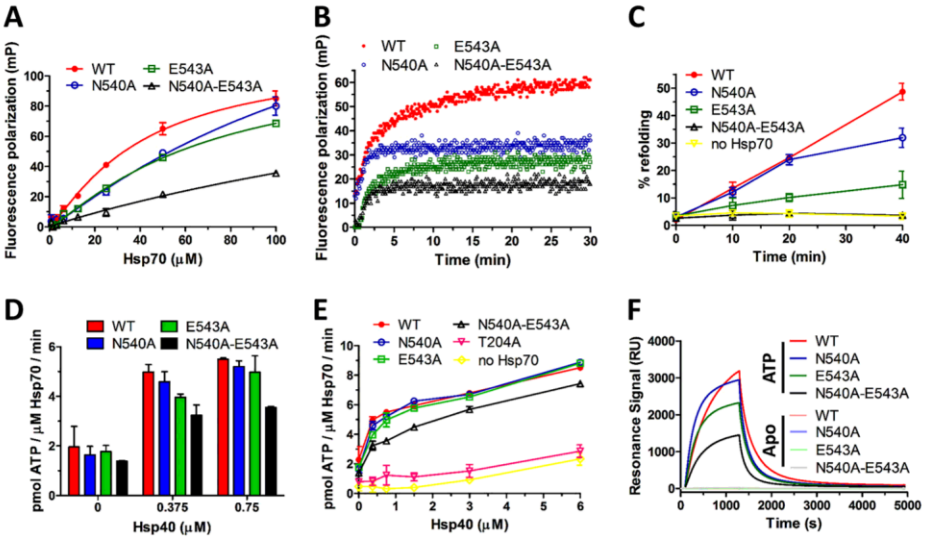

FIG. 6. **E543A and N540A-E543A mutants have severely impaired substrate binding/refolding activities and lower interaction with Hsp40.** *A,* Equilibrium binding curves of F-NRLLLTG peptide binding to Hsp70 WT and mutants under nucleotide-free conditions. Fluorescence polarization was determined at 30 nM peptide and increasing Hsp70 concentrations. Error bars represent S.D.; $n = 3$ independent experiments. *B,* Kinetics of F-NRLLLTG interaction with WT and mutant Hsp70s under nucleotide- free conditions determined by fluorescence polarization. Protein and peptide concentrations were 50 μM and 30 nM, respectively. *C,* Firefly luciferase was chemically denatured, mixed with Hsp70 WT or mutants (1 μM), Hsp40 (2 μM), Bag-1 (0.5 μM) and ATP (2 mM) and recovered luminescence was measured. Error bars represent S.D.; $n = 3$ independent experiments. *D,* ATPase activity of Hsp70 WT and mutants at lower Hsp40 concentrations, for full results see *E*. *E,* ATPase activity of Hsp70 WT and mutants (2 μM) was tested at various Hsp40 concentrations in malachite green assay. Error bars represent S.D.; $n = 3$ independent experiments. *F,* SPR measurement of Hsp70 WT and mutants binding to Hsp40 under nucleotide-free conditions (Apo) or in the presence of ATP.

induced structural changes in the ATP-bound state of Hsp70 protomer. Peptides belonging to group iv) include *48–68, 268–282, 294–302, 353–368, 547–564* and *550–576* (Fig. 5*D* and 5*E*, and supplemental Fig. S3*A*). The differential deuteration of these peptides in ATP-bound forms of E543A and N540A-E543A mutants might mirror their role in the dimerization interface. When projected onto the surface of DnaK (13) and Hsp70 dimer (homology-based model, see Experimental Procedures), group (4) peptides *48–68, 268–282 and 294–302* localize to the dimer interface together with *519–529* and *530–542* (Fig. 5*E*). The same is true for the dimer contacts in BiP and for the interface of Hsc70 NDB with Sse1 (supplemental Fig. S4*A*) (45). The interface regions identified for Hsp70 are not compatible with Sse1 dimer crystal structure (supplemental Fig. S4*A*) (14). However, although the regions covered by *353–368* and *547–564/550–576* peptides do not match any protein-protein contacts in dimeric Hsp70, they form an interface when projected onto the Sse1 dimer (supplemental Fig. S4*B*). Next, we searched for the residues mediating the intermolecular contacts in the respective dimeric structures (supplemental Fig. S4*A, S4C*). The intermolecular NBD-SBDα contacts are conserved in all of the analyzed proteins except the Sse1 dimer. However, this interface is present in Sse1-Hsc70 NBD heterodimers (supplemental Fig. S4*A*). Interestingly, although the intermolecular NBD-NBD contacts localize to the aligned peptide sequences, the residues mediating the interactions differ in Hsp70 isoforms (supplemental Fig. S4*A, S4C*). This suggests that differences in the NBD-NBD interface contribute to Hsp70 isoforms' varying dimerization propensities (Fig. 1*A*). Moreover, we observed that the highly conserved D529 (Hsp70 numbering) residue participates in intramolecular contacts involving NBD-NBD interface residues in all the analyzed proteins (supplemental Fig. S4*A*). To test the role of D529 in Hsp70 ATP-dependent dimers, we analyzed the dimerization properties of D529A mutant (supplemental Fig. S5*A* and S5*B*). This mutant can dimerize, although the ATP-bound monomer-dimer equilibrium is impaired compared with WT protein and the D529A substitution destabilized the SBDα subdomain αAB helixes in both conformational states (supplemental Fig. S5*C*). Because the αB helix contains N540 and E543 residues, the D529A-induced structural rearrangements in this region might account for the dimerization imbalance.

Taken together, the antiparallel Hsp70 ATP-dependent dimer assembles in solution through the interfaces captured in the previously solved crystal structures of Hsp70 isoforms (DnaK, BiP, Sse1-Hsc70 NBD) (12, 25, 45), although the identity of the residues mediating the interaction is isoform-specific. Moreover, our HDX data suggest that Hsp70 ATP-dependent dimers might fluctuate between BiP-like (12) and Sse1-like (14) dimer organizations.

Dimerization of ATP-bound Hsp70 Is Required for Effective Hsp70-Hsp40 Interaction and Hsp40-mediated Hsp70 Chaperoning Activity—The structural changes introduced to Hsp70

by mutating N540 and E543 impair its substrate binding capacity (Fig. 6*A* and 6*B*). To assess the chaperoning activity of dimerization deficient mutants, we measured their ability to refold denatured luciferase *in vitro* with Hsp40 and Bag1 cochaperones as the ATPase activating and nucleotide-exchange factors (Fig. 6*C*) (19, 46, 47). E543A and N540A-E543A mutants had severely impaired refolding capacity, whereas the N540A mutant allowed luciferase refolding, albeit to a lower degree than WT protein. Next, we determined Hsp40-stimulated ATPase activity. Although the ATPase activity measured at low Hsp40 concentrations (Fig. 6*D*) mirrored the dimerization defects of N540A, E543A and N540A-E543A proteins, at higher Hsp40 concentrations N540A and E543A mutants reached ATPase levels comparable to WT protein (Fig. 6*E*). The N540A-E543A mutant exhibited significantly lower activity across all Hsp40 concentrations. These results indicate that these mutants are compromised in their ability to associate and functionally cooperate with Hsp40 either during *in vitro* refolding or concentration-dependent ATPase stimulation (25). To test mutant protein binding to Hsp40 directly, we used an established surface plasmon resonance (SPR) assay (Fig. 6*F*) (25, 48). We did not detect interaction between Hsp40 and the Hsp70 variants under nucleotide-free conditions. Addition of ATP led to a high binding signal for WT protein. The binding curves of N540A, E543A and N540A-E543A mutants reflected their ability to form dimers (Fig. 3), with N540A-E543A having considerably diminished affinity to Hsp40. These data suggest that the ATP-dependent dimerization of human inducible Hsp70 is required for its efficient interaction with Hsp40, like the DnaK-DnaJ interaction (25).

Tomm34 and Chip Cochaperones Bind to Hsp70 ATP-induced Dimers With Different Outcome—To delineate the behavior of Hsp70 ATP-dependent dimers further, we evaluated engagement in multichaperone complexes by analyzing the binding of ATP-induced Hsp70 dimers to the TPR cochaperones Tomm34 (34 kDa) (29) and Chip (35 kDa) (49, 50). As a negative control we used Hsp70 lacking its C-terminal PTIEEVD motif that mediates the interaction with TPR domains (supplemental Fig. S6*A*, S6*B*) (22). In SEC, Chip eluted as a single peak with MW 130 kDa under both nucleotide conditions (Fig. 7*A*). In accordance with these data, it is known that Chip forms dimers that aberrantly separate in SEC as larger oligomers because of their non-globular shape (49, 51). We also verified Chip by native ESI-MS, which clearly showed a MW corresponding to dimeric molecules (supplemental Fig. S6*C*). The separation of Chip/Hsp70 mixtures under nucleotide-free conditions revealed that Chip was completely saturated by Hsp70 and the elution volume of the resulting complex corresponded to 260 kDa suggesting a 2:1 stoichiometry ($Chip_2$:Hsp70). Because the proteins were mixed in equimolar concentrations, a fraction of Hsp70 remained free as evidenced by the presence of the 95 kDa elution peak. The addition of ATP to the Chip/Hsp70 mixture led to the formation of one predominant peak with MW 315 kDa indicating the presence of a $Chip_2$:$Hsp70_2$ complex. As controls, we did not detect interactions between Chip and Hsp70ΔPTIEEVD with or without nucleotide addition (supplemental Fig. S6*A*). However, Hsp70ΔPTIEEVD was able to assemble as dimers in the presence of ATP. These data indicate that Chip dimers form a stable complex with ATP-induced Hsp70 dimers. This is supported by native ESI-MS (supplemental Fig. S6*D*). In the Apo state, complexes corresponding to $Chip_2$:Hsp70 and to a lesser extent $Chip_2$:$Hsp70_2$ was also detected. On incubation with ATP, we detected only $Chip_2$:$Hsp70_2$ complexes and Hsp70 dimers because of disruption of the larger MW complexes during ESI-MS. Moreover, the Hsp70 N540A-E543A mutant did not form ATP-induced $Chip_2$:$Hsp70_2$ complexes, exhibiting similar behavior to Hsp70 WT/Chip mixtures in the Apo state.

Tomm34 eluted as a single peak of 55 kDa representing its monomeric structure (Fig. 7*B*, see also Fig. 7*C* and 7*D*). The elution profiles of Tomm34/Hsp70 and Tomm34/Hsp70ΔPTIEEVD in the absence of ATP were almost identical, with clearly separated peaks for individual proteins (Fig. 7*B* and supplemental Fig. S6*B*). This was expected because Tomm34-Hsp70 interaction is both ATP- and PTIEEVD-dependent (29). Accordingly, Hsp70ΔPTIEEVD dimers formed in the presence of ATP did not interact with Tomm34 (supplemental Fig. S6*B*). Separation of Tomm34/Hsp70 mixture in the presence of ATP resulted in a dominant peak with MW corresponding to 130 kDa and a concomitant decrease in ATP-dependent Hsp70 dimers and Tomm34 peak intensities. Conversely, we observed an increase in the Hsp70 ATP-bound monomer peak (80 kDa) (Fig. 7*B*). SDS-PAGE revealed that the 130 kDa peak contains Tomm34 and Hsp70. The apparent MW of the 130 kDa peak suggests the stoichiometry of the Tomm34/Hsp70 complex to be 1:1. We also chemically cross-linked the individual Tomm34 or Hsp70 proteins or their complex and analyzed the resulting assemblies by Western blotting using Tomm34 and Hsp70 specific antibodies (Fig. 7*C*). The ATP-dependent Hsp70 dimer (migrating at approx. 150 kDa) dissociates upon interaction with Tomm34 and the resulting Tomm34:Hsp70 complex has 1:1 stoichiometry according to its migration at approx. 110 kDa in the denaturing gel. An ATP-dependent 1:1 complex between Hsp70 WT/N540A-E543A and Tomm34 was also detected by native ESI-MS, indicating that stable Hsp70 ATP-dependent dimerization is not required for the Hsp70-Tomm34 interaction (Fig. 7*D*). Taken together, the ATP-induced Hsp70 dimer can complex with TPR cochaperones. However, although Hsp70 homodimers remain intact upon interaction with Chip, they are destabilized during ATP-dependent interaction with Tomm34 and form a 1:1 heterodimer.

ATP-dependent Hsp70 Dimers Are Distributed In High-molecular Weight Protein Complexes Ex Vivo—To gain insight into the potential role of ATP-dependent Hsp70 dimer formation in the cellular proteome, we compared the distribution of

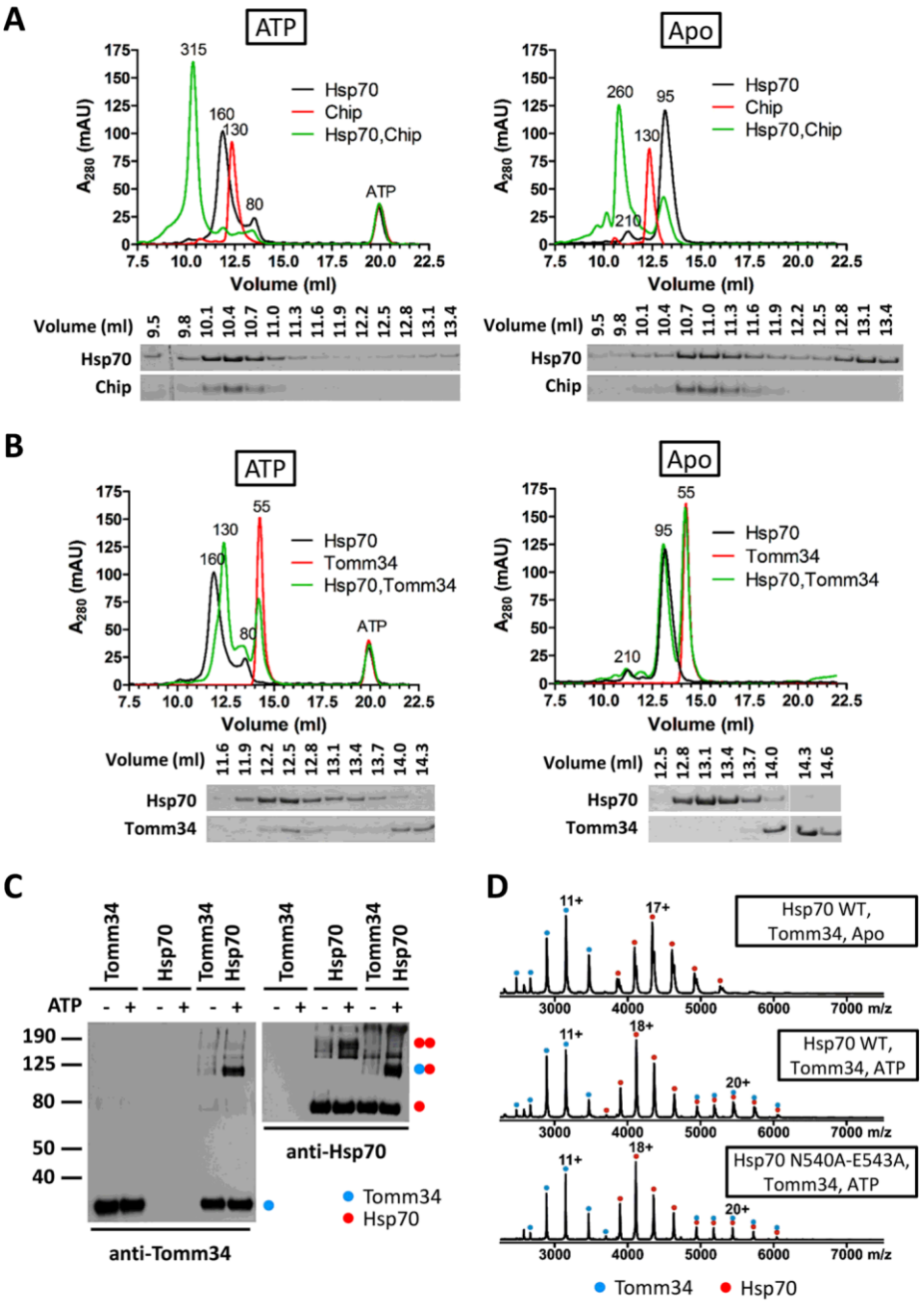

FIG. 7. **ATP-dependent dimer of Hsp70 associates with Chip and Tomm34 TPR domain cochaperones through different mechanisms.** *A* and *B*, Hsp70 WT and Chip or Tomm34 were mixed (both at 40 μM) and pre-incubated with or without ATP (0.2 mM, 20 min, 21 °C) before separation by analytical SEC. Apparent MW of eluting peaks is indicated (see Experimental Procedures). Proteins in the separated fractions were analyzed by SDS-PAGE and Coomassie staining. *C*, Hsp70, Tomm34 or both (40 μM each) were mixed in the presence or absence of ATP (0.2 mM) for 20 min at 21 °C. Glutaraldehyde was added (0.5 mM final concentration) for 10 mins and the reactions stopped with Tris, pH 8 (80 mM final concentration). Samples were diluted in 2× CSB loading buffer, separated by SDS-PAGE, blotted and probed by Tomm34 or Hsp70 antibodies. Blue and red dots, respectively, indicate positions of Tomm34 and Hsp70 monomers, homodimers and heterodimers. *D*, Native ESI-MS spectra of Hsp70 WT or N540A-E543A mutant mixtures with Tomm34 (20 μM) were acquired after pre-incubation without (Apo) or with ATP. The charged states corresponding to Tomm34/Hsp70 monomers and heterodimers are labeled with single and double dots, respectively.

HA-tagged WT and N540A-E543A proteins in cell lysates fractionated by SEC (Fig. 8*A*). Firstly, lysates were processed by preparative gel filtration to remove low-molecular weight compounds including ATP. Before SEC, the processed lysates were incubated in the presence or absence of ATP for 20 min. In the absence of ATP, both WT and N540A-E543A proteins were evenly distributed in the early fractions (elution volume 7.5–12 ml) and accumulated in the later fractions (elution volume 12.5–13.5 ml) that correspond to their low oligomeric/monomeric forms (see Fig. 3*B*). Pre-incubation with ATP led to N540A-E543A becoming mainly low oligomeric, with almost complete loss in the early fractions. In contrast, WT Hsp70 retained its uniform distribution in the early fractions with slightly increased population of low oligomeric species in the presence of ATP. To probe the conformational status of Hsp70 in cell lysates we also tested the level of Tomm34 in SEC fractions (29). Tomm34 shifted to earlier fractions after ATP pre-incubation. Of note, Tomm34 coeluted with the low oligomeric fractions of WT and N540A-E543A Hsp70, indicating the presence of 1:1 complexes. This result shows that both Hsp70 variants were in NBD-SBDβ docked conformation and interacted with Tomm34 in the ATP-treated samples. Analogously, we performed glutaraldehyde cross-linking of desalted total cell lysates from the cells

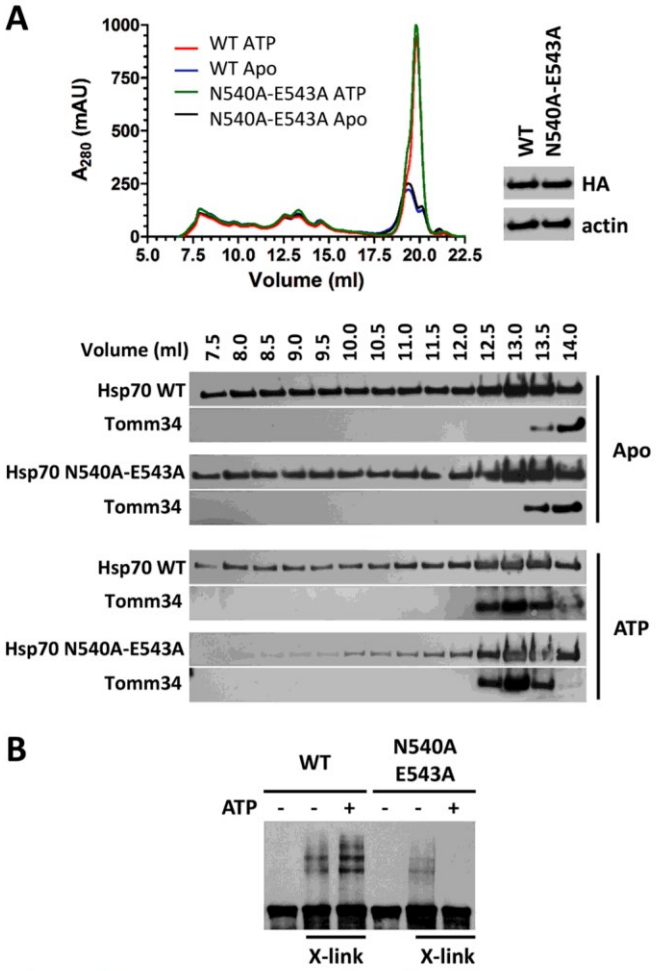

FIG. 8. **ATP-dependent dimerization of Hsp70 is required for its participation in high molecular weight complexes detected *ex vivo*.** *A*, Desalted lysates from HEK293 cells overexpressing HA-tagged Hsp70 WT or N540A-E543A mutant to the same level (evaluated by Western blotting using anti-HA antibody) were incubated with/without 2 mM ATP for 20 min at 21 °C before SEC. The presence of Hsp70 and Tomm34 proteins in the separated fractions was tested by Hsp70/Tomm34 antibodies. *B*, Desalted HEK293 cell lysates with overexpressed HA-tagged Hsp70 WT or N540A-E543A were incubated with/without 2 mM ATP for 20 min at 21 °C before mixing with glutaraldehyde (0.5 mM final concentration) for 10 min at 21 °C. The reaction was stopped by adding Tris, pH 8 (80 mM final concentration), samples were supplemented with 2× CSB loading buffer and analyzed by SDS-PAGE and Western blotting with Hsp70 antibody.

overexpressing HA-tagged WT and N540A-E543A proteins and separated the cross-linked complexes by SDS-PAGE (Fig. 8*B*). We observed an increase in the level of higher-molecular weight protein complexes containing HA-Hsp70 WT in the presence of ATP. On the contrary, the multiprotein complexes of HA-tagged N540A-E543A captured in the absence of ATP rapidly disassembled in the presence of ATP. These observations suggest that the ATP-dependent dimerization properties of Hsp70 are necessary for its participation in higher-molecular weight protein complexes in cells.

DISCUSSION

Formation and disassembly of a small population of ATP-dependent DnaK dimers plays a critical role in DnaJ-regulated DnaK ATPase activity (25, 26). Moreover, conservancy of residues involved in mediating homo-dimerization of ATP-bound DnaK in its eukaryotic homologs supports a functional role of the ATP-dependent dimer (52). Here, we demonstrated that human Hsc70 and Hsp70 proteins form ATP-dependent dimers in solution with markedly higher efficiency compared with DnaK (Fig. 1*A*). The higher affinity of self-interactions between ATP-bound Hsp70 monomers *versus* Apo monomers is demonstrated by efficient ATP-bound dimer formation at low concentrations of Hsp70 (10 μM) compared with the more than 200 μM of Apo Hsp70 needed to assemble into dimers (Fig. 2*A*) (24, 53). Interestingly, Hsc70 was shown to follow ATP-dependent monomerization similarly to BiP in number of previous studies using SEC and SAXS (54–57). The discordance in the results might be caused by the fact that Hsc70 in those studies was purified from animal tissues and/or separated on Superose 12 SEC column. It has been demonstrated that posttranslational modifications and buffer ionic-strength influence Hsp70 ATP-dependent dimerization (27) and that Superose 12 ionically interacts with separated proteins complicating the interpretation (58). Alternatively, the presence of Hsp40 contamination in purified Hsc70 proteins would lead to rapid Hsc70 ATP-bound dimer dissociation after ATP addition (Fig. 2*C*). Hsp40 was also reported to promote ATP-dependent dimerization/oligomerization of Hsp70/Hsc70 purified from animal tissues (59) or insect cells (27), indicating that the role of Hsp70 posttranslational modification might be decisive for its oligomerization properties. In addition, an SAXS study describing the structures of recombinant bacterially purified Hsc70 in ADP- and ATP-bound conformations revealed ATP-induced compaction of Hsc70 reflecting NBD-SBDβ docking in monomers (57). However, the authors later discovered that the expression construct they used contained a mutation causing E543K substitution (60). As we now demonstrate, E543 is crucial for ATP-dependent Hsp70 dimerization.

The structural analyses (SAXS, HDX, Fig. 4 and 5, and supplemental Fig. S3) with dimerization-deficient mutants of human Hsp70 (N540A, E543A, N540A-E543A, Fig. 3) revealed that Hsp70 predominantly assembles in solution as an antiparallel dimer, closely resembling the crystal packing of its homologs (6, 11–13, 45). A recent study suggested the presence of antiparallel human Hsp70 dimers in multichaperone complexes (27), however their subunit orientation in the ATP-bound state inferred from chemical cross-linking does not satisfy the topology of antiparallel Hsp70 ATP-dependent dimers captured in DnaK/BiP structures and described here (6, 11–13). This discrepancy could stem from the use of Hsp70 purified from eukaryotic expression system by Morgner *et al.* (27) (*i.e.* post-translationally modified) or be caused

by the error-prone intra- and inter-molecular cross-links differentiation because of the homo-dimeric nature of Hsp70 (61). Although the residues mediating NBD-SBDα contacts in the antiparallel dimer are conserved, the NBD-NBD interfaces show lower conservation, as documented by inspection of crystal structures and our homology-based Hsp70 dimer model (supplemental Fig. S4). Therefore, NBD-SBDα contacts might serve as an elemental dimer interface that is accompanied by homolog-specific NBD-NBD interactions allowing for functional differentiation of Hsp70 dimeric species. Mechanistically, stable dimerization of ATP-bound Hsp70 may prevent Hsp70 monomers from premature association with Hsp110 and Bag NEFs as documented by evidence that Hsp110/BAG interfaces with Hsp70 NBD largely overlap with NBD-NBD contacts in the Hsp70 ATP-dependent dimer (47, 62, 63). Accordingly, although Bag1M protein increased the dissociation rate of ADP analog from Hsc70, its role in the dissociation of ATP analog was negligible (64).

Contrary to previous results that DnaK dimerization mutants N537A and D540A did not perturb substrate binding equilibria (25), N540, E543A and N540A-E543A substitutions in human Hsp70 severely compromised its substrate binding thermodynamics (Fig. 6*A*) because of a large destabilization of the Hsp70 SBDα region (Fig. 5 and supplemental Fig. S3). The faster kinetics of substrate binding for the dimerization mutants (Fig. 6*B*) resembles the behavior of lidless DnaK and the D540A-E548A DnaK mutant (8, 16). Some DnaK/Hsp70 C-terminal truncation mutants exhibit intramolecular binding of the destabilized SBDα hydrophobic motifs into the substrate binding site of SBDβ (65, 66). This self-binding increases the intrinsic ATPase rate of these proteins (67–69). We do not expect the dimerization mutants to follow this mechanism because their basal ATPase activity is comparable to WT protein (Fig. 6*D*). Therefore, the elution profile of the predominantly monomeric N540A-E543A mutant (Fig. *3B*) showing a dominant peak at MW 95 kDa in the presence of ATP is likely to mirror complex processes involving both impaired ATP-bound monomer/dimer equilibrium and destabilization of the SBDα subdomain (Fig. 5), rather than increased ATP hydrolysis by this mutant.

Our data showed that the degree of dimerization defects in the analyzed mutants was mirrored by their decreased interaction with Hsp40 and refolding activity (Fig. *6CDEF*). Dimerization deficient E543A and N540A-E543A mutants did not refold denatured luciferase even at a saturating concentration of Hsp40 (2 μM, Fig. 6*C*). Because N540A-E543A binds substrates very weakly (Fig. 6*A* and 6*B*), its inactivity in the refolding assay cannot be clearly distinguished from its dimerization and Hsp40 binding defects. However, although N540A and E543A have comparable defects in substrate binding activity (Fig. 6*A*), N540A mediates a significantly higher level of luciferase refolding (Fig. 6*C*). In addition, N540A mutation allows a significant level of Hsp70 dimerization and Hsp40 interaction (Fig. 3*B,* 3*C,* 3*D*, Fig. 6*F*). Therefore, we speculate that Hsp40-mediated substrate transfer to ATP-bound Hsp70 requires chaperone transient dimerization. Evidence exists suggesting that substrate binding to SBDβ needs to be followed by SBDα closing over SBDβ for effective Hsp40/substrate-stimulated ATPase activity of Hsp70 (11, 26). Thus, transient stabilization of the SBDα subdomain of an Hsp70 protomer by its docking onto the NBD domain of the partner Hsp70 molecule might provide a time window for productive Hsp40-mediated substrate positioning into SBDβ before the SBDα subdomain closes over SBDβ. This hypothesis is consistent with the paradoxical observation that the DnaJ-DnaK interaction relies on both ATP-dependent DnaK dimerization (25) and dimer dissociation allowing free movement of the SBDα subdomain (26). Additionally, our SEC analysis of Hsp70 ATP-dependent dimers coincubated with Hsp40 (Fig. 2*C*) revealed complete dimer dissociation, however, the resulting monomers separated as both ATP-bound and ADP/Apo forms (apparent MW 80 and 95 kDa, respectively) indicating that Hsp40 dimer interaction with Hsp70 ATP-bound dimer does not activate the ATPase activity of both Hsp70 protomers. This observation suggests that $Hsp70_2$:$Hsp40_2$ interaction is asymmetrical.

Hsp70 isolated from cells is commonly observed in larger protein complexes (70–72). Our *ex vivo* experiments indicated that ATP-dependent Hsp70 dimerization is vital for Hsp70 participation in these high molecular weight complexes (Fig. 8*A*). Furthermore, antiparallel dimeric Hsp70 species were detected in *in vitro* reconstituted complexes involving Hsp90, Hop, Hsp40, and GR (Glucocorticoid receptor) (27), supporting the functional role of Hsp70 dimerization in multichaperone assemblies. The level of inducible Hsp70 is elevated under proteotoxic conditions and chronically increased in some pathologies, including cancer (73–78). Given that intracellular concentrations of Hsp70 can reach up to tens of μM under stress conditions (79, 80), the physiological importance of ATP-dependent Hsp70 dimers for overcoming proteotoxic stress becomes a likely hypothesis.

Considering the recently discovered regulatory role of ATP-induced dimerization for Hsp70 chaperoning activity (Hsp40 binding) (25, 26) and multichaperone complex formation (27), differential effects of TPR cochaperone binding to Hsp70 ATP-bound dimers (Fig. 7) are likely to be important for overall activity. Association of Hsp70 ATP-bound dimers with Chip may facilitate spatial coordination of Hsp40/Hsp70-mediated substrate processing and ubiquitination (50, 81). Conversely, the inhibitory role of Tomm34 on Hsp70-mediated refolding activity (29) can be attributed to its ability to dissociate Hsp70 ATP-bound dimers (Fig. 7*B* and 7*C*) necessary for substrate capture during effective Hsp70-Hsp40 interaction (18, 25, 26, 82, 83). We have previously suggested that the additional Tomm34-Hsp70 binding site is located between residues 533–543 in the SBDα subdomain (29). This region contains both residues (N540, E543) required for the formation of Hsp70 antiparallel dimers. It is yet to be determined whether

Tomm34 occupies the 533–543 region directly or modulates its availability for Hsp70 homodimerization through allosteric changes in the SBDα subdomain. Nevertheless, ATP-dependent Hsp70 dimer dissociation by Tomm34 provides structural support for our previously suggested model of Tomm34-mediated pre-protein shuttling between Hsp70 and Hsp90 enabling its cytosolic transport in semifolded but aggregation-proof form (29). In addition, our results support the notion that TPR domain cochaperone binding to EEVD motif of Hsp70 does not follow a uniform scaffolding mechanism and suggest that the interaction is cochaperone specific (50).

The thermodynamics of Hsp70-Tomm34 interactions determined by our previous ITC analysis (29) is likely to reflect multiple equilibria transitions (*e.g.* Hsp70 ATP-bound monomer/dimer equilibrium), complicating data interpretation. Hsp70:Tomm34 complex stoichiometry was determined to be 2:1, whereas the current study shows that Tomm34 associates with ATP-bound Hsp70 monomer (Fig. 7*B*, 7*C* and 7*D*). A plausible explanation for this discrepancy would be that Hsp70 dimer dissociation by Tomm34 binding to one of the protomers renders the other protomer incapable of further association with Tomm34.

In conclusion, ATP-dependent antiparallel Hsp70 dimerization is an evolutionary conserved mechanism for Hsp70 activity regulation that has been adapted by different Hsp70 homologs with various propensities. In contrast to bacterial DnaK and human BiP, human stress-induced Hsp70 is largely dimeric in the presence of ATP *in vitro* and *ex vivo*, which might reflect the specific role of stress-induced Hsp70 in the maintenance of cellular proteostasis under proteotoxic conditions. Moreover, Hsp70 ATP-bound dimers are used either as a scaffold for TPR domain cochaperone binding (Chip) or, conversely, cochaperone binding (Tomm34) leads to rapid disassembly, which may explain the inhibitory effect of Tomm34 on the Hsp70 chaperone system (29).

Acknowledgment—We thank Dr. P. J. Coates for critical reading of the manuscript.

DATA AVAILABILITY

The mass spectrometry proteomics data have been deposited to the ProteomeXchange Consortium via the PRIDE (https://www.ebi.ac.uk/pride/archive/) partner repository with the dataset identifier PXD010069. Small angle scattering datasets, atomic model and fits have been deposited to the Small Angle Scattering Biological Data Bank (www.sasbdb.org) as entry SASDDN6.

* This work was mainly supported by Czech Science Foundation (16-20860S), additional support was provided by the Ministry of Education, Youth and Sports of the Czech Republic (MEYS CR, LO1413, LQ1604 and LO1509), by the Ministry of Health of the Czech Republic - conceptual development of research organization (MMCI, 00209805) and EU CZ.1.05/1.1.00/02.0109 and OPPK CZ.2.16/3.1.00/24023. CIISB research infrastructure project LM2015043 funded by MEYS CR is gratefully acknowledged for the financial support of the measurements at the CF X-ray Diffraction and BioSAXS, CEITEC and at the Center of Molecular Structure, BioCeV. Part of the work was carried out with the support of Core Facility Biomolecular Interactions and Crystallization of CEITEC - Central European Institute of Technology under CEITEC - open access project LM2011020 funded by MEYS CR under the activity "Projects of major infrastructures for research, development and innovations".

S This article contains supplemental Figures and Tables.

‡‡ Current address: Heinrich Pette Institute – Leibniz Institute for Experimental Virology, Martinistraβe 52, 20251 Hamburg, Germany.

§§ To whom correspondence may be addressed. E-mail: pman@biomed.cas.cz.

¶¶ To whom correspondence may be addressed. E-mail: muller@mou.cz.

Author contributions: F.T., M.D., P. Muller, and P. Man designed research; F.T., M.D., P.V., J.C., V.M., J.H., A.K., J.M., T.K., B.V., P. Muller, and P. Man performed research; F.T., M.D., P.V., J.C., V.M., J.H., A.K., J.M., T.K., B.V., P. Muller, and P. Man analyzed data; F.T., M.D., P. Muller, and P. Man wrote the paper.

REFERENCES

1. Calamini, B., and Morimoto, R. I. (2012) Protein homeostasis as a therapeutic target for diseases of protein conformation. *Curr. Topics Med. Chem.* **12,** 2623–2640
2. Young, J. C., Agashe, V. R., Siegers, K., and Hartl, F. U. (2004) Pathways of chaperone-mediated protein folding in the cytosol. *Nat. Rev. Mol. Cell Biol.* **5,** 781–791
3. Young, J. C. (2010) Mechanisms of the Hsp70 chaperone system. *Biochim. Biol. Cell.* **88,** 291–300
4. Boorstein, W. R., Ziegelhoffer, T., and Craig, E. A. (1994) Molecular evolution of the HSP70 multigene family. *J. Mol. Evolution* **38,** 1–17
5. Radons, J. (2016) The human HSP70 family of chaperones: where do we stand? *Cell Stress Chaperones* **21,** 379–404
6. Yang, J., Zong, Y., Su, J., Li, H., Zhu, H., Columbus, L., Zhou, L., and Liu, Q. (2017) Conformation transitions of the polypeptide-binding pocket support an active substrate release from Hsp70s. *Nat. Communications* **8,** 1201
7. Pellecchia, M., Montgomery, D. L., Stevens, S. Y., Vander Kooi, C. W., Feng, H. P., Gierasch, L. M., and Zuiderweg, E. R. (2000) Structural insights into substrate binding by the molecular chaperone DnaK. *Nat. Structural Biol.* **7,** 298–303
8. Fernandez-Saiz, V., Moro, F., Arizmendi, J. M., Acebron, S. P., and Muga, A. (2006) Ionic contacts at DnaK substrate binding domain involved in the allosteric regulation of lid dynamics. *J. Biol. Chem.* **281,** 7479–7488
9. Zhang, P., Leu, J. I., Murphy, M. E., George, D. L., and Marmorstein, R. (2014) Crystal structure of the stress-inducible human heat shock protein 70 substrate-binding domain in complex with peptide substrate. *PLoS ONE* **9,** e103518
10. Swain, J. F., Dinler, G., Sivendran, R., Montgomery, D. L., Stotz, M., and Gierasch, L. M. (2007) Hsp70 chaperone ligands control domain association via an allosteric mechanism mediated by the interdomain linker. *Mol. Cell* **26,** 27–39
11. Kityk, R., Kopp, J., Sinning, I., and Mayer, M. P. (2012) Structure and dynamics of the ATP-bound open conformation of Hsp70 chaperones. *Mol. Cell* **48,** 863–874
12. Yang, J., Nune, M., Zong, Y., Zhou, L., and Liu, Q. (2015) Close and allosteric opening of the polypeptide-binding site in a human Hsp70 chaperone BiP. *Structure* **23,** 2191–2203
13. Qi, R., Sarbeng, E. B., Liu, Q., Le, K. Q., Xu, X., Xu, H., Yang, J., Wong, J. L., Vorvis, C., Hendrickson, W. A., Zhou, L., and Liu, Q. (2013) Allosteric opening of the polypeptide-binding site when an Hsp70 binds ATP. *Nat. Struct. Mol. Biol.* **20,** 900–907
14. Liu, Q., and Hendrickson, W. A. (2007) Insights into Hsp70 chaperone activity from a crystal structure of the yeast Hsp110 Sse1. *Cell* **131,** 106–120
15. Zhuravleva, A., and Gierasch, L. M. (2015) Substrate-binding domain conformational dynamics mediate Hsp70 allostery. *Proc. Natl. Acad. Sci. U.S.A.* **112,** E2865–E2873
16. Buczynski, G., Slepenkov, S. V., Sehorn, M. G., and Witt, S. N. (2001) Characterization of a lidless form of the molecular chaperone DnaK:

deletion of the lid increases peptide on- and off-rate constants. *J. Biol. Chem.* **276,** 27231–27236
17. Mayer, M. P., Schroder, H., Rudiger, S., Paal, K., Laufen, T., and Bukau, B. (2000) Multistep mechanism of substrate binding determines chaperone activity of Hsp70. *Nature structural biology* **7,** 586–593
18. Kityk, R., Kopp, J., and Mayer, M. P. (2018) Molecular Mechanism of J-Domain-Triggered ATP Hydrolysis by Hsp70 Chaperones. *Mol. Cell* **69,** 227–237 e224
19. Yu, H. Y., Ziegelhoffer, T., and Craig, E. A. (2015) Functionality of Class A and Class B J-protein cochaperones with Hsp70. *FEBS Lett.* **589,** 2825–2830
20. Bracher, A., and Verghese, J. (2015) The nucleotide exchange factors of Hsp70 molecular chaperones. *Front Mol. Biosci.* **2,** 10
21. Yam, A. Y., Albanese, V., Lin, H. T., and Frydman, J. (2005) Hsp110 cooperates with different cytosolic HSP70 systems in a pathway for de novo folding. *J. Biol. Chem.* **280,** 41252–41261
22. Scheufler, C., Brinker, A., Bourenkov, G., Pegoraro, S., Moroder, L., Bartunik, H., Hartl, F. U., and Moarefi, I. (2000) Structure of TPR domain-peptide complexes: critical elements in the assembly of the Hsp70-Hsp90 multichaperone machine. *Cell* **101,** 199–210
23. Allan, R. K., and Ratajczak, T. (2011) Versatile TPR domains accommodate different modes of target protein recognition and function. *Cell Stress Chaperones* **16,** 353–367
24. Aprile, F. A., Dhulesia, A., Stengel, F., Roodveldt, C., Benesch, J. L., Tortora, P., Robinson, C. V., Salvatella, X., Dobson, C. M., and Cremades, N. (2013) Hsp70 oligomerization is mediated by an interaction between the interdomain linker and the substrate-binding domain. *PLoS ONE* **8,** e67961
25. Sarbeng, E. B., Liu, Q., Tian, X., Yang, J., Li, H., Wong, J. L., Zhou, L., and Liu, Q. (2015) A functional DnaK dimer is essential for the efficient interaction with Hsp40 heat shock protein. *J. Biol. Chem.* **290,** 8849–8862
26. Liu, Q., Li, H., Yang, Y., Tian, X., Su, J., Zhou, L., and Liu, Q. (2017) A disulfide-bonded DnaK dimer is maintained in an ATP-bound state. *Cell Stress Chaperones* **22,** 201–212
27. Morgner, N., Schmidt, C., Beilsten-Edmands, V., Ebong, I. O., Patel, N. A., Clerico, E. M., Kirschke, E., Daturpalli, S., Jackson, S. E., Agard, D., and Robinson, C. V. (2015) Hsp70 forms antiparallel dimers stabilized by post-translational modifications to position clients for transfer to Hsp90. *Cell Reports* **11,** 759–769
28. Preissler, S., Chambers, J. E., Crespillo-Casado, A., Avezov, E., Miranda, E., Perez, J., Hendershot, L. M., Harding, H. P., and Ron, D. (2015) Physiological modulation of BiP activity by trans-protomer engagement of the interdomain linker. *Elife* **4,** e08961
29. Durech, M., Trcka, F., Man, P., Blackburn, E. A., Hernychova, L., Dvorakova, P., Coufalova, D., Kavan, D., Vojtesek, B., and Muller, P. (2016) Novel entropically driven conformation-specific interactions with Tomm34 protein modulate Hsp70 protein folding and ATPase activities. *Mol. Cell. Proteomics* **15,** 1710–1727
30. Chang, L., Bertelsen, E. B., Wisen, S., Larsen, E. M., Zuiderweg, E. R., and Gestwicki, J. E. (2008) High-throughput screen for small molecules that modulate the ATPase activity of the molecular chaperone DnaK. *Anal. Biochem.* **372,** 167–176
31. Franke, D., Petoukhov, M. V., Konarev, P. V., Panjkovich, A., Tuukkanen, A., Mertens, H. D. T., Kikhney, A. G., Hajizadeh, N. R., Franklin, J. M., Jeffries, C. M., and Svergun, D. I. (2017) ATSAS 2.8: a comprehensive data analysis suite for small-angle scattering from macromolecular solutions. *J. Appl. Crystallography* **50,** 1212–1225
32. Pettersen, E. F., Goddard, T. D., Huang, C. C., Couch, G. S., Greenblatt, D. M., Meng, E. C., and Ferrin, T. E. (2004) UCSF Chimera–a visualization system for exploratory research and analysis. *J. Computational Chem.* **25,** 1605–1612
33. Sali, A., and Blundell, T. L. (1993) Comparative protein modelling by satisfaction of spatial restraints. *J. Mol. Biol.* **234,** 779–815
34. Kadek, A., Kavan, D., Felice, A. K., Ludwig, R., Halada, P., and Man, P. (2015) Structural insight into the calcium ion modulated interdomain electron transfer in cellobiose dehydrogenase. *FEBS Lett.* **589,** 1194–1199
35. Jensen, P. F., Larraillet, V., Schlothauer, T., Kettenberger, H., Hilger, M., and Rand, K. D. (2015) Investigating the interaction between the neonatal Fc receptor and monoclonal antibody variants by hydrogen/deuterium exchange mass spectrometry. *Mol. Cell. Proteomics* **14,** 148–161
36. Zhang, Z., and Smith, D. L. (1993) Determination of amide hydrogen exchange by mass spectrometry: a new tool for protein structure elucidation. *Protein Sci.* **2,** 522–531
37. Schlecht, R., Erbse, A. H., Bukau, B., and Mayer, M. P. (2011) Mechanics of Hsp70 chaperones enables differential interaction with client proteins. *Nat. Struct. Mol. Biol.* **18,** 345–351
38. Wieteska, L., Shahidi, S., and Zhuravleva, A. (2017) Allosteric fine-tuning of the conformational equilibrium poises the chaperone BiP for post-translational regulation. *Elife* **6**
39. Ebong, I. O., Morgner, N., Zhou, M., Saraiva, M. A., Daturpalli, S., Jackson, S. E., and Robinson, C. V. (2011) Heterogeneity and dynamics in the assembly of the heat shock protein 90 chaperone complexes. *Proc. Natl. Acad. Sci. U.S.A.* **108,** 17939–17944
40. Stengel, F., Baldwin, A. J., Painter, A. J., Jaya, N., Basha, E., Kay, L. E., Vierling, E., Robinson, C. V., and Benesch, J. L. (2010) Quaternary dynamics and plasticity underlie small heat shock protein chaperone function. *Proc. Natl. Acad. Sci. U.S.A.* **107,** 2007–2012
41. Li, Z., Hartl, F. U., and Bracher, A. (2013) Structure and function of Hip, an attenuator of the Hsp70 chaperone cycle. *Nat. Struct. Mol. Biol.* **20,** 929–935
42. Woodcock, J. M., Goodwin, K. L., Sandow, J. J., Coolen, C., Perugini, M. A., Webb, A. I., Pitson, S. M., Lopez, A. F., and Carver, J. A. (2018) Role of salt bridges in the dimer interface of 14–3-3zeta in dimer dynamics, N-terminal alpha-helical order, and molecular chaperone activity. *J. Biol. Chem.* **293,** 89–99
43. Haladova, K., Mrazek, H., Jecmen, T., Halada, P., Man, P., Novak, P., Chmelik, J., Obsil, T., and Sulc, M. (2012) The combination of hydrogen/deuterium exchange or chemical cross-linking techniques with mass spectrometry: mapping of human 14–3-3zeta homodimer interface. *J. Structural Biol.* **179,** 10–17
44. Heintz, U., and Schlichting, I. (2016) Blue light-induced LOV domain dimerization enhances the affinity of Aureochrome 1a for its target DNA sequence. *Elife* **5,** e11860
45. Schuermann, J. P., Jiang, J., Cuellar, J., Llorca, O., Wang, L., Gimenez, L. E., Jin, S., Taylor, A. B., Demeler, B., Morano, K. A., Hart, P. J., Valpuesta, J. M., Lafer, E. M., and Sousa, R. (2008) Structure of the Hsp110:Hsc70 nucleotide exchange machine. *Mol. Cell* **31,** 232–243
46. Takayama, S., Bimston, D. N., Matsuzawa, S., Freeman, B. C., Aime-Sempe, C., Xie, Z., Morimoto, R. I., and Reed, J. C. (1997) BAG-1 modulates the chaperone activity of Hsp70/Hsc70. *EMBO J.* **16,** 4887–4896
47. Sondermann, H., Scheufler, C., Schneider, C., Hohfeld, J., Hartl, F. U., and Moarefi, I. (2001) Structure of a Bag/Hsc70 complex: convergent functional evolution of Hsp70 nucleotide exchange factors. *Science* **291,** 1553–1557
48. Mayer, M. P., Laufen, T., Paal, K., McCarty, J. S., and Bukau, B. (1999) Investigation of the interaction between DnaK and DnaJ by surface plasmon resonance spectroscopy. *J. Mol. Biol.* **289,** 1131–1144
49. Zhang, M., Windheim, M., Roe, S. M., Peggie, M., Cohen, P., Prodromou, C., and Pearl, L. H. (2005) Chaperoned ubiquitylation–crystal structures of the CHIP U box E3 ubiquitin ligase and a CHIP-Ubc13-Uev1a complex. *Mol. Cell* **20,** 525–538
50. Zhang, H., Amick, J., Chakravarti, R., Santarriaga, S., Schlanger, S., McGlone, C., Dare, M., Nix, J. C., Scaglione, K. M., Stuehr, D. J., Misra, S., and Page, R. C. (2015) A bipartite interaction between Hsp70 and CHIP regulates ubiquitination of chaperoned client proteins. *Structure* **23,** 472–482
51. Nikolay, R., Wiederkehr, T., Rist, W., Kramer, G., Mayer, M. P., and Bukau, B. (2004) Dimerization of the human E3 ligase CHIP via a coiled-coil domain is essential for its activity. *J. Biol. Chem.* **279,** 2673–2678
52. Malinverni, D., Marsili, S., Barducci, A., and De Los Rios, P. (2015) Large-scale conformational transitions and dimerization are encoded in the amino-acid sequences of Hsp70 chaperones. *PLoS Computational Biol.* **11,** e1004262
53. Trcka, F., Durech, M., Man, P., Hernychova, L., Muller, P., and Vojtesek, B. (2014) The assembly and intermolecular properties of the Hsp70-Tomm34-Hsp90 molecular chaperone complex. *J. Biol. Chem.* **289,** 9887–9901
54. Gao, B., Eisenberg, E., and Greene, L. (1996) Effect of constitutive 70-kDa heat shock protein polymerization on its interaction with protein substrate. *J. Biol. Chem.* **271,** 16792–16797

55. Benaroudj, N., Triniolles, F., and Ladjimi, M. M. (1996) Effect of nucleotides, peptides, and unfolded proteins on the self-association of the molecular chaperone HSC70. *J. Biol. Chem.* **271,** 18471–18476
56. Buxbaum, E., and Woodman, P. G. (1996) Binding of ATP and ATP analogues to the uncoating ATPase Hsc70 (70 kDa heat-shock cognate protein). *Biochem. J.* **318 (Pt 3)**, 923–929
57. Wilbanks, S. M., Chen, L., Tsuruta, H., Hodgson, K. O., and McKay, D. B. (1995) Solution small-angle X-ray scattering study of the molecular chaperone Hsc70 and its subfragments. *Biochemistry* **34,** 12095–12106
58. Lee, S. C., and Whitaker, J. R. (2004) Are molecular weights of proteins determined by superose 12 column chromatography correct? *Journal of agricultural and food chemistry* **52,** 4948–4952
59. King, C., Eisenberg, E., and Greene, L. (1995) Polymerization of 70-kDa heat shock protein by yeast DnaJ in ATP. *J. Biol. Chem.* **270,** 22535–22540
60. Ha, J. H., Hellman, U., Johnson, E. R., Li, L., McKay, D. B., Sousa, M. C., Takeda, S., Wernstedt, C., and Wilbanks, S. M. (1997) Destabilization of peptide binding and interdomain communication by an E543K mutation in the bovine 70-kDa heat shock cognate protein, a molecular chaperone. *J. Biol. Chem.* **272,** 27796–27803
61. Lima, D. B., Melchior, J. T., Morris, J., Barbosa, V. C., Chamot-Rooke, J., Fioramonte, M., Souza, T., Fischer, J. S. G., Gozzo, F. C., Carvalho, P. C., and Davidson, W. S. (2018) Characterization of homodimer interfaces with cross-linking mass spectrometry and isotopically labeled proteins. *Nat. Protocols* **13,** 431–458
62. Arakawa, A., Handa, N., Ohsawa, N., Shida, M., Kigawa, T., Hayashi, F., Shirouzu, M., and Yokoyama, S. (2010) The C-terminal BAG domain of BAG5 induces conformational changes of the Hsp70 nucleotide-binding domain for ADP-ATP exchange. *Structure* **18,** 309–319
63. Williamson, D. S., Borgognoni, J., Clay, A., Daniels, Z., Dokurno, P., Drysdale, M. J., Foloppe, N., Francis, G. L., Graham, C. J., Howes, R., Macias, A. T., Murray, J. B., Parsons, R., Shaw, T., Surgenor, A. E., Terry, L., Wang, Y., Wood, M., and Massey, A. J. (2009) Novel adenosine-derived inhibitors of 70 kDa heat shock protein, discovered through structure-based design. *J. Med. Chem.* **52,** 1510–1513
64. Brehmer, D., Rudiger, S., Gassler, C. S., Klostermeier, D., Packschies, L., Reinstein, J., Mayer, M. P., and Bukau, B. (2001) Tuning of chaperone activity of Hsp70 proteins by modulation of nucleotide exchange. *Nat. Structural Biol.* **8,** 427–432
65. Umehara, K., Hoshikawa, M., Tochio, N., and Tate, S. I. (2018) Substrate binding switches the conformation at the lynchpin site in the substrate-binding domain of human Hsp70 to enable allosteric interdomain communication. *Molecules* **23,** 528
66. Wang, H., Kurochkin, A. V., Pang, Y., Hu, W., Flynn, G. C., and Zuiderweg, E. R. (1998) NMR solution structure of the 21 kDa chaperone protein DnaK substrate binding domain: a preview of chaperone-protein interaction. *Biochemistry* **37,** 7929–7940
67. Swain, J. F., Schulz, E. G., and Gierasch, L. M. (2006) Direct comparison of a stable isolated Hsp70 substrate-binding domain in the empty and substrate-bound states. *J. Biol. Chem.* **281,** 1605–1611
68. Sun, L., Edelmann, F. T., Kaiser, C. J., Papsdorf, K., Gaiser, A. M., and Richter, K. (2012) The lid domain of Caenorhabditis elegans Hsc70 influences ATP turnover, cofactor binding and protein folding activity. *PLoS ONE* **7,** e33980
69. Freeman, B. C., Myers, M. P., Schumacher, R., and Morimoto, R. I. (1995) Identification of a regulatory motif in Hsp70 that affects ATPase activity, substrate binding and interaction with HDJ-1. *EMBO J.* **14,** 2281–2292
70. Faou, P., and Hoogenraad, N. J. (2012) Tom34: a cytosolic cochaperone of the Hsp90/Hsp70 protein complex involved in mitochondrial protein import. *Biochim. Biophys. Acta* **1823,** 348–357
71. Chavez, J. D., Schweppe, D. K., Eng, J. K., and Bruce, J. E. (2016) In Vivo Conformational Dynamics of Hsp90 and Its Interactors. *Cell Chem. Biol.* **23,** 716–726
72. Klucken, J., Shin, Y., Masliah, E., Hyman, B. T., and McLean, P. J. (2004) Hsp70 Reduces alpha-Synuclein Aggregation and Toxicity. *J. Biol. Chem.* **279,** 25497–25502
73. Sherman, M. Y., and Gabai, V. L. (2015) Hsp70 in cancer: back to the future. *Oncogene* **34,** 4153–4161
74. Yaglom, J. A., Wang, Y., Li, A., Li, Z., Monti, S., Alexandrov, I., Lu, X., and Sherman, M. Y. (2018) Cancer cell responses to Hsp70 inhibitor JG-98: Comparison with Hsp90 inhibitors and finding synergistic drug combinations. *Sci. Reports* **8,** 3010
75. Kundrat, L., and Regan, L. (2010) Balance between folding and degradation for Hsp90-dependent client proteins: a key role for CHIP. *Biochemistry* **49,** 7428–7438
76. Kawazoe, Y., Nakai, A., Tanabe, M., and Nagata, K. (1998) Proteasome inhibition leads to the activation of all members of the heat-shock-factor family. *Eur. J. Biochem.* **255,** 356–362
77. Woo, J. A., Liu, T., Zhao, X., Trotter, C., Yrigoin, K., Cazzaro, S., Narvaez, E., Khan, H., Witas, R., Bukhari, A., Makati, K., Wang, X., Dickey, C., and Kang, D. E. (2017) Enhanced tau pathology via RanBP9 and Hsp90/Hsc70 chaperone complexes. *Hum. Mol. Genet.* **26,** 3973–3988
78. Lackie, R. E., Maciejewski, A., Ostapchenko, V. G., Marques-Lopes, J., Choy, W. Y., Duennwald, M. L., Prado, V. F., and Prado, M. A. M. (2017) The Hsp70/Hsp90 Chaperone Machinery in Neurodegenerative Diseases. *Frontiers Neurosci.* **11,** 254
79. De Los Rios, P., and Barducci, A. (2014) Hsp70 chaperones are non-equilibrium machines that achieve ultra-affinity by energy consumption. *Elife* **3,** e02218
80. Nollen, E. A., Brunsting, J. F., Song, J., Kampinga, H. H., and Morimoto, R. I. (2000) Bag1 functions in vivo as a negative regulator of Hsp70 chaperone activity. *Mol. Cell Biol.* **20,** 1083–1088
81. Zhang, H. T., Zeng, L. F., He, Q. Y., Tao, W. A., Zha, Z. G., and Hu, C. D. (2016) The E3 ubiquitin ligase CHIP mediates ubiquitination and proteasomal degradation of PRMT5. *Biochim. Biophys. Acta* **1863,** 335–346
82. Jin, Y., Awad, W., Petrova, K., and Hendershot, L. M. (2008) Regulated release of ERdj3 from unfolded proteins by BiP. *EMBO J.* **27,** 2873–2882
83. Petrova, K., Oyadomari, S., Hendershot, L. M., and Ron, D. (2008) Regulated association of misfolded endoplasmic reticulum lumenal proteins with P58/DNAJc3. *EMBO J.* **27,** 2862–2872

Publikace II

Vandová, V. & Vaňková, P., Ďurech, M., Houser, J., Kavan, D., Man, P., Müller, P. & Trčka, F.

HSPA1A conformational mutants reveal a conserved structural unit in Hsp70 proteins.

Biochim. Biophys. Acta - Gen. Subj. **1864**, 129458 (2020)

Můj příspěvěk k práci: *návrh experimentů, provedení HDX-MS s interpretací dat a jejich grafickou prezentací, příprava manuskriptu*

BBA - General Subjects 1864 (2020) 129458

Contents lists available at ScienceDirect

BBA - General Subjects

journal homepage: www.elsevier.com/locate/bbagen

HSPA1A conformational mutants reveal a conserved structural unit in Hsp70 proteins

Veronika Vandova[a,1], Pavla Vankova[b,c,1], Michal Durech[a], Josef Houser[d,e], Daniel Kavan[b,c], Petr Man[b,c], Petr Muller[a,*], Filip Trcka[a,*]

[a] Regional Centre for Applied Molecular Oncology, Masaryk Memorial Cancer Institute, Zluty kopec 7, 656 53 Brno, Czech Republic
[b] BioCeV - Institute of Microbiology of the Czech Academy of Sciences, v.v.i., Prumyslova 595, 252 50 Vestec, Czech Republic
[c] Department of Biochemistry, Faculty of Science, Charles University, Hlavova 8, 128 43 Prague, Czech Republic
[d] Central European Institute of Technology, Masaryk University, Kamenice 5, 625 00 Brno, Czech Republic
[e] National Centre for Biomolecular Research, Faculty of Science, Masaryk University, Kotlarska 2, 611 37 Brno, Czech Republic

ARTICLE INFO

Keywords:
Allostery
Molecular chaperones
Heat-shock protein 70
Folding
Mutation

ABSTRACT

Background: The Hsp70 proteins maintain proteome integrity through the capacity of their nucleotide- and substrate-binding domains (NBD and SBD) to allosterically regulate substrate affinity in a nucleotide-dependent manner. Crystallographic studies showed that Hsp70 allostery relies on formation of contacts between ATP-bound NBD and an interdomain linker, accompanied by SBD subdomains docking onto distinct sites of the NBD leading to substrate release. However, the mechanics of ATP-induced SBD subdomains detachment is largely unknown.

Methods: Here, we investigated the structural and allosteric properties of human HSPA1A using hydrogen/deuterium exchange mass spectrometry, ATPase assays, surface plasmon resonance and fluorescence polarization-based substrate binding assays.

Results: Analysis of HSPA1A proteins bearing mutations at the interface of SBD subdomains close to the interdomain linker (amino acids L399, L510, I515, and D529) revealed that this region forms a folding unit stabilizing the structure of both SBD subdomains in the nucleotide-free state. The introduced mutations modulate HSPA1A allostery as they localize to the NBD-SBD interfaces in the ATP-bound protein.

Conclusions: These findings show that residues forming the hydrophobic structural unit stabilizing the SBD structure are relocated during ATP-activated detachment of the SBD subdomains to different NBD-SBD docking interfaces enabling HSPA1A allostery.

General significance: Mutation-induced perturbations tuned HSPA1A sensitivity to peptide/protein substrates and to Hsp40 in a way that is common for other Hsp70 proteins. Our results provide an insight into structural rearrangements in the SBD of Hsp70 proteins and highlight HSPA1A-specific allostery features, which is a prerequisite for selective targeting in Hsp-related pathologies.

1. Introduction

Hsp70 proteins are crucial components of the chaperone network that maintains homeostasis of the cellular proteome (proteostasis) [1]. In recent years, a tremendous advance in understanding the allosteric control of Hsp70 proteins has been achieved by crystallization of bacterial Hsp70 chaperone – DnaK [2,3]. DnaK, as well as other Hsp70 proteins, has an N-terminal nucleotide-binding domain (NBD) and a C-terminal substrate-binding domain (SBD). A highly conserved hydrophobic linker joins the NBD with the SBD that has two functional parts:

Abbreviations: ADP, adenosine diphosphate; ATP, adenosine triphosphate; Bag-1, Bcl2-associated athanogene 1; B-PES, biotinylated 2-phenyl-ethynesulfonamide; GST, glutathione S-transferase; Hip, Hsc70-interacting protein; HDX, hydrogen/deuterium exchange; Hsc, heat shock cognate; Hsp, heat shock protein; NBD, nucleotide-binding domain; NEF, nucleotide exchange factor; PES, 2-phenyl-ethynesulfonamide; PET-16, triphenyl(phenylethynyl)phosphonium bromide; PDB, protein data bank; SBD, substrate-binding domain; SBP, streptavidin-binding peptide; SPR, surface plasmon resonance; TEV, tobacco etch virus; Tomm34, translocase of outer mitochondrial membrane 34; WT, wild type

* Corresponding authors.
E-mail addresses: muller@mou.cz (P. Muller), pilif.trcka@gmail.com (F. Trcka).
[1] Both authors contributed equally to this work.

https://doi.org/10.1016/j.bbagen.2019.129458
Received 11 May 2019; Received in revised form 22 August 2019; Accepted 15 October 2019
Available online 30 October 2019

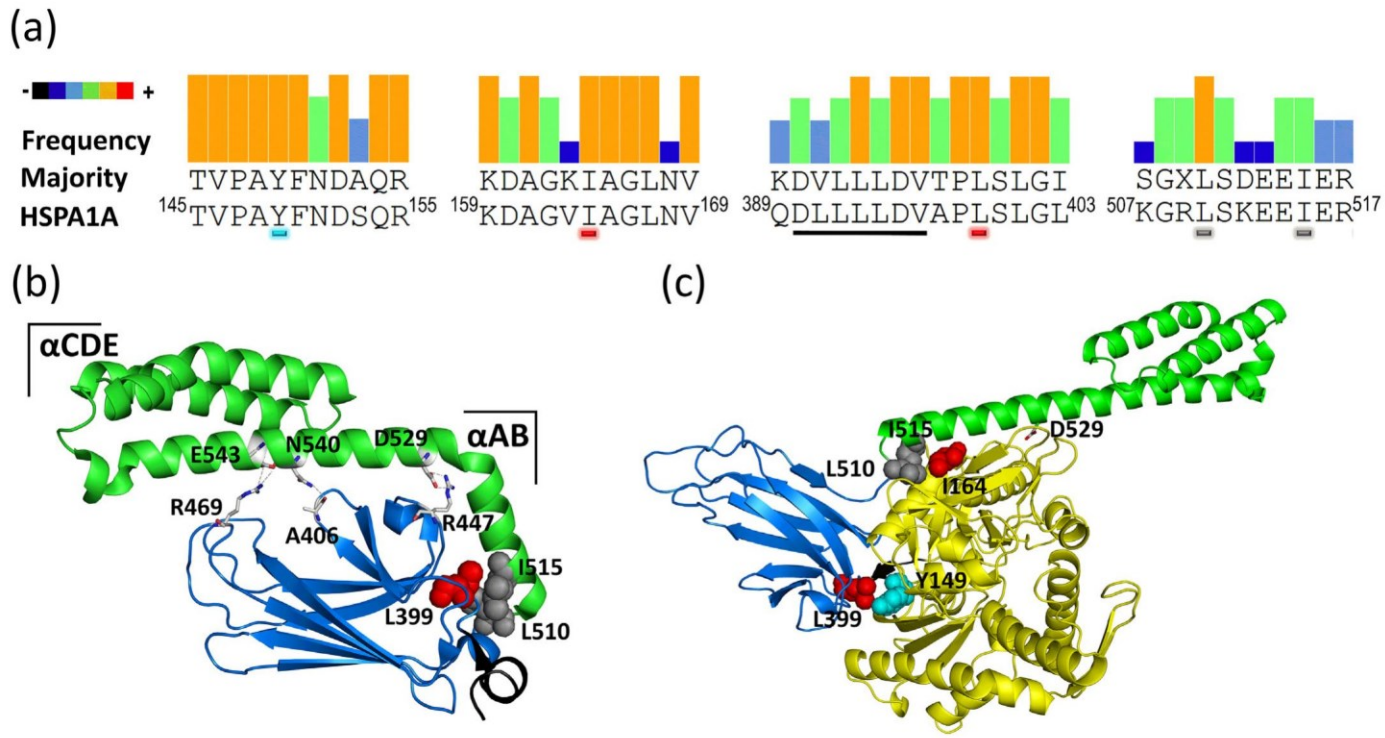

Fig. 1. Hydrophobic residues in αA helix together with L399 are important for HSPA1A structural integrity in both nucleotide states. (a) Multiple sequence alignment of selected HSPA1A regions demonstrating their conservation. Amino acids highlighted in cyan, red and grey are represented as spheres in the structures shown in (b) and (c). The black line marks a hydrophobic core of the interdomain linker which is displayed in (b) and (c) in black. (b) Crystal structure of HSPA1A SBD (PDB ID: 4PO2). Amino acids important for SBDα-SBDβ positioning are shown as sticks. Residues L399 (red spheres) and L510/I515 (grey spheres) form a hydrophobic pocket. SBDα, SBDβ and the interdomain linker are shown in green, marine and black, respectively. (c) A homology model of HSPA1A [18] depicting the position of highlighted SBD residues in the ATP-bound state. NBD residues I164 and Y149 stabilizing the contacts with the SBD are highlighted in red and cyan, respectively. NBD, SBDα, SBDβ and the interdomain linker are shown in yellow, green, marine and black, respectively. The images were created in PyMOL.

i) β-sheet SBDβ constituting a substrate binding groove; and ii) SBDα consisting of five α-helical segments forming a lid covering SBDβ. In the absence of ATP, the NBD and SBD behave like independent species. Upon ATP binding, the protein undergoes allosteric changes initiated by insertion of the linker into the NBD, followed by docking of the SBDβ subdomain to one site of the NBD and of SBDα to another site in the NBD (Fig. 1) [3,4]. Hsp70 in its domain-docked conformation is fully prepared to hydrolyse ATP, however, docking of the SBD prevents hydrolysis [4,5]. The SBD in the ATP bound state is characterized by relaxed structure with high on/off rates of substrate binding, representing its low-affinity state. An incoming substrate induces structural changes in the substrate binding groove, triggering SBD to NBD signaling and leading to SBD undocking from the NBD, allowing ATP hydrolysis. At this step, SBDβ traps the substrate by adopting the high-affinity state secured by SBDα. The position of SBDα in respect to SBDβ is mediated by a network of electrostatic and hydrophobic interactions [6,7].

Although the end-point domain-docked conformation is captured in the crystal structures, the detailed mechanism of its establishment, especially the SBD rearrangements, is largely unknown. It has been demonstrated that the SBD intradomain structural units and their conformational dynamics are implicated in the regulation of Hsp70 interdomain allosteric control [8,9]. Delineation of the SBD structural elements is therefore crucial for understanding of ATP-induced changes enabling the SBD docking onto the NBD.

As the substrate-induced stimulation of Hsp70 ATPase activity is suboptimal, the J-domain of Hsp40 co-chaperone contacts the linker/SBDβ interface in the domain-docked state [10]. This strengthens the substrate-induced SBD to NBD signaling and increases ATP hydrolysis rate. Conversely, a slow rate of ADP dissociation from the NBD is accelerated by co-chaperones with the function of nucleotide-exchange factors (NEF) [11]. In the course of evolution, a new class of co-chaperones bearing so-called tetratricopeptide repeat (TPR) domains that mediate their interaction with the conserved C-terminal EEVD motif of eukaryotic Hsp70 has emerged [12–15]. Despite the diversity of compartments and processes in which distinct Hsp70s take part in eukaryotic cells, the core elements of their ATP-driven molecular allostery are largely conserved [16]. However, a growing body of evidence describes various fine-tuning mechanisms that modulate the allostery of different Hsp70 proteins [17–21].

In this study, we have delineated the structural and allosteric features of human stress-inducible HSPA1A isoform mutated at evolutionary conserved residues in the SBD - L399, L510, I515, and D529. Previous computational and biochemical studies have suggested that these amino acid positions are involved in the SBD stabilization, however, without direct structural evidence [6,22,23]. We showed that these residues form a structural unit stabilizing the SBDβ subdomain by restricting the mobility of the linker region and SBDα. This data suggests that ATP-induced destabilization of the described SBD structural unit enables SBDα-SBDβ detachment and their docking to the NBD. Moreover, as L399, L510, and I515 residues localize also to the NBD-SBD docking sites, we probed the allosteric behaviour of the prepared mutants. These analyses showed that HSPA1A protein exhibits unique allosteric features, namely insensitivity to peptide substrates, differentiating it from prokaryotic DnaK and other eukaryotic isoforms. Since HSPA1A protein is highly expressed in pathologies including cancer and neurodegenerative diseases [24,25], a detailed knowledge of its structure and allosteric behavior might help us to design selective strategies to block its activity.

2. Materials and methods

2.1. Cloning and protein preparation

All coding sequences were cloned by Gateway recombination technology (Invitrogen, Carlsbad, CA, USA). The full coding sequences of human *HSPA1A* (Hsp70, UniProt ID: P0DMV8-1) variants were cloned into pDEST17 and pT7-SBP vectors containing an N-terminal His_6 or SBP tag, respectively. HSPA1A point mutations were prepared using QuickChange Site-Directed Mutagenesis Kit (Agilent Technologies, Santa Clara, CA, USA) according to the manufacturer's instructions. The full coding sequences of human *BAG1* (Bag-1, UniProt ID: Q99933-4), *DNAJB1* (Hsp40, UniProt ID: P25685-1), *ST13* (Hip, UniProt ID: P50502-1) and *TOMM34* (Tomm34, UniProt ID: Q15785-1) genes were cloned into pDEST15 containing an N-terminal His_6-GST tag cleavable by tobacco etch virus (TEV) protease. All cloned genes were expressed in *E. coli* BL21(DE3) RIPL cells as described previously [13].

Cells expressing His_6-tagged HSPA1A proteins were resuspended in His binding buffer (50 mM Hepes, pH 7.6, 0.3 M KCl, 5 mM imidazole, 5% glycerol). After purification using a HisTrap column (GE Healthcare, Piscataway, NJ, USA), HSPA1A proteins were dialyzed against buffer A (20 mM Tris, pH 7.2, 100 mM KCl) for 24 h, applied to a HiTrap Q column (GE Healthcare) and eluted by a linear gradient of buffer B (20 mM Tris, pH 7.2, 1 M KCl). Fractions containing purified HSPA1A proteins were concentrated and subjected to gel filtration using a HiPrep 16/60 Sephacryl S-100 HR column. His_6-GST-tagged proteins and SBP-tagged HSPA1A mutants were purified as described previously [13]. The full length p53 (UniProt ID: P04637-1) protein was purified as described previously [26].

2.2. Pull-down assays

Before performing pull-down experiments, all proteins were exchanged into pull-down assay buffer (50 mM Hepes, pH 7.5, 0.15 M KAc, 2 mM $MgCl_2$). For SBP pull-downs, 70 pmol of various SBP-tagged HSPA1A constructs bound to streptavidin agarose beads were incubated with 140 pmol of Hip or Tomm34 proteins in buffers containing 0.4 mM ATP or ADP or no nucleotides (as indicated). After 1 h incubation at 4 °C, beads were washed with matching buffers, proteins were eluted with 2 mM biotin and analyzed by SDS-PAGE/Coomassie (Hip) and western blotting (Tomm34). Pull-down assays with biotinylated Hsp40 (EZ-Link™, Thermo Fischer Scientific, Waltham, MA, USA) and HSPA1A variants was performed analogously except that the samples for western blotting were eluted by boiling in 2× loading sample buffer for 10 min.

2.3. Antibodies

Monoclonal antibodies to Tomm34, Hsp40 and HSPA1A used in this study were previously prepared and characterized in-house. Blots were developed with rabbit anti-mouse IgG secondary antibody conjugated with horseradish peroxidase (Dako, Santa Clara, CA, USA).

2.4. Luciferase refolding assay

Firefly luciferase (50 nM, Promega, Madison, WI, USA) incubated with HSPA1A (1 μM), Hsp40 (2 μM), and Bag-1 (0.5 μM) proteins in 50 mM Hepes, pH 7.5, 150 mM KAc, 2 mM $MgCl_2$, 5 mM DTT, 5 mM ATP was thermally denatured at 42 °C for 30 min. The refolding reaction was started by shifting the temperature to 37 °C. At given time points, 2 μl of the reaction were mixed with D-luciferin (100 μM in 100 μl) and the luciferase activity was measured at 21 °C using an Infinite M1000 Pro (Tecan, Männedorf, Switzerland) at emission wavelength of 560 nm and 500/100 ms settle/integration time. The signal from samples with native luciferase was set as 100%. As negative controls we measured the luciferase activity of denatured luciferase only.

2.5. Malachite green ATPase assay

Experiments were performed according to previous protocols [13,27]. HSPA1A WT or its mutants (2 μM) were titrated with Hsp40 protein in 50 mM Hepes, pH 7.5, 0.15 M KAc, 2 mM $MgCl_2$, 1 mM ATP for 3 h at 37 °C. In the peptide assays, we used HSPA1A (2 μM) and 300 μM NR peptide (NRLLLTG). All the reactions contained 1% DMSO as the peptide was diluted from DMSO-dissolved stock. The synergy between Hsp40 and protein substrate was evaluated using HSPA1A WT or its mutants (2 μM) in the presence of either 1 μM Hsp40, 4 μM full-length p53 protein, or both. After incubation, malachite green reagent was added into each well in clear 96 well plates and 34% sodium citrate was immediately added to halt the non-enzymatic hydrolysis of ATP. The samples were incubated for another 15 min before measuring absorbance at 620 nm. A phosphate standard curve was used to calculate ATPase rate as pmol ATP/μM HSPA1A/min. The final ATPase activities of HSPA1A proteins were obtained by subtraction of the background ATPase activities detected in the assay buffer, NR peptide, p53, and p53/Hsp40 mixture, respectively.

2.6. Peptide binding

Fluorescein-NRLLLTG peptide binding experiments were performed in 50 mM Hepes, pH 7.5, 0.15 M KAc, 2 mM $MgCl_2$, 0.01% Tween 20. BSA (1 μM) was added to the reaction buffer to reduce non-specific binding to plates. To obtain equilibrium binding curves, mixtures containing 30 nM peptide were titrated with different concentrations of WT and mutant HSPA1A proteins and incubated overnight at 4 °C. Peptide binding kinetics and peptide release were analyzed using peptide and protein concentrations of 30 nM and 50 μM (kinetics)/25 μM (release), respectively, where 0.4 mM ATP was added after overnight incubation at 4 °C to measure release. To distinguish non-specific binding, we used BSA with the same concentration as analyzed protein. All reactions were carried out in a total volume of 12 μl in 384-well black Nunc Plates (Thermo Fischer Scientific). Fluorescence polarization was measured at 25 °C using an Infinite M1000 Pro (Tecan, Männedorf, Switzerland) with excitation and emission wavelengths of 470 and 520 nm, respectively. Data analysis was performed using GraphPad Prism version 5.03 for Windows (GraphPad Software, San Diego, CA, USA).

2.7. Surface plasmon resonance (SPR)

SPR was carried out on a Biacore T200 system (GE Healthcare). All SPR measurements were performed at 25 °C in SPR buffer (50 mM Hepes, pH 7.5, 0.15 M KAc, 2 mM $MgCl_2$, 0.005% Tween 20). Biotinylated Hsp40 (EZ-Link™, Thermo Fischer Scientific) was immobilized on Series S Sensor chip SA (GE Healthcare) to a final response of 600 RU. The first channel on the sensor was blocked with biotin and used as a blank. WT, D529A, L399D, L510D and I515D HSPA1A protein variants (0.2 μM) were mixed with 4 mM ATP or buffer (9:1 volume ratio), incubated for 1 min and injected for 10 min at a flow rate of 10 μl/min, followed by 1.5 h dissociation. The data were plotted after subtracting the blank channel response. In the repeated experiment with HSPA1A WT, L399A and L399D variants, biotinylated Hsp40 was immobilized in SPR buffer on the SA Sensor chip to a final response of 230 RU. Next, HSPA1A proteins (0.2 μM) were mixed with 4 mM ATP or buffer (9:1 volume ratio), incubated for 10 min and injected for 5 min at a flow rate of 10 μl/min. This was followed by dissociation for 2 h and regeneration of the chip by the addition of 2 M urea for 1 min and 20 min stabilization of the chip by SPR buffer flow. Both experiments were performed in two technical, reproducible replicates and we present here one representative result. Each experimental series contained WT HSPA1A at the beginning and at the end of the analysis to control for potential inactivation of coupled Hsp40.

2.8. Preparation of biotin-conjugated PES and PES-binding assay

The biotinylated form of PES (2-phenylethynesulfonamide or pifithrin-μ, Sigma-Aldrich, St. Louis, MO, USA) was produced by mixing 200 mM EZ-Link™ Sulfo-NHS-SS-Biotin (ThermoFisher Scientific) and 100 mM PES (both diluted in DMSO) with the pull-down assay buffer (50 mM Hepes, pH 7.5, 0.15 M KAc, 2 mM $MgCl_2$) to give 20 mM and 30 mM final concentrations, respectively, followed by a 30 min incubation at RT.

Before performing PES-binding assay, the biotinylated PES (B-PES) was diluted to 5 mM with pull-down assay buffer. B-PES (30 μl of 5 mM solution per sample) was incubated with streptavidin agarose beads for 30 min at 4 °C. After washing with assay buffer, 5 μg of HSPA1A proteins (WT, L399D, L510D, I515D and D529A) pre-incubated for 30 min at 4 °C in 30 μl of assay buffer containing 0.4 mM ADP, were added to the beads. After 1 h incubation at 4 °C, beads were washed with matching buffers. The proteins were eluted by boiling in 2× loading sample buffer for 10 min and analyzed by SDS-PAGE and immunoblotting.

2.9. Hydrogen/deuterium exchange (HDX) mass spectrometry

The level of hydrogen/deuterium exchange (HDX) was monitored on HSPA1A and its point mutants L399A, L399D, L510A, L510D, I515A, I515D, and D529A in the absence or presence of ATP. The proteins were pre-incubated with 5-molar excess of ATP (or appropriate volume of buffer) for 30 min prior to the exchange. Deuterium labeling was initiated by 5-fold dilution into D_2O-based 50 mM Hepes, pD 7.5, 0.1 M KAc, 2 mM $MgCl_2$ at 21 °C. Exchange was quenched by 9-fold dilution into 1 M glycine, pH 2.3 and freezing in liquid nitrogen. Exchange times were 20, 120, 1200 and 7200 s. Each sample was quickly thawed and injected into LC-system, where it was digested with immobilized pepsin column (bed volume 66 μl) and the peptides were trapped and desalted on a peptide microtrap (Optimize Technologies). Digestion and desalting was done at a flow rate of 100 μl/min (LC-20AD pump, Shimadzu) with 0.4% formic acid in water. After 3 min, desalted peptides were eluted onto a ZORBAX 300SB-C18 column (0.5 × 35 mm, 3.5 μm, Agilent Technologies) and separated by a linear gradient of 10–25% B in 7 min, followed by a quick step to 99% B, where A was 0.4% formic acid/2% acetonitrile in water, B was 0.4% formic acid/95% acetonitrile in water. The solvent was delivered at a constant flow rate of 20 μl/min (Agilent Technologies 1200). All components of the LC-system were kept at 0 °C to minimize loss of deuterium.

The LC-system was connected directly to an electrospray ionization source of a 15 T FT-ICR mass spectrometer (solariX XR, Bruker Daltonics). Data were exported using DataAnalysis 4.1 and deuterium uptake was analyzed by the in-house developed program, Deutex [18]. Peptides generated by pepsin digestion were identified in a separate data-dependent LC-MS/MS run and the data were searched against a database containing sequences of HSPA1A WT, all of the single point mutants and pepsin. Fully deuterated samples were analyzed and used for back-exchange correction [28]. The peptides detected in HDX-MS are presented in italics.

2.10. Molecular docking simulations

The AutoDock Vina plugin for PyMOL was applied for molecular docking studies [29]. PES and PET-16 compounds were prepared as pdb file using CORINA Classic converter (https://www.mn-am.com/online_demos/corina_demo). The crystal structure of HSPA1A SBD was downloaded (PDB ID: 4PO2). The druggable pocket of HSPA1A SBD was chosen on the basis of DnaK SBD co-crystal with PET-16 inhibitor (PDB ID: 4R5G) using DoGSiteScorer Binding site detection tool (https://proteins.plus/) [30]. The grid centre was set as coordinates of x, y, z = 43.17, 19.04 and 58.16. The other parameters for AutoDock Vina were set as default. The docking results were viewed using PyMOL (www.pymol.org).

2.11. Software

Multiple sequence alignments based on data available in [16] were performed using DNASTAR Lasergene Suite (www.dnastar.com). Molecular structures were rendered using PyMOL.

3. Results

3.1. Hydrophobic residues in αA helix of HSPA1A SBDα subdomain stabilize both conformational states

In our previous study, we demonstrated that the disruption of D529-R447 ionic contact by D529A mutation leads to a destabilization of HSPA1A SBDβ subdomain, with increased solvent exposure of amino acid segment 440–456 (SBDβ loop $L_{4,5}$), and, unexpectedly, also the 394–401 region [13] (Fig. 1b). Interestingly, this region overlaps a conserved interdomain linker hydrophobic core ^{390}DLLLLDV^{396} (Fig. 1a) and contains a strongly invariant residue L399. As described previously, L399 forms a hydrophobic pocket with L510 and I515 in helix αA of the SBDα subdomain [7,22,23,31] (Fig. 1b). Since D529 localizes close to a kink between helix αB and αA and also participates in a charged network with the residues in helix αA [6], we speculate that the D529-mediated ionic interactions and L399-L510, I515 hydrophobic pocket represent mutually dependent structural units stabilizing the SBDβ subdomain including the C-terminal part of the interdomain linker through efficient positioning of the SBDα subdomain. In order to test this hypothesis, we have analyzed the structural and substrate binding properties of D529A mutant along with alanine/aspartate mutants at amino acid residues 399, 510, and 515. Moreover, residues forming the hydrophobic pocket in the Apo state are likely involved in the ATP-induced structural changes as L399 is located at the SBDβ-NBD interface of domain-docked Hsp70 [2,3,32,33], and L510/I515 participate in the NBD-SBDα interaction together with I164 of the NBD [2,13,32] (Fig. 1c). Thus, we also delineated the ATP-dependent activities of D529A, L399A/D, L510A/D, and I515A/D proteins.

3.2. L399 and I515 secure the SBD structure in cooperation with D529

To characterize the structural defects caused by the introduced mutations, we analyzed the mutants together with WT HSPA1A using hydrogen/deuterium exchange (HDX) mass spectrometry (Fig. 2). Inspection of the proteins revealed that the pattern of structural changes is similar between L399D, I515D and D529A mutants (Fig. 2a, Supplementary Fig. S1a). These proteins exhibit large deprotection of the SBDα subdomain covered by peptides *487–520, 519–542* and *530–546* in the early times of incubation (20 s/120 s). Since peptide *487–513* shows little deuteration change compared to *487–520*, we localize the initial destabilization to amino acids 513–520, representing the αA helix of SBDα (Supplementary Fig. S2). A kinetic analysis of αA/αB helices deuteration (peptide *519–542*) showed that the rapid deuterium exchange in the WT protein was further accelerated by L399D, I515D and D529A mutations, however, all proteins reached the same level of deuteration after 7200 s (Supplementary Fig. S2). This observation indicates that the inherent mobility of the SBDα subdomain is strongly augmented in L399D, I515D and D529A proteins suggesting a complete SBDα-SBDβ detachment [34]. Conversely, L399A, I515A, and L510D mutants exhibited moderate destabilization of the SBDα αA/αB helices reflecting partly functional SBDα-SBDβ association.

The destabilization of SBDα was accompanied in L399D, I515D and D529A mutants by substantial rearrangements in the linker/SBDβ regions *394–401* ($L_{L,1}$ loop), *402–410* ($L_{1,2}$ loop), *413–427* ($L_{2,3}$ loop and β3 sheet), *428–439* ($L_{3,4}$ loop; this region is stable in I515D mutant), and *440–455* (β4 sheet and $L_{4,5}$ loop) (Fig. 2b, Supplementary Fig. S1b). Segments located further towards the C-terminus (*456–475, 479–486*)

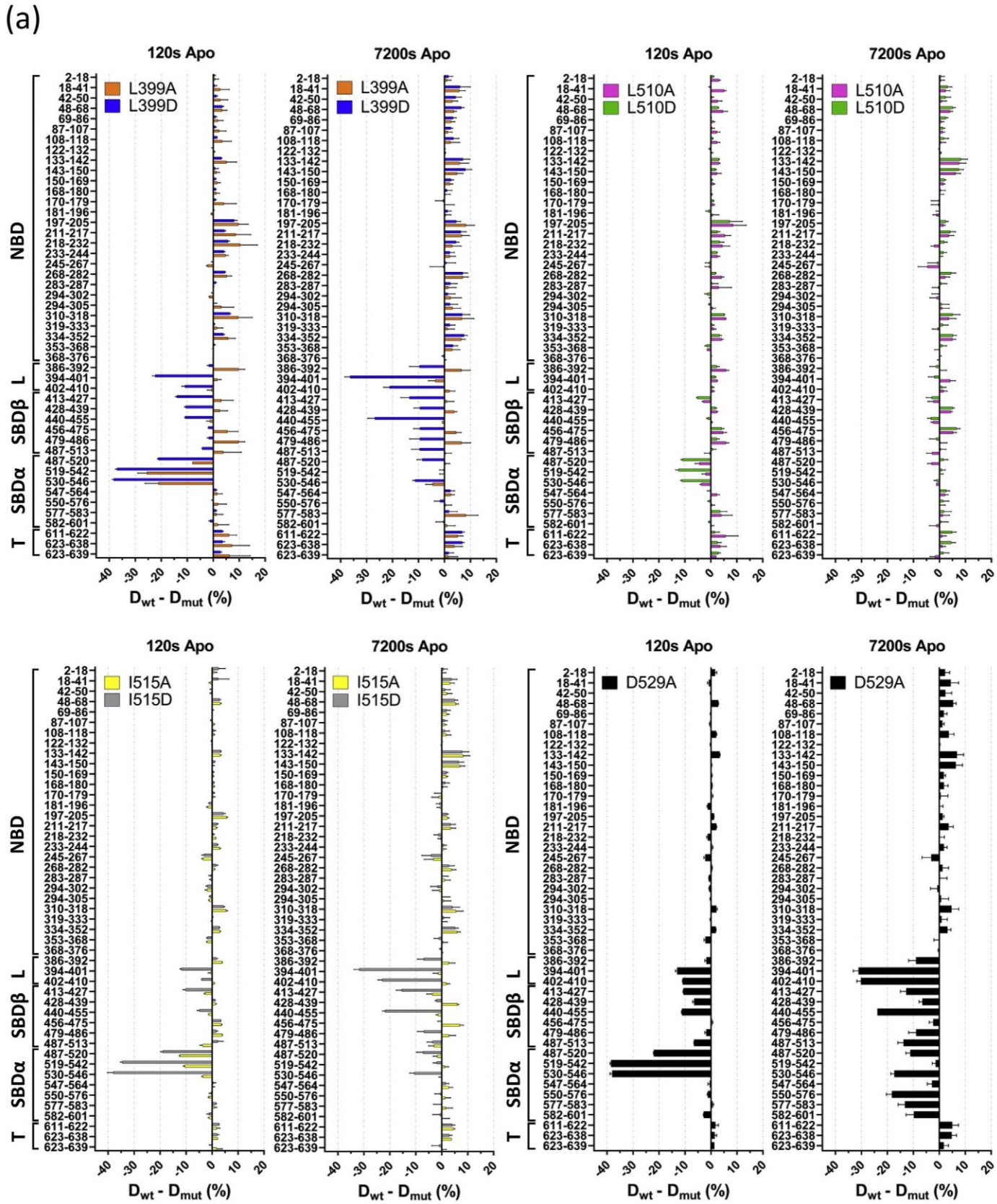

Fig. 2. L399, I515 and D529 secure the SBD structure in a mutually-dependent manner. (a) Deuteration level (%) differences between HSPA1A WT, D529A, L399A/D, L510A/D and I515A/D peptides in nucleotide-free state (Apo) after 120 and 7200 s incubation in deuterated buffer (for other incubation times see Supplementary Fig. S1a). Numbers at the left indicate the HSPA1A peptide fragments; schematic representation at the left shows HSPA1A domain constitution; L, interdomain linker; T, C-terminal tail. Experiments were performed in independent triplicates. Error bars represent S. D. (b) The deuteration level differences between HSPA1A WT and D529A, L399D and I515D SBD peptides in the Apo state after 120 s of deuteration are represented on the crystal structure of HSPA1A SBD domain (PDB ID: 4PO2) in a red-white-blue palette (-55 - 0 - 55%) deprotected-intact-protected). For other incubation times see Supplementary Fig. S1b. The figures were created in PyMOL.

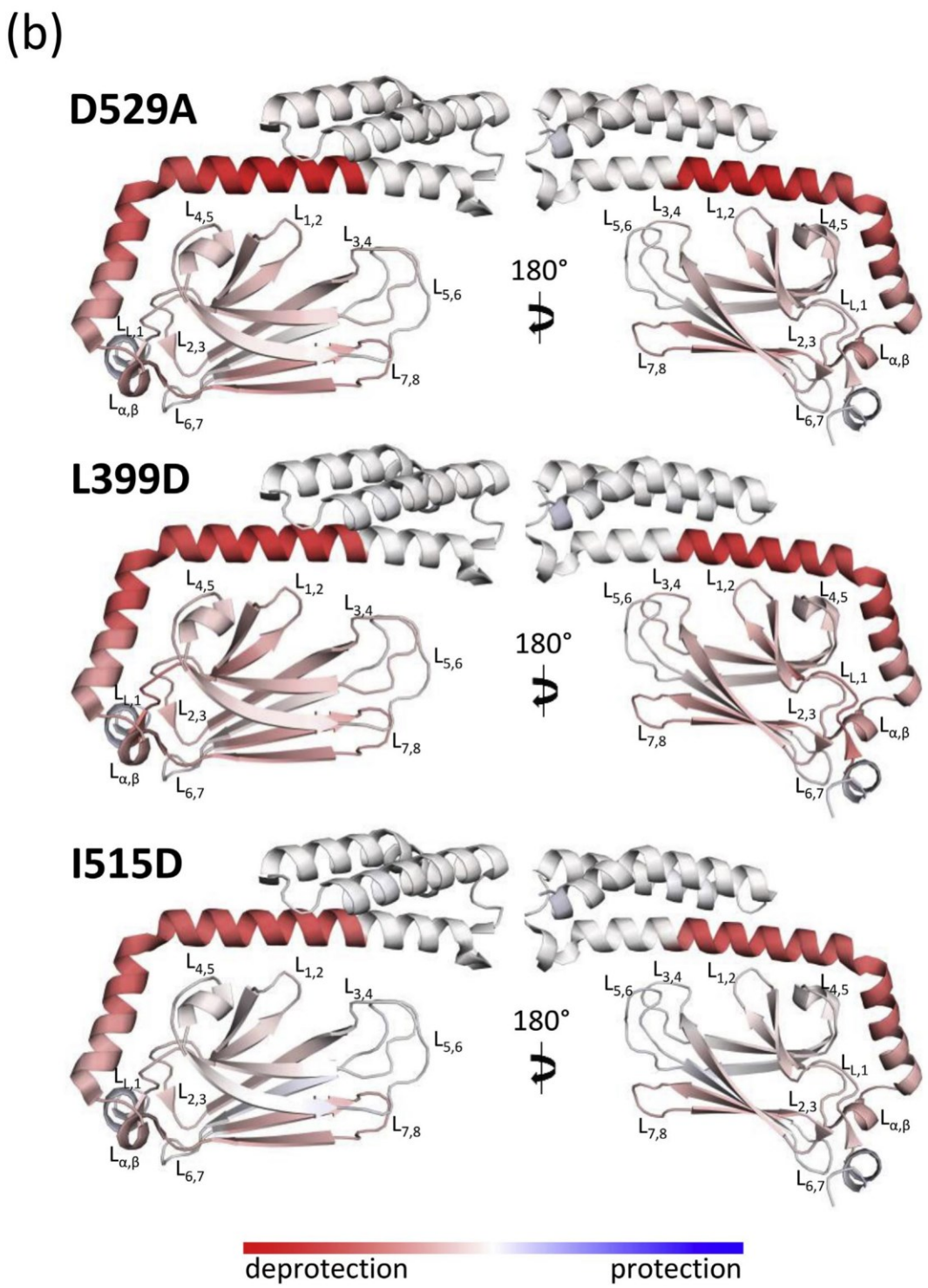

Fig. 2. (*continued*)

of SBDβ were affected to a lesser degree in D529A and L399D mutants only (7200 s, Fig. 2a–b). These structural changes localize to functionally important SBDβ regions, namely substrate binding cleft, and together with SBDα detachment are likely to perturb HSPA1A substrate-binding activity (Supplementary Fig. S3).

In support of our initial hypothesis, these data indicate that introduction of the charged residue (D) in positions L399/I515 and disruption of the ionic contacts in D529A have strikingly similar detrimental effects on HSPA1A SBD structure including the linker region. On the contrary, L399A/L510D/I515A mutations affect the structure of SBDα only, showing that the hydrophobic pocket surrounding L399 stabilizes the αA/αB helices and that the charge in the 510 position is not critical for maintaining the integrity of the SBDβ subdomain.

3.3. HSPA1A mutants with destabilized SBDβ/SBDα subdomains have impaired substrate-binding activity and interaction with an SBD allosteric inhibitor

The structural rearrangements detected in the HSPA1A mutants (Fig. 2 and Supplementary Fig. S3) suggest that the substrate binding activity of these proteins is compromised. To test this notion, we measured the kinetics of model substrate peptide binding by

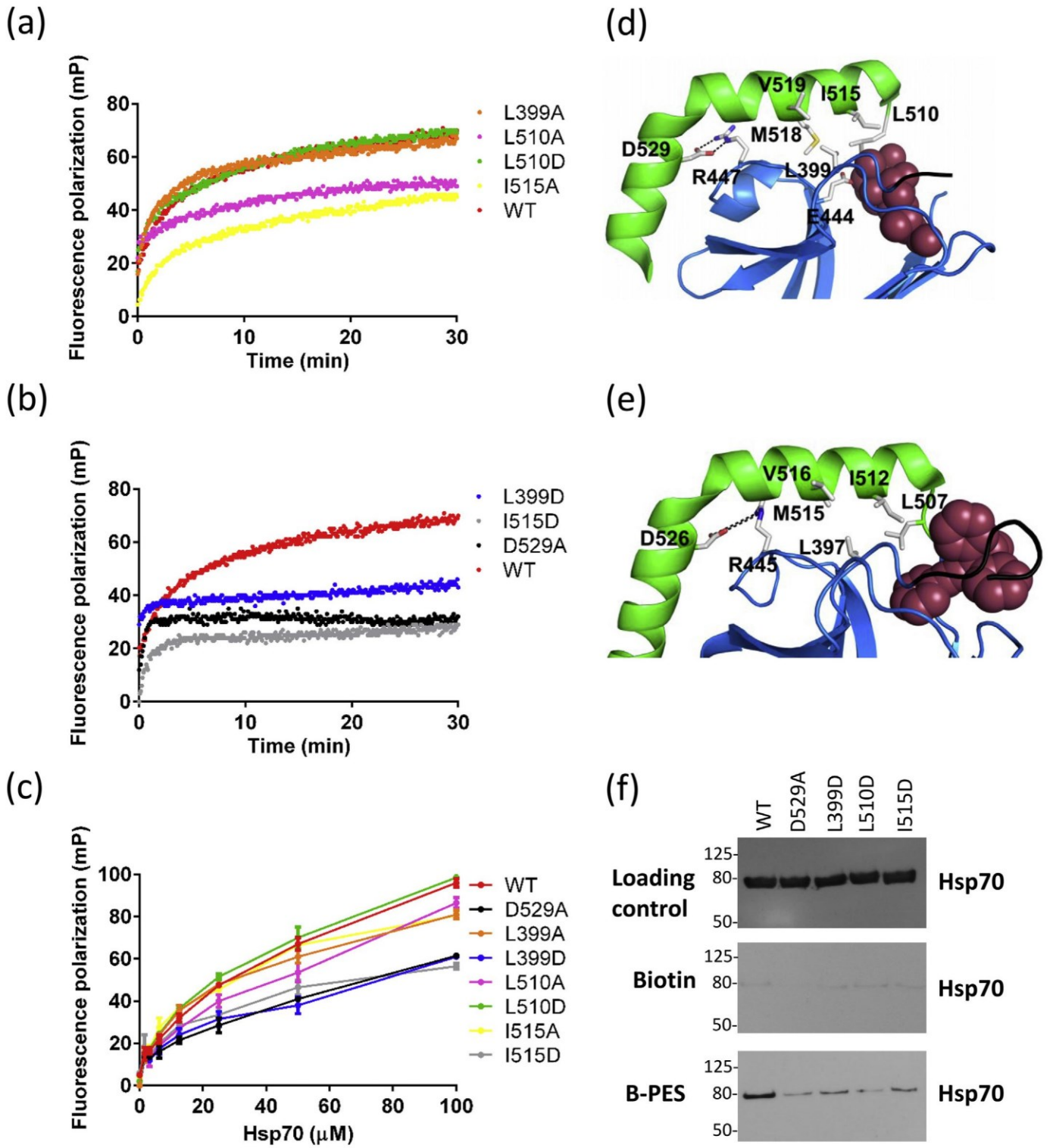

Fig. 3. Destabilization of SBDα/SBDβ subdomains compromises substrate binding activity and the interaction with SBD-targeting inhibitor. (a) and (b) Kinetics of fluorescein-NRLLLTG peptide interaction with WT and HSPA1A mutants under nucleotide-free conditions determined by fluorescence polarization measurement. Protein and peptide concentrations were 50 μM and 30 nM, respectively. For clarity, proteins exhibiting WT-like kinetics of binding are presented in (a), whereas proteins with faster kinetics of binding compared to WT are presented in (b) (all curves together are shown in Supplementary Fig. S4). (c) Equilibrium binding curves of fluorescein-NRLLLTG peptide binding to HSPA1A WT and mutants under nucleotide-free conditions. Fluorescence polarization was determined at 30 nM peptide and increasing Hsp70 concentrations. Experiments were performed in independent triplicates. Error bars represent S. D. (d) Structure of HSPA1A SBD co-crystalized with novolactone inhibitor (PDB ID: 4WV7). SBDα, SBDβ and novolactone are shown in green, marine and raspberry, respectively. (e) Structure of DnaK SBD co-crystalized with PET-16 inhibitor (PDB ID: 4R5G). SBDα, SBDβ and PET-16 are shown in green, marine and raspberry, respectively.

fluorescence polarization (Fig. 3a–b). The analyzed proteins divide into two groups according to the profiles of their peptide binding kinetics (Fig. 3a–b, Supplementary Fig. S4). L399A, L510A/D and I515A mutants displayed slow WT-like kinetics of peptide binding, indicating unaffected substrate capture activity (Fig. 3a). Conversely, D529A, L399D, and I515D variants exhibited fast peptide binding kinetics characteristic for the Hsp70 mutants with substrate binding defects (Fig. 3b) [6,13]. The equilibrium binding levels corroborated the kinetic results, showing that D529A, L399D and I515D mutants have impaired substrate binding capacity (Fig. 3c). These results indicate that it is the combined destabilization of the SBDβ/SBDα subdomains observed in D529A, L399D and I515D mutants (Fig. 2), rather than loosening of the αA/αB helices structure (namely peptides *487–520, 519–542, and 530–546*) found in L399A, L510A/D, I515A variants that renders HSPA1A unable to stably bind peptide substrates (Fig. 3a-c and Supplementary Fig. S3).

The recently solved crystal structures of two allosteric inhibitors, novolactone and PET-16, targeting the SBD of Hsp70 revealed that L399-centered $L_{L,1}$-$L_{\alpha,\beta}$ contacts might be involved in inhibitor binding through stabilization of the binding pocket (Fig. 3d–e and Supplementary Fig. S3) [35,36]. The naturally occurring compound novolactone is firstly coordinated into the binding site between SBDα and SBDβ subdomains and eventually covalently attached to E444, preventing the active allostery of Hsp70 (Fig. 3d) [35]. The synthetic inhibitor, PET-16 (triphenyl(phenylethynyl)phosphonium bromide), coordinates into the same pocket and a similar binding mode is expected for its derivative 2-phenyl-ethynesulfonamide (PES) exhibiting comparable biological effects *in vivo* (Fig. 3e) [36,37]. To test whether L399D, L510D, I515D and D529A mutations destabilizing the SBDα/SBDβ contacts (Figs. 2, 3a-c) affect binding of the inhibitors, we evaluated the interaction of the mutants with commercially available PES which we conjugated to NHS-biotin for affinity precipitation (Fig. 3f and Supplementary Fig. S5). Our results showed interaction of WT HSPA1A protein with biotinylated PES above the level of the background control (immobilized biotin). L399D, L510D, I515D and D529A variants all bound with lower efficiency, suggesting that mutations interfering with SBDα/SBDβ interface stability compromise the structure of the PES binding pocket.

3.4. L399, L510, and I515 are important for HSPA1A protein conformational activity as revealed by the interaction with Hip and Tomm34 co-chaperones and HDX mass spectrometry

Having inspected the structural and functional properties of HSPA1A variants in the Apo state, we proceeded to probe their conformational activity. To this end, we tested the interaction with Hip and Tomm34 co-chaperones (Fig. 4a). These TPR co-chaperones bind preferentially to distinct Hsp70 conformations: Hip interacts with the NBD in the ADP-bound state [38] and Tomm34 prefers the SBDα determinants in the ATP-bound state [13]. The assays were performed at 4 °C to minimize the intrinsic HSPA1A ATPase activity [39]. As L399 is likely to form a hydrophobic pocket buried at the NBD-SBDβ interface (Fig. 1c, Fig. 4b), we evaluated the role of the side chain size at this position by substituting the leucine (L) also for phenylalanine (F). As expected, all tested HSPA1A proteins interacted with Hip in the presence of ADP since the introduced mutations are located in the SBD (Fig. 4a). Conversely, WT, D529A, and L399F proteins exhibited loss of the interaction with Hip in the presence of ATP, indicating their ability to adopt an intact ATP-bound state. Complementary results were obtained by probing the ATP-dependent interaction with Tomm34, where WT-like levels of Tomm34-HSPA1A interaction were observed only for D529A and L399F proteins. This observation supports the role of 399 position side chain size/charge in the formation of hydrophobic contacts between the NBD and SBDβ (Fig. 4b), as L399A/D mutants exhibit defects in interaction with Tomm34. Furthermore, L510/I515 positions in SBDα do not tolerate both small hydrophobic amino acid (A) and aspartate (D) most likely due to the disruption of NBD-SBDα docking (I164 residue on the NBD) (Fig. 1c).

Next, we compared the HDX levels of WT, L399A/D, L510A/D, I515A/D, and D529A proteins in the presence and absence of ATP (Fig. 5). WT and D529A proteins exhibited ATP-induced protection of the NBD coupled with allosterically transduced deprotection of the SBDβ subdomain [13]. Importantly, peptides covering IA subdomain of NBD (*143–150, 150–169, 168–180, 170–179*), the interdomain linker (*386–392, 394–401*) and SBDβ loops $L_{2,3}$ (*413–427*) and $L_{6,7}$ (*479–486*) forming the NBD-SBDβ docking interface showed lower deuteration levels in the ATP-bound state of WT and D529A proteins [2,3,13]. Conversely, L399A/D, L510A/D, I515A/D mutants bound ATP as documented by decreased deuteration of peptides containing ATP-coordinating residues (G202, E268, K271, S275, and G339) [40], however, the protection of peptides covering the NBD-SBDβ interface is absent indicating that these proteins do not form stable domain-docked state. It is of note that segments of L399A/D, L510A/D, and I515A/D proteins' SBDβ are partly deprotected in the presence of ATP (7200 s of deuteration) suggesting that the mutants retained certain degree of allosteric control. Taken together, these results showed that L399, L510, and I515 residues play an important role in local interaction communities involved in the stabilization of HSPA1A ATP-bound state.

3.5. Allostery is partly preserved in L399, L510 and I515 residues mutants

To further dissect the interdomain communication defects found in the analyzed mutants (Figs. 4, Fig. 5), we measured their ability to release bound substrate peptide after ATP binding to the NBD (Fig. 6a). The level of peptide release detected in all mutants was lower in comparison with the WT protein and mirrored the propensity of the proteins to open the SBDβ subdomain in the presence of ATP with alanine mutants releasing more effectively (Fig. 5). These results indicate that although disabling the structural features of the stable ATP-bound conformation (Figs. 4a and 5), L399A, L510A/D, and I515A mutations in the L399-centered hydrophobic pocket residues allow for residual levels of interdomain communication. L399D and I515D variants had the most compromised substrate release activity (11 and 14% of WT, respectively), reflecting severe defects in their interdomain communication (Figs. 4a and 5).

In a complementary assay, we evaluated the sensitivity of the mutants to substrate by measuring their ATPase activity accelerated by the NR substrate peptide (Fig. 6b). T204A mutant with diminished ATPase activity [13,41] was used as a control. As the SBD plays an inhibitory role in the ATPase cycle of Hsp70, the impairment of allostery leads to an increase of basal chaperone ATPase activity [4,5]. Indeed, the basal ATPase rates of the L399A/D, L510A/D and I515A/D mutants were elevated. However, substrate peptide addition did not affect the ATPase activity of the analyzed proteins, with the exception of L399D and I515D mutants that displayed moderately accelerated ATPase activity. These results indicate that, in contrast to DnaK [42], the ATPase activity of HSPA1A is not accelerated by the NR peptide. Interestingly, impairment of allosteric control sensitizes HSPA1A to peptide-mediated stimulation of ATP hydrolysis as exemplified by L399D and I515D variants.

3.6. Mutants with an active SBD to NBD allosteric pathway show decreased ATPase stimulation by Hsp40

To test the ability of the mutants to be stimulated by Hsp40 co-chaperone and protein substrates, we measured their ATPase activity in the presence of either Hsp40 (DnajB1), WT p53 protein, or both (Fig. 6c). We chose WT p53 as a protein containing intrinsically disordered regions [43,44], which represent a generic structural feature of Hsp70 substrates as documented by the canonical DnaK interactor σ^{32} [45,46]. Again, the basal ATPase activity of L399A/D, L510A/D and I515A/D mutants in this experiment revealed their 2.7, 4.8, 2.5, 1.7,

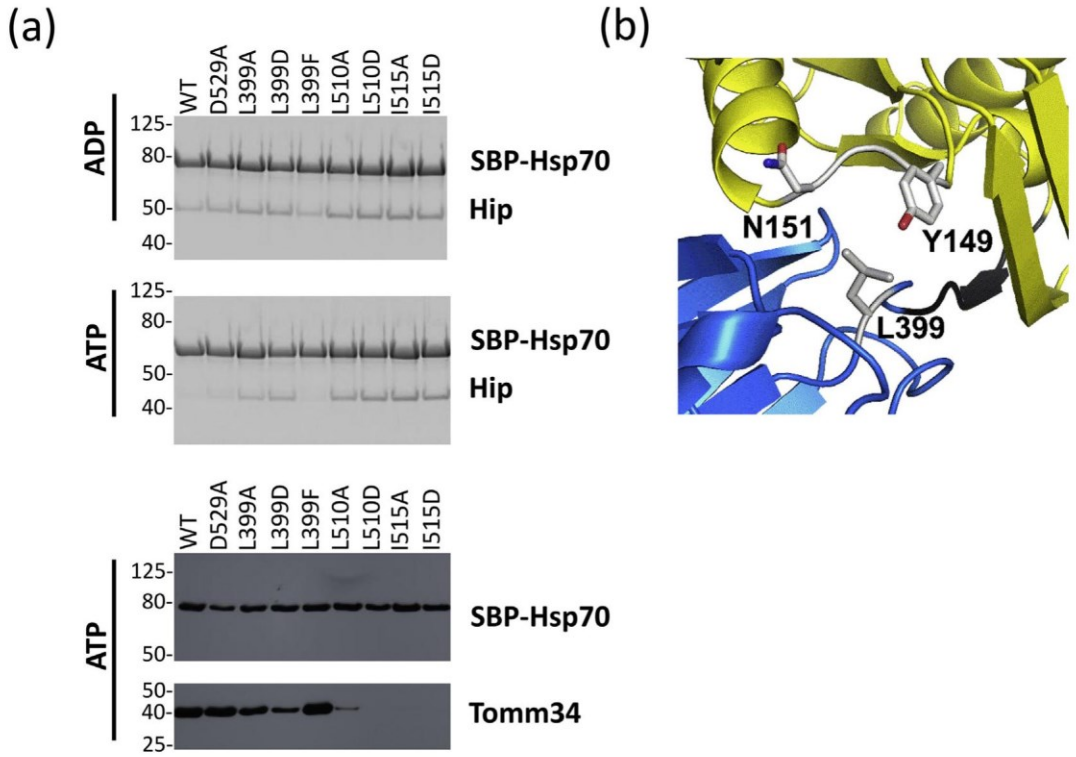

Fig. 4. L399, L510 and I515 stabilize the ATP-bound state of HSPA1A as reflected by the interaction with conformation-specific co-chaperones. (a) 70 pmol of SBP-tagged HSPA1A constructs bound to streptavidin agarose beads were incubated with either 140 pmol of Hip or Tomm34 proteins in buffers containing 0.4 mM ATP, ADP or no nucleotides (as indicated). Eluted proteins were separated by SDS-PAGE and analyzed by either Coomassie staining (Hip) or western blotting (Tomm34). (b) NBD-SBD interface of HSPA1A homology model [18] in the ATP-bound state, with L399, N151 and Y149 represented as sticks. The NBD and SBD are shown in yellow and marine, respectively. The image was created in PyMOL.

2.4 and 2.5-fold increased activity, respectively, compared to WT HSPA1A. D529A had a basal ATPase level comparable to WT. The addition of p53 increased the ATPase activity of all the proteins approximately two-fold (ranging from 1.7 to 2.6) compared to their basal rates. Hsp40 stimulated the ATPase activity of the WT and D529A proteins 4.5 and 4.4-fold, respectively. In contrast, L399A, L510A/D and I515A/D mutants were accelerated by only 1.6 to 2.8-fold and L399D did not respond to Hsp40 addition (1.2-fold acceleration). The combined presence of both Hsp40 and p53 increased the ATPase activity of WT and D529A HSPA1A proteins 10-fold, whereas L399A/D, L510A/D and I515A/D variants were accelerated 3.2, 2.1, 4.5, 5.4, 3.9 and 3.6-fold, respectively. These results indicate that the mutants' ATPase activity can be stimulated by p53 protein presence. The acceleration of ATP hydrolysis by Hsp40, however, is reduced in the mutant proteins due to either their elevated intrinsic ATPase activity (namely L399D) or HSPA1A-Hsp40 cooperation defects. To further evaluate HSPA1A-Hsp40 cooperation, we tested the ability of the studied mutants to refold thermally denatured firefly luciferase in an Hsp40-assisted manner (Fig. 6d). Bag1 protein was used as NEF [47]. L399D, I515D and D529A proteins showed severe defects in luciferase refolding. In contrast, L399A, L510D and I515A exhibited an intermediate refolding activity and L510A reached WT-like levels of refolding. This indicates that the most predictive feature of HSPA1A variants' refolding activity is their substrate binding capacity (see Fig. 3a–c) rather than the level of Hsp40-mediated ATPase activity acceleration (Fig. 6c).

Together, these results showed that HSPA1A ATPase is more readily stimulated by protein substrates than by peptides. The conformational defects imposed on HSPA1A by mutations in the linker/SBDβ and SBDα subdomains leave the allosteric pathway from the SBD to the NBD largely intact (p53-mediated stimulation of ATPase activity) [4]. Conversely, the synergy between Hsp40 and the substrate in triggering ATP hydrolysis is compromised due to the altered HSPA1A-Hsp40 cooperation, however, without significant effect on Hsp40-assisted luciferase refolding.

3.7. HSPA1A-Hsp40 cooperation loss is not due to defects in the HSPA1A-Hsp40 interaction

The above results, together with current knowledge of the Hsp70-Hsp40 interaction [41], suggested that the analyzed mutants might have modulated ability to directly associate with Hsp40 due to the impairments in allostery control (Figs. 4, 5, 6) and substrate binding capacity (Fig. 3a–c). To probe the mutants' ability to bind Hsp40, we performed streptavidin affinity precipitation using biotinylated Hsp40 protein (Fig. 7a). In the absence of ATP, only D529A exhibited moderate binding to immobilized Hsp40. Strikingly, all of the analyzed proteins interacted with Hsp40 after ATP addition. To evaluate the HSPA1A-Hsp40 interaction in detail, we used an established SPR [41,48,49] experiment in which WT, D529A, L399D, L510D and I515D variants were passed over immobilized biotinylated Hsp40 in the presence or absence of ATP (Fig. 7b and Supplementary Fig. S6). The low resonance response in the absence of ATP reflected the binding propensities of the analyzed proteins (Fig. 7a), with D529A showing the highest signal. The level of binding was significantly elevated by ATP addition, albeit with differing magnitude and binding curve shape for each variant (Fig. 7b and Supplementary Fig. S6). While L510D and D529A displayed similar maximal responses to WT HSPA1A, I515D reached lower values. This result recapitulated previous findings that I515C mutant of Hsc70 has a lower level of binding to the J-domain of auxilin [50]. Interestingly, L399D exhibited considerably higher resonance response than the WT protein. To further verify whether mutations at L399 (L399A/D) increase the binding to Hsp40, we used a more stringent SPR procedure with a regeneration step included (see

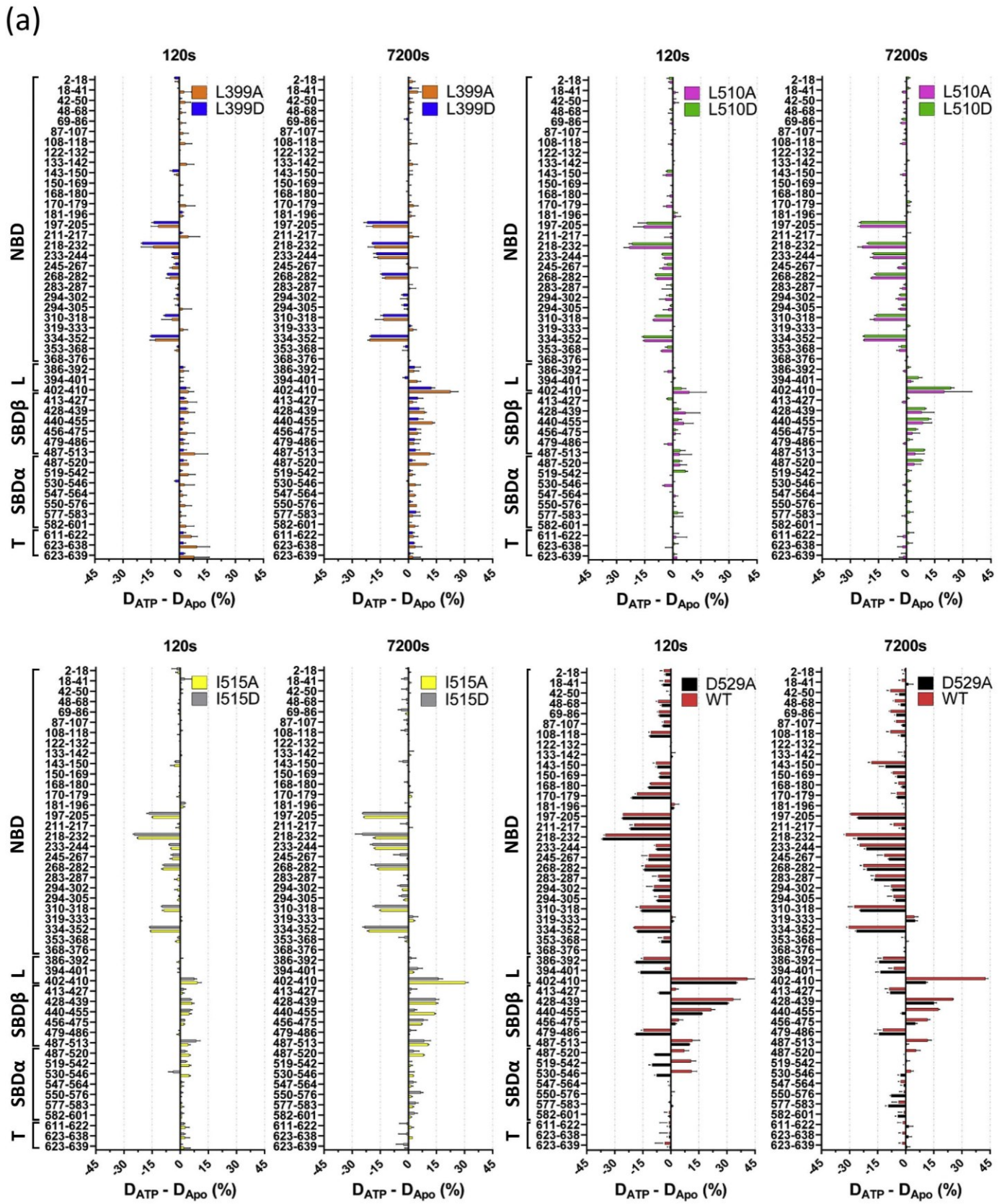

Fig. 5. Domain docking is perturbed in L399, L510 and I515 residues mutants. Deuteration level (%) differences between HSPA1A WT, D529A, L399A/D, L510A/D and I515A/D peptides in the ATP-bound state and the nucleotide-free state (Apo) after 120 and 7200 s incubation in deuterated buffer. Numbers at the left indicate the HSPA1A peptide fragments; schematic representation at the left shows HSPA1A domain constitution; L, interdomain linker; T, C-terminal tail. Experiments were performed in independent triplicates. Error bars represent S. D.

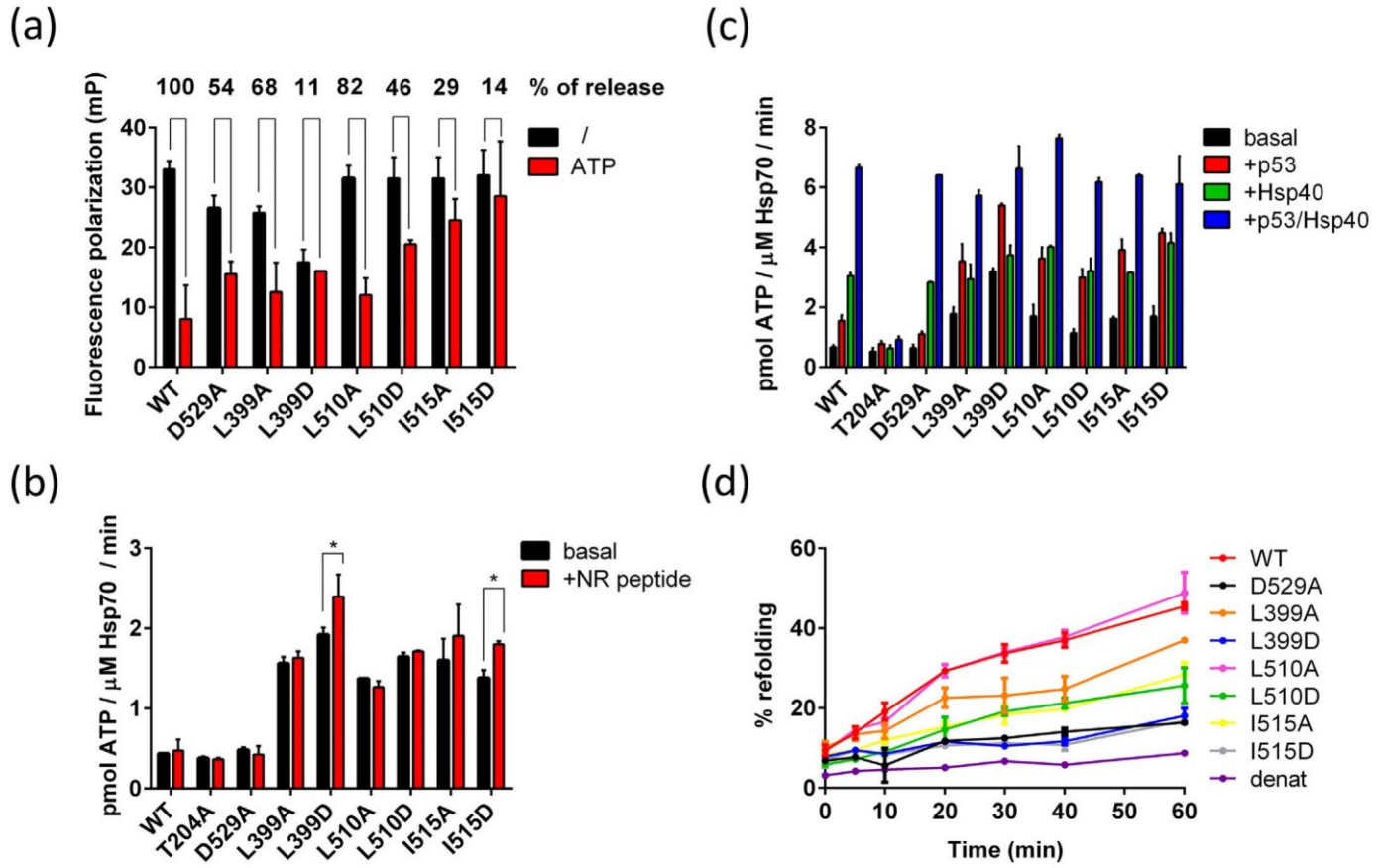

Fig. 6. ATPase activity of HSPA1A variants with impaired allosteric control is sensitive to both peptide and protein substrates but unresponsive to Hsp40 stimulation. (a) ATP-induced substrate peptide release from HSPA1A proteins. HSPA1A proteins (25 µM) were incubated overnight with 30 nM fluorescein-labelled substrate peptide at 4 °C to reach binding equilibrium. Next, ATP (0.4 mM) or buffer was added and fluorescence polarization was measured. The % of release compares the decrease of fluorescence polarization caused by ATP addition among the analyzed proteins, with the decrease for WT protein being set as 100%. (b) The ATPase activity of HSPA1A variants (2 µM) incubated with or without 300 µM NR peptide (NRLLLTG) evaluated by malachite green assay. The T204A mutant lacking ATPase activity was used as a negative control. The asterisk indicates a significant difference in ATPase activity as determined by the Mann–Whitney test ($p < .05$). (c) The ATPase activity of HSPA1A variants (2 µM) in the presence of 1 µM Hsp40, 4 µM full-length p53 or both. T204A mutant was used as a negative control. (d) Firefly luciferase mixed with HSPA1A WT or mutants (1 µM), Hsp40 (2 µM), Bag-1 (0.5 µM) and ATP (5 mM) was thermally denatured (42 °C) and the luminescence recovered at 37 °C was measured. Activity of denatured luciferase recovered in the absence of chaperones was used as negative control. All experiments were performed in independent triplicates. Error bars represent S. D.

Section 2.7) (Fig. 7c–d). Indeed, this experiment revealed that L399A/D mutants have higher levels of ATP-induced binding to Hsp40 than the WT protein.

Together, although the analyzed mutants (except D529A) have compromised both allostery (Figs. 4, 5, 6) and functional cooperation with Hsp40 (Fig. 6c), they are able to physically contact Hsp40 in an ATP-dependent manner differing from the WT protein. This observation is particularly interesting for the L399D mutant, which is largely conformationally inactive, substrate-binding deficient [41] and almost insensitive to Hsp40-mediated ATPase acceleration (Figs. 3a–c, 6c).

4. Discussion

The SBD plays an inhibitory role in Hsp70 ATPase activity both by regulating linker availability in the Apo state [5] and by preventing back rotation of the NBD lobes enabling ATP hydrolysis in the ATP-bound state [2–4,10,33]. Although the exact molecular mechanism of ATP-induced changes in the SBD is currently unknown, it is clear, that the SBD conformational dynamics and inter-subdomain interactions modulate Hsp70 chaperone activity [8,9].

Here, we revealed that the SBD of D529A as well as L399D, and I515D mutants in the Apo state share strikingly similar structural features (Fig. 2a and Supplementary Fig. S1, Fig. S3, Table 1): i) destabilization of SBDβ propagated from the C-terminal part of the linker region ^{394}LDVAPLSL^{401} containing L399 residue; ii) highly increased mobility of the SBDα subdomain. These structural features are mirrored in increased substrate binding kinetics of the mutants (Fig. 3a–b) resembling the behaviour of lid-less Hsp70 variants in the Apo state [6,21,51,52] or the SBD in the context of ATP-bound Hsp70 [3,33]. Thus, we propose that residues L399, I515, and D529 represent members of a stable local community maintaining the SBD integrity through regulation of SBDα/SBDβ positioning and stabilization of the linker region in HSPA1A [23,53,54].

Controversial results were obtained for DnaK, where the overall structure of the lid-less SBD construct (393–507) in the substrate-free state was determined to be highly flexible unless stabilized by peptide binding [55,56]. Later study, however, described that the peptide-bound state and the empty state of the optimized SBD construct containing αAB helices (387-552-L542Y/L543E) assume largely similar structure indicating that destabilization of the substrate-free lid-less SBD construct (393–507) was caused by the absence of the lid [55,57]. Additionally, D526A mutation in DnaK (D529A in HSPA1A) has been previously shown to affect the thermal stability of the SBD domain and peptide binding kinetics [6]. These results support our findings that highly conserved I515 and D529 residues in the SBDα maintain the structure of both SBD subdomains allowing favourable kinetics of

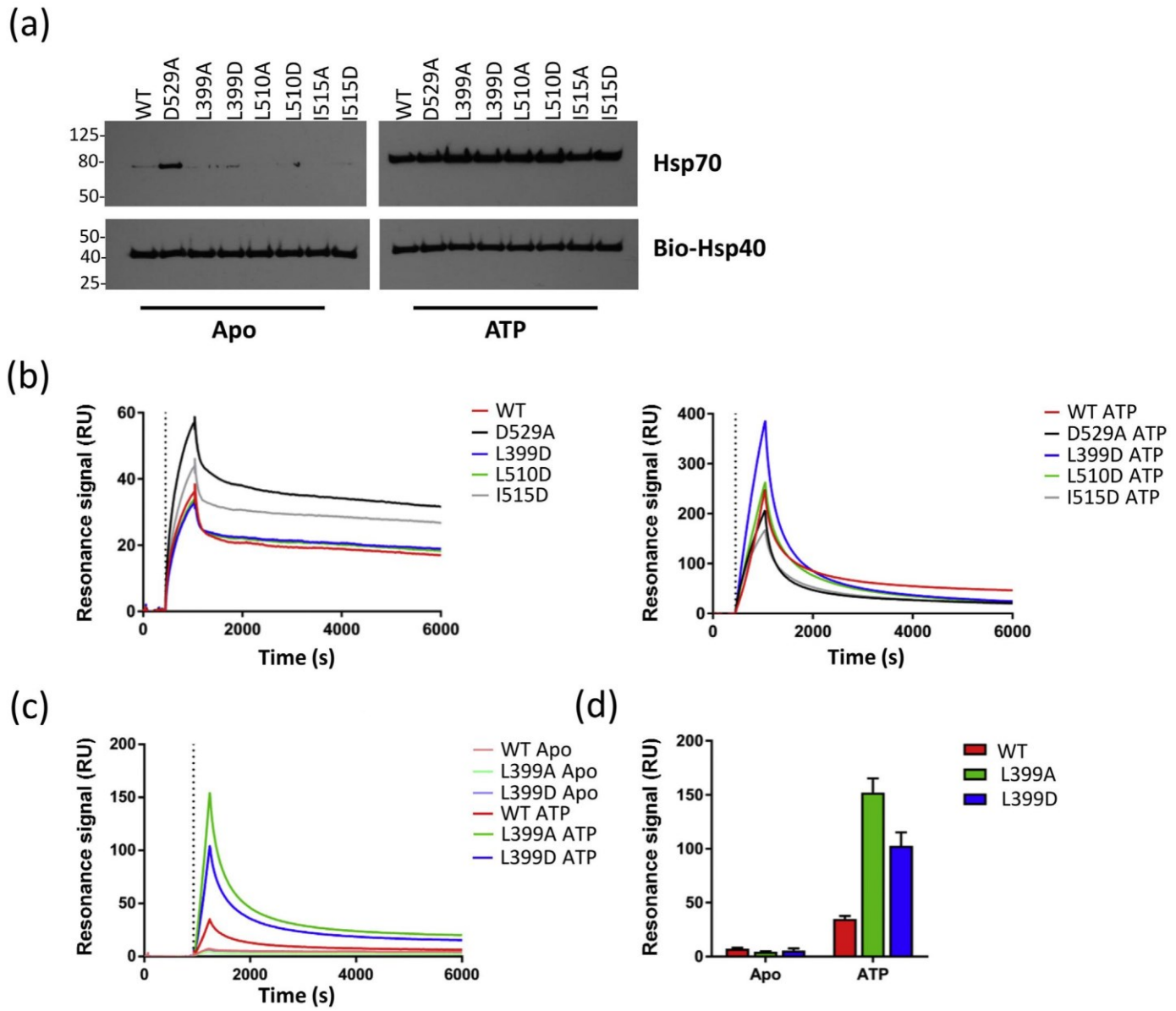

Fig. 7. HSPA1A mutants interact with Hsp40. (a) Biotinylated Hsp40 (B-Hsp40, 70 pmol) bound to streptavidin agarose beads was incubated with HSPA1A proteins (140 pmol) in the absence (Apo) or presence of 0.4 mM ATP before elution by boiling and SDS-PAGE/western blot analysis. (b) Surface plasmon resonance measurement of HSPA1A WT, D529A, L399D and I515D binding to chip-bound biotinylated Hsp40 under nucleotide-free conditions (Apo) or in the presence of ATP. Two technical replicates were measured with comparable results, one of which is presented here. The dotted line denotes the time of sample injection onto the chip. (c) Modified SPR measurement (see Section 2.7) of HSPA1A WT, L399A and L399D binding to immobilized Hsp40 under nucleotide-free conditions (Apo) or in the presence of ATP. Two technical replicates were measured with comparable results, one of which is presented here. (d) The maximal resonance values from (c). Error bars represent S. D.

substrate binding. Interestingly, R470-D552 contact in BiP protein (corresponding to R447-D529 in HSPA1A) is physiologically modified by ADP ribosylation at R470 residue leading to inactivation of BiP substrate-binding activity in starved cells [21]. This suggests that the L399-I515-D529 ensemble can be targeted by cellular post-translational machineries to modulate Hsp70 activity under various conditions.

In addition to physiological modifications, we showed that weakening of the αA helix interaction with the $L_{L,1}$ loop compromised the binding of PES inhibitor (Fig. 3f). The binding specificity of this inhibitor was recently questioned [58], however, our molecular docking analyses revealed its docking into the αA-$L_{L,1}$ cavity of HSPA1A, which is occupied by its derivative PET-16 in the PET-16-DnaK crystal structure (Supplementary Fig. S7) [36]. Therefore, we conclude that pharmacological targeting of the αA-$L_{L,1}$ cavity might interfere with the HSPA1A SBD structure and protein allostery through modulation of L399-I515-D529 ensemble as exemplified by PES/PET-16 inhibitors [36,59]. Interestingly, an allosteric coupling between the movements of the SBDα and the linker has been described [60]. We suggest that the coupling of the SBDα/linker motions is regulated by the L399-I515-D529 structural unit. These findings suggest, that the L399-I515-D529 community plays a vital role in the structural integrity of the SBD in HSPA1A Apo state and is amenable to physiological or pharmacological modifications.

What is the role of the L399-I515-D529 ensemble in HSPA1A conformational change? In order to allow for HSPA1A conformational changes upon ATP binding, the L399-I515-D529 community must be disassembled (Fig. 1). Such a situation is mimicked in the Apo state by the introduced mutations as discussed above (Fig. 2). The L399-I515-D529 community destabilization upon ATP binding is likely to follow after an ATP-induced folding of the ^{391}LLLLDV^{396} linker sequence into a

Table 1
Structural, allosteric and chaperone properties of HSPA1A mutants.

		WT	D529A	L399A	L399D	L510A	L510D	I515A	I515D
Structure and binding activity of the SBD in the Apo state	SBDα subdomain destabilization (Fig. 2)	–	High	Intermediate	High	Low	Low	Low	High
	SBDβ destabilization (Fig. 2)	–	High	Low	High	Low	Low	Low	High
	Interdomain linker destabilization (Fig. 2)[a]	–	High	Low	High	Low	Low	Low	High
	Substrate peptide binding kinetics (Fig. 3a-b)	Slow	Fast	Slow	Fast	Slow	Slow	Slow	Fast
Allostery	ATP-dependent interaction with Tomm34 co-chaperone (Fig. 4a)	Yes	Yes	Decreased	Decreased	No	No	No	No
	ATP-induced domain-docking (Fig. 5)[b]	Yes	Yes	No	No	No	No	No	No
	ATP-induced SBDβ destabilization (Fig. 5)	High	High	Low	Low	Low	Low	Low	Low
	ATP-induced substrate release (% of WT; Fig. 6a)	100%	54%	68%	11%	82%	46%	29%	14%
	Peptide-induced ATPase activity (Fig. 6b)	No	No	No	Yes	No	No	No	Yes
	Interaction with Hsp40 (Fig. 7)	Yes	Yes	Yes	Yes	Yes	Yes	Yes	Yes
Chaperone activities	Basal ATPase activity (pmol ATP/μM Hsp70/min; Fig. 6b)	0.436 ± 0.004	0.482 ± 0.023	1.563 ± 0.058	1.921 ± 0.062	1.373 ± 0.005	1.647 ± 0.035	1.601 ± 0.189	1.381 ± 0.069
	Luciferase refolding activity (%; Fig. 6d)	45.53 ± 0.93	16.35 ± 0.78	37.02 ± 0.31	18.05 ± 1.90	48.88 ± 5.12	25.66 ± 0.4.44	28.41 ± 3.02	16.81 ± 0.45

[a] Peptide 394–401.
[b] Peptides 143–150, 150–169, 168–180, 170–179, 386–392, 394–401, 413–427 and 479–486.

β-sheet configuration in the NBD as the folding of the linker into the NBD precedes the NBD-SBDβ docking [2,3,33] (Fig. 8, Supplementary Fig. S8). A potential role of the linker insertion into the NBD as a direct trigger for L399-I515-D529 unit disassembly is suggested by a molecular dynamics study showing that the hydrophobic region of the linker forms stable contacts with the SBD providing the necessary rigidity [61]. However, additional experiments are required to address the role of linker mobility in the L399-I515-D529 ensemble destabilization.

At the NBD-SBDβ interface L399 interacts with Y149 residue in a size/charge-dependent manner as revealed by our mutational analyses and inspection of various Hsp70 crystal structures [3,33,62] (Figs. 1, 4, Supplementary Fig. S8). The NBD-SBD docking is further secured by SBDα and SBDβ residues (R416, N417, E444, L510, I515) uncovered by SBDα detachment after L399-I515-D529 community disassembly (Figs. 1, 2 and 8, Supplementary Fig. S3 and S8b). Interestingly, we observed an elevated D529A-Hsp40 interaction in the absence of ATP (Fig. 7a-b). The increased mobility of the linker/SBDβ/SBDα region induced by D529A substitution (Fig. 2) might to a degree satisfy the structural requirements for HSPA1A-Hsp40 interaction [10] independently of ATP [63,64]. L510 (A/D) and I515 (A/D) substitutions in the αA helix destabilize the NBD-SBDα interaction, most likely mediated through I164 residue (Figs. 1 and 8, Supplementary Fig. S8a) [13,32,33]. It is of interest to note that DnaK truncation mutant lacking the SBDα subdomain (1–507) has largely intact ATP-induced peptide release, peptide-stimulated ATPase activity and domain docking suggesting that SBDα is not required for allosteric transitions in DnaK [9,51,56]. In contrast, L510A/D and I515A/D mutants of HSPA1A are not able to achieve stable domain-docked conformation (Fig. 5) and I515D mutant has severe defects in allostery and chaperoning function (Fig. 6a,d). A recent evidence suggests that the NBD-SBDα interface of eukaryotic Hsp70 proteins and namely HSPA1A has been “tuned” in the course of evolution to stabilize the domain-docked state significantly more than in DnaK [9,17,33]. Particularly interesting is the eukaryote-specific insertion of R509 (HSPA1A numbering) stabilizing the NBD-SBDα interface together with L510/I515-I164 contacts [17,33]. Therefore, destabilization of the NBD-SBDα interface induced by L510A/D and I515A/D mutations in HSPA1A leads to distinct modulation of allostery in comparison to the deletion of the SBDα subdomain in DnaK.

The impaired ability of HSPA1A point mutants to achieve the ATP-bound conformation is mirrored in their perturbed allosteric control and Hsp40 interaction. The ATPase activity of HSPA1A is not stimulated by peptide substrates unless allostery is compromised by L399D and I515D mutations (Fig. 6b). A similar observation for HSPA1A I164L and R509E mutants was recently described suggesting that weakening of the NBD-SBDα contacts render HSPA1A more sensitive to peptide stimulation [17]. However, as L399D and I515D mutations affect different intramolecular interfaces (NDB-SBDβ and NBD-SBDα, respectively, Fig. 1, Supplementary Fig. S8), we propose that the defects of HSPA1A allosteric control in general are responsible for its increased peptide-induced ATPase rate. In addition, the ATPase rate of Hsc70 is intrinsically sensitive to peptide stimulation similarly to DnaK [17,42]. This indicates that HSPA1A and Hsc70 differ in their ability to transmit allosteric signals from the SBD to the NBD, which might account for their distinct roles [4,65]. Conversely, the presence of a large substrate protein (p53) triggers SBD to NBD signaling in HSPA1A independently of intact allosteric control (Fig. 6c). It is possible that bulky substrates contact the SBD of HSPA1A more extensively, eliciting SBD to NBD signaling and accelerate NBD-SBD undocking in allosterically defective proteins to further promote their increased ATPase activity [66].

ATPase stimulation by Hsp40 is compromised in the proteins with elevated intrinsic ATPase rate, however, these allosterically defective proteins exhibit ATP-induced binding to Hsp40 (Figs. 6c and 7). We propose that modulation of allosteric control increasing the ATPase activity disable efficient Hsp40-mediated interdomain linker adjustment, preventing optimal positioning of the catalytic residues for

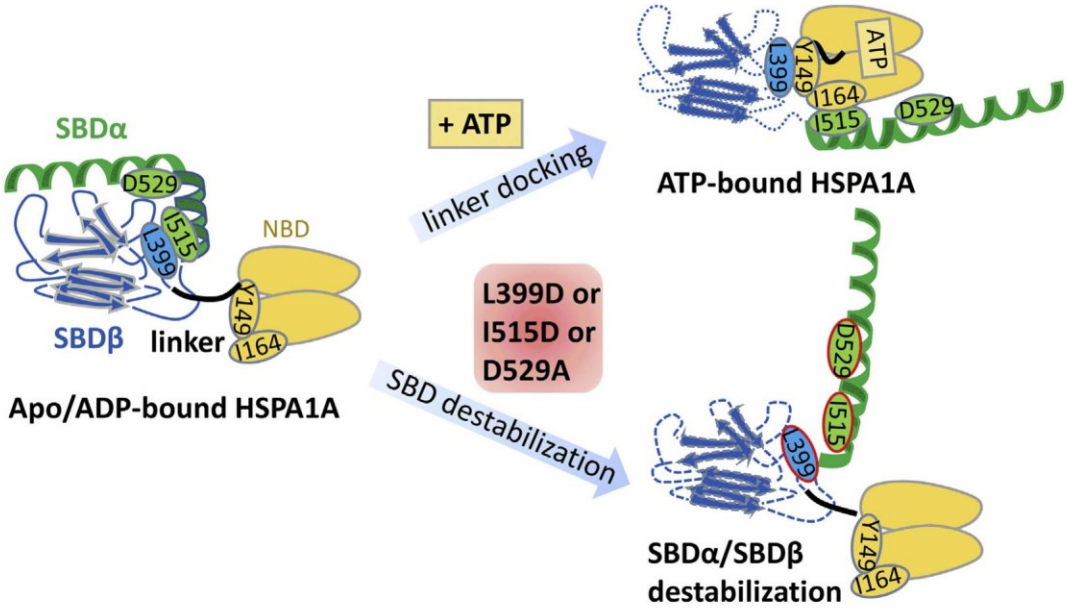

Fig. 8. The role of L399, I515 and D529 in HSPA1A structural transitions. L399D, I515 and D529 residues form a local community stabilizing the interface of SBDα/SBDβ subdomains in the Apo/ADP-bound state of HSPA1A. Upon ATP binding, the flexible interdomain linker becomes structured by docking into the NBD. The L399-I515-D529 community is disassembled and L399 is recruited to the NBD-SBD interface (Y149 residue). Detached SBDα/SBDβ subdomains dock onto the NBD through the newly exposed surfaces increasing the flexibility of SBDβ (dashed lines). I515 together with L510 secure the SBDα contacts with the NBD (I164). Introduction of L399D, I515D and D529A mutations to the Apo state mimics the ATP-induced disassembly of the L399-I515-D529 unit and causes SBD destabilization (dashed lines).

further ATP hydrolysis acceleration [10]. Although the Hsp70-Hsp40 interaction is abrogated in certain allosterically inactive Hsp70 variants (*e.g.* DnaK-A4-V389A/L390A/L391A/L392A and DnaK-D2-L390D/L391D) [41], binding of allosterically defective DnaK V389A variant to DnaJ has been reported [67]. This suggests that site-specific perturbations of Hsp70 allostery are required to prevent Hsp40 binding. Interestingly, L399A/D mutants had significantly higher levels of binding to Hsp40 than WT protein (Fig. 7c–d). It is likely, that L399 displacement from the NBD-SBDβ interface (Figs. 4, Fig. 5 Supplementary Fig. S8b) caused by A/D mutations facilitate Hsp40 docking by increasing the mobility of the SBDβ and linker in respect to the NBD [10]. However, further investigation is needed to explain this behavior of L399A/D mutants. Moreover, different kinetics of mutants' binding to Hsp40 compared to WT was observed (Fig. 7b and Supplementary Fig. S6). Concordantly, modulated kinetics of DnaK D526N mutant association with DnaJ was previously determined by SPR [68], indicating that Hsp70-Hsp40 interactions can be “tuned” by the mutations introduced to the SBD [69].

5. Conclusions

Taken together, our data provide an important insight into the conformational activity of human HSPA1A. We delineated the mutual interdependence of L399-centered residues and D529 electrostatic community in maintaining the structure of the SBDβ. Next, we disclosed the importance of ATP-induced L399 repositioning for the establishment of L399-Y149 contacts at the NBD-SBDβ interface, a feature likely to be general and necessary for all Hsp70 proteins with active allostery [2,5] (Fig. 8). Conversely, a unique behavior of HSPA1A ATPase activity in response to peptide substrates was observed, documenting the differential allosteric “tuning” in Hsp70 homologs [17–21]. The information provided here of the distinct characteristics of HSPA1A structure and Hsp40 interaction will aid the design of novel isoform-specific Hsp70 inhibitors to treat human pathologies including cancer and neurodegenerative diseases [70,71].

Author contributions

F.T., V.V., P.V., P.Ma. and P.Mu. designed research; V.V., P.V., F.T., M.D., P.Ma., D.K., and J.H. performed research and analyzed data; V.V., P.V., and F.T. wrote the manuscript. The final version of the manuscript was commented and approved by all authors.

Acknowledgements

We gratefully thank Dr. P. J. Coates for critical reading and language editing of the manuscript. This work was supported by Czech Science Foundation (16-20860S). Additional institutional and instrumental support from the Ministry of Education, Youth and Sports of the Czech Republic (MEYS CR, LO1413 and LQ1604), the Ministry of Health of the Czech Republic - conceptual development of research organization (MMCI, 00209805) and EU CZ.1.05/1.1.00/02.0109 is gratefully acknowledged. We acknowledge the Biomolecular Interactions and Crystallization Core Facility of CEITEC MU and Centre of Molecular Structure at BioCeV supported by the CIISB research infrastructure (LM2015043 funded by MEYS CR) for their support with obtaining scientific data presented in this paper.

Appendix A. Supplementary data

Supplementary data to this article can be found online at https://doi.org/10.1016/j.bbagen.2019.129458.

References

[1] T. Moran Luengo, M.P. Mayer, S.G.D. Rudiger, The Hsp70-Hsp90 chaperone cascade in protein folding, Trends Cell Biol. 29 (2019) 164–177.
[2] R. Qi, E.B. Sarbeng, Q. Liu, K.Q. Le, X. Xu, H. Xu, J. Yang, J.L. Wong, C. Vorvis, W.A. Hendrickson, L. Zhou, Q. Liu, Allosteric opening of the polypeptide-binding site when an Hsp70 binds ATP, Nat. Struct. Mol. Biol. 20 (2013) 900–907.
[3] R. Kityk, J. Kopp, I. Sinning, M.P. Mayer, Structure and dynamics of the ATP-bound open conformation of Hsp70 chaperones, Mol. Cell 48 (2012) 863–874.
[4] R. Kityk, M. Vogel, R. Schlecht, B. Bukau, M.P. Mayer, Pathways of allosteric regulation in Hsp70 chaperones, Nat. Commun. 6 (2015) 8308.
[5] J.F. Swain, G. Dinler, R. Sivendran, D.L. Montgomery, M. Stotz, L.M. Gierasch,

Hsp70 chaperone ligands control domain association via an allosteric mechanism mediated by the interdomain linker, Mol. Cell 26 (2007) 27–39.
[6] V. Fernandez-Saiz, F. Moro, J.M. Arizmendi, S.P. Acebron, A. Muga, Ionic contacts at DnaK substrate binding domain involved in the allosteric regulation of lid dynamics, J. Biol. Chem. 281 (2006) 7479–7488.
[7] P. Zhang, J.I. Leu, M.E. Murphy, D.L. George, R. Marmorstein, Crystal structure of the stress-inducible human heat shock protein 70 substrate-binding domain in complex with peptide substrate, PLoS One 9 (2014) e103518.
[8] A. Zhuravleva, L.M. Gierasch, Substrate-binding domain conformational dynamics mediate Hsp70 allostery, Proc. Natl. Acad. Sci. U. S. A. 112 (2015) E2865–E2873.
[9] A. Zhuravleva, E.M. Clerico, L.M. Gierasch, An interdomain energetic tug-of-war creates the allosterically active state in Hsp70 molecular chaperones, Cell 151 (2012) 1296–1307.
[10] R. Kityk, J. Kopp, M.P. Mayer, Molecular mechanism of J-domain-triggered ATP hydrolysis by Hsp70 chaperones, Mol. Cell 69 (227–237) (2018) e4.
[11] A. Bracher, J. Verghese, The nucleotide exchange factors of Hsp70 molecular chaperones, Front. Mol. Biosci. 2 (2015) 10.
[12] R.K. Allan, T. Ratajczak, Versatile TPR domains accommodate different modes of target protein recognition and function, Cell Stress Chaperones 16 (2011) 353–367.
[13] M. Durech, F. Trcka, P. Man, E.A. Blackburn, L. Hernychova, P. Dvorakova, D. Coufalova, D. Kavan, B. Vojtesek, P. Muller, Novel entropically driven conformation-specific interactions with Tomm34 protein modulate Hsp70 protein folding and ATPase activities, Mol. Cell. Proteomics 15 (2016) 1710–1727.
[14] H. McDonough, C. Patterson, CHIP: a link between the chaperone and proteasome systems, Cell Stress Chaperones 8 (2003) 303–308.
[15] C. Scheufler, A. Brinker, G. Bourenkov, S. Pegoraro, L. Moroder, H. Bartunik, F.U. Hartl, I. Moarefi, Structure of TPR domain-peptide complexes: critical elements in the assembly of the Hsp70-Hsp90 multichaperone machine, Cell 101 (2000) 199–210.
[16] D. Malinverni, S. Marsili, A. Barducci, P. De Los Rios, Large-scale conformational transitions and dimerization are encoded in the amino-acid sequences of Hsp70 chaperones, PLoS Comput. Biol. 11 (2015) e1004262.
[17] W. Meng, E.M. Clerico, N. McArthur, L.M. Gierasch, Allosteric landscapes of eukaryotic cytoplasmic Hsp70s are shaped by evolutionary tuning of key interfaces, Proc. Natl. Acad. Sci. U. S. A. 115 (2018) 11970–11975.
[18] F. Trcka, M. Durech, P. Vankova, J. Chmelik, V. Martinkova, J. Hausner, A. Kadek, J. Marcoux, T. Klumpler, B. Vojtesek, P. Muller, P. Man, Human stress-inducible Hsp70 has a high propensity to form ATP-dependent antiparallel dimers that are differentially regulated by cochaperone binding, Mol. Cell. Proteomics 18 (2019) 320–337.
[19] L. Sun, F.T. Edelmann, C.J. Kaiser, K. Papsdorf, A.M. Gaiser, K. Richter, The lid domain of caenorhabditis elegans Hsc70 influences ATP turnover, cofactor binding and protein folding activity, PLoS One 7 (2012) e33980.
[20] J.H. Seo, J.H. Park, E.J. Lee, T.T. Vo, H. Choi, J.Y. Kim, J.K. Jang, H.J. Wee, H.S. Lee, S.H. Jang, Z.Y. Park, J. Jeong, K.J. Lee, S.H. Seok, J.Y. Park, B.J. Lee, M.N. Lee, G.T. Oh, K.W. Kim, ARD1-mediated Hsp70 acetylation balances stress-induced protein refolding and degradation, Nat. Commun. 7 (2016) 12882.
[21] J.E. Chambers, K. Petrova, G. Tomba, M. Vendruscolo, D. Ron, ADP ribosylation adapts an ER chaperone response to short-term fluctuations in unfolded protein load, J. Cell Biol. 198 (2012) 371–385.
[22] D. Penkler, O. Sensoy, C. Atilgan, O. Tastan Bishop, Perturbation-response scanning reveals key residues for allosteric control in Hsp70, J. Chem. Inf. Model. 57 (2017) 1359–1374.
[23] G. Stetz, G.M. Verkhivker, Computational analysis of residue interaction networks and coevolutionary relationships in the Hsp70 chaperones: a community-hopping model of allosteric regulation and communication, PLoS Comput. Biol. 13 (2017) e1005299.
[24] C. Boudesco, S. Cause, G. Jego, C. Garrido, Hsp70: a cancer target inside and outside the cell, Methods Mol. Biol. 1709 (2018) 371–396.
[25] C.G. Evans, L. Chang, J.E. Gestwicki, Heat shock protein 70 (hsp70) as an emerging drug target, J. Med. Chem. 53 (2010) 4585–4602.
[26] C.A. Midgley, C.J. Fisher, J. Bartek, B. Vojtesek, D. Lane, D.M. Barnes, Analysis of p53 expression in human tumours: an antibody raised against human p53 expressed in Escherichia coli, J. Cell Sci. 101 (Pt 1) (1992) 183–189.
[27] L. Chang, E.B. Bertelsen, S. Wisen, E.M. Larsen, E.R. Zuiderweg, J.E. Gestwicki, High-throughput screen for small molecules that modulate the ATPase activity of the molecular chaperone DnaK, Anal. Biochem. 372 (2008) 167–176.
[28] Z.Q. Zhang, D.L. Smith, Determination of amide hydrogen-exchange by mass-spectrometry - a new tool for protein-structure elucidation, Protein Sci. 2 (1993) 522–531.
[29] O. Trott, A.J. Olson, Software news and update AutoDock Vina: improving the speed and accuracy of docking with a new scoring function, efficient optimization and multithreading, J. Comput. Chem. 31 (2010) 455–461.
[30] A. Volkamer, D. Kuhn, T. Grombacher, F. Rippmann, M. Rarey, Combining global and local measures for structure-based druggability predictions, J. Chem. Inf. Model. 52 (2012) 360–372.
[31] H. Wang, A.V. Kurochkin, Y. Pang, W. Hu, G.C. Flynn, E.R. Zuiderweg, NMR solution structure of the 21 kDa chaperone protein DnaK substrate binding domain: a preview of chaperone-protein interaction, Biochemistry 37 (1998) 7929–7940.
[32] Q. Liu, W.A. Hendrickson, Insights into Hsp70 chaperone activity from a crystal structure of the yeast Hsp110 Sse1, Cell 131 (2007) 106–120.
[33] J. Yang, M. Nune, Y. Zong, L. Zhou, Q. Liu, Close and allosteric opening of the polypeptide-binding site in a human Hsp70 chaperone BiP, Structure 23 (2015) 2191–2203.
[34] R. Schlecht, A.H. Erbse, B. Bukau, M.P. Mayer, Mechanics of Hsp70 chaperones enables differential interaction with client proteins, Nat. Struct. Mol. Biol. 18 (2011) 345–351.
[35] A.Q. Hassan, C.A. Kirby, W. Zhou, T. Schuhmann, R. Kityk, D.R. Kipp, J. Baird, J. Chen, Y. Chen, F. Chung, D. Hoepfner, N.R. Movva, R. Pagliarini, F. Petersen, C. Quinn, D. Quinn, R. Riedl, E.K. Schmitt, A. Schitter, T. Stams, C. Studer, P.D. Fortin, M.P. Mayer, H. Sadlish, The novolactone natural product disrupts the allosteric regulation of Hsp70, Chem. Biol. 22 (2015) 87–97.
[36] J.I. Leu, P. Zhang, M.E. Murphy, R. Marmorstein, D.L. George, Structural basis for the inhibition of HSP70 and DnaK chaperones by small-molecule targeting of a C-terminal allosteric pocket, ACS Chem. Biol. 9 (2014) 2508–2516.
[37] J.I. Leu, T. Barnoud, G. Zhang, T. Tian, Z. Wei, M. Herlyn, M.E. Murphy, D.L. George, Inhibition of stress-inducible HSP70 impairs mitochondrial proteostasis and function, Oncotarget 8 (2017) 45656–45669.
[38] Z. Li, F.U. Hartl, A. Bracher, Structure and function of Hip, an attenuator of the Hsp70 chaperone cycle, Nat. Struct. Mol. Biol. 20 (2013) 929–935.
[39] J.S. McCarty, G.C. Walker, DnaK as a thermometer: threonine-199 is site of autophosphorylation and is critical for ATPase activity, Proc. Natl. Acad. Sci. U. S. A. 88 (1991) 9513–9517.
[40] A. Arakawa, N. Handa, M. Shirouzu, S. Yokoyama, Biochemical and structural studies on the high affinity of Hsp70 for ADP, Protein Sci. 20 (2011) 1367–1379.
[41] M.P. Mayer, T. Laufen, K. Paal, J.S. McCarty, B. Bukau, Investigation of the interaction between DnaK and DnaJ by surface plasmon resonance spectroscopy, J. Mol. Biol. 289 (1999) 1131–1144.
[42] S. Popp, L. Packschies, N. Radzwill, K.P. Vogel, H.J. Steinhoff, J. Reinstein, Structural dynamics of the DnaK-peptide complex, J. Mol. Biol. 347 (2005) 1039–1052.
[43] M. Wells, H. Tidow, T.J. Rutherford, P. Markwick, M.R. Jensen, E. Mylonas, D.I. Svergun, M. Blackledge, A.R. Fersht, Structure of tumor suppressor p53 and its intrinsically disordered N-terminal transactivation domain, Proc. Natl. Acad. Sci. U. S. A. 105 (2008) 5762–5767.
[44] S. Kannan, D.P. Lane, C.S. Verma, Long range recognition and selection in IDPs: the interactions of the C-terminus of p53, Sci. Rep. 6 (2016) 23750.
[45] K. Liberek, T.P. Galitski, M. Zylicz, C. Georgopoulos, The DnaK chaperone modulates the heat shock response of *Escherichia coli* by binding to the sigma 32 transcription factor, Proc. Natl. Acad. Sci. U. S. A. 89 (1992) 3516–3520.
[46] F. Rodriguez, F. Arsene-Ploetze, W. Rist, S. Rudiger, J. Schneider-Mergener, M.P. Mayer, B. Bukau, Molecular basis for regulation of the heat shock transcription factor sigma32 by the DnaK and DnaJ chaperones, Mol. Cell 32 (2008) 347–358.
[47] J.N. Rauch, J.E. Gestwicki, Binding of human nucleotide exchange factors to heat shock protein 70 (Hsp70) generates functionally distinct complexes in vitro, J. Biol. Chem. 289 (2014) 1402–1414.
[48] E.B. Sarbeng, Q. Liu, X. Tian, J. Yang, H. Li, J.L. Wong, L. Zhou, Q. Liu, A functional DnaK dimer is essential for the efficient interaction with Hsp40 heat shock protein, J. Biol. Chem. 290 (2015) 8849–8862.
[49] S. Yamamoto, S. Nakano, K. Owari, K. Fuziwara, N. Ogawa, M. Otaka, K. Tamaki, S. Watanabe, A. Komatsuda, H. Wakui, K. Sawada, H. Kubota, H. Itoh, Gentamicin inhibits HSP70-assisted protein folding by interfering with substrate recognition, FEBS Lett. 584 (2010) 645–651.
[50] J. Jiang, K. Prasad, E.M. Lafer, R. Sousa, Structural basis of interdomain communication in the Hsc70 chaperone, Mol. Cell 20 (2005) 513–524.
[51] F. Moro, V. Fernandez, A. Muga, Interdomain interaction through helices a and B of DnaK peptide binding domain, FEBS Lett. 533 (2003) 119–123.
[52] G. Buczynski, S.V. Slepenkov, M.G. Sehorn, S.N. Witt, Characterization of a lidless form of the molecular chaperone DnaK: deletion of the lid increases peptide on- and off-rate constants, J. Biol. Chem. 276 (2001) 27231–27236.
[53] G. Stetz, G.M. Verkhivker, Dancing through life: molecular dynamics simulations and network-centric modeling of allosteric mechanisms in Hsp70 and Hsp110 chaperone proteins, PLoS One 10 (2015) e0143752.
[54] G. Ozbaykal, A. Rana Atilgan, C. Atilgan, In silico mutational studies of Hsp70 disclose sites with distinct functional attributes, Proteins 83 (2015) 2077–2090.
[55] S.Y. Stevens, S. Cai, M. Pellecchia, E.R. Zuiderweg, The solution structure of the bacterial HSP70 chaperone protein domain DnaK(393-507) in complex with the peptide NRLLLTG, Protein Sci. 12 (2003) 2588–2596.
[56] M. Pellecchia, D.L. Montgomery, S.Y. Stevens, C.W. Vander Kooi, H.P. Feng, L.M. Gierasch, E.R. Zuiderweg, Structural insights into substrate binding by the molecular chaperone DnaK, Nat. Struct. Biol. 7 (2000) 298–303.
[57] J.F. Swain, E.G. Schulz, L.M. Gierasch, Direct comparison of a stable isolated Hsp70 substrate-binding domain in the empty and substrate-bound states, J. Biol. Chem. 281 (2006) 1605–1611.
[58] R. Schlecht, S.R. Scholz, H. Dahmen, A. Wegener, C. Sirrenberg, D. Musil, J. Bomke, H.M. Eggenweiler, M.P. Mayer, B. Bukau, Functional analysis of Hsp70 inhibitors, PLoS One 8 (2013) e78443.
[59] G. Stetz, G.M. Verkhivker, Probing allosteric inhibition mechanisms of the Hsp70 chaperone proteins using molecular dynamics simulations and analysis of the residue interaction networks, J. Chem. Inf. Model. 56 (2016) 1490–1517.
[60] M. Liebscher, A. Roujeinikova, Allosteric coupling between the lid and interdomain linker in DnaK revealed by inhibitor binding studies, J. Bacteriol. 191 (2009) 1456–1462.
[61] C.A. English, W. Sherman, W. Meng, L.M. Gierasch, The Hsp70 interdomain linker is a dynamic switch that enables allosteric communication between two structured domains, J. Biol. Chem. 292 (2017) 14765–14774.
[62] S.M. Wilbanks, D.B. McKay, How potassium affects the activity of the molecular chaperone Hsc70. II. Potassium binds specifically in the ATPase active site, J. Biol. Chem. 270 (1995) 2251–2257.
[63] A.L. Lai, E.M. Clerico, M.E. Blackburn, N.A. Patel, C.V. Robinson, P.P. Borbat, J.H. Freed, L.M. Gierasch, Key features of an Hsp70 chaperone allosteric landscape revealed by ion-mobility native mass spectrometry and double electron-electron

resonance, J. Biol. Chem. 292 (2017) 8773–8785.
[64] R. Banerjee, G.G. Jayaraj, J.J. Peter, V. Kumar, K. Mapa, Monitoring conformational heterogeneity of the lid of DnaK substrate-binding domain during its chaperone cycle, FEBS J. 283 (2016) 2853–2868.
[65] H. Jaiswal, C. Conz, H. Otto, T. Wolfle, E. Fitzke, M.P. Mayer, S. Rospert, The chaperone network connected to human ribosome-associated complex, Mol. Cell. Biol. 31 (2011) 1160–1173.
[66] A. Mashaghi, S. Bezrukavnikov, D.P. Minde, A.S. Wentink, R. Kityk, B. Zachmann-Brand, M.P. Mayer, G. Kramer, B. Bukau, S.J. Tans, Alternative modes of client binding enable functional plasticity of Hsp70, Nature 539 (2016) 448–451.
[67] D.P. Kumar, C. Vorvis, E.B. Sarbeng, V.C. Cabra Ledesma, J.E. Willis, Q. Liu, The four hydrophobic residues on the Hsp70 inter-domain linker have two distinct roles, J. Mol. Biol. 411 (2011) 1099–1113.
[68] W.C. Suh, W.F. Burkholder, C.Z. Lu, X. Zhao, M.E. Gottesman, C.A. Gross, Interaction of the Hsp70 molecular chaperone, DnaK, with its cochaperone DnaJ, Proc. Natl. Acad. Sci. U. S. A. 95 (1998) 15223–15228.
[69] B.A. Schilke, S.J. Ciesielski, T. Ziegelhoffer, E. Kamiya, M. Tonelli, W. Lee, G. Cornilescu, J.K. Hines, J.L. Markley, E.A. Craig, Broadening the functionality of a J-protein/Hsp70 molecular chaperone system, PLoS Genet. 13 (2017) e1007084.
[70] M.Y. Sherman, V.L. Gabai, Hsp70 in cancer: back to the future, Oncogene 34 (2015) 4153–4161.
[71] W.B. Pratt, J.E. Gestwicki, Y. Osawa, A.P. Lieberman, Targeting Hsp90/Hsp70-based protein quality control for treatment of adult onset neurodegenerative diseases, Annu. Rev. Pharmacol. Toxicol. 55 (2015) 353–371.

Publikace III

Trčka, F., Ďurech, M., **Vaňková, P.**, Vandová, V., Šimončík, O., Kavan, D., Vojtěšek, B., Müller, P. & Man, P.

The interaction of the mitochondrial protein importer TOMM34 with HSP70 is regulated by TOMM34 phosphorylation and binding to 14-3-3 adaptors.

J. Biol. Chem. **295**, 8928–8944 (2020)

Můj příspěvěk k práci: *in vitro fosforylace proteinů s kvantifikací pomocí ESI-MS a LC-MS/MS, provedení HDX-MS a nESI-MS s interpretací dat a jejich grafická prezentace*

JBC ARTICLE

The interaction of the mitochondrial protein importer TOMM34 with HSP70 is regulated by TOMM34 phosphorylation and binding to 14-3-3 adaptors

Received for publication, January 18, 2020, and in revised form, April 28, 2020 Published, Papers in Press, May 5, 2020, DOI 10.1074/jbc.RA120.012624

Filip Trcka[1], Michal Durech[1], Pavla Vankova[2,3], Veronika Vandova[1], Oliver Simoncik[1], Daniel Kavan[2,3], Borivoj Vojtesek[1], Petr Muller[1,*], and Petr Man[2,*]

From the [1]Regional Centre for Applied Molecular Oncology, Masaryk Memorial Cancer Institute, Brno, Czech Republic, [2]BioCeV, Institute of Microbiology of the Czech Academy of Sciences, Vestec, Czech Republic, and the [3]Department of Biochemistry, Faculty of Science, Charles University, Prague, Czech Republic

Edited by Karen G. Fleming

Translocase of outer mitochondrial membrane 34 (TOMM34) orchestrates heat shock protein 70 (HSP70)/HSP90–mediated transport of mitochondrial precursor proteins. Here, using *in vitro* phosphorylation and refolding assays, analytical size-exclusion chromatography, and hydrogen/deuterium exchange MS, we found that TOMM34 associates with 14-3-3 proteins after its phosphorylation by protein kinase A (PKA). PKA preferentially targeted two serine residues in TOMM34: Ser^{93} and Ser^{160}, located in the tetratricopeptide repeat 1 (TPR1) domain and the interdomain linker, respectively. Both of these residues were necessary for efficient 14-3-3 protein binding. We determined that phosphorylation-induced structural changes in TOMM34 are further augmented by binding to 14-3-3, leading to destabilization of TOMM34's secondary structure. We also observed that this interaction with 14-3-3 occludes the TOMM34 interaction interface with ATP-bound HSP70 dimers, which leaves them intact and thereby eliminates an inhibitory effect of TOMM34 on HSP70-mediated refolding *in vitro*. In contrast, we noted that TOMM34 in complex with 14-3-3 could bind HSP90. Both TOMM34 and 14-3-3 participated in cytosolic precursor protein transport mediated by the coordinated activities of HSP70 and HSP90. Our results provide important insights into how PKA-mediated phosphorylation and 14-3-3 binding regulate the availability of TOMM34 for its interaction with HSP70.

Two highly conserved families of molecular chaperones, HSP70 and HSP90, represent core machineries surveying folding and conformational status of cellular proteome (1, 2). Some client proteins of HSP70/HSP90 are either terminally folded or directed for degradation when misfolded to prevent their aggregation (3, 4). A working model for a subset of clients destined to particular cellular compartments, namely mitochondria, suggests that these precursors are kept in a semi-folded transfer-competent state by cycling between HSP70 and HSP90 organized in large multiprotein complexes (5–8). To be imported, mitochondrial precursors processed by HSP70/HSP90 complexes are delivered to the translocase of outer mitochondrial membrane (TOM) complex, which serves as the main gate for diverse precursors transferred into mitochondria (5, 7, 9, 10). TOM is a multiprotein complex consisting of receptors and transmembrane channels. TOM20 and TOM22 receptors of TOM facilitate the transport of precursors containing cleavable presequences, as well as β-barrel proteins (11–13). The transfer of noncleavable hydrophobic precursors, such as the carrier precursors, is mediated by TOM70 receptor (5, 8). The precursors delivered via different receptors are then translocated through the transmembrane channel formed by TOM40 β-barrel protein (14). Recent studies in yeast demonstrated that the metabolic switch from respiration to fermentation is accompanied by a decrease of mitochondrial import capacity, which is induced by protein kinase A (PKA)–mediated phosphorylation of TOM components (15–18). These data indicate that mitochondrial import can be tuned by post-translational modification of the TOM import machinery.

In the multiprotein HSP70/HSP90 complexes transferring mitochondrial precursors, a group of co-chaperone proteins containing two or more tetratricopeptide repeat (TPR) domains enable recurrent precursor shuttling by physically bridging HSP70 to HSP90 (6, 7). This process is mediated through accommodation of the C-terminal HSP70/HSP90 EEVD motifs by conserved charged residues in the TPR domains, forming a so-called two-carboxylate clamp (19, 20). The function of TPR domain co-chaperones goes beyond mere scaffolding because they were reported to regulate the ATPase and folding activities of HSP70/HSP90 (6, 21, 22). In higher eukaryotes, the TOMM34 (34-kDa translocase of the outer mitochondrial membrane) co-chaperone, bearing two TPR domains joined by a flexible interdomain linker, participates with HSP70/HSP90 in mitochondrial precursor protein transport in the cytosol (7, 22, 23). At the molecular level, the TPR2 domain of TOMM34 accommodates the EEVD motif of HSP90 (23). The interaction between HSP70 and TOMM34 is more extensive and requires contacts between the ATP-bound conformation of HSP70 and determinants in the TPR1 domain and the interdomain linker (21). Formation of the HSP70·TOMM34 complex leads to rapid disassembly of ATP-bound dimers of human HSP70 (HSPA1A) and inhibition of HSP70/HSP40-mediated refolding (24). Nevertheless, the

This article contains supporting information.

*For correspondence: Petr Muller, muller@mou.cz; Petr Man, pman@biomed.cas.cz.

physiological role of TOMM34 in precursor protein transport is largely unknown.

14-3-3 dimeric adaptor proteins recognizing phosphorylated targets are involved in a plethora of cellular processes such as cell-cycle control, growth factor signaling, apoptosis, and protein trafficking, including precursor protein transport into mitochondria (25–31). The α-helical structure of 14-3-3 monomers is highly similar to TPR domains and contains residues that electrostatically interact with phosphorylated segments of their partner proteins (19, 32). Mode I R*XX*(pS/pT)*X*(P/G), mode II R*X*(F/Y)*X*(pS/pT)*X*(P/G), and mode III (pS/pT)X_{1-2}–COOH were identified as optimal binding sites for 14-3-3 proteins; however, noncanonical modes of binding also exist (33–35). Motifs recognized by 14-3-3 proteins are predominantly found in structurally disordered regions of the partner proteins (36). Binding of 14-3-3 adaptors has a variety of effects on the bound phosphorylated proteins, including induction of structural changes and steric blockage of interaction interfaces with other proteins or with DNA (34, 37, 38).

In this study, we identified PKA-modified TOMM34 as a novel interaction partner of 14-3-3 proteins. TOMM34 phosphorylation induces structural changes in its TPR domains that are augmented by 14-3-3 protein binding and modulate the interaction of TOMM34 with HSP70. TOMM34 complexed with 14-3-3γ is largely excluded from interaction with HSP70, leaving HSP70/HSP40-mediated refolding intact. Our data suggest a role of both TOMM34 and 14-3-3 proteins in chaperone-assisted transport of precursors to mitochondria and show that post-translational modification of cytosolic, as well as TOM components of the mitochondrial import cascade, are involved in context-dependent regulation of the mitochondrial proteome.

Results

TOMM34 phosphorylation by PKA induces its binding to 14-3-3 proteins

We have shown previously that the TOMM34 TPR1 domain and the highly flexible interdomain linker (amino acids ~140–190) play a role in ATP-dependent TOMM34·HSP70 complex formation (21). Because a number of serine and threonine residues are present in the TPR1 domain and the linker, post-translational modifications of these residues might regulate TOMM34 interaction with HSP70. Therefore, we performed a prediction analysis of potential kinase target sites in TOMM34 (Table S2) (39). This analysis revealed two high-scoring PKA motifs containing serine residues: Ser^{93} localized in the TPR1 domain and Ser^{160} present in the interdomain linker (Fig. 1*a*). Both of these sites were shown to be phosphorylated *in vivo* (40). To test whether PKA mediates phosphorylation of these sites, we performed *in vitro* phosphorylation of TOMM34 by PKA and analyzed the resulting phosphosites by MS (Fig. 1*b* and Table S3). We observed that PKA phosphorylates Ser^{93} and Ser^{160} with 94 and 65% efficiency, respectively. The higher modification level of Ser^{93} likely reflects the preference of PKA for the ^{91}RRASA^{95} motif compared with ^{157}RWNSLP^{162} (41). Other TOMM34 residues were phosphorylated to considerably lower degrees, with the exception of Ser^{280} exhibiting 24% modification (Fig. 1*b* and Table S3). Interestingly, both Ser^{93} and Ser^{160} are localized in motifs predicted to be recognized by 14-3-3 adaptor proteins, in contrast to Ser^{280} (42) (Fig. 1*a* and Table S4). Moreover, Ser^{160} resides in a highly flexible region of TOMM34, a structural feature facilitating binding of 14-3-3 proteins (Fig. 1*a*) (23, 43, 44). To test whether TOMM34 binds 14-3-3 proteins, we performed size-exclusion chromatography (SEC) analysis of PKA-phosphorylated pTOMM34 alone and preincubated with six 14-3-3 isoforms: β, γ, ϵ, σ, τ, and ζ (Fig. 2 and Fig. S1). Phosphorylation of TOMM34 does not change its SEC mobility, and nonphosphorylated TOMM34 protein does not interact with 14-3-3γ (Fig. 2 and Fig. S1*b*). The experiments showed that pTOMM34 forms early-eluting complexes with all tested 14-3-3 isoforms but with differing efficiency and peak distribution. Together, these experiments revealed that TOMM34 is readily phosphorylated by PKA at Ser^{93}, Ser^{160}, and Ser^{280} residues, and this modification enables 14-3-3 isoforms binding.

Ser^{160} phosphorylation by PKA is crucial for 14-3-3 dimer binding

To define the contribution of individual serine residue phosphorylation on the interactions between pTOMM34 and 14-3-3, we analyzed the binding of *in vitro* phosphorylated WT, S93A, S160A, and S93A/S160A TOMM34 variants to 14-3-3γ protein using SEC (Fig. 3). WT, pWT TOMM34 and 14-3-3γ proteins eluted as single peaks with elution volumes of 14.3 and 13.7 ml, respectively. Complex pWT·14-3-3γ eluted in a main peak with elution volume of 12.5 ml and a minor peak (shoulder of 14-3-3γ elution peak) eluting at ~13.1 ml. The elution profile of pS93A/14-3-3γ protein mixture revealed largely intact complex formation; however, the main elution peak shifted to elution volume of 12.8 ml. Importantly, only a small fraction of pS160A/14-3-3γ protein mixture formed a complex with elution volume 12.5 ml, and mixture of p(S93A/S160A) with 14-3-3γ eluted as noninteracting single proteins. Coomassie staining of selected fractions separated in Phos-tag gels (45), together with MS analysis of phosphosites (% of phosphorylated peptides in the selected fractions), enabled the distinction of individual phosphorylated forms (Fig. 3*c* and Table S3*b*). We observed that the main elution peak of the pWT·14-3-3γ complex (12.8 ml) contains TOMM34 protein phosphorylated simultaneously at both Ser^{93} (98%) and Ser^{160} (99%) residues. Noninteracting pWT fraction (14.3 ml) contains residual nonphosphorylated protein, $pSer^{93}$ (93%), and only 7% $pSer^{160}$ protein. Further, 98% of $pSer^{160}$ in the pS93A/14-3-3γ sample is complexed with 14-3-3γ (elution volume 12.8 ml). Interestingly, because the bulk pWT and pS93A proteins are phosphorylated at Ser^{160} to 65 and 58%, respectively (Fig. 1 and Table S3*a*), the 14-3-3γ–interacting fractions are highly enriched for $pSer^{160}$ modification. Conversely, $pSer^{93}$ species in pS160A/14-3-3γ protein mixture remain largely in the unbound TOMM34 fraction. These results clearly show that Ser^{160} phosphorylation by PKA is both necessary and sufficient for the interaction between pTOMM34 and 14-3-3γ. However, the simultaneous presence of a phosphate group on Ser^{93} and Ser^{160} accelerates pTOMM34·14-3-3γ complex

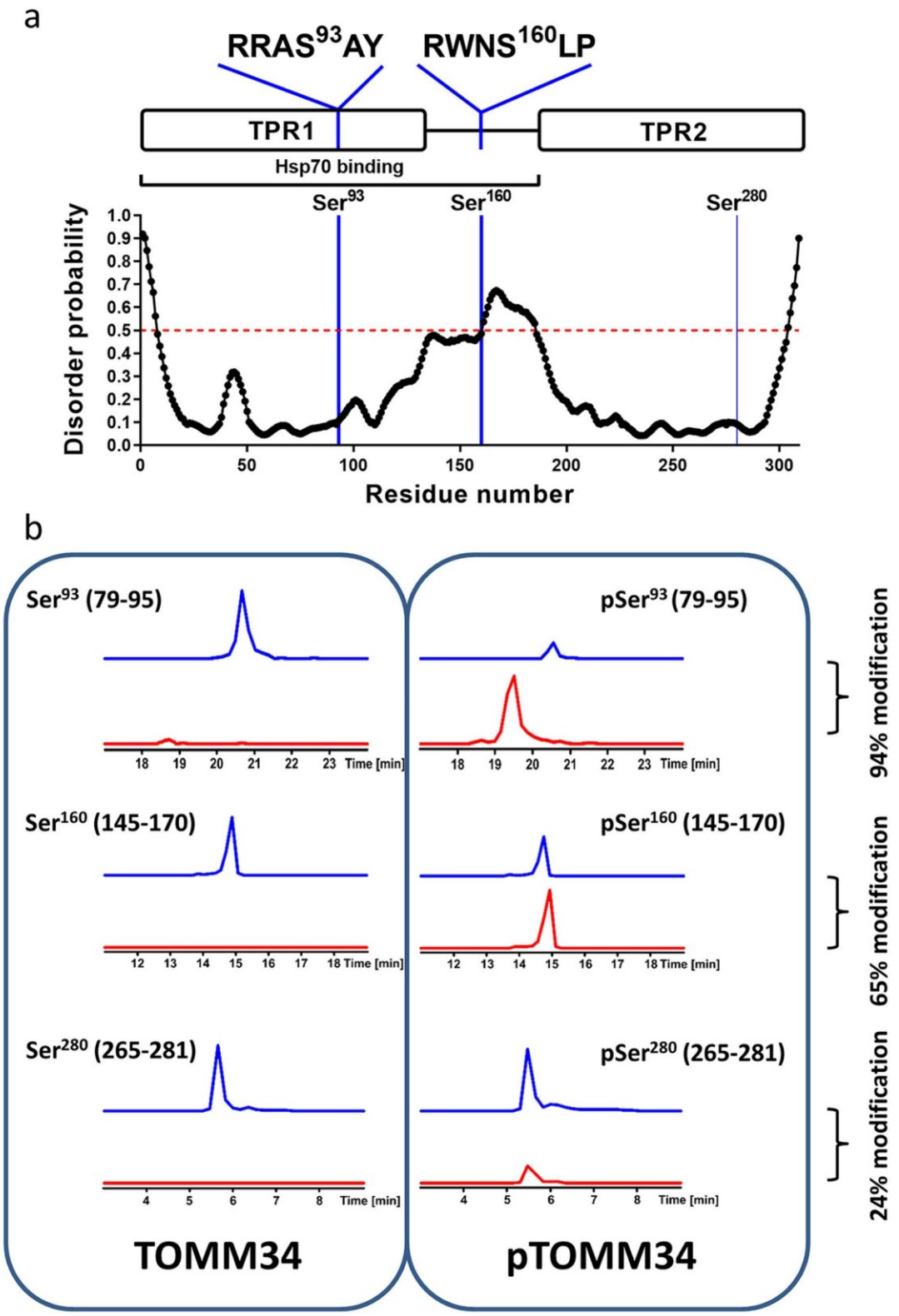

Figure 1. Unstructured and structured regions of TOMM34 contain PKA-targeted serine residues. *a*, prediction of TOMM34 disordered regions (43). The *red dashed line* denotes the prediction threshold. TOMM34 domain structure with the indicated location and sequence context of the preferentially PKA-targeted serine residues is depicted. The regions of TOMM34 implicated in the interaction with HSP70 (TPR1 domain and interdomain linker) are marked. *b*, summed extracted ion chromatograms for selected TOMM34 peptides covering PKA phosphorylation sites Ser^{93} (peptides 79–95), Ser^{160} (peptides 145–170), and Ser^{280} (peptides 265–281). Traces for nonphosphorylated (*blue*) and phosphorylated (*red*) versions of the peptides derived from nonphosphorylated TOMM34 and PKA-phosphorylated TOMM34 (pTOMM34) are shown. The level of the targeted sites phosphorylation is indicated as percentages.

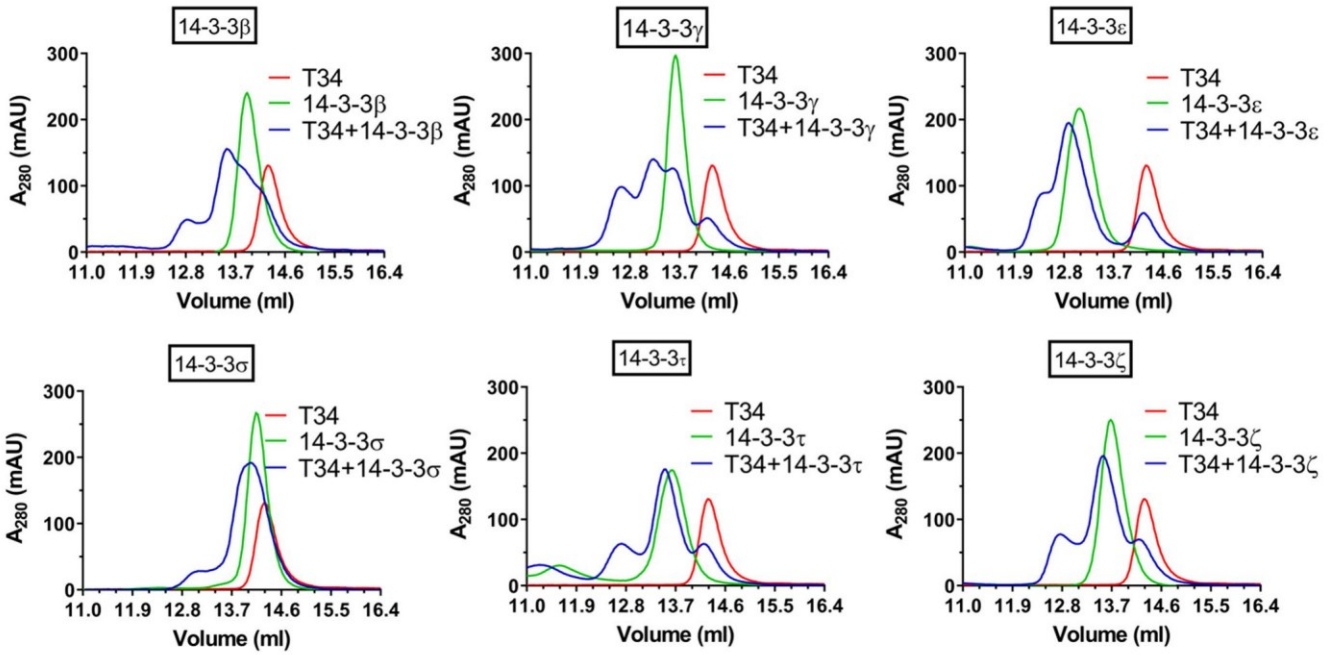

Figure 2. PKA-phosphorylated TOMM34 interacts with 14-3-3 proteins. PKA-phosphorylated TOMM34 (T34, 35 μM) was preincubated with various 14-3-3 isoforms (70 μM) for 30 min at 21 °C before separation by analytical SEC.

mobility in SEC, suggesting that the architecture of Ser^{93}/$pSer^{160}$·14-3-3γ and $pSer^{93}$/$pSer^{160}$·14-3-3γ differ. The phosphorylation of Ser^{280} does not contribute to the interaction between pTOMM34 and 14-3-3γ. To determine the stoichiometry of pTOMM34·14-3-3γ assembly, we performed native electrospray ionization MS with TOMM34/14-3-3γ mixture (Fig. S2). We detected ions corresponding selectively to pTOMM34 complexed with 14-3-3γ dimer, excluding the possibility of 14-3-3γ monomer binding to TOMM34 protein (46).

Phosphorylation induces destabilization of TOMM34 secondary structure strengthened by 14-3-3γ binding

To gain insight into the structural consequences of TOMM34 phosphorylation by PKA and subsequent 14-3-3γ binding, we performed hydrogen/deuterium exchange (HDX)–MS measurement of nonphosphorylated/phosphorylated WT, S93A, S160A, and S93A/S160A TOMM34 in the presence and absence of 14-3-3γ (Fig. 4). This method measures the level of peptide bond hydrogens exchange for deuterium present in the reaction buffer, reflecting the changes in hydrogen bonding and in solvent accessibility of the corresponding protein regions (47). The deuteration levels were followed on peptides/phosphopeptides derived from TOMM34, pTOMM34 and 14-3-3γ proteins reflecting site-specific structural changes introduced by phosphorylation. Introduction of alanine substitutions (S93A, S160A, and S93A/S160A) had virtually no effect on the overall TOMM34 deuteration, indicating that these mutations do not affect TOMM34 secondary structure (Fig. S3). PKA-mediated phosphorylation of WT TOMM34, targeting preferentially Ser^{93}, Ser^{160}, and Ser^{280} residues (Fig. 1 and Table S3), led to destabilization of the TPR2 domain detectable at early deuteration intervals (20 s, 2 min) followed by TPR1 domain destabilization at longer incubation times (20 min, 2 h) (Fig. 4*a*). The analyses of pS93A, pS160A, and p(S93A/S160A) variants revealed that $pSer^{160}$ has a minor role in phosphorylation-induced changes in TOMM34 (Fig. 4*a*). Conversely, mutants lacking Ser^{93} phosphorylation (pS93A and p(S93A/S160A)) exhibited similar deuteration profiles that differ from the pWT protein (Fig. 4*a*). These differences include slightly reduced destabilization of TPR2 domain opening and particularly the absence of TPR1 destabilization. These findings support the role of Ser^{93} phosphorylation for the stability of the TPR1 domain. The rapid opening of the TPR2 domain region, localized in proximity to Ser^{280}, is present in all phosphorylated TOMM34 variants, demonstrating that Ser^{280} phosphorylation regulates local structural features of the TPR2 domain.

To test the structural effects of 14-3-3γ association with TOMM34, we measured HDX of PKA-phosphorylated WT and phosphoablative variants in the presence or absence of 14-3-3γ (Fig. 4*b*). We recapitulated that the $pSer^{160}$ modification is crucial for pTOMM34·14-3-3γ interaction (Fig. 3), because both pS160A and p(S93A/S160A) variants showed lower HDX changes in the presence of 14-3-3γ compared with pWT and pS93A proteins (Fig. 4*b*). Interestingly, pWT association with 14-3-3γ leads to simultaneous destabilization of both TPR domains (Fig. 4*b*). Comparable structural loosening in the TPR2 domain is detectable also in the pS93A·14-3-3γ complex, but in contrast, TOMM34 lacking Ser^{93} phosphorylation has compromised TPR1 destabilization. These observations are in agreement with our SEC analyses (Fig. 3), suggesting that Ser^{160} phosphorylation is both necessary and sufficient for 14-3-3γ binding to TOMM34, whereas Ser^{93} phosphorylation is required for additional positioning of bound 14-3-3γ. A subtle structural loosening of the TPR2 domain in the presence of 14-3-3γ is

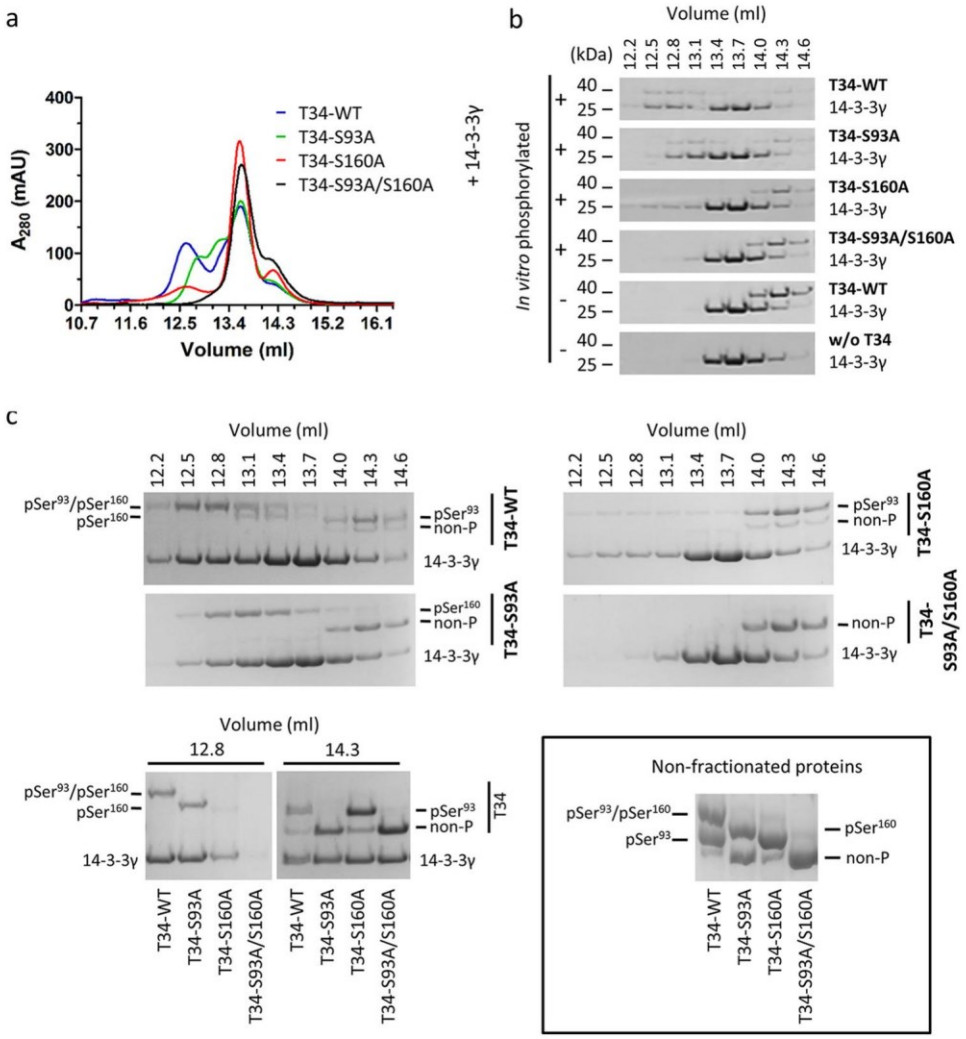

Figure 3. Ser^{160} phosphorylation by PKA is crucial for 14-3-3 dimers binding. *a*, PKA-phosphorylated TOMM34 variants (T34, 35 μM) were preincubated with 14-3-3γ protein (70 μM) for 30 min at 21 °C before separation by analytical SEC. *b*, indicated fractions from (*a*) and from SEC separations of nonphosphorylated TOMM34/14-3-3γ (see Fig. 2 and Fig. S1) were analyzed by gel electrophoresis and Coomassie staining. *c*, indicated fractions from (*a*) and (*b*) as well as nonfractioned proteins were separated in Phos-tag gels retarding the migration of phosphorylated proteins and stained by Coomassie (45). MS-identified phosphoforms of TOMM34 in 14-3-3γ-bound (elution volume, 12.8 ml) and unbound (elution volume, 14.3 ml) fractions are indicated.

observed also in nonphosphorylated TOMM34, indicating that 14-3-3γ transiently contacts this part of the TOMM34 protein.

HDX levels monitored in 14-3-3γ peptides were largely unchanged by TOMM34 or its variants, mirroring the structural rigidity of dimeric 14-3-3 (48, 49). However, several regions showed differential deuteration (Fig. 4, *c* and *d*). We observed phosphorylation-independent opening of the C-terminal end of helix H9 in 14-3-3γ, which was slightly enhanced in the presence of phosphorylated TOMM34 proteins. This region might be responsible for the above-mentioned contacts with the TPR2 domain of nonphosphorylated TOMM34. 14-3-3γ helices 3, 5, and 7, which map to the phosphopeptide-binding groove, were protected from deuterium exchange selectively by phosphorylated TOMM34 (Fig. 4*d*) (50). Conversely, the protection of helix 8 cannot be ascribed directly to phosphopeptide accommodation and implies the presence of an additional protein–protein interface between phosphorylated TOMM34 and 14-3-3γ as has been shown previously for other 14-3-3 interaction partners (38, 51).

Together, using HDX-MS, we have determined that phosphorylation of TOMM34 Ser^{93} by PKA is responsible for overall structural opening of the TPR1 domain and has a role in positioning of 14-3-3γ during pTOMM34·14-3-3γ complex formation mediated through phosphorylation of the TOMM34 Ser^{160} residue. 14-3-3γ is likely to interact with TOMM34 through accommodating its phosphosites in the ligand-binding groove and also by an additional interface localized at helix 8 of 14-3-3γ (38, 50, 51).

Phosphorylation of Ser^{160} modulates TOMM34 interaction with HSP70

The HDX-MS (Fig. 4, *a* and *b*) analyses suggested that TOMM34 phosphorylation by PKA at Ser^{93} and Ser^{280} residues destabilizes its TPR1 and TPR2 domains, respectively, and destabilization is further strengthened by pSer^{160}–dependent 14-3-3γ recruitment. Because the TPR1 and TPR2 domains interact with the C termini of HSP70 and HSP90, respectively, to enable efficient binding of the molecular chaperones (21,

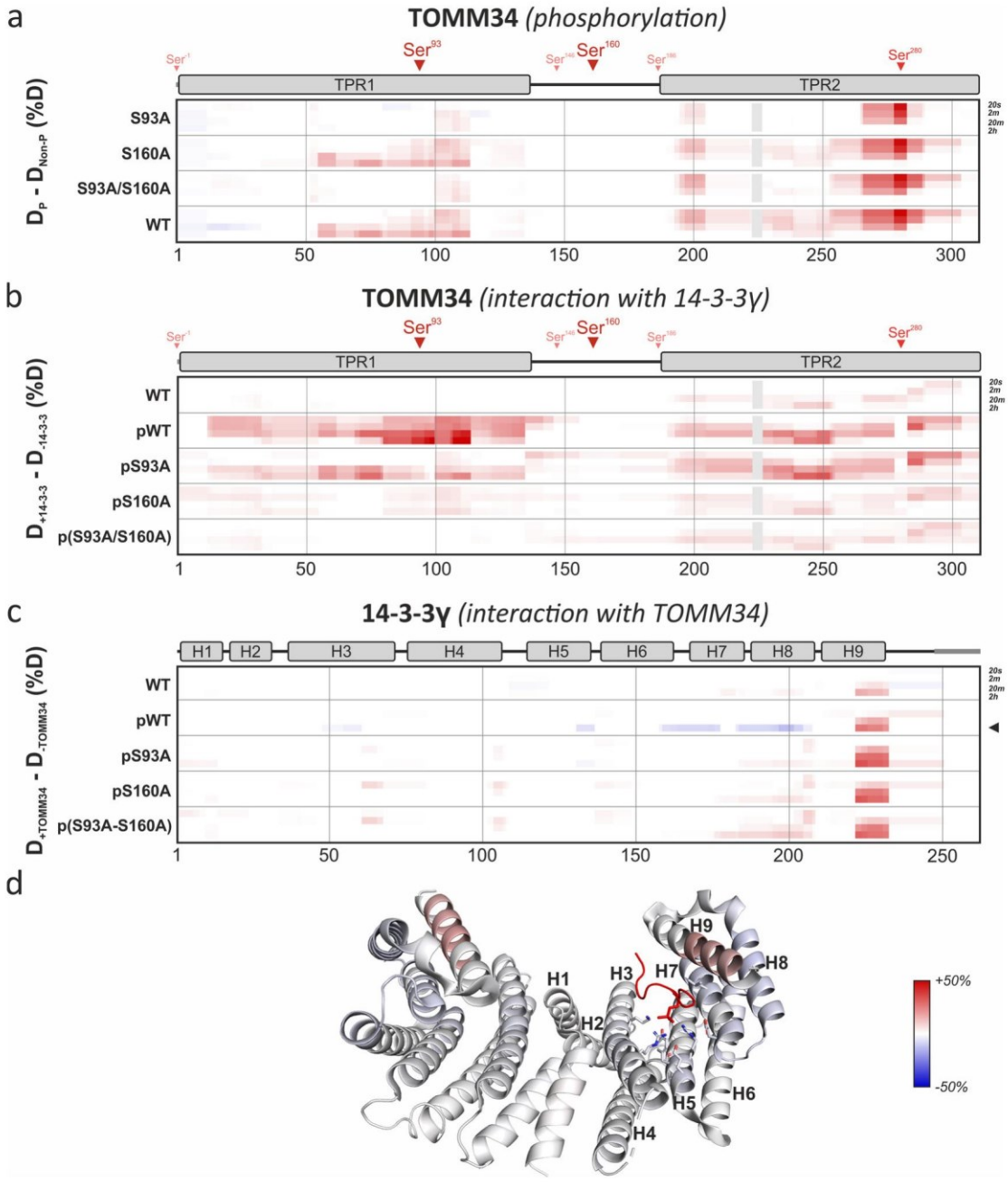

Figure 4. Phosphorylation induces destabilization of TOMM34 secondary structure augmented by 14-3-3γ binding. Time resolved deuteration level differences between selected experimental conditions (indicated on the *left side*) presented in the form of heat maps. *Horizontal gray lines* separate individual experimental conditions. Within each experimental condition, the *four rows* correspond to exchange times (20 s, 2 min, 20 min, and 2 h from *top* to *bottom*), indicated on the *right side*. The *vertical gray lines* mark sequence positions (spaced by 50 amino acids). *a*, difference between phosphorylated (p) TOMM34 WT, S93A, S160A, and/or S93A/S160A proteins and their nonphosphorylated forms. TOMM34 domain structure is depicted above the heat map with PKA-modified sites indicated by *arrowheads* (see Fig. 1). Regions in *gray boxes* were not covered. *b*, differences between nonphosphorylated TOMM34 WT and phosphorylated (p) TOMM34 WT, S93A, S160A, and/or S93A/S160A proteins in the presence and absence of 14-3-3γ protein. *c*, differences between 14-3-3γ protein incubated in the presence or absence of nonphosphorylated TOMM34 WT and PKA-phosphorylated (p) TOMM34 WT, S93A, S160A, and/or S93A/S160A. 14-3-3γ domain structure is depicted above the heat map. *d*, deuteration level differences between 14-3-3γ protein incubated with and without PKA-phosphorylated TOMM34 protein after 2 h of deuteration (indicated in *c* by an *arrowhead*) mapped on the structure of 14-3-3γ dimer in complex with phosphopeptide (in *red*) (PBD code 6A5S; Ref. 50). Residues involved in phosphoserine interaction (Lys^{50}, Arg^{57}, Arg^{132}, Tyr^{133}, Glu^{136}, Leu^{177}, and Glu^{185}) and α-helices are highlighted in one of 14-3-3γ protomers.

23), we tested the interaction of phosphorylated TOMM34 variants with HSP70 and HSP90 C-terminal EEVD peptides in the presence of 14-3-3γ by fluorescence polarization (Fig. 5*a*). We observed that all nonphosphorylated proteins, as well as phosphorylated TOMM34 variants bearing a S93A mutation, bound HSP70 EEVD peptide with comparable affinity as nonphosphorylated WT protein. Conversely, proteins phosphorylated at Ser^{93} residue exhibited reduced association with HSP70 EEVD peptide independently of 14-3-3γ. Experiments with HSP90 C-terminal EEVD peptide did not show a phosphorylation/14-3-3γ–dependent decrease of TOMM34 interaction with the peptide (Fig. 5*a*). 14-3-3γ did not exhibit binding to EEVD peptides. To further delineate the structural consequences of HSP70/HSP90 EEVD peptides binding to phosphorylated

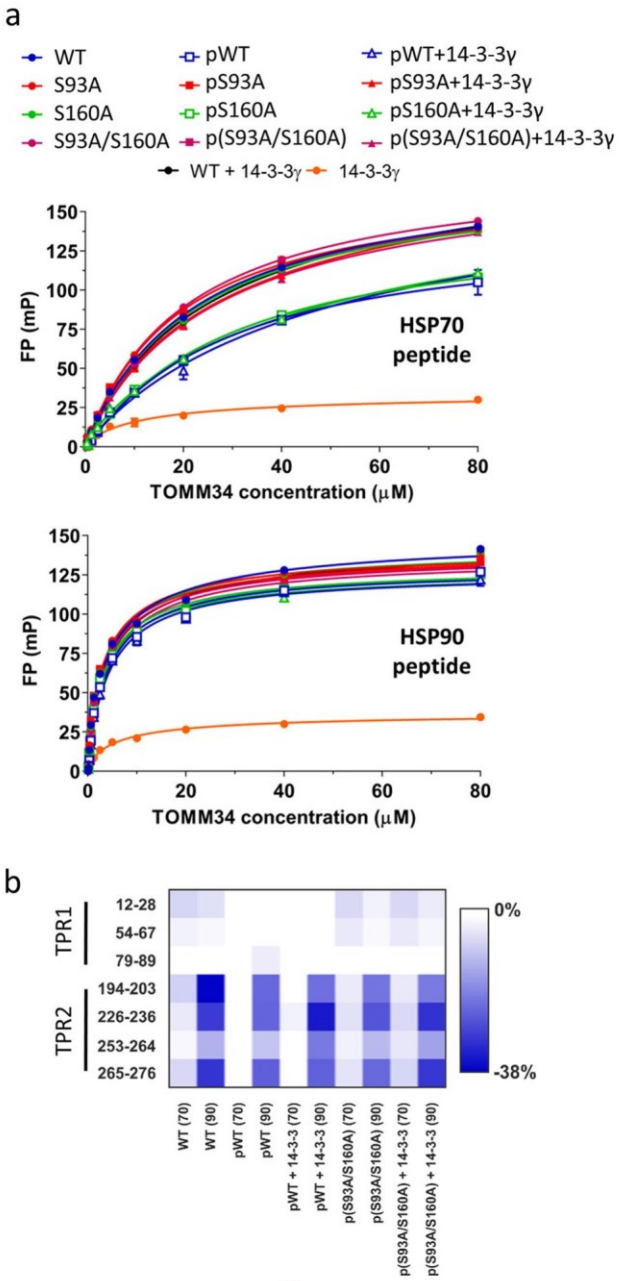

Figure 5. Phosphorylation of Ser^{93} decreases TOMM34 interaction with HSP70 C-terminal EEVD motif. *a*, equilibrium binding curves of fluorescein-labeled C-terminal HSP70 (GGSGSGPTIEEVD) or HSP90 (GDDDTSRMEEVD) peptides binding to nonphosphorylated and PKA-phosphorylated (p) TOMM34 WT, S93A, S160A, and/or S93A/S160A proteins in the presence or absence of 14-3-3γ measured by fluorescence polarization. *Error bars* represent S.D.; $n = 3$ independent experiments. *b*, deuteration level differences (percentage of deuteration) between selected peptides covering the respective two-carboxylate clamps of TPR1 and TPR2 domains in nonphosphorylated and PKA-phosphorylated (p) TOMM34 WT and/or S93A/S160A proteins detected in the presence of HSP70 (*70*) and HSP90 (*90*) C-terminal peptides and in the peptides' absence. The effect of 14-3-3γ presence on peptide-induced deuteration changes is also shown.

TOMM34 variants in the presence of 14-3-3γ, we performed HDX-MS (Fig. 5*b* and Fig. S4). Differences in deuteration of peptides covering the two-carboxylate clamp residues accommodating HSP70/HSP90 C-terminal motifs revealed an unchanged ability of HSP90 EEVD peptide to induce protection of the TOMM34 TPR2 domain (23). On the contrary, protection of the TPR1 domain, the main binding site for HSP70 EEVD peptide, was reduced (23). Again, the effect of 14-3-3γ on the peptide-induced deuteration changes was low. These results revealed that although destabilization of the TPR1 domain by Ser^{93} phosphorylation (Fig. 4*a*) decreases affinity to the HSP70 C terminus (Fig. 5*a*), the loosening of TPR2 by Ser^{280} modification is not accompanied by diminished binding of HSP90 EEVD peptide. The role of 14-3-3γ in reducing the affinity of pTOMM34 for HSP70/HSP90 EEVD motifs is negligible.

Having investigated the binding of HSP70/HSP90 C-terminal peptides, we proceeded with analyses of full-length protein interactions by pulldown with streptavidin-binding peptide (SBP)-tagged proteins (Fig. 6). Because the TOMM34·HSP70 interaction is ATP-dependent (21, 24), the corresponding buffers were supplemented with ATP. All the nonphosphorylated TOMM34 variants interacted with SBP-HSP70 to the same level in the presence of ATP, indicating that the introduced mutations do not affect binding (Fig. 6*a*). Expectedly, no interaction was detected between SBP-HSP70 and phosphorylated TOMM34 variants in the absence of ATP. Surprisingly, PKA treatment decreased the association of TOMM34 pWT and pS93A proteins with SBP-HSP70, whereas pS160A and p(S93A/S160A) proteins exhibited unaffected binding to SBP-HSP70. These results show that phosphorylation of Ser^{160}, rather than pSer^{93}–mediated structural changes of the TPR1 domain (Figs. 4*a*), decreases TOMM34 binding to full-length HSP70. SBP-HSP90 pulldown showed that all phosphorylated TOMM34 variants are able to bind HSP90, recapitulating that the opening of the TPR2 domain by Ser^{280} phosphorylation does not preclude HSP90 binding (Figs. 4*a* and 5).

To delineate the influence of 14-3-3γ binding on the interactions between TOMM34 and HSP70, we performed SBP-pulldown assay using the S93A/S160A variant that is unable to bind 14-3-3γ (Fig. 3). We detected a phosphorylation-dependent and 14-3-3γ–independent decrease of TOMM34 binding to SBP-HSP70 (Fig. 6*b*). 14-3-3γ protein was not co-precipitated with residual WT TOMM34 interacting with SBP-HSP70. This result indicates that the pWT·14-3-3γ complex is excluded from interaction with SBP-HSP70. Conversely, SBP-HSP90·pWT·14-3-3γ assembly is effectively pulled down using the same experimental setup (Fig. 6*b*). Collectively, the data show that although phosphorylation of Ser^{93} decreases binding of the TOMM34 TPR1 domain to HSP70 EEVD peptide, the interaction of full-length HSP70 with phosphorylated TOMM34 is precluded mainly by phosphorylation at Ser^{160}.

pTOMM34 complexed with 14-3-3γ dimer does not disrupt ATP-dependent HSP70 dimer

We next used SEC to further study interactions between HSP70, TOMM34, and 14-3-3γ, because this method does not require immobilization (Fig. 7, *a* and *b*). All analyses were performed in the presence of ATP. First, we evaluated HSP70 and TOMM34 protein samples in the absence of 14-3-3γ. HSP70 eluted as a major peak with elution volume 11.9 ml, which corresponds to the ATP-bound HSP70 dimer (24). The HSP70 dimer was disrupted by interaction with nonphosphorylated

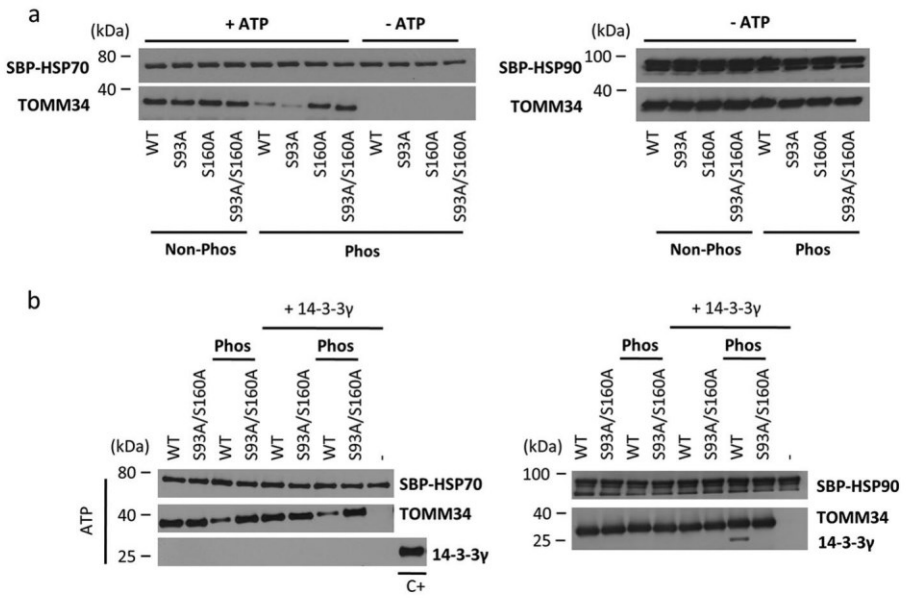

Figure 6. Phosphorylation of Ser^{160} modulates TOMM34 interaction with HSP70 protein. *a*, SBP pulldown analysis of the interaction between SBP–HSP70/SBP–HSP90 and nonphosphorylated (*Non-phos*) and PKA-phosphorylated (*Phos*) TOMM34 protein variants. Because the interaction of TOMM34 with HSP70 is ATP-dependent (21), these experiments were performed in the presence or absence of ATP. *b*, SBP pulldown analysis of SBP–HSP70/SBP–HSP90 interaction with nonphosphorylated and PKA-phosphorylated TOMM34 and/or S93A/S160A proteins in the presence and the absence of 14-3-3γ. *C+* denotes purified 14-3-3γ protein used as a positive control for Western blotting.

TOMM34, forming a complex with 1:1 stoichiometry (24) eluting at ~12.4 ml. Interestingly, the presence of phosphorylated TOMM34 also led to HSP70 dimer disruption, although the pTOMM34·HSP70 complex was less abundant, and a significant portion of HSP70 redistributed into early-eluting oligomeric fractions. This observation suggests that the decreased level of pTOMM34 binding to HSP70 detected by pulldown analysis (Fig. 6*a*) is caused by modulated mechanism/kinetics of pTOMM34/HSP70 interaction compared with nonphosphorylated TOMM34 protein. To unravel the role of 14-3-3γ in TOMM34·HSP70 complex formation, we first analyzed HSP70/14-3-3γ protein mixture, showing that 14-3-3γ does not interact with the ATP-bound HSP70 dimer and leaves it intact (Fig. 7*a*). Nonphosphorylated TOMM34 interacts with HSP70, disrupting its dimeric structure independently of the presence of 14-3-3γ. Strikingly, pTOMM34/HSP70/14-3-3γ mixtures eluted as two main peaks with elution volumes 12.5 and 13.1 ml, respectively. Although the peak at 13.1 ml corresponds to pTOMM34·14-3-3γ late eluting assembly enriched for HSP70 monomers, the 12.5-ml peak contains early-eluting pTOMM34·14-3-3γ complex together with HSP70, as shown by Coomassie staining (Fig. 7, *a* and *b*). That the elution profile of pTOMM34·14-3-3γ complexes is unchanged by the presence of HSP70 (Fig. 7*b*) strongly suggests that pTOMM34 complexed with 14-3-3γ is largely excluded from interaction with HSP70. This is further demonstrated by the presence of a 12.5-ml peak shoulder corresponding to ATP-bound HSP70 dimer (elution volume of ~11.9 ml).

To further test whether pTOMM34 complexed with 14-3-3γ loses its interaction with ATP-bound HSP70 dimers, we performed chemical cross-linking with glutaraldehyde and analyzed the resulting complexes by SDS-PAGE/Western blotting using antibodies recognizing HSP70, TOMM34, and 14-3-3γ proteins (Fig. 7*c* and Fig. S5). ATP-induced HSP70 dimer migrated at ~150 kDa. The addition of nonphosphorylated WT TOMM34 and S93A/S160A proteins led to HSP70 dimer disruption, and comparable levels of HSP70·WT and HSP70·S93A/S160A complexes appeared migrating at 110 kDa. In contrast, both pWT and p(S93A/S160A) proteins disrupted HSP70 dimers; however, the level of pWT·HSP70 assembly was lower compared with the p(S93A/S160A)·HSP70 complex. This observation corresponds with our SEC analysis of pWT/HSP70 samples (Fig. 7*a*) showing that pTOMM34 contacts HSP70 dimer inducing its disassembly, but the resulting pTOMM34·HSP70 complex is less stable. Importantly, the simultaneous presence of p(S93A/S160A) and 14-3-3γ led to HSP70 dimer disassembly, and a p(S93A/S160A)·HSP70 complex was formed. Conversely, a significant fraction of HSP70 dimer is preserved in the presence of the pTOMM34·14-3-3γ complex, and the level of pTOMM34·HSP70 assembly is strongly decreased. Surprisingly, pTOMM34·14-3-3γ assembly was detected migrating at ~70 kDa by TOMM34 antibody, indicating 1:1 stoichiometry (Fig. 7*b*), which is in contrast to our native ESI analysis of pTOMM34·14-3-3γ complex stoichiometry (1:2, Fig. S2). The corresponding signal for p(S93A/S160A)·14-3-3γ complex is less populated. Detection using 14-3-3γ antibody showed the presence of 14-3-3γ monomers/dimers and only a weak signal for corresponding pTOMM34·14-3-3γ dimer tripartite complex (Fig. S5). Coomassie staining of pWT and p(S93A/S160A) proteins cross-linked to 14-3-3γ revealed clear separation of pWT, p(S93A/S160A) and 14-3-3γ monomers/dimers (Fig. S5). These observations suggest that the pTOMM34 complex with 14-3-3γ dimer is inefficiently cross-linked and decays in the presence of SDS leaving only traces of pTOMM34·14-3-3γ assembly with 1:1 stoichiometry detectable by Western blotting. Alternatively, the epitopes of antibodies raised against 14-3-3γ and TOMM34 are not

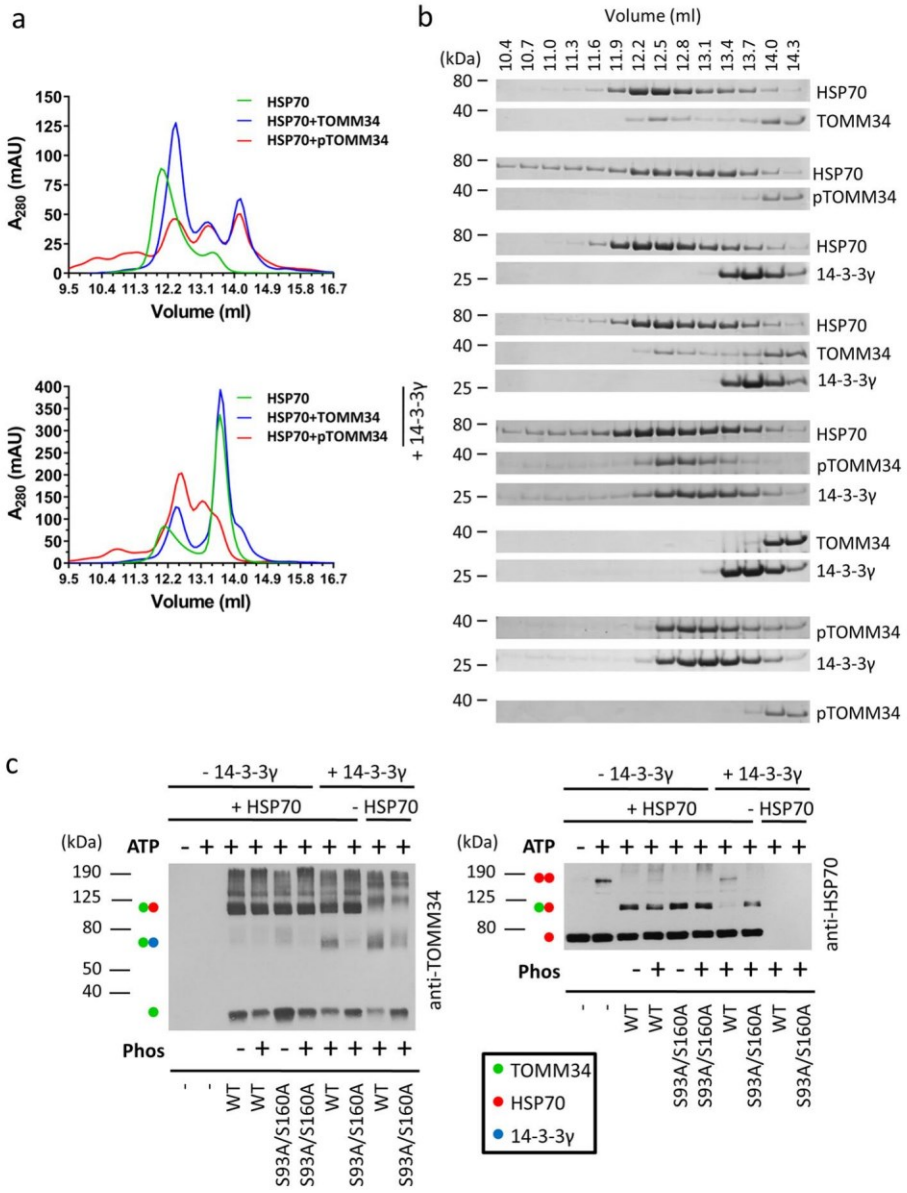

Figure 7. Binding of pTOMM34 to 14-3-3γ dimer prevents disruption of ATP-dependent HSP70 dimer. *a*, phosphorylated/nonphosphorylated TOMM34 WT preincubated with/without 14-3-3γ (30 min, 21 °C) was mixed with HSP70 in the presence of 0.2 mM ATP and incubated 20 min at 21 °C before separation by analytical SEC. The final concentrations of TOMM34, 14-3-3γ, and HSP70 in the protein mixtures were 35, 70, and 35 μM, respectively. *b*, indicated fractions from (*a*) were analyzed by gel electrophoresis and Coomassie staining. *c*, intact or PKA-phosphorylated WT and/or S93A/S160A (final concentration, 60 μM) proteins were mixed with 14-3-3γ (final concentration, 120 μM) or buffer. HSP70 protein (60 μM) preincubated with or without ATP (0.4 mM) was added to TOMM34/14-3-3γ samples in 1:1 ratio, and the mixture was chemically cross-linked by glutaraldehyde addition. The reactions were stopped after 10 min with Tris, pH 8, and separated by SDS-PAGE, blotted, and probed with anti-TOMM34 and HSP70 antibodies. Molecular mass markers and captured protein assemblies are indicated by *numbers* and *dots*, respectively.

readily accessible in the cross-linked tripartite complex. Taken together, the SEC and chemical cross-linking analyses revealed that the modulated interaction of phosphorylated TOMM34 protein with HSP70 is largely prevented by interaction of pTOMM34 with 14-3-3γ dimers, leaving the ATP-bound HSP70 dimer intact.

Binding of pTOMM34 to 14-3-3γ eliminates TOMM34's inhibitory role in HSP70-mediated refolding

TOMM34 protein at high concentrations inhibits HSP70/HSP40-mediated luciferase refolding, likely through HSP70 dimer disruption (21, 24). Therefore, we tested the influence of TOMM34 phosphorylation by PKA on HSP70/HSP40-mediated luciferase refolding (Fig. 8*a*). We detected that both WT and S93A/S160A proteins either phosphorylated or nonphosphorylated completely inhibited luciferase refolding. This observation reflects the finding that HSP70 dimers are disrupted by both modified and unmodified TOMM34 proteins (Fig. 7). Next, we monitored HSP70/HSP40-mediated luciferase refolding in the presence of constant pTOMM34 concentration and increasing concentrations of 14-3-3γ (Fig. 8*b* and Fig. S6). pTOMM34-inhibited luciferase refolding was recovered by 14-3-3γ in a concentration-dependent mode. At equimolar concentrations of pTOMM34 and 14-3-3γ dimers (5 μM), the refolding efficiency reached the level of TOMM34-free refolding mixtures.

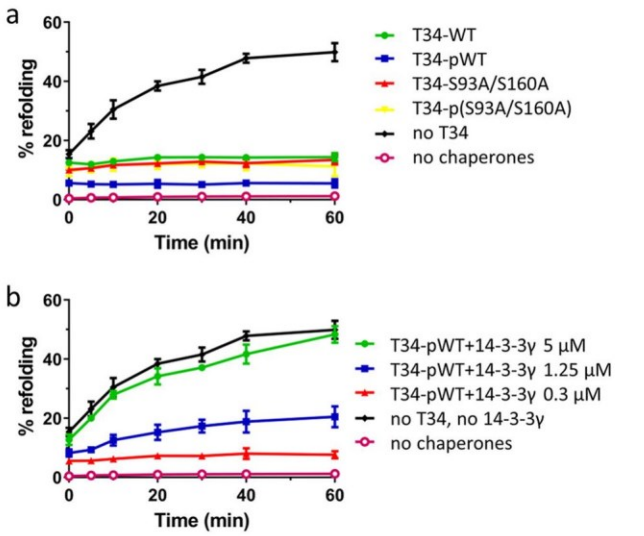

Figure 8. Sequestration of pTOMM34 by 14-3-3γ eliminates TOMM34's inhibitory role in HSP70-mediated refolding. *a*, firefly luciferase incubated with HSP70 (1 μM), HSP40 (2 μM), and BAG1 (0.5 μM) proteins was thermally denatured at 42 °C for 30 min in the presence of 5 μM nonphosphorylated/PKA-phosphorylated TOMM34 WT and S93A/S160A proteins. The kinetics of luciferase reactivation was measured after shifting the reaction temperature to 37 °C. *b*, firefly luciferase denatured as in (*a*) was refolded in the presence of 5 μM PKA-phosphorylated TOMM34 WT protein and increasing concentrations of 14-3-3γ dimer (0.3, 1.25, and 5 μM). The signal from samples with native luciferase was set as 100%. As negative controls, we measured the luciferase activity of denatured luciferase only. *Error bars* represent S.D.; $n = 3$ independent experiments.

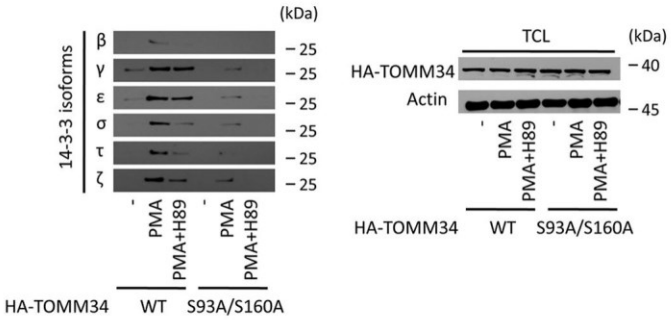

Figure 9. 14-3-3 isoforms interact with TOMM34 *ex vivo* in a phosphorylation-dependent manner. *TOMM34*$^{-/-}$ MCF-7 cells transfected with pCMV-N-HA-TOMM34 WT and pCMV-N-HA-TOMM34-S93A/S160A constructs were treated with PMA (0.3 μM), PKA inhibitor H89 (20 μM), and vehicle control (DMSO, -) for 12 h, collected, and lysed. Next, biotinylated 14-3-3 isoforms prebound to streptavidin–agarose beads were incubated with the cell lysates at 4 °C for 1 h. The eluted complexes were analyzed by gel electrophoresis and Western blotting using anti-HA antibody.

Together, the refolding assays suggest that complex formation between pTOMM34 and 14-3-3γ prevents TOMM34-mediated decomposition of ATP-bound HSP70 dimers and allows for productive luciferase refolding.

14-3-3 Isoforms interact with TOMM34 ex vivo

To verify whether the interactions between 14-3-3 isoforms and pTOMM34 detected *in vitro* (Fig. 2) are physiologically relevant, we performed *ex vivo* pulldown of HA-tagged TOMM34 WT and S93A/S160A proteins reintroduced into *TOMM34*$^{-/-}$ MCF-7 cells (52) using biotinylated 14-3-3 proteins (Fig. 9). To induce cellular signaling, the cells were treated with 12-*O*-tetradecanoylphorbol-13-acetate (PMA) (53–55). Because PKA kinase is encoded by several genes in the human genome (56), we decided to use H89 PKA kinase inhibitor with relaxed specificity (57, 58) to ensure robust inhibition of all kinases sharing PKA-like activity. This allowed us to distinguish phosphorylation/PKA-dependent pTOMM34·14-3-3 complexes. We observed that all the analyzed 14-3-3 isoforms (β, γ, ε, σ, τ, and ζ) interacted with TOMM34 in a PMA-dependent manner, and the interaction was decreased in PMA/H89 co-treated samples. S93A/S160A variant also exhibited PMA-induced binding to 14-3-3 isoforms that was sensitive to H89; however, the levels of pulled down S93A/S160A protein were lower. These results indicate that TOMM34 interaction with 14-3-3 isoforms takes place in cells and is heavily dependent on Ser^{93}/Ser^{160} phosphorylation by PKA or possibly other kinases inhibited by H89 inhibitor (57). Nevertheless, the residual PMA-induced S93A/S160A interaction with 14-3-3 isoforms suggests that an pSer^{93}– and pSer^{160}–independent mechanism of TOMM34/14-3-3 binding also exists *in vivo*.

Discussion

TOMM34·HSP70 complex formation requires both accommodation of the HSP70 EEVD C-terminal motif by the TOMM34 TPR1 domain and docking of so-far-unknown determinants in the TOMM34 interdomain linker to HSP70 in the ATP-bound conformation (21, 23). The TPR1 domain and the interdomain linker of TOMM34 contain several serine/threonine residues, suggesting that their modification might regulate interaction between TOMM34 and HSP70.

Here, we have shown that Ser^{93} (TPR1 domain) and Ser^{160} (interdomain linker) TOMM34 residues are effectively phosphorylated by PKA (Fig. 1 and Tables S2 and S3). The phosphorylation of Ser^{93} induces destabilization of the TPR1 domain (Fig. 4*a*). Opening of the TPR1 domain can be ascribed to repulsive electrostatic interactions introduced by the phosphate group into a structurally stable region of TPR1 domain (Fig. 1*a*) (23, 59). These structural rearrangements are a likely cause of diminished HSP70 EEVD peptide binding because the two-carboxylate clamp of TPR1 domain preferentially accommodates the C terminus of HSP70 (Fig. 5*b*) (23). However, the interaction of the phosphorylated S160A TOMM34 variant (bearing pSer^{93}) with full-length HSP70 is unaffected (Fig. 6*a*). This indicates that the reduced binding of the HSP70 EEVD motif into a destabilized TPR1 domain does not preclude the formation of a high-affinity interaction interface between ATP-bound HSP70 and TOMM34 *in vitro* (21). PKA modification of residue Ser^{93} might, however, regulate the TOMM34/HSP70 interaction *in vivo*, where the TOMM34 TPR1 domain competes with other TPR co-chaperones for binding to the HSP70 C terminus (60, 61). Analogously, phosphorylation of Ser^{280} residue interferes with TPR2 stability (Fig. 4*a*), however, without reducing the affinity of HSP90 C-terminal peptide toward this domain *in vitro* (Fig. 5).

The phosphorylation of Ser^{160} does not have an effect on TOMM34 structure (Fig. 4*a*). This observation is in line with that fact that Ser^{160} is located in the flexible solvent-exposed

interdomain linker (23) (Fig. 1*a*). Importantly, Ser^{160} phosphorylation modulated the TOMM34/HSP70 interaction (Figs. 6–8). Although the ATP-bound HSP70 dimer (24) is effectively disrupted by phosphorylated TOMM34, the level of pTOMM34·HSP70 assembly is substantially reduced compared with TOMM34·HSP70 (Fig. 7, *a* and *b*) unless stabilized by chemical cross-linking (Fig. 7*c* and Fig. S5). Because the TOMM34 interdomain linker is involved in the entropically driven TOMM34 interactions with HSP70, the presence of the phosphate group at Ser^{160} is likely to preclude the formation of a stable protein–protein interface (21). The exact topology of this interface is unknown. These observations also indicate that dissociation of ATP-bound HSP70 dimers is independent of the stable TOMM34·HSP70 complex formation. Accordingly, pTOMM34 exhibits an inhibitory effect on HSP70/HSP40-mediated refolding (Fig. 8), which requires the presence of ATP-dependent HSP70 dimers (24). It is of note that disassembly of HSP70 dimers selectively by pTOMM34 is accompanied by HSP70 oligomerization (Fig. 7, *a* and *b*). We speculate that the released HSP70 monomers lacking stabilization through interaction with TOMM34 oligomerize to form a mixed population of molecules in different nucleotide states (21, 62). However, detailed analysis of these oligomers is yet to be performed. Taken together, the mechanism of PKA phosphorylation-induced reduction of TOMM34 binding to HSP70 is 2-fold: $pSer^{93}$ diminishes TPR1-EEVD interactions, and $pSer^{160}$ perturbs the interaction interface formed between the TOMM34 interdomain linker and HSP70.

Structural changes triggered in proteins phosphorylated at particular motifs are often secured by subsequent binding of 14-3-3 proteins (63–65). All tested 14-3-3 isoforms (β, γ, ϵ, σ, τ, and ζ) bound phosphorylated TOMM34 *in vitro* and *ex vivo* (Figs. 2 and 9), and pTOMM34·14-3-3γ assembly was analyzed in detail. Phosphorylation of Ser^{160} in the context of the $^{152}RXX(pS/pT)X(P/R)WNSLP^{162}$ consensus binding motif localized in the flexible interdomain region is both necessary and sufficient for pTOMM34·14-3-3γ interaction (Figs. 3 and 4) (36, 65). However, the distinct SEC profiles of pWT and pS93A proteins in complex with 14-3-3γ (Fig. 3) indicate that the architecture of these assemblies differ. The structural analysis supports this notion by showing that pS93A retains 14-3-3γ–induced TPR2 destabilization but lacks the opening of TPR1 domain observed in pWT protein (Fig. 4*b*). 14-3-3γ forms a structurally stable dimer (48) that interacts with TOMM34 monomer (Figs. 4 and 7*b* and Figs. S2 and S5). We suggest that the phosphorylated Ser^{160} residue serves as a "gatekeeper" enabling the initial contact of TOMM34 with one of the two amphipathic grooves in the 14-3-3γ dimer (66, 67). Subsequently, the phosphorylated Ser^{93} residue can be accommodated by the second amphipathic groove. Although the $^{90}RRASAY^{95}$ motif deviates from the consensus mainly by lacking proline residue at +2 positon (65), it was shown that the amphipathic grooves of 14-3-3 proteins can coordinate noncanonical sequences (34). Simultaneous binding of two distinct phosphosites in one peptide/protein to 14-3-3 dimers has been previously described (34, 68–70). Moreover, a bidentate 14-3-3 binding was shown to induce conformational changes in $Nth1_{1-751}$ enzyme regulating its activity (34). The presence of a flexible solvent-exposed interdomain linker allows the TPR1 and TPR2 domains of TOMM34 to be mutually oriented with a certain degree of freedom (23, 71). Thus, simultaneous accommodation of phosphorylated Ser^{93} and Ser^{160} residues by structurally rigid 14-3-3γ (Fig. 4, *c* and *d*) (32, 48, 66) might force TOMM34 TPR domains to assume a more defined orientation. As TOMM34 becomes generally more solvent-accessible in the presence of 14-3-3γ (Fig. 4*b*), the bidentate binding mode of 14-3-3γ might impose constraints on TOMM34 structure, leading to its structural loosening. This mode of interaction is rather unusual because studies dealing with the structural consequences of 14-3-3 binding mostly report 14-3-3–induced stabilization of the partner protein (38, 49, 51). However, the fast deuteration kinetics of the flexible protein regions may abrogate the detection of the stabilizing interaction event, as seen with other 14-3-3–interacting proteins (38). Similarly, the protein–protein contacts mediated mainly by electrostatic and side-chain interactions may also show minimal or no detectable changes in peptide bond hydrogen-exchange rates (23, 38, 49). As the gatekeeper $pSer^{160}$ modification resides in a flexible part of TOMM34 protein (Fig. 1), the putative local stabilizing effects of 14-3-3 binding, therefore, could be undetectable by HDX-MS. Moreover, our data support the existence of an additional interaction interface between pTOMM34 and 14-3-3γ involving the surface of helix 8 (Fig. 4, *b–d*). Similar interfaces encompassing helix 8 of 14-3-3 proteins have been reported previously (38, 51). Conversely, phosphorylation-independent transient contacts are likely to occur between the TOMM34 TPR2 domain and helix 9 of 14-3-3γ (Fig. 4, *b–d*) (72, 73). Helix 9 is commonly a part of phosphopeptide-binding grooves and becomes stabilized by the presence of phosphorylated protein partner (38, 51). In contrast, helix 9 was also shown to exhibit intrinsic flexibility in the presence of nonphosphorylated interaction partner that was increased in the presence of phosphorylated interactor, allowing the assembly to reach a more compact conformation (67). This model is supported by our HDX data (Fig. 4, *c* and *d*), although more detailed structural data are needed to fully delineate pTOMM34·14-3-3γ complex architecture and the role of helix 9.

Importantly, formation of a complex of pTOMM34 with 14-3-3γ dimer eliminates its ability to disrupt ATP-bound HSP70 dimers and interact with HSP70 (Fig. 7), allowing HSP70/HSP40-mediated refolding in the presence of pTOMM34 (Fig. 8*b*). We propose that 14-3-3γ sterically occludes the TOMM34 interdomain linker, thereby preventing its interaction with ATP-bound HSP70 (21). Conversely, destabilization of the TPR2 domain in pTOMM34·14-3-3γ assembly (Fig. 4*b*) does not inhibit HSP90·pTOMM34·14-3-3γ complex formation (Fig. 6). Thus, Ser^{160} phosphorylation and subsequent 14-3-3 protein binding might serve as a specific mechanism for suspending HSP70 from TOMM34 alone or as a part of HSP70·TOMM34·HSP90 tripartite complex (Fig. 10) (21, 23). Whether this mode of TOMM34·14-3-3 interaction is generic for other 14-3-3 isoforms awaits further investigation; however, peak distribution heterogeneity of TOMM34 complexes with different 14-3-3 isoforms (Fig. 2) suggests possible structural/functional diversification of TOMM34·14-3-3 assemblies (32, 48).

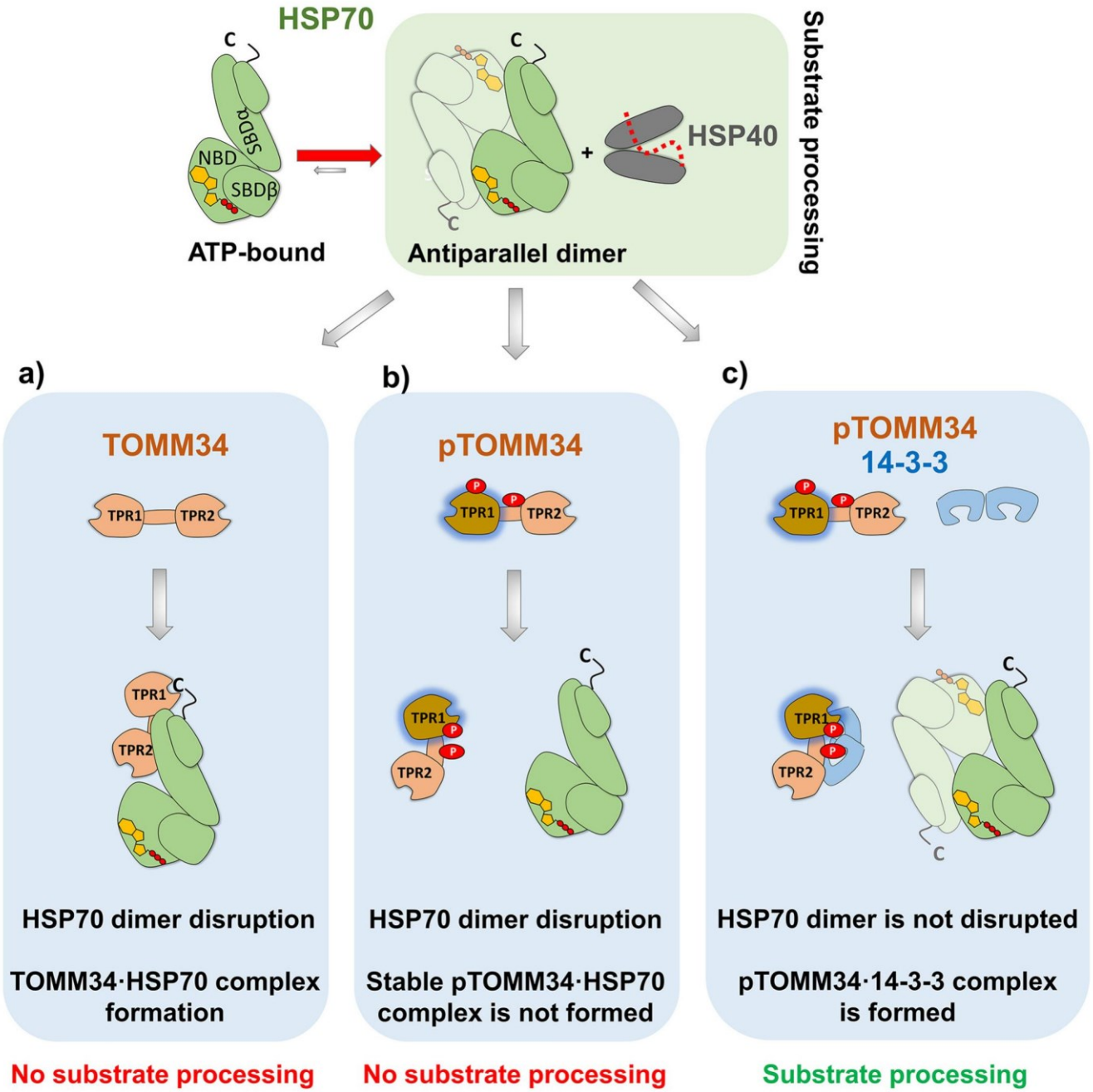

Figure 10. TOMM34 interaction with HSP70 dimers is regulated by its PKA-mediated phosphorylation and 14-3-3 binding. ATP-bound HSP70 antiparallel dimers cooperate with HSP40 during protein substrate (*dotted red line*) processing (24). *a*, nonphosphorylated TOMM34 stably interacts with HSP70 in the ATP-bound state through TPR1-EEVD (*c*) contacts and an interface encompassing the TOMM34 interdomain linker (21, 24). This interaction leads to HSP70 dimer disruption, preventing substrate processing. *b*, PKA mediates TOMM34 phosphorylation (pTOMM34) on Ser^{93} and Ser^{160} residues (*red circles*), leading to structural loosening of the TPR1 domain and perturbation of the interaction interface formed between the TOMM34 interdomain linker and HSP70. pTOMM34 transiently interacts with HSP70, disrupting its dimeric structure and substrate processing activity, but a stable pTOMM34·HSP70 complex is not formed. *c*, 14-3-3 binding to pTOMM34 sequesters TOMM34 from HSP70 dimers leaving their substrate processing activity intact.

What is the physiological outcome of PKA-mediated TOMM34 interaction with 14-3-3 proteins? From a systemic perspective, *TOMM34* (74) was reported to be transactivated by NRF1 and NRF2, transcription factors governing the expression of mitochondrial respiratory subunits (75) and Tom20/Tom70 translocases (76, 77). At the protein level, TOMM34 participates on preprotein transport in the cytosol as a component of large multichaperone complexes in which it coordinates HSP70 and HSP90 (7, 23). Elevated levels of TOMM34 inhibited import of mitochondrial precursor proteins containing N-terminal presequences translocated by the Tom20 pathway (ornithine transcarbamylase), as well as of carrier proteins (phosphate carrier, PiC; ADP/ATP carrier protein, ACC) characterized by multiple integral targeting elements imported via a Tom70-dependent mechanism (7, 8, 11, 78). In contrast, an antibody against TOMM34 blocked mitochondrial import of preproteins bearing presequences (79). These data suggest that tightly regulated levels of TOMM34 are necessary for effective

transport of a variety of import-competent precursors from ribosomes to mitochondria. In recent years, PKA has been shown to suppress mitochondrial protein import by phosphorylating Tom70 (15), Tom40 (16), and Tom22 (17) translocases upon metabolic switch from respiratory to glycolytic metabolism. Interestingly, PKA can be sequestered to the proximity of the outer mitochondrial membrane by protein kinase A anchor proteins (AKAPs) (80, 81) to perform a plethora of functions including regulation of apoptosis by Bad protein phosphorylation (18, 82). Local accumulation of PKA at the surface of TOM might therefore integrate signaling and metabolic demands of the cell by tuning of mitochondrial import pathways, with TOMM34 as a newly identified PKA target. In mammals, 14-3-3 proteins were first described to participate in mitochondrial import by recognizing presequences of preprotein; however, later studies showed that they also facilitate the import of β-barrel proteins lacking presequences (26–31). These observations reveal a more general role of 14-3-3 proteins in mitochondrial import, although the exact mechanism of their action remains elusive. A recurrent bidirectional transfer of precursor proteins between HSP70 and HSP90 seems to be vital for maintaining their import-competent conformation while preventing aggregation (5, 6). We suggest that the action of TOMM34 and 14-3-3 proteins coordinated by PKA phosphorylation of TOMM34 helps to fine-tune shuttling of various transport-competent precursors between HSP70 and HSP90 by timely destabilization of TOMM34 binding to HSP70. This process would be further regulated by the level of PKA activation under different signaling and metabolic circumstances (15–17).

Collectively, we have described TOMM34 protein phosphorylated by PKA as a novel interaction partner of 14-3-3 adaptor proteins. This interaction, established via phosphorylation of residues Ser^{160} and Ser^{93}, leads to large structural changes in TOMM34 and prevents TOMM34 binding to HSP70 eliminating its inhibitory role on HSP70/HSP40-mediated refolding. Because the mechanism of HSP70/HSP90–regulated precursor protein transport to mitochondria is largely unknown, our data suggest novel testable hypotheses about the role of TOMM34 and 14-3-3 proteins in this process.

Experimental procedures

Cloning and protein preparation

All coding sequences were cloned by Gateway recombination technology (Invitrogen). The full coding sequences of the human *TOMM34* (NM_006809.4), *DNAJB1* (HSP40, NM_006145.2), and human *BAG1* (BAG1s, NM_001172415.1) genes, sequences coding for TOMM34 point mutants (S93A, S160A, S93A/S160A), were cloned into a vector containing an N-terminal His_6-GST tag cleavable by tobacco etch virus protease. The sequences coding for TOMM34 WT and S93A/S160A point mutant were furthermore cloned into a vector containing an N-terminal SBP tag. The full coding sequences of the human *HSPA1A* (HSP70, NM_005345.5) and *HSP90AA1* (HSP90α, NM_001017963.2) genes were cloned into a vector containing an N-terminal His_6 or SBP tag cleavable by tobacco etch virus protease. All cloned genes were expressed in BL21(DE3) RIPL cells and purified as described previously (21). 14-3-3 protein isoforms (β, γ, ϵ, σ, τ, and ζ) were cloned into a vectors containing either N- or C-terminal His_6 tag (see Table S1) and expressed in BL21(DE3) RIPL. Bacteria expressing 14-3-3 proteins were grown in LB medium at 37 °C with an A_{600} of up to 0.5. Induction of gene expression was achieved by adding isopropyl β-D-thiogalactopyranoside to the culture (final concentration, 1 mM). The bacterial culture was grown at 30 °C for another 3-4 h and then pelleted by centrifugation. Next, the cells were resuspended in His-binding buffer (50 mM Hepes, pH 7.6, 0.3 M KCl, 5 mM imidazole, 5% glycerol). Cell suspensions were enriched with lysozyme (1 mg/ml) and phenylmethylsulfonyl fluoride (1 mM) and then sonicated. Bacterial lysates were obtained by centrifugation for 30 min at 12,000 × g. His_6-tagged 14-3-3 proteins were captured on a HisTrap column and eluted with 250 mM imidazole. The eluted fractions were subsequently subjected to buffer exchange into His-binding buffer to remove imidazole. All proteins were finally exchanged into final assay buffers using 7-kDa molecular mass cutoff Zeba spin desalting columns (Thermo Fisher Scientific).

Cell culture, transfection, and treatment

TOMM34$^{-/-}$ MCF-7 cells were cultured in Dulbecco's modified Eagle's medium supplemented with 10% fetal bovine serum and 300 mg/liter L-glutamine in a humidified atmosphere of 5% CO_2 at 37 °C. Transient transfections of cells (grown to 70% confluency on 15-mm-diameter dishes) with the plasmids pCMV-N-HA-TOMM34 WT and pCMV-N-HA-TOMM34-S93A/S160A (10 μg of DNA) were performed by Lipofectamine 3000 according to the manufacturer's manual (Thermo Fisher Scientific). 12 h after transfection, the cells were split to three 15-mm-diameter dishes and cultured for another 6 h before treatment with PMA (0.3 μM), PKA inhibitor H89 (Selleckchem, Munich, Germany, 20 μM), and vehicle control (DMSO) for 12 h. Next, the cells were collected and lysed in 50 mM Hepes, pH 7.5, 150 mM KCl, 2 mM $MgCl_2$, 5 mM NaF, 1% Nonidet P-40 supplemented with proteinase and phosphatase inhibitors mixture (Sigma–Aldrich).

Site-directed mutagenesis

The full-length *TOMM34* coding sequences were mutated to encode desired mutations using QuikChange site-directed mutagenesis kit (Agilent Technologies, Santa Clara, CA, USA) and mutagenic oligonucleotides according to the manufacturer's instructions.

In vitro phosphorylation assay

TOMM34 and all its variants (40 μM) were incubated with PKA (New England Biolabs, Ipswich, MA, USA; 62,500 units/mg TOMM34) and ATP (2 mM) in PKA assay buffer at 30 °C for 24 h. After incubation, the phosphorylation reaction was stopped by exchanging the buffer to 50 mM Hepes, pH 7.5, 150 mM KAc, and 2 mM $MgCl_2$ (HKM buffer).

Analytical size-exclusion chromatography

Separations by SEC were carried out using Superdex 200 Increase 10/300 GL (GE Healthcare) pre-equilibrated with

HKM buffer. 75 μl of phosphorylated/nonphosphorylated TOMM34 proteins (35 μm) preincubated with/without different 14-3-3 isoforms (70 μM) for 30 min at 21 °C was injected and isocratically eluted at 0.3 ml/min. In experiments testing the influence of TOMM34·14-3-3γ complex formation on HSP70 dimers, phosphorylated/nonphosphorylated TOMM34 preincubated with/without 14-3-3γ (30 min, 21 °C) was mixed with HSP70 in the presence of 0.2 mM ATP and incubated for 20 min at 21 °C. The final concentrations of TOMM34, 14-3-3γ, and HSP70 in the protein mixtures were 35, 70, and 35 μM, respectively. Injection volume and flow rate was as described above. From each run, 300-μl fractions corresponding to protein peaks were collected and analyzed using standard or Phostag (Wako Pure Chemical Industries, Osaka, Japan) gel electrophoresis followed by Coomassie staining.

Pulldown assay for biotinylated proteins ex vivo

10 μg of biotinylated 14-3-3 isoforms (EZ-Link™ Thermo Fisher Scientific) per sample were prebound to streptavidin–agarose beads and incubated at 4 °C for 1 h with *TOMM34*$^{-/-}$ MCF-7 cell lysates prepared after cell transfection and treatment as described above. After washing with assay buffer (50 mM Hepes, pH 7.5, 150 mM KCl, 2 mM $MgCl_2$, 5 mM NaF, 1% Nonidet P-40), the bound complexes were eluted by boiling the beads in × loading sample buffer for 10 min and analyzed by SDS-PAGE and Western blotting.

SBP pulldown assays

Before performing pulldown experiments, all proteins were exchanged to HKM buffer. Next, 60 pmol of SBP-tagged HSP70 or HSP90 was incubated with streptavidin–agarose beads at 4 °C for 30 min After washing with assay buffer, 60 pmol of phosphorylated/nonphosphorylated TOMM34 variants (WT or mutant proteins) preincubated with/without 120 pmol of 14-3-3γ (30 min, 21 °C) were added to the beads. Mixtures containing SBP–HSP70 were supplemented with/without 0.2 mM ATP. After 1 h of incubation at 4 °C, the beads were washed with ATP-containing/ATP-free buffers. Finally, the proteins were eluted with 2 mM biotin in assay buffer and analyzed by Coomassie staining or Western blotting.

Antibodies

Monoclonal anti-TOMM34 and anti-HA tag antibodies used in this study were prepared in-house. Monoclonal anti-14-3-3γ was purchased from Santa Cruz Biotechnology (Dallas, TX, USA). For SBP-tagged protein detection, we used peroxidase-conjugated streptavidin (Sigma–Aldrich) diluted in 5% milk in the presence of avidin (10 ng/μl). Avidin was added to prevent streptavidin binding to biotinylated proteins present in the milk. The blots were developed with polyclonal anti-mouse/rabbit IgG secondary antibodies conjugated with horseradish peroxidase (Dako, Santa Clara, CA, USA).

Luciferase refolding assay

Firefly luciferase (50 nM, Promega) incubated with HSP70 (1 μM), HSP40 (2 μM), and BAG1 (0.5 μM) proteins in HKM buffer supplemented with 5 mM DTT, 5 mM ATP was thermally denatured at 42 °C for 30 min in the presence of 5 μM phosphorylated/nonphosphorylated TOMM34 WT or S93A/S160A and increasing concentrations of 14-3-3γ dimer (0.3, 1.25, and 5 μM). The refolding reaction was started by shifting the temperature to 37 °C. At given time points, 2 μl of the reaction were mixed with D-luciferin (100 μM in 100 μl of 50 mM glycylglycine, pH 7.8, 30 mM $MgSO_4$, 4 mM DTT), and the luciferase activity was measured at 21 °C using an Infinite M1000 Pro (Tecan, Männedorf, Switzerland) at emission wavelengths of 560 nm and 500/100 ms settle/integration time. The signal from samples with native luciferase was set as 100%. As negative controls, we measured the luciferase activity of denatured luciferase only.

Peptide binding

Phosphorylated/nonphosphorylated TOMM34 WT, S93A, S160A, and S93A/S160A in various concentrations were titrated against 30 nM fluorescein-labeled C-terminal HSP70 (GGSGSGPTIEEVD) or HSP90 (GDDDTSRMEEVD) peptide in HKM buffer supplemented with 0.01% Tween 20. In titrations containing 14-3-3γ protein, the molar ratio between 14-3-3γ and TOMM34 was 2:1. All reactions were carried out in a total volume of 12 μl in a 384-well black Nunc Plate (Thermo Fisher Scientific). The plate was incubated for 1 h at room temperature with shaking. Fluorescence polarization was measured at 21 °C using an Infinite M1000 Pro (Tecan) with excitation and emission wavelengths of 470 and 520 nm, respectively. The analysis was performed using GraphPad Prism, version 5.03, for Windows (GraphPad Software, San Diego, CA, USA).

Chemical cross-linking

Intact or PKA-phosphorylated TOMM34 WT or S93A/S160A proteins (final concentration, 60 μM) were mixed with 14-3-3γ (final concentration, 120 μM) or buffer in HKM buffer supplemented with 0.4 mM ATP and incubated for 30 min at 21 °C. Next, HSP70 protein (60 μM) preincubated with or without ATP (0.4 mM) for 30 min at 21 °C was added to TOMM34/14-3-3γ samples in 1:1 ratio, and the mixture was incubated for 1 min at 21 °C. Glutaraldehyde was added (final concentration, 1 mM), and the reactions stopped after 10 and 20 min with Tris, pH 8 (final concentration, 80 mM). The samples were diluted 100× in 2× CSB loading buffer, and 5 μl was separated by SDS-PAGE, blotted, and probed with TOMM34, HSP70, and 14-3-3γ antibodies.

MS and hydrogen/deuterium exchange

Native ESI-MS analysis of TOMM34 and 14-3-3γ was performed on proteins alone or mixed in 1:2 molar ratio (TOMM34:14-3-3γ, 10 μM:20 μM). After preincubation in HKM buffer, the proteins were buffer exchanged into 200 mM ammonium acetate, pH 7.5, using Zeba Spin columns (0.5 ml, 7-kDa cutoff). The samples were loaded to homemade quartz tips and electrosprayed to Waters Synapt G2Si. MS settings was a follows: spray voltage, 1.2 kV; trap collision energy, 70 V; sampling cone voltage, 20 V; source offset, 10 V; trap gas, 4 ml/min; and source temperature, 30 °C.

HDX was followed for all TOMM34 variants (WT, S93A, S160A, S93A/S160A) in phosphorylated and nonphosphorylated

state. Nonphosphorylated and phosphorylated WT and phosphorylated mutant forms of TOMM34 were also studied in the presence of 14-3-3γ. Finally, nonphosphorylated and phosphorylated WT and phosphorylated S93A/S160A mutant were analyzed in complex with HSP70 or HSP90 C-terminal peptides or with the peptides and 14-3-3γ. TOMM34 concentration during HDX (initiated by a 5-fold dilution into D_2O based HKM buffer) was 10 μM. 14-3-3γ was used in 2-molar excess and C-terminal peptides in 5-molar excess to TOMM34. Exchange was followed for 20 s, 2 min, 20 min, and 2 h and then quenched by 1:9 dilution into 0.5 M glycine (pH 2.3) and subjected to rapid freezing in liquid nitrogen. Each sample was thawed, online-digested on immobilized pepsin column (66-μl bed volume), desalted, and separated using water–acetonitrile gradient (10–45% B in 7 min) on a setup consisting of a trap cartridge (ACQUITY UPLC BEH C18, 130 Å, 1.7 μM, 2.1 mm × 5 mm, Waters) and an analytical column (ACQUITY UPLC BEH C18, 130 Å, 1.7 μM, 1 mm × 100 mm, Waters). Digestion and desalting by 0.4% formic acid (FA) in water was driven by the 1260 Infinity II quaternary pump (Agilent Technologies) pumping at 100 μl/min and lasted 3 min. Separation was done using the 1290 Infinity II LC system (Agilent Technologies) pumping at 40 μl/min and using the following solvents: A: 0.1% FA, 2% acetonitrile in water; and B: 0.1% FA, 2% water in acetonitrile. All steps were performed at pH 2.5 and 0 °C to minimize back-exchange. The LC system was interfaced to an ESI FT-ICR MS (15T Solarix XR, Bruker Daltonics) operating in positive MS mode. Hydrogen/deuterium data processing used the in-house developed program Deutex as described previously (24, 83). Identification of pepsin generated peptides was achieved by separate LC–MS/MS analyses and database searching (MASCOT, MatrixScience) against a custom database containing sequences of the studied protein forms and proteases. Phosphorylation of Ser and Thr was included as a variable modification. Estimation of the phosphorylation extent on the identified sites via extracted ion chromatograms was done in DataAnalysis 5.0 (Bruker Daltonics).

Data availability

All data are contained within the article and the accompanying supporting information.

Acknowledgments—We thank Dr. P. J. Coates for critical reading of the manuscript.

Author contributions—F. T., P. Muller, and P. Man conceptualization; F. T., M. D., P. V., D. K., and P. Man formal analysis; F. T., M. D., P. V., and D. K. validation; F. T., M. D., P. V., V. V., O. S., D. K., and P. Man investigation; F. T., M. D., P. V., V. V., D. K., and P. Man visualization; F. T., M. D., P. V., V. V., O. S., D. K., P. Muller, and P. Man methodology; F. T. writing-original draft; F. T., M. D., P. V., V. V., O. S., D. K., B. V., P. Muller, and P. Man writing-review and editing; P. V., D. K., and P. Man data curation; P. V., D. K., and P. Man software; V. V. and O. S. resources; B. V., P. Muller, and P. Man supervision; B. V., P. Muller, and P. Man funding acquisition; B. V., P. Muller, and P. Man project administration.

Funding and additional information—This work was mainly supported by Czech Science Foundation Grant 16-20860S. Additional experiments were funded by Czech Science Foundation Grant 19-03796S. Further institutional and instrumental support from the Ministry of Education, Youth and Sports of the Czech Republic through Grant LQ1604, Czech Infrastructure for Integrative Structural Biology (CIISB) through Grant LM2015043, and the European Union through Grant CZ.1.05/1.1.00/02.0109, the Ministry of Health of the Czech Republic Conceptual Development of Research Organization through Grant 00209805 is gratefully acknowledged.

Conflict of interest—The authors declare that they have no conflicts of interest with the contents of this article.

Abbreviations—The abbreviations used are: HSP, heat shock protein; ESI, electrospray ionization; HDX, hydrogen/deuterium exchange; PKA, protein kinase A; SBP, streptavidin-binding peptide; SEC, size-exclusion chromatography; TOM, translocase of outer mitochondrial membrane; TPR, tetratricopeptide repeat; -P, PKA-phosphorylated; PMA, 12-O-tetradecanoylphorbol-13-acetate; FA, formic acid.

References

1. Morán Luengo, T., Mayer, M. P., and Rüdiger, S. G. D. (2019) The Hsp70–Hsp90 chaperone cascade in protein folding. *Trends Cell Biol.* **29,** 164–177 CrossRef Medline
2. Mayer, M. P. (2010) Gymnastics of molecular chaperones. *Mol. Cell* **39,** 321–331 CrossRef Medline
3. Davis, A. K., Pratt, W. B., Lieberman, A. P., and Osawa, Y. (2020) Targeting Hsp70 facilitated protein quality control for treatment of polyglutamine diseases. *Cell. Mol. Life Sci.* **77,** 977–996 CrossRef Medline
4. Morán Luengo, T., Kityk, R., Mayer, M. P., and Rüdiger, S. G. D. (2018) Hsp90 breaks the deadlock of the HSP70 chaperone system. *Mol. Cell* **70,** 545–552.e9 CrossRef Medline
5. Bhangoo, M. K., Tzankov, S., Fan, A. C., Dejgaard, K., Thomas, D. Y., and Young, J. C. (2007) Multiple 40-kDa heat-shock protein chaperones function in Tom70-dependent mitochondrial import. *Mol. Biol. Cell* **18,** 3414–3428 CrossRef Medline
6. Brychzy, A., Rein, T., Winklhofer, K. F., Hartl, F. U., Young, J. C., and Obermann, W. M. (2003) Cofactor Tpr2 combines two TPR domains and a J domain to regulate the Hsp70/Hsp90 chaperone system. *EMBO J.* **22,** 3613–3623 CrossRef Medline
7. Faou, P., and Hoogenraad, N. J. (2012) Tom34: a cytosolic cochaperone of the Hsp90/Hsp70 protein complex involved in mitochondrial protein import. *Biochim. Biophys. Acta* **1823,** 348–357 CrossRef Medline
8. Young, J. C., Hoogenraad, N. J., and Hartl, F. U. (2003) Molecular chaperones Hsp90 and Hsp70 deliver preproteins to the mitochondrial import receptor Tom70. *Cell* **112,** 41–50 CrossRef Medline
9. Wiedemann, N., and Pfanner, N. (2017) Mitochondrial machineries for protein import and assembly. *Annu. Rev. Biochem.* **86,** 685–714 CrossRef Medline
10. Jores, T., Lawatscheck, J., Beke, V., Franz-Wachtel, M., Yunoki, K., Fitzgerald, J. C., Macek, B., Endo, T., Kalbacher, H., Buchner, J., and Rapaport, D. (2018) Cytosolic Hsp70 and Hsp40 chaperones enable the biogenesis of mitochondrial β-barrel proteins. *J. Cell Biol.* **217,** 3091–3108 CrossRef Medline
11. Abe, Y., Shodai, T., Muto, T., Mihara, K., Torii, H., Nishikawa, S., Endo, T., and Kohda, D. (2000) Structural basis of presequence recognition by the mitochondrial protein import receptor Tom20. *Cell* **100,** 551–560 CrossRef Medline
12. Jores, T., Klinger, A., Gross, L. E., Kawano, S., Flinner, N., Duchardt-Ferner, E., Wöhnert, J., Kalbacher, H., Endo, T., Schleiff, E., and Rapaport, D. (2016) Characterization of the targeting signal in mitochondrial β-barrel proteins. *Nat. Commun.* **7,** 12036 CrossRef Medline
13. Moczko, M., Bömer, U., Kübrich, M., Zufall, N., Hönlinger, A., and Pfanner, N. (1997) The intermembrane space domain of mitochondrial Tom22 functions as a trans binding site for preproteins with N-terminal targeting sequences. *Mol. Cell Biol.* **17,** 6574–6584 CrossRef Medline

14. Hill, K., Model, K., Ryan, M. T., Dietmeier, K., Martin, F., Wagner, R., and Pfanner, N. (1998) Tom40 forms the hydrophilic channel of the mitochondrial import pore for preproteins. *Nature* **395,** 516–521 CrossRef Medline
15. Schmidt, O., Harbauer, A. B., Rao, S., Eyrich, B., Zahedi, R. P., Stojanovski, D., Schönfisch, B., Guiard, B., Sickmann, A., Pfanner, N., and Meisinger, C. (2011) Regulation of mitochondrial protein import by cytosolic kinases. *Cell* **144,** 227–239 CrossRef Medline
16. Rao, S., Schmidt, O., Harbauer, A. B., Schönfisch, B., Guiard, B., Pfanner, N., and Meisinger, C. (2012) Biogenesis of the preprotein translocase of the outer mitochondrial membrane: protein kinase A phosphorylates the precursor of Tom40 and impairs its import. *Mol. Biol. Cell* **23,** 1618–1627 CrossRef Medline
17. Gerbeth, C., Schmidt, O., Rao, S., Harbauer, A. B., Mikropoulou, D., Opalińska, M., Guiard, B., Pfanner, N., and Meisinger, C. (2013) Glucose-induced regulation of protein import receptor Tom22 by cytosolic and mitochondria-bound kinases. *Cell Metab.* **18,** 578–587 CrossRef Medline
18. Dagda, R. K., and Das Banerjee, T. (2015) Role of protein kinase A in regulating mitochondrial function and neuronal development: implications to neurodegenerative diseases. *Rev. Neurosci.* **26,** 359–370 CrossRef Medline
19. Scheufler, C., Brinker, A., Bourenkov, G., Pegoraro, S., Moroder, L., Bartunik, H., Hartl, F. U., and Moarefi, I. (2000) Structure of TPR domain–peptide complexes: critical elements in the assembly of the Hsp70–Hsp90 multichaperone machine. *Cell* **101,** 199–210 CrossRef Medline
20. Brinker, A., Scheufler, C., Von Der Mulbe, F., Fleckenstein, B., Herrmann, C., Jung, G., Moarefi, I., and Hartl, F. U. (2002) Ligand discrimination by TPR domains: relevance and selectivity of EEVD-recognition in Hsp70·Hop·Hsp90 complexes. *J. Biol. Chem.* **277,** 19265–19275 CrossRef Medline
21. Durech, M., Trcka, F., Man, P., Blackburn, E. A., Hernychova, L., Dvorakova, P., Coufalova, D., Kavan, D., Vojtesek, B., and Muller, P. (2016) Novel entropically driven conformation-specific interactions with Tomm34 protein modulate Hsp70 protein folding and ATPase activities. *Mol. Cell. Proteomics* **15,** 1710–1727 CrossRef Medline
22. Lee, C. T., Graf, C., Mayer, F. J., Richter, S. M., and Mayer, M. P. (2012) Dynamics of the regulation of Hsp90 by the co-chaperone Sti1. *EMBO J.* **31,** 1518–1528 CrossRef Medline
23. Trcka, F., Durech, M., Man, P., Hernychova, L., Muller, P., and Vojtesek, B. (2014) The assembly and intermolecular properties of the Hsp70–Tomm34–Hsp90 molecular chaperone complex. *J. Biol. Chem.* **289,** 9887–9901 CrossRef Medline
24. Trcka, F., Durech, M., Vankova, P., Chmelik, J., Martinkova, V., Hausner, J., Kadek, A., Marcoux, J., Klumpler, T., Vojtesek, B., Muller, P., and Man, P. (2019) Human stress-inducible Hsp70 has a high propensity to form ATP-dependent antiparallel dimers that are differentially regulated by cochaperone binding. *Mol. Cell. Proteomics* **18,** 320–337 CrossRef Medline
25. Park, J. H., Jang, H. R., Lee, I. Y., Oh, H. K., Choi, E. J., Rhim, H., and Kang, S. (2017) Amyotrophic lateral sclerosis-related mutant superoxide dismutase 1 aggregates inhibit 14-3-3–mediated cell survival by sequestration into the JUNQ compartment. *Hum. Mol. Genet.* **26,** 3615–3629 CrossRef Medline
26. Hachiya, N., Alam, R., Sakasegawa, Y., Sakaguchi, M., Mihara, K., and Omura, T. (1993) A mitochondrial import factor purified from rat liver cytosol is an ATP-dependent conformational modulator for precursor proteins. *EMBO J.* **12,** 1579–1586 CrossRef Medline
27. Hachiya, N., Komiya, T., Alam, R., Iwahashi, J., Sakaguchi, M., Omura, T., and Mihara, K. (1994) MSF, a novel cytoplasmic chaperone which functions in precursor targeting to mitochondria. *EMBO J.* **13,** 5146–5154 CrossRef Medline
28. Hachiya, N., Mihara, K., Suda, K., Horst, M., Schatz, G., and Lithgow, T. (1995) Reconstitution of the initial steps of mitochondrial protein import. *Nature* **376,** 705–709 CrossRef Medline
29. Komiya, T., Hachiya, N., Sakaguchi, M., Omura, T., and Mihara, K. (1994) Recognition of mitochondria-targeting signals by a cytosolic import stimulation factor, MSF. *J. Biol. Chem.* **269,** 30893–30897 Medline
30. Komiya, T., and Mihara, K. (1996) Protein import into mammalian mitochondria: characterization of the intermediates along the import pathway of the precursor into the matrix. *J. Biol. Chem.* **271,** 22105–22110 CrossRef Medline
31. Komiya, T., Sakaguchi, M., and Mihara, K. (1996) Cytoplasmic chaperones determine the targeting pathway of precursor proteins to mitochondria. *EMBO J.* **15,** 399–407 CrossRef Medline
32. Gardino, A. K., Smerdon, S. J., and Yaffe, M. B. (2006) Structural determinants of 14-3-3 binding specificities and regulation of subcellular localization of 14-3-3–ligand complexes: a comparison of the X-ray crystal structures of all human 14-3-3 isoforms. *Semin. Cancer Biol.* **16,** 173–182 CrossRef Medline
33. Yaffe, M. B., Rittinger, K., Volinia, S., Caron, P. R., Aitken, A., Leffers, H., Gamblin, S. J., Smerdon, S. J., and Cantley, L. C. (1997) The structural basis for 14-3-3:phosphopeptide binding specificity. *Cell* **91,** 961–971 CrossRef Medline
34. Alblova, M., Smidova, A., Docekal, V., Vesely, J., Herman, P., Obsilova, V., and Obsil, T. (2017) Molecular basis of the 14-3-3 protein-dependent activation of yeast neutral trehalase Nth1. *Proc. Natl. Acad. Sci. U.S.A.* **114,** E9811–E9820 CrossRef Medline
35. Ottmann, C., Marco, S., Jaspert, N., Marcon, C., Schauer, N., Weyand, M., Vandermeeren, C., Duby, G., Boutry, M., Wittinghofer, A., Rigaud, J. L., and Oecking, C. (2007) Structure of a 14-3-3 coordinated hexamer of the plant plasma membrane H^+-ATPase by combining X-ray crystallography and electron cryomicroscopy. *Mol. Cell* **25,** 427–440 CrossRef Medline
36. Bustos, D. M., and Iglesias, A. A. (2006) Intrinsic disorder is a key characteristic in partners that bind 14-3-3 proteins. *Proteins* **63,** 35–42 CrossRef Medline
37. Silhan, J., Vacha, P., Strnadova, P., Vecer, J., Herman, P., Sulc, M., Teisinger, J., Obsilova, V., and Obsil, T. (2009) 14-3-3 protein masks the DNA binding interface of forkhead transcription factor FOXO4. *J. Biol. Chem.* **284,** 19349–19360 CrossRef Medline
38. Rezabkova, L., Man, P., Novak, P., Herman, P., Vecer, J., Obsilova, V., and Obsil, T. (2011) Structural basis for the 14-3-3 protein-dependent inhibition of the regulator of G protein signaling 3 (RGS3) function. *J. Biol. Chem.* **286,** 43527–43536 CrossRef Medline
39. Blom, N., Gammeltoft, S., and Brunak, S. (1999) Sequence and structure-based prediction of eukaryotic protein phosphorylation sites. *J. Mol. Biol.* **294,** 1351–1362 CrossRef Medline
40. Hornbeck, P. V., Zhang, B., Murray, B., Kornhauser, J. M., Latham, V., and Skrzypek, E. (2015) PhosphoSitePlus, 2014: mutations, PTMs and recalibrations. *Nucleic Acids Res* **43,** D512–D520 CrossRef Medline
41. Hennrich, M. L., Marino, F., Groenewold, V., Kops, G. J., Mohammed, S., and Heck, A. J. (2013) Universal quantitative kinase assay based on diagonal SCX chromatography and stable isotope dimethyl labeling provides high-definition kinase consensus motifs for PKA and human Mps1. *J. Proteome Res.* **12,** 2214–2224 CrossRef Medline
42. Madeira, F., Tinti, M., Murugesan, G., Berrett, E., Stafford, M., Toth, R., Cole, C., MacKintosh, C., and Barton, G. J. (2015) 14-3-3-Pred: improved methods to predict 14-3-3-binding phosphopeptides. *Bioinformatics* **31,** 2276–2283 CrossRef Medline
43. Ishida, T., and Kinoshita, K. (2007) PrDOS: prediction of disordered protein regions from amino acid sequence. *Nucleic Acids Res* **35,** W460–W464 CrossRef Medline
44. Uhart, M., and Bustos, D. M. (2014) Protein intrinsic disorder and network connectivity: the case of 14-3-3 proteins. *Front. Genet.* **5,** 10 CrossRef Medline
45. Kinoshita, E., Kinoshita-Kikuta, E., Takiyama, K., and Koike, T. (2006) Phosphate-binding tag, a new tool to visualize phosphorylated proteins. *Mol. Cell. Proteomics* **5,** 749–757 CrossRef Medline
46. Sluchanko, N. N., and Gusev, N. B. (2012) Oligomeric structure of 14-3-3 protein: what do we know about monomers?. *FEBS Lett.* **586,** 4249–4256 CrossRef Medline
47. Oganesyan, I., Lento, C., and Wilson, D. J. (2018) Contemporary hydrogen deuterium exchange mass spectrometry. *Methods* **144,** 27–42 CrossRef Medline
48. Yang, X., Lee, W. H., Sobott, F., Papagrigoriou, E., Robinson, C. V., Grossmann, J. G., Sundström, M., Doyle, D. A., and Elkins, J. M. (2006) Structural basis for protein–protein interactions in the 14-3-3 protein family. *Proc. Natl. Acad. Sci. U.S.A.* **103,** 17237–17242 CrossRef Medline

49. Kacirova, M., Kosek, D., Kadek, A., Man, P., Vecer, J., Herman, P., Obsilova, V., and Obsil, T. (2015) Structural characterization of phosducin and its complex with the 14-3-3 protein. *J. Biol. Chem.* **290,** 16246–16260 CrossRef Medline
50. Xu, Y., Ren, J., He, X., Chen, H., Wei, T., and Feng, W. (2019) YWHA/14-3-3 proteins recognize phosphorylated TFEB by a noncanonical mode for controlling TFEB cytoplasmic localization. *Autophagy* **15,** 1017–1030 CrossRef Medline
51. Macakova, E., Kopecka, M., Kukacka, Z., Veisova, D., Novak, P., Man, P., Obsil, T., and Obsilova, V. (2013) Structural basis of the 14-3-3 protein-dependent activation of yeast neutral trehalase Nth1. *Biochim. Biophys. Acta* **1830,** 4491–4499 CrossRef Medline
52. Muller, P., Coates, P. J., Nenutil, R., Trcka, F., Hrstka, R., Chovanec, J., Brychtova, V., and Vojtesek, B. (2019) Tomm34 is commonly expressed in epithelial ovarian cancer and associates with tumour type and high FIGO stage. *J. Ovarian Res.* **12,** 30 CrossRef Medline
53. Baillie, G., MacKenzie, S. J., and Houslay, M. D. (2001) Phorbol 12-myristate 13-acetate triggers the protein kinase A–mediated phosphorylation and activation of the PDE4D5 cAMP phosphodiesterase in human aortic smooth muscle cells through a route involving extracellular signal regulated kinase (ERK). *Mol. Pharmacol.* **60,** 1100–1111 CrossRef Medline
54. Wu, J., Li, J., Huang, K. P., and Huang, F. L. (2002) Attenuation of protein kinase C and cAMP-dependent protein kinase signal transduction in the neurogranin knockout mouse. *J. Biol. Chem.* **277,** 19498–19505 CrossRef Medline
55. Tai, T. C., and Wong, D. L. (2003) Protein kinase A and protein kinase C signaling pathway interaction in phenylethanolamine *N*-methyltransferase gene regulation. *J. Neurochem.* **85,** 816–829 CrossRef Medline
56. Søberg, K., Moen, L. V., Skålhegg, B. S., and Laerdahl, J. K. (2017) Evolution of the cAMP-dependent protein kinase (PKA) catalytic subunit isoforms. *PLoS One* **12,** e0181091 CrossRef Medline
57. Limbutara, K., Kelleher, A., Yang, C. R., Raghuram, V., and Knepper, M. A. (2019) Phosphorylation changes in response to kinase inhibitor H89 in PKA-null cells. *Sci. Rep.* **9,** 2814 CrossRef Medline
58. García-Bermúdez, J., Sánchez-Aragó, M., Soldevilla, B., Del Arco, A., Nuevo-Tapioles, C., and Cuezva, J. M. (2015) PKA phosphorylates the ATPase inhibitory factor 1 and inactivates its capacity to bind and inhibit the mitochondrial H^+-ATP synthase. *Cell Rep.* **12,** 2143–2155 CrossRef Medline
59. Kumar, A., Gopalswamy, M., Wolf, A., Brockwell, D. J., Hatzfeld, M., and Balbach, J. (2018) Phosphorylation-induced unfolding regulates p19 (INK4d) during the human cell cycle. *Proc. Natl. Acad. Sci. U.S.A.* **115,** 3344–3349 CrossRef Medline
60. Muller, P., Ruckova, E., Halada, P., Coates, P. J., Hrstka, R., Lane, D. P., and Vojtesek, B. (2013) C-terminal phosphorylation of Hsp70 and Hsp90 regulates alternate binding to co-chaperones CHIP and HOP to determine cellular protein folding/degradation balances. *Oncogene* **32,** 3101–3110 CrossRef Medline
61. Assimon, V. A., Southworth, D. R., and Gestwicki, J. E. (2015) Specific binding of tetratricopeptide repeat proteins to heat shock protein 70 (Hsp70) and heat shock protein 90 (Hsp90) is regulated by affinity and phosphorylation. *Biochemistry* **54,** 7120–7131 CrossRef Medline
62. Aprile, F. A., Dhulesia, A., Stengel, F., Roodveldt, C., Benesch, J. L., Tortora, P., Robinson, C. V., Salvatella, X., Dobson, C. M., and Cremades, N. (2013) Hsp70 oligomerization is mediated by an interaction between the interdomain linker and the substrate-binding domain. *PLoS One* **8,** e67961 CrossRef Medline
63. Muslin, A. J., Tanner, J. W., Allen, P. M., and Shaw, A. S. (1996) Interaction of 14-3-3 with signaling proteins is mediated by the recognition of phosphoserine. *Cell* **84,** 889–897 CrossRef Medline
64. Oldfield, C. J., Meng, J., Yang, J. Y., Yang, M. Q., Uversky, V. N., and Dunker, A. K. (2008) Flexible nets: disorder and induced fit in the associations of p53 and 14-3-3 with their partners. *BMC Genomics* **9,** S1 CrossRef Medline
65. Johnson, C., Crowther, S., Stafford, M. J., Campbell, D. G., Toth, R., and MacKintosh, C. (2010) Bioinformatic and experimental survey of 14-3-3-binding sites. *Biochem. J.* **427,** 69–78 CrossRef Medline
66. Yaffe, M. B. (2002) How do 14-3-3 proteins work?: Gatekeeper phosphorylation and the molecular anvil hypothesis. *FEBS Lett.* **513,** 53–57 CrossRef Medline
67. Masone, D., Uhart, M., and Bustos, D. M. (2017) On the role of residue phosphorylation in 14-3-3 partners: AANAT as a case study. *Sci. Rep.* **7,** 46114 CrossRef Medline
68. Molzan, M., and Ottmann, C. (2012) Synergistic binding of the phosphorylated S233- and S259-binding sites of C-RAF to one 14-3-3ζ dimer. *J. Mol. Biol.* **423,** 486–495 CrossRef Medline
69. Obsil, T., Ghirlando, R., Anderson, D. E., Hickman, A. B., and Dyda, F. (2003) Two 14-3-3 binding motifs are required for stable association of Forkhead transcription factor FOXO4 with 14-3-3 proteins and inhibition of DNA binding. *Biochemistry* **42,** 15264–15272 CrossRef Medline
70. Kostelecky, B., Saurin, A. T., Purkiss, A., Parker, P. J., and McDonald, N. Q. (2009) Recognition of an intra-chain tandem 14-3-3 binding site within PKCϵ. *EMBO Rep.* **10,** 983–989 CrossRef Medline
71. Bhaskara, R. M., de Brevern, A. G., and Srinivasan, N. (2013) Understanding the role of domain-domain linkers in the spatial orientation of domains in multi-domain proteins. *J. Biomol. Struct. Dynamics* **31,** 1467–1480 CrossRef
72. Ottmann, C., Yasmin, L., Weyand, M., Veesenmeyer, J. L., Diaz, M. H., Palmer, R. H., Francis, M. S., Hauser, A. R., Wittinghofer, A., and Hallberg, B. (2007) Phosphorylation-independent interaction between 14-3-3 and exoenzyme S: from structure to pathogenesis. *EMBO J.* **26,** 902–913 CrossRef Medline
73. Ito, T., Nakata, M., Fukazawa, J., Ishida, S., and Takahashi, Y. (2014) Phosphorylation-independent binding of 14-3-3 to NtCDPK1 by a new mode. *Plant Signal. Behavior* **9,** e977721 CrossRef
74. Blesa, J. R., Prieto-Ruiz, J. A., Abraham, B. A., Harrison, B. L., Hegde, A. A., and Hernández-Yago, J., *et al* (2008) NRF-1 is the major transcription factor regulating the expression of the human TOMM34 gene. *Biochem. Cell Biol.* **86,** 46–56 CrossRef Medline
75. Scarpulla, R. C. (2011) Metabolic control of mitochondrial biogenesis through the PGC-1 family regulatory network. *Biochim. Biophys. Acta* **1813,** 1269–1278 CrossRef Medline
76. Blesa, J. R., Prieto-Ruiz, J. A., Hernández, J. M., and Hernández-Yago, J. (2007) NRF-2 transcription factor is required for human TOMM20 gene expression. *Gene* **391,** 198–208 CrossRef Medline
77. Blesa, J. R., Hernández, J. M., and Hernández-Yago, J. (2004) NRF-2 transcription factor is essential in promoting human Tomm70 gene expression. *Mitochondrion* **3,** 251–259 CrossRef Medline
78. Brix, J., Rüdiger, S., Bukau, B., Schneider-Mergener, J., and Pfanner, N. (1999) Distribution of binding sequences for the mitochondrial import receptors Tom20, Tom22, and Tom70 in a presequence-carrying preprotein and a non-cleavable preprotein. *J. Biol. Chem.* **274,** 16522–16530 CrossRef Medline
79. Chewawiwat, N., Yano, M., Terada, K., Hoogenraad, N. J., and Mori, M. (1999) Characterization of the novel mitochondrial protein import component, Tom34, in mammalian cells. *J. Biochem.* **125,** 721–727 CrossRef Medline
80. Wang, L., Sunahara, R. K., Krumins, A., Perkins, G., Crochiere, M. L., Mackey, M., Bell, S., Ellisman, M. H., and Taylor, S. S. (2001) Cloning and mitochondrial localization of full-length D-AKAP2, a protein kinase A anchoring protein. *Proc. Natl. Acad. Sci. U.S.A.* **98,** 3220–3225 CrossRef Medline
81. Cardone, L., de Cristofaro, T., Affaitati, A., Garbi, C., Ginsberg, M. D., Saviano, M., Varrone, S., Rubin, C. S., Gottesman, M. E., Avvedimento, E. V., and Feliciello, A. (2002) A-kinase anchor protein 84/121 are targeted to mitochondria and mitotic spindles by overlapping amino-terminal motifs. *J. Mol. Biol.* **320,** 663–675 CrossRef Medline
82. Affaitati, A., Cardone, L., de Cristofaro, T., Carlucci, A., Ginsberg, M. D., Varrone, S., Gottesman, M. E., Avvedimento, E. V., and Feliciello, A. (2003) Essential role of A-kinase anchor protein 121 for cAMP signaling to mitochondria. *J. Biol. Chem.* **278,** 4286–4294 CrossRef Medline
83. Kavan, D., and Man, P. (2011) MSTools: web based application for visualization and presentation of HXMS data. *Int. J. Mass Spectrometry* **302,** 53–58 CrossRef

Publikace IV

Vaňková, P., Salido, E., Timson, D. J., Man, P. & Pey, A. L.

A Dynamic Core in Human NQO1 Controls the Functional and Stability Effects of Ligand Binding and Their Communication across the Enzyme Dimer.

Biomolecules **9**, 1–17 (2019)

Můj příspěvěk k práci: *návrh experimentů, provedení ESI-MS, nESI-MS a HDX-MS s interpretací dat, příprava manuskriptu*

biomolecules

MDPI

Article

A Dynamic Core in Human NQO1 Controls the Functional and Stability Effects of Ligand Binding and Their Communication across the Enzyme Dimer

Pavla Vankova [1,2], Eduardo Salido [3], David J. Timson [4], Petr Man [1,*] and Angel L. Pey [5,*]

[1] Institute of Microbiology, Academy of Sciences of the Czech Republic, Videnska 1083, 142 20 Prague 4, Czech Republic. pavla.vankova@biomed.cas.cz
[2] Department of Biochemistry, Faculty of Science, Charles University, Hlavova 2030/8, 128 43 Prague 2, Czech Republic
[3] Center for Rare Diseases (CIBERER), Hospital Universitario de Canarias, Universidad de La Laguna, 38320 Tenerife, Spain; edsalido@gmail.com
[4] School of Pharmacy and Biomolecular Sciences, University of Brighton, Huxley Building, Lewes Road, Brighton BN2 4GJ, UK; D.Timson@brighton.ac.uk
[5] Department of Physical Chemistry and Unit of Excellence in Chemistry, University of Granada, Av. Fuentenueva s/n, E-18071 Granada, Spain
* Correspondence: pman@biomed.cas.cz (P.M.); angelpey@ugr.es (A.L.P.)

Received: 23 October 2019; Accepted: 10 November 2019; Published: 12 November 2019

Abstract: Human NAD(P)H:quinone oxidoreductase 1 (NQO1) is a multi-functional protein whose alteration is associated with cancer, Parkinson's and Alzheimer´s diseases. NQO1 displays a remarkable functional chemistry, capable of binding different functional ligands that modulate its activity, stability and interaction with proteins and nucleic acids. Our understanding of this functional chemistry is limited by the difficulty of obtaining structural and dynamic information on many of these states. Herein, we have used hydrogen/deuterium exchange monitored by mass spectrometry (HDXMS) to investigate the structural dynamics of NQO1 in three ligation states: without ligands ($NQO1_{apo}$), with FAD ($NQO1_{holo}$) and with FAD and the inhibitor dicoumarol ($NQO1_{dic}$). We show that $NQO1_{apo}$ has a minimally stable folded core holding the protein dimer, with FAD and dicoumarol binding sites populating binding non-competent conformations. Binding of FAD significantly decreases protein dynamics and stabilizes the FAD and dicoumarol binding sites as well as the monomer:monomer interface. Dicoumarol binding further stabilizes all three functional sites, a result not previously anticipated by available crystallographic models. Our work provides an experimental perspective into the communication of stability effects through the NQO1 dimer, which is valuable for understanding at the molecular level the effects of disease-associated variants, post-translational modifications and ligand binding cooperativity in NQO1.

Keywords: protein structural dynamics; NQO1; ligand binding; protein stability; allostery; protein degradation

1. Introduction

Human NAD(P)H:quinone oxidoreductase 1 (NQO1; EC 1.6.5.2) is a multifunctional stress protein mostly localized in the cellular cytosol [1]. NQO1 expression is upregulated as a response to different types of cellular stress and through several mechanisms, including the antioxidant response through Nrf2-mediated and Ah2 signaling pathways [1–4].

NQO1 displays multiple enzymatic and non-enzymatic functions [1–5]. NQO1 catalyzes different reactions with cytoprotective and metabolic roles, such as the two-electron reduction of quinones to form hydroquinones [2,6] (Figure 1), redox cycling of quinones [2], reduction of coenzyme Q_{10} and vitamin E to their antioxidant form [2], scavenging reactive oxygen species [1–3,7], reduction of catecholamines and vitamin K [1,2] and maintenance of the NADH/NAD^+ redox balance [3,8]. The main features of these biochemical reactions involving NQO1 have been investigated in detail mainly through enzymological and structural analyses. Structurally, the enzyme forms obligate functional homodimers, with two active sites located in the monomer:monomer interface (MMI), and each monomer consists of two different domains: i) an N-terminal domain spanning residues 1–224 that contains part of the active site and is involved in the tight binding of one FAD molecule per monomer and protein dimerization; ii) a C-terminal domain (residues 225–274) that contributes to stabilizing the protein dimer and to the binding of the NAD(P)H coenzyme and the substrates [1,4,9–14]. The functional cycle of NQO1 generally involves two steps according to a *ping-pong* mechanism: first, in the reductive half-reaction, an NAD(P)H molecule binds to the enzyme and rapidly reduces the FAD to $FADH_2$ (with a second-order rate constant of ~10^6 $M^{-1}{\cdot}s^{-1}$) with the subsequent release of the oxidized nicotinamide dinucleotide; and second, in a very fast oxidative half-reaction (with a second-order rate constant >10^9 $M^{-1}{\cdot}s^{-1}$), the substrate binds and is reduced by the $FADH_2$, thus regenerating the flavin in oxidized form and releasing the reduced product [1,10]. This catalytic cycle is known to be inhibited by different coumarin-based molecules (the best characterized is the biscoumarin, dicoumarol) that act as competitive inhibitors by blocking the NAD(P)H access to the active site and partially occupying the NAD(P)H binding site [1,15]. Importantly, comparison of the crystal structures of NQO1 with FAD bound ($NQO1_{holo}$) with that containing also dicoumarol bound ($NQO1_{dic}$) have revealed that inhibitor binding causes only minor structural rearrangements in the conformation, which localize at the surface of the catalytic site [15]. Among non-enzymatic functions, we must highlight the ability of NQO1 to develop protein: protein and protein: RNA interactions [1,2,16–20]. In particular, protein:protein interactions involving NQO1 are relevant to understand its multiple roles in physiological and pathological processes. NQO1 interacts with key transcription factors associated with cancer (e.g., p53, p73α and HIF-1α) [17,18] and proteins involved in HIV infection (e.g., Tat protein) [19], and these interactions increase the intracellular stability of these protein partners by preventing their degradation by the proteasome. These protein:protein interactions presumably depend on the functional state of NQO1: binding of NADH may increase the strength of these interactions, while dicoumarol binding has the opposite effect [9,17,19]. In addition, $NQO1_{holo}$ binds to the 20S particle of the proteasome and inhibits its proteolytic activity, while FAD withdrawal (i.e., $NQO1_{apo}$) renders NQO1 susceptible to degradation by this mechanism [16].

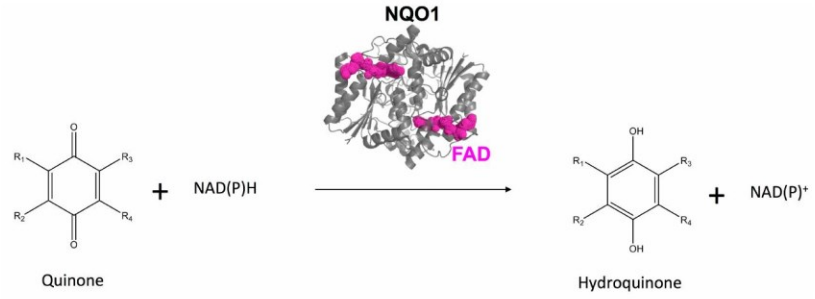

Figure 1. NQO1 catalyzes the two-electron reduction of a wide range of quinones. This enzyme also reduces other organic and inorganic species, such as superoxide radicals and iron(III) ions.

Alterations in NQO1 stability and function are associated to different extents with a variety of human diseases, including cancer, neurological disorders (such as Parkinson´s and Alzheimer´s diseases, multiple sclerosis and schizophrenia) and cardiovascular diseases [1,21]. In these cases, either the wild-type (WT) NQO1 protein and/or a common polymorphic variant (rs1800566, causing

a Pro187Ser amino acid exchange) have been found to be associated with increased disease predisposition. The Pro187Ser variant decreases NQO1 activity due to a large defect in FAD binding (10- to 40-fold lower affinity than that of WT) and in conformational stability, leading to its rapid intracellular degradation by the proteasome [1,10,14,16,22–25]. In general, reduced NQO1 activity or protein levels are commonly observed under these pathological conditions [1,26], although for the particular case of cancer, overexpression of NQO1 is also associated with cancer progression, which makes pharmacological inhibition of NQO1 (e.g., by dicoumarol or related compounds) a potential therapeutic strategy to treat this disease if it selectively targets cancer cells [27–29]. Linked to some of these pathological conditions, the intracellular stability of NQO1 WT is controlled by the population of the $NQO1_{apo}$ state, which is efficiently targeted to the ubiquitin-dependent proteasomal degradation pathway [14,25,30]. Recent works also demonstrated that alterations in the phosphorylation pattern of NQO1 WT at different sites might be associated with these pathological states, likely through effects on the FAD binding affinity and consequently on the intracellular stability of NQO1 WT [26,30,31].

NQO1 is an excellent model to decipher the role of protein dynamics in the function and stability of flavin-dependent enzymes, the role of ligand binding in disease-associated protein stability, and the molecular mechanisms by which mutations cause loss-of-function genetic diseases [1,5,9,10,14,25,30–34]. FAD binding to NQO1 WT triggers a large conformational change, which can be observed by some biophysical techniques (circular dichroism, infrared and NMR spectroscopies or small-angle X-ray scattering), and increases the kinetic stability of the protein dimer, although high-resolution structural information is only available for the $NQO1_{holo}$ state [9–11,14,22,34,35]. This structural change is accompanied by significant changes in overall protein flexibility (evidence provided by proteolysis experiments and structure-based analyses of FAD binding energetics) [10,14,34], presumably linked to the fast degradation of $NQO1_{apo}$ vs. $NQO1_{holo}$ in the cell [14,25], although no high-resolution experimental information on these dynamic changes is available [14]. Regarding dicoumarol binding, the comparison of the X-ray crystallographic structures of $NQO1_{holo}$ and $NQO1_{dic}$ has revealed only local changes in protein structure at the active site [15], and thus, this did not provide details on the remarkable stabilizing effect of dicoumarol binding on the overall conformational stability and the dynamics of the C-terminal domain [14]. A critical role of protein dynamics in the mechanisms causing alterations in NQO1 function due to the Pro187Ser polymorphism and other rare cancer-associated mutations, phosphorylation at specific sites as well as the effect of suppressor mutations of the Pro187Ser phenotype have been put forward from experimental and computational studies [5,9,10,14,30–34,36]. Thus, they also await high-resolution information on the changes in protein dynamics due to these site-specific changes in different ligation states ($NQO1_{apo}$, $NQO1_{holo}$ and $NQO1_{dic}$).

We report herein a detailed experimental analysis on the structural dynamics of human NQO1 in three functionally relevant ligation states ($NQO1_{apo}$, $NQO1_{holo}$ and $NQO1_{dic}$). Our results uncover the existence of a dynamic network within the NQO1 dimer that readily responds to the binding of functional ligands and help to explain their effects on NQO1 function and stability *in vitro* and *in vivo*. Our work also provides an experimental benchmark to understand the allosteric effects of disease-associated variants, post-translational modifications and ligand binding in NQO1.

2. Materials and Methods

2.1. Protein Expression and Purification

Protein expression and purification was carried out as described [30]. *E. coli* BL21(DE3) cells were transformed with pET46 Ek/LIC vector containing the cDNA of human WT NQO1 [22] and grown for 16 h in LBA medium (LB containing 0.1 $mg \cdot ml^{-1}$ ampicillin at 37 °C). This culture was diluted 40-fold in fresh LBA and grown at 37 °C for 3 h. Expression was then triggered by the addition of IPTG (isopropyl β-D-1-thiogalactopyranoside) at a final concentration of 0.5 mM. Induced cells were incubated for 6 h at 25 °C, harvested by centrifugation, washed with binding buffer (BB, 20 mM sodium phosphate, 300 mM NaCl and 50 mM imidazole at pH 7.4) and frozen overnight at −80 °C.

Then, cells were thawed and resuspended in BB containing 1 mM PMSF (phenylmethylsulfonyl fluoride) and lysed by sonication. Crude extracts were clarified by centrifugation (20 min at 20,000× g and 4 °C), and supernatants were loaded into immobilized metal affinity chromatography (IMAC) columns (GE Healthcare) equilibrated in BB. Columns were washed with BB, and the protein was eluted with elution buffer (BB containing 500 mM imidazole). The eluate was exchanged to 50 mM K-HEPES (2-[4-(2-hydroxyethyl)piperazin-1-yl]ethanesulfonic acid, potassium salt) pH 7.4 using PD-10 columns (GE Healthcare), centrifuged for 30 min at 20,000× *g* and 4 °C, and the UV–visible spectra of the supernatants were registered in a HP8453 UV–Visible spectrophotomer (Agilent). This purified holo-protein containing high levels of FAD bound (70%–80% based on the absorbance ratio at 450 nm and 280 nm; see also [30,33,36]) was stored at −80 °C upon flash freezing in liquid N_2. Further purification of the NQO1 dimer was carried out by size-exclusion chromatography using a HiLoad® 16/600 Superdex® 200 prep grade (GE Healthcare) and using 20 mM K-HEPES 200 mM NaCl at pH 7.4 as the mobile phase. This purified protein was subsequently used to obtain apo-protein upon treatment with BB containing 2 M urea and 2 M KBr, 1 mM DTT (1,4-dithiothreitol) and 1 mM PMSF at 4 °C, and separation of the apo-protein and the FAD released was carried out by IMAC at 4 °C. Apo-proteins were finally exchanged to 50 mM K-HEPES at pH 7.4 using PD-10 columns at 4 °C, concentrated using VIVASPIN 6 30,000 MWCO PES devices (Sartorius) and stored at −80 °C after flash freezing in liquid N_2. The purity and integrity of the holo- and apo-protein was checked by polyacrylamide gel electrophoresis in the presence of sodium dodecylsulphate (SDS-PAGE; Figure S1). The holo-protein was also found to display enzyme kinetic parameters (Figure S1) consistent with those previously reported using the same protein construct and purification procedure [9,22].

Purified proteins were also verified by mass spectrometry. The intact mass was analyzed through direct infusion on ESI-FT-ICR MS (Figure S2), showing that the protein was expressed intact and lacking the N-terminal Met. The dimeric state of $NQO1_{apo}$ and $NQO1_{holo}$ was verified by native ESI-MS (Figure S3).

2.2. Hydrogen/Deuterium Exchange Mass Spectrometry (HDXMS

Amide hydrogen/deuterium exchange (HDX) of NQO1 was followed for its apo ($NQO1_{apo}$) and holo ($NQO1_{holo}$) forms, and the holo form was also analyzed in the presence of dicoumarol ($NQO1_{dic}$). Prior to the exchange, the $NQO1_{holo}$ and $NQO1_{dic}$ at 20 μM concentration were pre-incubated with 10 molar excess of FAD for 5 min. $NQO1_{dic}$ was then further mixed with 10 molar excess of dicoumarol and incubated for another 5 min. The exchange reaction was initiated by a 10-fold dilution into a D_2O-based 50 mM K-HEPES, pD 7.4, 1 mM TCEP (tris(2-carboxyethyl)phosphine). The exchange was thus followed at 2 μM protein concentration. Deuterium labelling was quenched by 0.5 M Glycine-HCl, pH 2.3, which was added at 1:1 ratio. The samples were then frozen in liquid N_2. Exchange was followed for 10 s, 30 s, 2 min, 5 min, 20 min, 1 h and 3 h, where 10 s, 5 min and 3 h samples were done in replicate. Each sample was quickly thawed and injected into a cooled LC system. Here, the protein was digested on custom-made nepenthesin-2 (Nep-2) and pepsin columns coupled in tandem (each having a bed volume of 66 μL), and the resulting peptides were trapped on a VanGuard Pre-column (ACQUITY UPLC BEH C18, 130Å, 1.7 μm, 2.1 mm × 5 mm, Waters, Milford, MA,USA), where they were desalted. The solvent used for digestion and desalting (0.4% formic acid (FA) in water) was pumped by a 1260 Infinity II Quaternary pump (Agilent Technologies, Waldbronn, Germany) at a flow rate of 200 $\mu L \cdot min^{-1}$. After three minutes of digestion and desalting, the peptides were separated on an analytical column (ACQUITY UPLC BEH C18, 130 Å, 1.7 μm, 1 mm × 100 mm, Waters, Milford, MA, USA) using linear gradient (5%–45% B in 7 min) followed by a quick step to 99% B lasting 5 min. Solvent A was 0.1% FA/2% acetonitrile (ACN) in water, B was 0.1% FA/98% ACN in water. The gradient was delivered by the 1290 Infinity II LC System (Agilent Technologies, Waldbronn, Germany) at a flow of 40 $\mu L \cdot min^{-1}$. Digestion, desalting and separation were done at 0 °C and pH 2.3 to minimize deuterium loss. The LC system was connected directly to an electrospray ionization source of a 15T FT-ICR mass spectrometer (solarix XR, Bruker Daltonics, Bremen, Germany) operating in broad-band MS mode. Data were peak-picked and exported using DataAnalysis v. 5.0 (Bruker Daltonics, Bremen, Germany) and then processed by the in-house developed program

Deutex (unpublished). Peptides arising from the digestion were identified through separate data-dependent LC-MS/MS analyses (using the same setup as described above) and database searching by the MASCOT algorithm v. 2.4 (Matrix Science, London, United Kingdom) against a custom-build database containing sequences of pepsin, nepenthesin-2 and NQO1. Fully deuterated samples were prepared and used for back-exchange correction as described previously [37,38]. Differences in deuteration can be considered as significant if they exceed 0.25 Da (calculated as 3× the average standard deviation).

The optimization of digestion conditions, including numerous proteolytical setups, showed that the serial combination of nepenthesin-2 with pepsin, operated at 200 $\mu L \cdot min^{-1}$, provided the best results in terms of sequence coverage (98.9%, missing the last three amino acids), number of peptides (140), average peptide length (8.3) and redundancy (4.1) (Figure S4). At this point, it should be also noted that the region between 100 and 110 yielded peptides of considerable hydrophobicity for which the signal intensity/quality was just at the threshold level, and thus conclusions derived from their analyses must be made with caution. The redundant peptide set was used to calculate deuteration in the shortest possible segments using the overlapping peptides. This analysis provided more detailed non-redundant information (high-resolution set). Data in this high-resolution set are mainly described in the manuscript (Figures 2–7, Figure S6 and Table S1), while those using experimental peptides (low resolution set) are found in Figures S7–S11 and Table S2. Note that the high-resolution set essentially leads to the same key conclusions as the low resolution one but, in principle, the former narrows the region for which HDX kinetics is assessed.

To report data on NQO1 segments from HDXMS, we did not consider the His-tag and used the native sequence from Met1 to Lys274. Therefore, the numbering used throughout the manuscript differs from that reported in some crystal structures of NQO1, which did not include Met1 and thus numbered the residues from Val1 to Lys273 (Val2 to Lys274 in the native sequence).

3. Results and Discussion

3.1.A Stable Folded Core in NQO1$_{apo}$ with Highly Dynamic Functional Sites

The results of HDX kinetics for NQO1$_{apo}$ are shown in Figure 2A. Results are presented as the % of the maximal (theoretical) deuterium incorporation for each segment (%D). Virtually all peptides characterized in this work for NQO1 complied with EX2 behavior (the presence of a tiny contribution from the EX1 regime can be detected in a few NQO1 peptides; see Figure S5). In the EX2 mechanism, the intrinsic exchange rate constant (k_{int}) is much lower than the rate constant (k_{cl}) for the conversion between non-exchanging (NE-NH) and exchanging (E-NH) states, according to the Linderstrøm-Lang model (Scheme: 1):

$$NE\text{–}NH \underset{k_{cl}}{\overset{k_{op}}{\leftrightarrow}} E\text{–}NH \xrightarrow{k_{int}} exchanged\ NH$$

Scheme 1. Linderstrøm-Lang model for HDX kinetics.

Assuming a pure EX2 behavior, the rate constant for exchange of individual backbone amides would be equal to the product of the equilibrium constant between NE-NH and E-NH ($K_{op} = k_{op}/k_{cl}$) and k_{int} [39]. Therefore, for this very simple mechanism (note that the conformational equilibrium is simply two-state and experimental HDX is rarely pure EX2), the experimental rate constant for exchange reflects to some extent the local stability (e.g., due to hydrogen bonding and burial in the structure) of the secondary structure.

Overall, the HDX kinetics was very heterogeneous among different protein segments of NQO1$_{apo}$ (Figure 2A). Most of the segments showed fast HDX kinetics (typically exchanging more than 20%D in the seconds-minutes time scales) while only a few peptides showed essentially no exchange after 3 h (%D < 20). Thus, in a first approach, we simply discerned between exchanging and

non-exchanging segments considering the %D after 3 h (%D < 20 vs. %D ≥ 20, respectively). The functional implications of this simple analysis were considered regarding those residues in different segments belonging to three functional sites: the FAD binding site (FBS), the dicoumarol binding site (DBS) and the monomer: monomer interface (MMI)(see Figure 2A), as provided by analysis of an X-ray crystallographic structure (PDB 2F1O [15]). It is worth noting that in this structure, the FBS and DBS are located adjacent to each other in the NQO1 monomer (actually, FAD is structurally part of the DBS), and both sites are close to the MMI (Figure 2B). Importantly, most of the residues that belong to the FBS, DBS and MMI are classified as exchanging in $NQO1_{apo}$ (%D ≥ 20; Figure 2A,B).

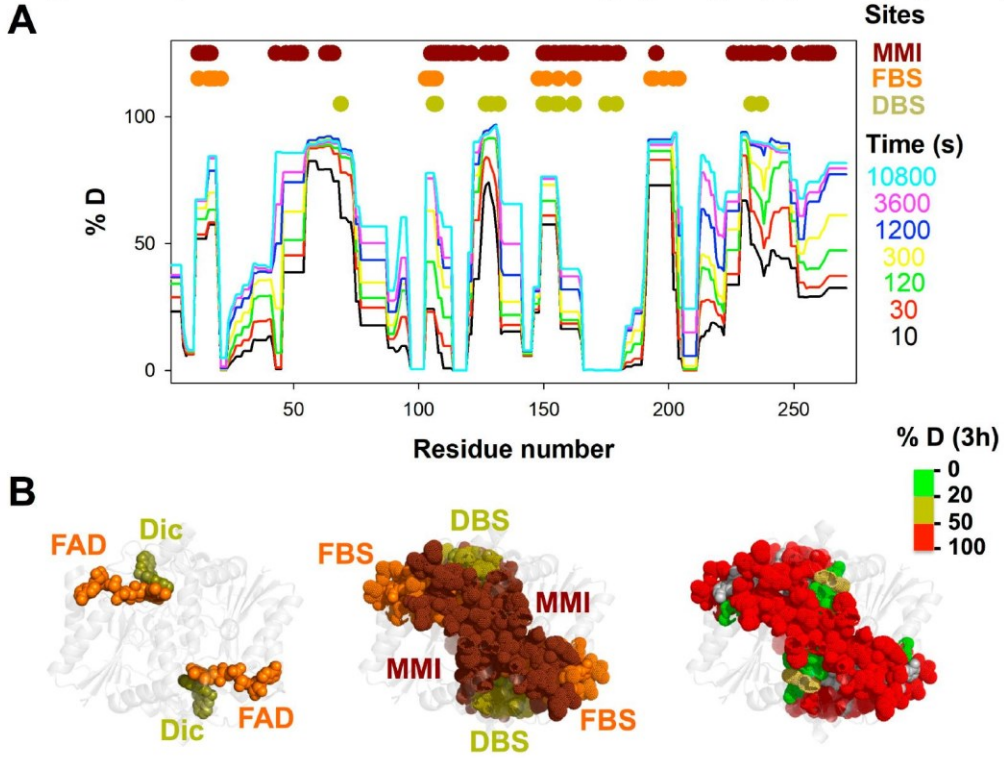

Figure 2. Overall HDX kinetics of $NQO1_{apo}$. (**A**) HDX kinetics for segments of $NQO1_{apo}$. Residues belonging to the monomer: monomer interface (MMI), FAD binding site (FBS) and dicoumarol binding site (DBS) are indicated as colored circles. These sites were retrieved from the analysis of the NQO1 structure (PDB 2F1O; [15]) using the PISA server (https://www.ebi.ac.uk/pdbe/pisa/); (**B**) Structural representation of HDX after 3 h [%D (3 h)] in $NQO1_{apo}$. For visual aid, the left panel shows the location of bound FAD and dicoumarol, the middle panel shows those residues belonging to the MMI, FBS and DBS, and the right panel displays the %D after 3 h for residues belonging to these functional sites.

Within non-exchanging segments, we found that these contained mostly residues buried in the crystallographic structure of NQO1 (in a ternary complex with FAD and dicoumarol bound, PDB 2F1O; $NQO1_{dic}$) (Figure 3A). Thus, these sequences likely represent regions that are critical for the acquisition and maintenance of a minimally stable dimeric fold in $NQO1_{apo}$ (note that $NQO1_{apo}$ is dimeric in solution but more expanded and flexible, and with lower conformational stability, than $NQO1_{holo}$ [9,14]). This minimal core involves helices α1, α3 and α4 and sheets β1 and β3–β5 (Figures 3A and S8). This core may also contribute to the acquisition of a minimally folded monomeric state that becomes stabilized in the dimeric state by the interactions between helices α3 and α4 across the monomers (i.e. the MMI) (Figures 3B and S8).

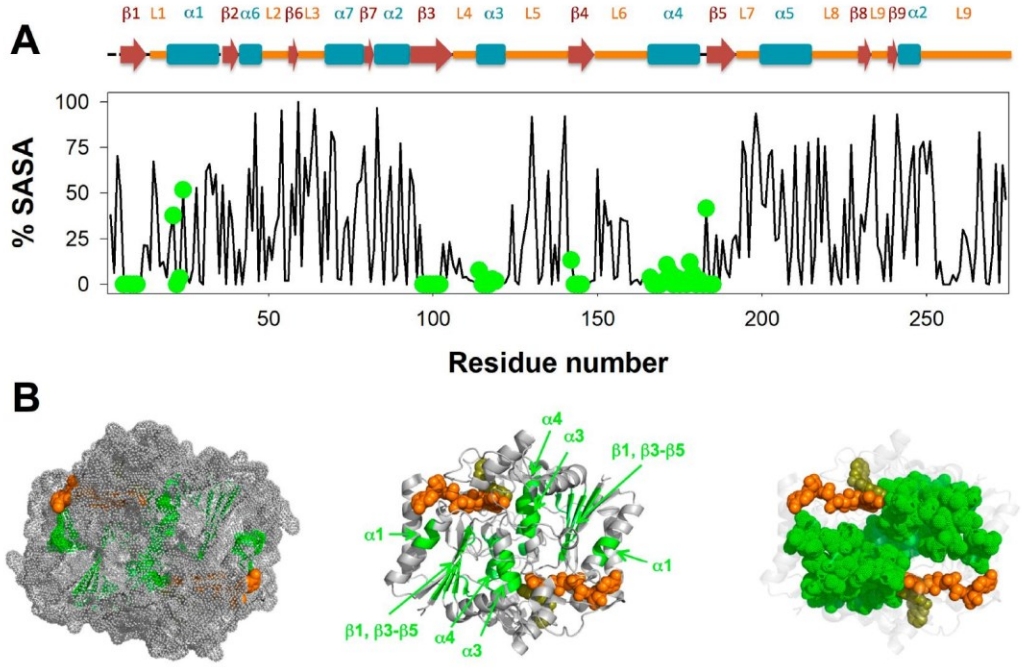

Figure 3. Non-exchanging segments define a minimally stable core in NQO1$_{apo}$. (**A**) Plot of the % SASA (solvent accessible surface area) for individual residues (considering backbone and side-chain) calculated from the structure of NQO1$_{dic}$ (PDB 2F1O [15]) using GETAREA (http://curie.utmb.edu/getarea.html; this algorithm does not consider the ligands in the calculation). Secondary structure elements are depicted according to [11]; residues belonging to non-exchanging segments are displayed as green circles; (**B**) Structural representation of non-exchanging segments (using PDB 2F1O [15]). The left panel shows a surface representation highlighting the burial of the minimally stable core. The middle panel shows segments belonging to this core plotted onto secondary structure elements. The right panel shows that this core may contribute to the stable folding of the individual monomers as well as their assembly into the dimer, with only a few stable contacts with the FAD (in orange ball representation) and the dicoumarol (in yellow ball representation).

Importantly, the FBS and DBS in NQO1$_{apo}$ are overall exchanging (Figures 2B, 3B and S8B), with the main exceptions being some marginal contacts in helices α1 and α3 (FBS) and α4 (DBS) (Figures 3B and S8B). Thus, our HDX analyses support that the conformational ensemble of NQO1$_{apo}$ is essentially populated by states non-competent for FAD or dicoumarol binding due to the high structural dynamics of their binding sites [9,14,34].

3.2. Complex HDX Kinetics

To provide deeper insight into the structural dynamics of NQO1$_{apo}$, we carefully analyzed the HDX kinetics for all protein segments (Figure S6). It should be noted that these HDX kinetics were very consistent with those obtained directly from peptides experimentally characterized (Figure S7 and S11). For the majority of the cases, HDX kinetics was described very well by a simple function with two kinetic phases (see Figures S6 and S7 for fittings, and Tables S1 and S2 for the best-fit values): a burst-phase corresponding to HDX mostly occurring within the experimental dead time (i.e., very few seconds), and thus characterized by a single parameter: its amplitude A$_{burst}$; and a slow phase that occurred typically in a scale of several seconds to minutes, characterized by two parameters: its amplitude A$_{slow}$ and an apparent first-order rate constant (k$_{slow}$), following this equation:

$$\%\, D(t) = A_{burst} + A_{slow} \cdot (1 - exp^{-k_{slow} \cdot t})$$

We chose to use this phenomenological description of HDX kinetics mainly for two reasons. First, it provided a simple scenario from which, using three characteristic parameters (A_{burst}, A_{slow} and k_{slow}), we could compare the HDX kinetics of different segments of $NQO1_{apo}$ (see Figure 4; note that this approach also worked very well with the HDX kinetics of $NQO1_{holo}$ and $NQO1_{dic}$; see Figures S6–S7 and Tables S1–S2). Second, although HDX kinetics analyzed using more complex functions (e.g., the two kinetic phases each containing a characteristic rate constant) may provide in some cases better fits, this would put the analyses at two intertwined risks: increasing the fitting parameters would make comparisons between behaviors more difficult, and importantly, in many cases these fittings show evident signs of overparametrization.

Kinetic analyses of HDX for protein segments considered as exchanging (>20%D after 3 h) revealed certain interesting behaviors. First, for many protein segments (of different lengths), we observed a significant contribution to the HDX kinetics from both the burst and slow phases (Figures 4 and S9, and Tables S1–S2). As indicated above, the HDX kinetics of NQO1 in all three ligation states is vastly consistent with EX2 kinetics, and thus, the observed kinetics depends to some extent on the equilibrium constant between non-exchanging and exchanging states [40]. Therefore, the presence of two clearly differentiated kinetic phases suggests the existence of complexity (i.e., heterogeneity) in the conformational ensemble of $NQO1_{apo}$, and plausibly, the significant population of at least two conformational substates with different HDX behavior, which may or may not significantly reequilibrate upon the intrinsic HDX step. Interestingly, although ligand binding affects these two kinetic phases ($NQO1_{holo}$ and $NQO1_{dic}$, see Figures S6–S7 and Tables S1–S2), both these phases still contribute to the HDX kinetics in these ligation states, suggesting that a certain degree of conformational heterogeneity remains upon ligand binding. Second, although in the EX2 scenario the overall kinetics depends on the intrinsic HDX rate constant, and therefore, on the individual backbone amides and their vicinity [40], some sort of correlated behavior at larger scales than small protein segments (e.g., secondary structure elements) is observed (Figures 4B and S9). Consistent with the above-mentioned proposal of a stable core of $NQO1_{apo}$ with highly dynamic FBS and DBS (simply made by analysis of %D after 3 h, Figure 3), these kinetic analyses suggest that secondary structure elements outside the stable core typically exchanged quite fast (i.e., with large burst phases and with k_{slow} often in the range of 10^{-1} to 10^{-2} s^{-1}; Figures 4B and S9).

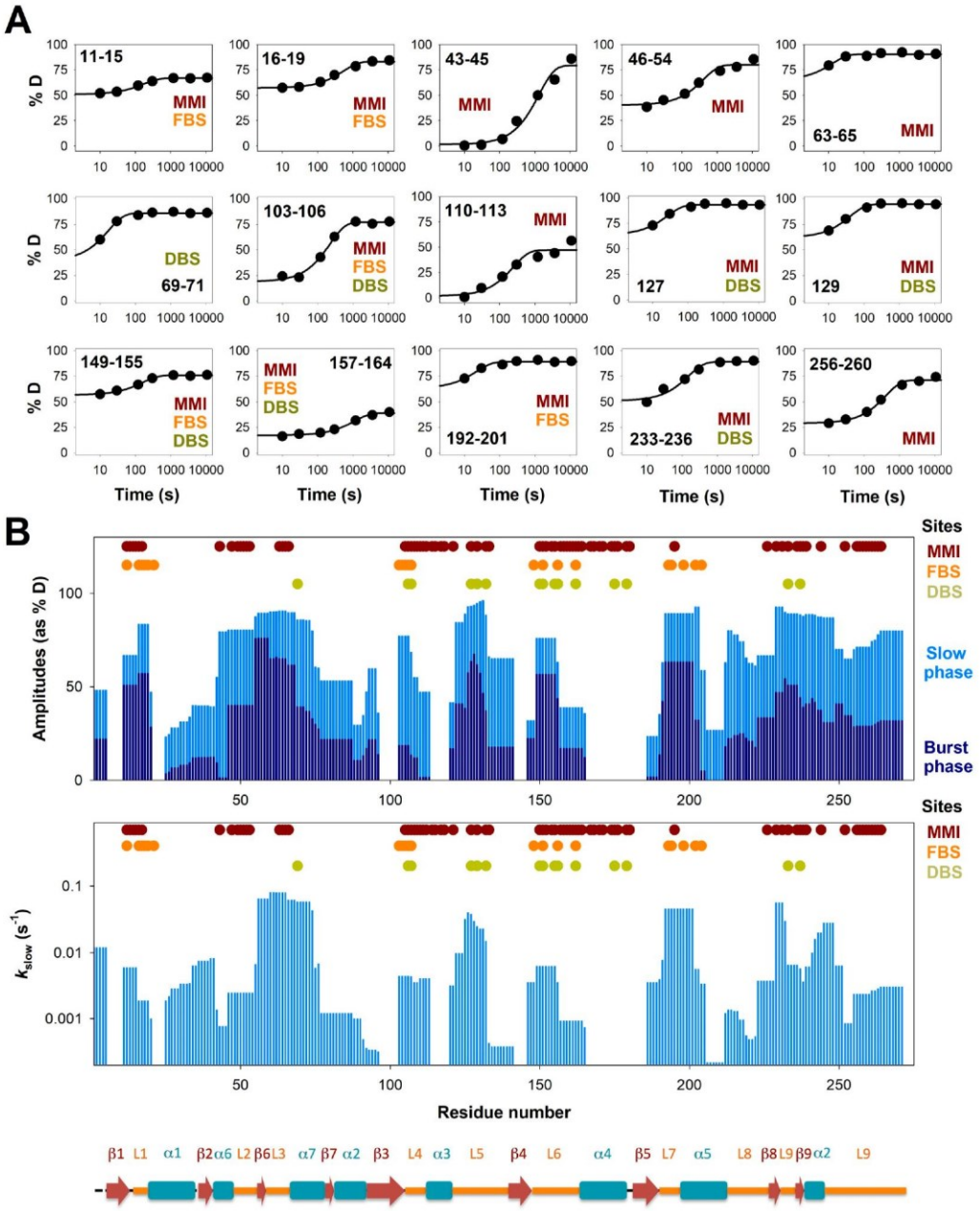

Figure 4. Segment-specific HDX kinetics of NQO1$_{apo}$. (**A**) Fittings of HDX kinetics for selected segments typically showing at least 50%D incorporation after 3 h and considered part of the functional sites (MMI, FBS and DBS). (**B**) Plots of the amplitudes for the burst- and slow-phase in HDX for segments (upper panel) and rate constants for the slow phase (lower panel) for segments with at least 20%D after 3 h. The elements of the secondary structure along the protein sequence are also indicated.

3.3. FAD and Dicoumarol Binding Cause Large-Scale Changes in Protein Structural Dynamics

FAD binding to NQO1$_{apo}$ is known to cause significant overall changes in protein structure and dynamics: it increases the content in the ordered secondary structure, reduces the protein hydrodynamic volume, and substantially enhances protein stability and resistance towards proteolytic attack [9,14,22,34,35]. In addition, structural and biophysical analyses have shown that NQO1 must contain bound FAD in order to bind dicoumarol with high affinity [9,14]. We first compared the %D incorporated to NQO1$_{holo}$ and NQO1$_{apo}$ after 3 h of reaction (Figure 5A–B), observing some interesting changes upon FAD binding. Particularly large differences were observed

in loop L1 (involved in the MMI and the FBS), loop L4 (involved in the MMI, the FBS and the DBS) and helix α5 (involved in the FBS). The stabilization observed for the MMI thus explains the increased thermostability of the NQO1 dimer upon FAD binding. The much lower structural dynamics of the FBS upon FAD binding is also consistent with an induced-fit mechanism, in which binding competent states (with high structural stability) are marginally populated in the absence of FAD, according to a recent proposal based on binding structure-thermodynamic relationships [34]. Interestingly, these results also imply that FAD is not only required for dicoumarol binding as a part of the DBS, but also that FAD binding modifies the dynamics of protein structural elements involved in the binding of the inhibitor (Figure 5C). It is worth noting that FAD binding also significantly slows down (3- to 5-fold) HDX of other regions such as sheet β6, helix α7 and loop L3 (Figures 6 and S6, and Table S1), some of them not directly involved in the MMI, FBS or DBS.

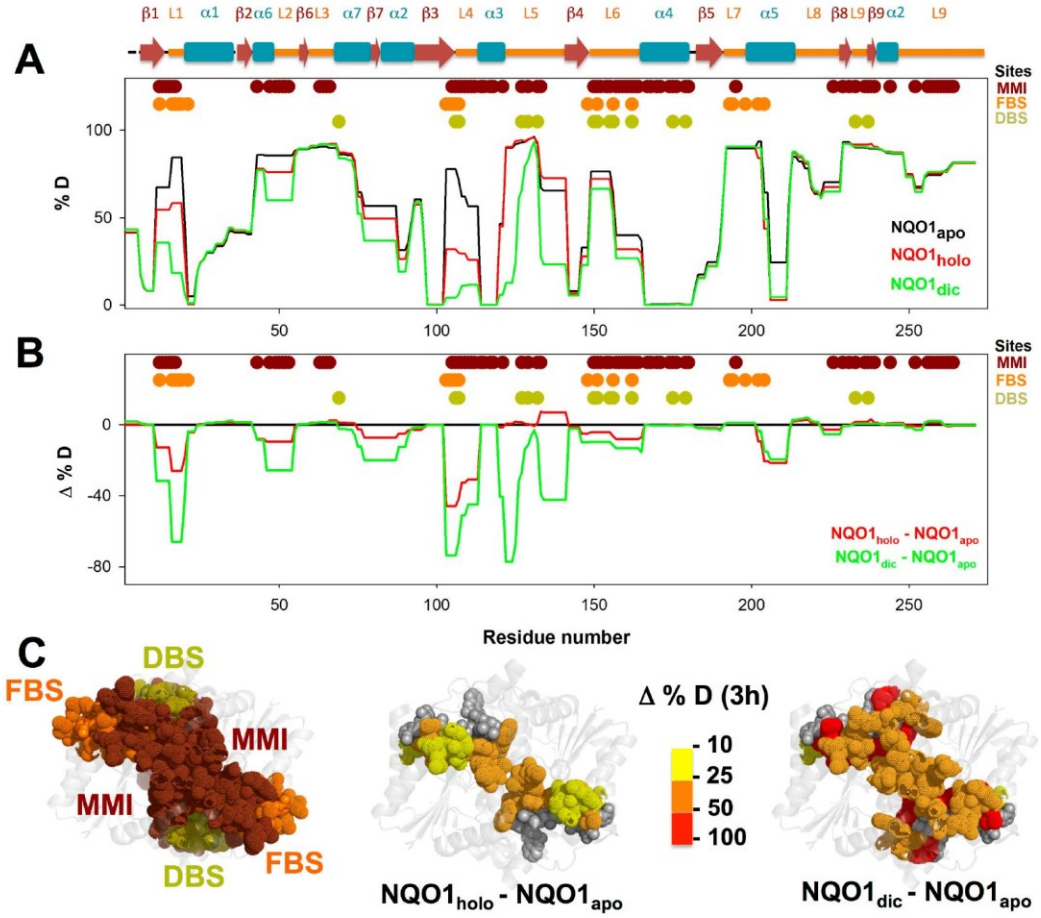

Figure 5. Overall HDX kinetics for segments of NQO1 upon binding FAD and dicoumarol. (**A** and **B**) HDX for segments of $NQO1_{apo}$, $NQO1_{holo}$ and $NQO1_{dic}$. Panel A shows %D after 3 h, and Panel B the difference in this parameter (Δ%D) between $NQO1_{holo}$ or $NQO1_{dic}$ and $NQO1_{apo}$. Residues belonging to the MMI, FBS and DBS are indicated (retrieved as described in Figure 2). (**C**) Δ%D after 3 h in NQO1 upon FAD and dicoumarol binding plotted onto the NQO1 structure (PDB 2F1O). For comparison, the left panel shows the location of MMI, FBS and DBS, the middle and right panels show those residues belonging to the sites that displayed at least a decrease of 10%D after 3 h in $NQO1_{holo}$ (middle panel) or $NQO1_{dic}$ (right panel) vs. $NQO1_{apo}$.

Dicoumarol binding to $NQO1_{holo}$ is also known to increase the protein ordered secondary structure, thermal stability and resistance of the N-terminal domain towards proteolysis [9,14]. According to this evidence, we observed that dicoumarol binding to $NQO1_{holo}$ decreased the %D after 3 h to an even larger extent than FAD binding, and these effects seemed to propagate to more distant regions in the protein structure, extensively affecting regions involved in the MMI, the FBS and DBS

(Figure 5). The regions affected by dicoumarol binding were actually the very same set of structural regions affected by FAD binding with the exception of helix α5 (Figure 5). In contrast to FAD, dicoumarol binding also caused a dramatic reduction in %D in sheet β4 and loop L5, which contain residues belonging to the MMI and the DBS (Figure 5). In addition, dicoumarol binding slowed down the HDX kinetics of helix α7 and loops L4 and L5 (Figures 6 and S6–S7, and Tables S1–S2) by several orders of magnitude.

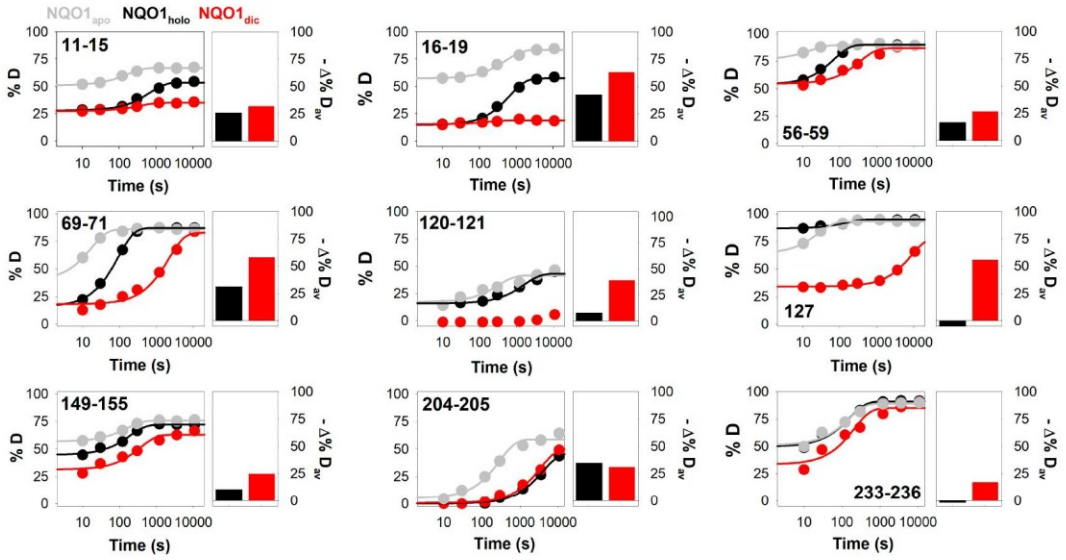

Figure 6. Changes in segment-specific HDX kinetics of NQO1 upon FAD and dicoumarol binding. Right panels show fittings of HDX kinetics for selected individual segments using a single exponential function with a burst-phase for $NQO1_{apo}$ (**grey**), $NQO1_{holo}$ (**black**) and $NQO1_{dic}$ (**red**). These data were used to calculate $\Delta\%D_{av}$, as an average of the time points with maximal differences between a given NQO1 form ($NQO1_{holo}$, black; $NQO1_{dic}$, red) and $NQO1_{apo}$, as a single metric to quantify changes in HDX kinetics (left panels).

Clearly, the HDX kinetics of NQO1 in all three ligation states ($NQO1_{apo}$, $NQO1_{holo}$ and $NQO1_{dic}$) were complex overall (Figures 6 and S6–S7). Therefore, it was not straightforward to provide a single metric from the global kinetic analysis reported so far in this work, even when a simple kinetic model was used. To quantify the effects of ligand binding (and potentially of mutations) on the structural dynamics of NQO1, we sought a single metric that would respond, at least semi-quantitatively, to the different types of change observed upon ligand binding (Figure 5 and 6). We must note that these changes include a variety of effects on the amplitudes of the two kinetic phases (sometimes increasing, decreasing, not changing or even shifting between the amplitudes of the burst and the slow phases upon ligand binding) and also on the rate constant of the slow phase (in some cases, this phase was too fast or slow to be measured adequately) (see Tables S1 and S2). Notably, all these effects on the HDX kinetics can be simplified to a common effect: at least a few of the data in the time-dependent measurements differ from two samples when these samples are paired for a given time point (see Figure 6 for representative examples). Thus, we decided to simply calculate the difference between the two paired proteins species for a given time and protein segment, and for each segment, to average the three time points with a maximal difference in these time series. Indeed, this simple metric (called $\Delta\%D_{av}$) was able to detect and rank the effects of ligand binding on NQO1 HDX due to changes in amplitudes and kinetic rate constants (Figure 6).

We compared again the behavior of $NQO1_{holo}$ vs. $NQO1_{apo}$ using $\Delta\%D_{av}$ (Figures 7A and S10A). The results showed that FAD binding substantially reduced the backbone dynamics of residues 11–20 (loop L1 and helix α1), 46–76 (loops L2 and L3, helix α7 and sheet β6), 103–113 (sheet β6 and loop L4), 149–165 (loop L6) and 191–211 (loop L7 and helix α5) (Figure 7A). These regions include most of

the residues involved in the MMI and FBS, and also some belonging to the DBS (Figure 7A–B). When we evaluated the effect of dicoumarol binding, we observed further structural stabilization of all these regions (with the exception of residues 191–211) and a specific stabilization of two additional regions mostly involved in the MMI and DBS: a dramatic stabilization of the segment 120–141 (loop 5) and a moderate effect in the segment 223–240 (loops L8 and L9 and sheets β8 and β9).

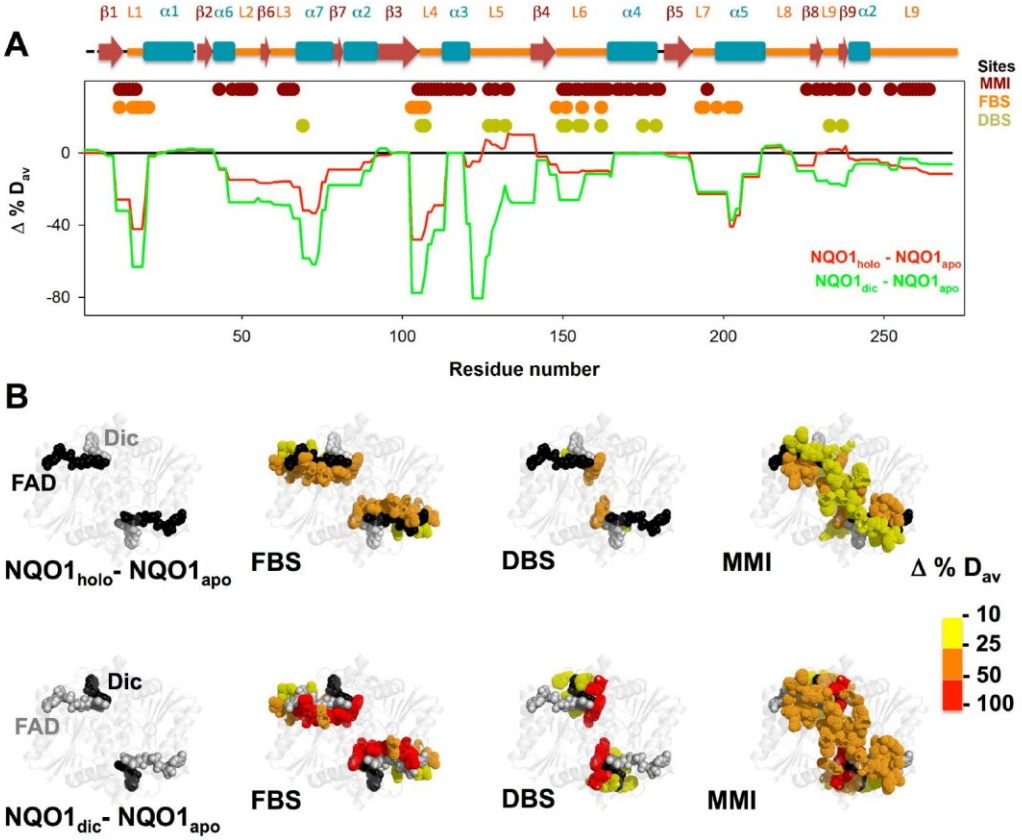

Figure 7. Changes in HDX kinetics of NQO1 upon binding FAD and dicoumarol as changes in $\%D_{av}$ ($\Delta\%D_{av}$). (**A**) $\Delta\%D_{av}$ for NQO1 segments upon binding FAD ($NQO1_{holo}$) and dicoumarol ($NQO1_{dic}$), using $NQO1_{apo}$ as a reference. Residues belonging to the MMI, FBS and DBS are indicated (retrieved as in Figure 2). (**B**) Representation of $\Delta\%D_{av}$ onto the structure of NQO1 (using PDB 2F1O). The upper row shows results for the $\Delta\%D_{av}$ of $NQO1_{holo}$ and the lower row represents $NQO1_{dic}$. Different panels in each row show results for residues involved in the FBS, DBS or MMI.

3.4. Insights into Cooperative Effects upon FAD and Dicoumarol Binding from Analysis of Structural Dynamics

In addition to the overall conformational and functional consequences of FAD and dicoumarol binding to NQO1, some experimental techniques have revealed complexity in the functional chemistry of this enzyme [22,23,41]. This behavior is not unexpected since binding of FAD to $NQO1_{apo}$ and dicoumarol to $NQO1_{holo}$ is described by a general formalism for binding of a ligand (L) to a macromolecule (P, NQO1 dimer) with two binding sites (Scheme 2) [42]:

$$P + L \overset{K_1}{\longleftrightarrow} PL \qquad PL + L \overset{K_2}{\longleftrightarrow} PL_2$$

Scheme 2. General formalism for a macromolecule P (NQO1 dimer) with two ligand (L) binding sites.

in which K_1 and K_2 describe the step-wise equilibrium constants as follows:

$$K_1 = \frac{[PL]}{[P] \cdot [L]}$$

$$K_2 = \frac{[PL_2]}{[PL] \cdot [L]}$$

For a P with two equivalent and non-interacting binding sites, these two step-wise equilibrium binding constants are related through a simple relationship: $K_1 = 4 \cdot K_2$. Significant deviations from this relationship imply the existence of non-equivalent or interacting sites: $K_1 > 4 \cdot K_2$ implies either negative cooperativity or non-equivalent binding sites, while $K_1 < 4 \cdot K_2$ unequivocally identifies positive cooperativity. It must be noted that, in this scenario, the largest differences between cooperative and non-cooperative binding are found for the dependence of the population of the half-ligated species [PL] (e.g., NQO1 dimer with one FAD bound) on [L] [22,23,42].

The NQO1 dimer contains two binding sites for either FAD or dicoumarol. Interestingly, calorimetric titrations of $NQO1_{apo}$ with FAD and $NQO1_{holo}$ with dicoumarol, as well as inhibition studies in the case of dicoumarol, have identified the existence of negative cooperativity in the binding of both ligands [22,23,41]. A detailed structural characterization of the communication between ligand binding sites underlying these cooperative effects is challenging for several reasons. First, in the ligand binding equilibrium, the unligated (P), half-ligated (PL) and fully-ligated (PL_2) species contribute structurally and energetically to the observed cooperative binding. However, to date, no structural information on the P or PL states for FAD binding is available (i.e., no high-resolution structure of $NQO1_{apo}$ or the intermediate species with a single FAD molecule bound per dimer), while for dicoumarol binding, no structural information for PL ($NQO1_{holo}$ with a single dicoumarol molecule bound per dimer) is available. Although our current HDXMS study does not report on half-ligated species, we were able to identify a network of interacting residues in $NQO1_{apo}$ that connect structurally and energetically the FBS and the DBS between monomers through the MMI interface. Therefore, our results suggest the existence of a highly dynamic structural network connecting these binding sites between the monomers in NQO1, and these results may also provide a blueprint for future experimental and computational mutagenesis studies aimed at perturbing and analyzing the role of this network in ligand binding energetics and cooperativity. In support of this hypothesis, recent work has shown that the mutation Gly151Ser (Gly150 according to the crystal structure) essentially prevents the communication of ligand binding effects between the two DBS across the NQO1 dimer [41]. Gly151 is located in the beginning of loop L6, and it undergoes a noticeable decrease in structural dynamics upon dicoumarol binding (Figure 7), which might constitute part of the allosteric signal generated by dicoumarol binding to one site (to form the half-ligated state PL), which communicates to the other subunit contributing to the negative cooperativity for dicoumarol binding. More globally, our analyses from HDXMS support the idea that dicoumarol binding triggers changes in NQO1 dynamics for certain (but not all) regions predicted by studies using a Gaussian network approach on structural models for the P and PL states [41]. In agreement with this recent study, we observed that dicoumarol binding affected the dynamics of loops L3 and L5, sheets β6 and β7, and helices α2, α5 and α7, which showed the largest changes in dynamics when the slowest frequency modes were analyzed upon formation of the PL state by a Gaussian network model (Figure 7 vs. [41]).

4. Conclusions

The multifunctional nature of NQO1 is likely controlled, to a large extent, by changes in protein structural dynamics triggered by the binding of small molecules (FAD, NAD(P)H, substrates, inhibitors) as well as by interaction with other biomacromolecules (proteins and nucleic acids). These structural and energetic aspects are critical to improve our understanding of these interactions under physiological and pathological conditions. In this work, we showed that the use of HDXMS can be instrumental to provide unprecedented detail of the effects of ligand binding on the functional chemistry of NQO1 linked to changes in protein structural dynamics. This approach may provide

novel insights into the regulation of NQO1 activity and stability *in vivo*, as well as the mechanisms by which these properties are regulated and/or dysregulated by disease-associated single amino acid exchanges and post-translational modifications.

NQO1 is one of the human flavoproteins for which intracellular protein levels are more strongly coupled to the intracellular availability of the flavin cofactor [25]. Our current understanding of this phenomenon proposes that this sensitivity of protein stability is due to efficient recognition and degradation of human apo-flavoproteins by the ubiquitin-dependent proteasomal pathway [14,25,30]. The lack of high-resolution information on the structure and dynamics of human apo-flavoproteins, due to the instability of these apo-proteins, has prevented us from a deep understanding of these recognition mechanisms. The detailed analysis reported herein for $NQO1_{apo}$ supports that HDXMS can also be used to improve our understanding of this phenomenon as well as the mechanisms by which disease-associated mutations and post-translational modifications may alter protein structural dynamics, leading to alternative recognition mechanisms by the proteasomal degradation pathway [14,30,34,36].

In this work, we identified a minimally stable core that allows $NQO1_{apo}$ to exist as a dimer, although this dimer constitutes a highly dynamic conformational ensemble and with marginal conformational stability. This core may serve as a wiring network that allows the communication of ligand binding and mutational effects between domains and between subunits through this minimally stable MMI (see [9,22,23,32,33]), and cooperative effects upon FAD and dicoumarol binding [22,23,41].

Our study also allows us to discuss the deleterious effects of the common cancer-associated polymorphism Pro187Ser. Pro187 belongs to sheet β5, as a part of the stable core of the monomer in $NQO1_{apo}$ state (Figure 3). Thus, the strong structural perturbation presumably caused by Pro187Ser substitution could readily cause long-range effects on the structural dynamics of $NQO1_{apo}$ by disrupting this stable core, and these effects could propagate within the monomer and between subunits in the dimer. This interpretation agrees with previous experimental, computational and structural perturbation analyses carried out on the Pro187Ser variant [5,14,22,30–34,36]. Consequently, even in $NQO1_{apo}$, the cancer-associated polymorphism Pro187Ser would destabilize the NQO1 monomer, and this effect could easily propagate to the MMI, the FBS and the DBS, thus contributing to explain the low conformational stability of P187S *in vitro*, its low affinity for FAD and dicoumarol, and its accelerated degradation by the proteasome [9,10,14,22–25,34].

Our analyses also support that HDXMS can provide unprecedented structural insight into the catalytic cycle of NQO1. First, our results indicate that FAD binding shifts the conformational ensemble of NQO1 towards more stable and competent states for either NAD(P)H or dicoumarol binding (i.e., at the DBS). This effect is further strengthened upon the binding of the inhibitor, suggesting that the structural dynamics of the DBS (and plausibly of the NAD(P)H binding site; [15]) acts by limiting the available ligand binding poses of NAD(P)H. This would optimize hydride transfer from the adenine dinucleotide coenzyme to the FAD, thus contributing to high rate constants experimentally measured for the reductive half-reaction catalyzed by NQO1 [10].

Supplementary Materials: The following are available online at www.mdpi.com/xxx/s1. In the Supplementary information file, Figures S1–S11 and Tables S1 and S2 can be found.

Author Contributions: conceptualization, A.L.P.; methodology, P.V., P.M. and A.L.P.; software, P.V. and P.M.; validation, P.V., P.M. and A.L.P.; formal analysis, P.V., P.M. and A.L.P.; investigation, P.V., E.S., P.M. and A.L.P.; resources, E.S., P.M. and A.L.P.; data curation, P.V., D.J.T., P.M. and A.L.P.; writing—original draft preparation, P.V., P.M. and A.L.P.; writing—review and editing, P.V., E.S., D.J.T., P.M. and A.L.P.; visualization, P.M. and A.L.P.; supervision, P.M. and A.L.P.; project administration, P.M. and A.L.P.; funding acquisition, E.S., P.M. and A.L.P.

Funding: This research was funded by the ERDF/Spanish Ministry of Science, Innovation and Universities—State Research Agency (Grant RTI2018-096246-B-I00, to A.L.P.), the Spanish Ministry of Economy and Competitiveness (Grant SAF2015-69796, to E.S.) and Junta de Andalucía (Grant P11-CTS-07187, to ALP). Access to an EU_FT–ICR_MS network installation was funded by the EU Horizon 2020 grant 731077. Additional support from Aula FUNCANIS-UGR, EU and MEYS CZ funds CZ.1.05/1.1.00/02.0109, LQ1604 and LM2015043 is gratefully acknowledged.

Acknowledgments: We acknowledge assistance from Dr. Noel Mesa-Torres in protein expression and purification.

Conflicts of Interest: The authors declare no conflict of interest.

References

1. Beaver, S.K.; Mesa-Torres, N.; Pey, A.L.; Timson, D.J. NQO1: A target for the treatment of cancer and neurological diseases, and a model to understand loss of function disease mechanisms. *Biochim. Biophys. Acta Proteins Proteom.* **2019**, *1867*, 663–676.
2. Ross, D.; Siegel, D. Functions of NQO1 in cellular protection and CoQ10 metabolism and its potential role as a redox sensitive molecular switch. *Front. Physiol.* **2017**, *8*, 595.
3. Ross, D.; Siegel, D. NQO1 in protection against oxidative stress. *Curr. Opin. Toxicol.* **2018**, *7*, 67–72.
4. Pey, A.L.; Megarity, C.F.; Medina-Carmona, E.; Timson, D.J. Natural small molecules as stabilizers and activators of cancer-associated NQO1 polymorphisms. *Curr. Drug Targets* **2016**, 17, *1506*–1514.
5. Pey, A.L.; Megarity, C.F.; Timson, D.J. NAD (P) H quinone oxidoreductase (NQO1): An enzyme which needs just enough mobility, in just the right places. *Biosci. Rep.* **2019**, *39*, BSR20180459**.**
6. Dinkova-Kostova, A.T.; Talalay, P. NAD (P) H: Quinone acceptor oxidoreductase 1 (NQO1), a multifunctional antioxidant enzyme and exceptionally versatile cytoprotector. *Arch. Biochem. Biophys.* **2010**, *501*, 116–123.
7. Siegel, D.; Gustafson, D.L.; Dehn, D.L.; Han, J.Y.; Boonchoong, P.; Berliner, L.J.; Ross, D. NAD (P) H: Quinone oxidoreductase 1: Role as a superoxide scavenger. *Mol. Pharmacol.* **2004**, *65*, 1238–1247.
8. Siegel, D.; Dehn, D.D.; Bokatzian, S.S.; Quinn, K.; Backos, D.S.; DiFrancesco, A.; Bernier, M.; Reisdorph, N.; deCabo, R.; Ross, D. Redox modulation of NQO1. *PLoS ONE* **2018**, *13*, e0190717.
9. Medina-Carmona, E.; Neira, J.L.; Salido, E.; Fuchs, J.E.; Palomino-Morales, R.; Timson, D.J.; Pey, A.L. Site-to-site interdomain communication may mediate different loss-of-function mechanisms in a cancer-associated NQO1 polymorphism. *Sci. Rep.* **2017**, *7*, 44352.
10. Lienhart, W.D.; Gudipati, V.; Uhl, M.K.; Binter, A.; Pulido, S.A.; Saf, R.; Zangger, K.; Gruber, K.; Macheroux, P. Collapse of the native structure caused by a single amino acid exchange in human NAD (P) H: Quinone oxidoreductase[1]. *FEBS J.* **2014**, *281*, 4691–4704.
11. Faig, M.; Bianchet, M.A.; Talalay, P.; Chen, S.; Winski, S.; Ross, D.; Amzel, L.M. Structures of recombinant human and mouse NAD (P) H: Quinone oxidoreductases: Species comparison and structural changes with substrate binding and release. *Proc. Natl. Acad. Sci. USA* **2000**, *97*, 3177–3182.
12. Li, R.; Bianchet, M.A.; Talalay, P.; Amzel, L.M. The three-dimensional structure of NAD (P) H: Quinone reductase, a flavoprotein involved in cancer chemoprotection and chemotherapy: Mechanism of the two-electron reduction. *Proc. Natl. Acad. Sci. USA* **1995**, *92*, 8846–8850.
13. Chen, S.; Deng, P.S.; Bailey, J.M.; Swiderek, K.M. A two-domain structure for the two subunits of NAD (P) H: Quinone acceptor oxidoreductase. *Protein Sci.* **1994**, *3*, 51–57.
14. Medina-Carmona, E.; Palomino-Morales, R.J.; Fuchs, J.E.; Padín-Gonzalez, E.; Mesa-Torres, N.; Salido, E.; Timson, D.J.; Pey, A.L. Conformational dynamics is key to understanding loss-of-function of NQO1 cancer-associated polymorphisms and its correction by pharmacological ligands. *Sci. Rep.* **2016**, *6*, 20331.
15. Asher, G.; Dym, O.; Tsvetkov, P.; Adler, J.; Shaul, Y. The crystal structure of NAD (P) H quinone oxidoreductase 1 in complex with its potent inhibitor dicoumarol. *Biochemistry* **2006**, *45*, 6372–6378.
16. Moscovitz, O.; Tsvetkov, P.; Hazan, N.; Michaelevski, I.; Keisar, H.; Ben-Nissan, G.; Shaul, Y.; Sharon, M. A mutually inhibitory feedback loop between the 20S proteasome and its regulator, NQO1. *Mol. Cell* **2012**, *47*, 76–86.
17. Asher, G.; Tsvetkov, P.; Kahana, C.; Shaul, Y. A mechanism of ubiquitin-independent proteasomal degradation of the tumor suppressors p53 and p73. *Genes Dev.* **2005**, *19*, 316–321.
18. Oh, E.T.; Kim, J.W.; Kim, J.M.; Kim, S.J.; Lee, J.S.; Hong, S.S.; Goodwin, J.; Ruthenborg, R.J.; Jung, M.G.; Lee, H.J.; et al. NQO1 inhibits proteasome-mediated degradation of HIF-1alpha. *Nat. Commun.* **2016**, *7*, 13593.
19. Lata, S.; Ali, A.; Sood, V.; Raja, R.; Banerjea, A.C. HIV-1 Rev downregulates Tat expression and viral replication via modulation of NAD (P) H: Quinine oxidoreductase 1 (NQO1). *Nat. Commun.* **2015**, *6*, 7244.
20. DiFrancesco, A.; DiGermanio, C.; Panda, A.C.; Huynh, P.; Peaden, R.; Navas-Enamorado, I.; Bastian, P.; Lehrmann, E.; Diaz-Ruiz, A.; Ross, D.; et al. Novel RNA-binding activity of NQO1 promotes SERPINA1 mRNA translation. *Free Radic. Biol. Med.* **2016**, *99*, 225–233.

21. Betancor-Fernandez, I.; Timson, D.J.; Salido, E.; Pey, A.L. Natural (and unnatural) small molecules as pharmacological chaperones and inhibitors in cancer. *Handb. Exp. Pharmacol.* **2018**, *45*, 345–383.
22. Pey, A.L.; Megarity, C.F.; Timson, D.J. FAD binding overcomes defects in activity and stability displayed by cancer-associated variants of human NQO1. *Biochim. Biophys. Acta* **2014**, *1842*, 2163–2173.
23. Claveria-Gimeno, R.; Velazquez-Campoy, A.; Pey, A.L. Thermodynamics of cooperative binding of FAD to human NQO1: Implications to understanding cofactor-dependent function and stability of the flavoproteome. *Arch. Biochem. Biophys.* **2017**, *636*, 17–27.
24. Siegel, D.; Anwar, A.; Winski, S.L.; Kepa, J.K.; Zolman, K.L.; Ross, D. Rapid polyubiquitination and proteasomal degradation of a mutant form of NAD (P) H: Quinone oxidoreductase 1. *Mol. Pharmacol.* **2001**, *59*, 263–268.
25. Martinez-Limon, A.; Alriquet, M.; Lang, W.H.; Calloni, G.; Wittig, I.; Vabulas, R.M. Recognition of enzymes lacking bound cofactor by protein quality control. *Proc. Natl. Acad. Sci. USA* **2016**, *113*, 12156–12161.
26. Luo, S.; SuKang, S.; Wang, Z.H.; Liu, X.; Day, J.X.; Wu, Z.; Peng, J.; Xiang, D.; Springer, W.; Ye, K. Akt Phosphorylates NQO1 and Triggers its Degradation, Abolishing Its Antioxidative Activities in Parkinson's Disease. *J. Neurosci.* **2019**, *39*, 7291–7305.
27. Nolan, K.A.; Scott, K.A.; Barnes, J.; Doncaster, J.; Whitehead, R.C.; Stratford, I.J. Pharmacological inhibitors of NAD (P) H quinone oxidoreductase, NQO1: Structure/activity relationships and functional activity in tumour cells. *Biochem. Pharmacol.* **2010**, *80*, 977–981.
28. Nolan, K.A.; Zhao, H.; Faulder, P.F.; Frenkel, A.D.; Timson, D.J.; Siegel, D.; Ross, D.; Burke, T.R., Jr.; Stratford, I.J.; Bryce, R.A. Coumarin-based inhibitors of human NAD (P) H: Quinone oxidoreductase-1. Identification, structure–activity, off-target effects and in vitro human pancreatic cancer toxicity. *J. Med. Chem.* **2007**, *50*, 6316–6325.
29. Scott, K.A.; Barnes, J.; Whitehead, R.C.; Stratford, I.J.; Nolan, K.A. Inhibitors of NQO1: Identification of compounds more potent than dicoumarol without associated off-target effects. *Biochem. Pharmacol.* **2011**, *81*, 355–363.
30. Medina-Carmona, E.; Rizzuti, B.; Martin-Escolano, R.; Pacheco-Garcia, J.L.; Mesa-Torres, N.; Neira, J.L.; Guzzi, R.; Pey, A.L. Phosphorylation compromises FAD binding and intracellular stability of wild-type and cancer-associated NQO1: Insights into flavo-proteome stability. *Int. J. Biol. Macromol.* **2019**, *125*, 1275–1288.
31. Mesa-Torres, N.; Betancor-Fernández, I.; Oppici, E.; Cellini, B.; Salido, E.; Pey, A.L. Evolutionary divergent suppressor mutations in conformational diseases. *Genes* **2018**, *9*, 352.
32. Medina-Carmona, E.; Betancor-Fernández, I.; Santos, J.; Mesa-Torres, N.; Grottelli, S.; Batlle, C.; Naganathan, A.N.; Oppici, O.; Cellini, B.; Ventura, S.; et al. Insight into the specificity and severity of pathogenic mechanisms associated with missense mutations through experimental and structural perturbation analyses. *Hum. Mol. Genet.* **2019**, *28*, 1–15.
33. Pey, A.L. Biophysical and functional perturbation analyses at cancer-associated P187 and K240 sites of the multifunctional NADP (H): Quinone oxidoreductase 1. *Int. J. Biol. Macromol.* **2018**, *118*, 1912–1923.
34. Munoz, I.G.; Morel, B.; Medina-Carmona, E.; Pey, A.L. A mechanism for cancer-associated inactivation of NQO1 due to P187S and its reactivation by the consensus mutation H80R. *FEBS Lett.* **2017**, *591*, 2826–2835.
35. Lienhart, W.D.; Strandback, E.; Gudipati, V.; Koch, K.; Binter, A.; Uhl, M.K.; Rantasa, D.M.; Bourgeois, B.; Madl, T.; Zangger, K.; et al. Catalytic competence, structure and stability of the cancer-associated R139W variant of the human NAD (P) H: Quinone oxidoreductase 1 (NQO 1). *FEBS J.* **2017**, *284*, 1233–1245.
36. Medina-Carmona, E.; Fuchs, J.E.; Gavira, J.A.; Mesa-Torres, N.; Neira, J.L.; Salido, E.; Palomino-Morales, R.; Burgos, M.; Timson, D.J.; Pey, A.L. Enhanced vulnerability of human proteins towards disease-associated inactivation through divergent evolution. *Hum. Mol. Genet.* **2017**, *26*, 3531–3544.
37. Zhang, Z.; Smith, D.L. Determination of amide hydrogen exchange by mass spectrometry: A new tool for protein structure elucidation. *Protein Sci.* **1993**, *2*, 522–531.
38. Trcka, F.; Durech, M.; Vankova, P.; Chmelik, J.; Martinkova, V.; Hausner, J.; Kadek, A.; Marcoux, J.; Klumpler, T.; Vojtesek, B.; et al. Human stress-inducible Hsp70 has a high propensity to form ATP-dependent antiparallel dimers that are differentially regulated by Cochaperone binding. *Mol. Cell Proteom.* **2019**, *18*, 320–337.
39. Bai, Y. Hydrogen Exchange Experiments: Detection and Characterization of Protein Folding Intermediates. In *Protein Folding, Misfolding and Aggregation*; Muñoz, V., Ed.; Royal Society of Chemistry: Cambridge, UK, 2008; pp. 70–83.

40. Konermann, L.; Pan, J.; Liu, Y.H. Hydrogen exchange mass spectrometry for studying protein structure and dynamics. *Chem. Soc. Rev.* **2011**, *40*, 1224–1234.
41. Megarity, C.F.; Abdel-Bettley, H.; Caraher, M.C.; Scott, K.A.; RA, W.; Jowitt, T.A.; Gutierrez, A.; Bryce, R.A.; Nolan, K.A.; Stratford, I.J.; et al. Negative cooperativity in NAD (P) H quinone oxidoreductase 1 (NQO1). *ChemBioChem* **2019**, doi:10.1002/cbic.201900313.
42. Wyman, J.; Gill, S.J. *Binding and Linkage: Functional Chemistry of Biological Macromolecules*; University Science Books: Mill Valley, CA, USA, 1990.